



Misfire detection for internal combustion aircraft engines

DISSERTATION
zur Erlangung des akademischen Grades
DOKTOR DER TECHNISCHEN WISSENSCHAFTEN

Angefertigt am Institut für
Elektrische Messtechnik und Messsignalverarbeitung

vorgelegt von
Dipl.-Ing.(FH) Andreas Mair
Oberschlierbach 27
4553 Oberschlierbach

Angenommen auf Antrag von:
Univ.-Prof. Dipl.-Ing. Dr. techn. Georg Brasseur
Univ.-Prof. Dipl.-Ing. Dr. techn. Peter Dietmaier

Oberschlierbach, März 2011

I. KURZFASSUNG

Stand der Technik heutiger Kleinflugzeuge sind Kolbenverbrennungskraftmaschinen, welche mit Vergaser ausgerüstet sind. Vergaserbedüsung, Abgasgrenzwerte, Kaltstarteigenschaften, Zertifizierungsvorgaben sowie Sicherheitsthemen stellen einige wichtige Punkte dar, welche man beim Einsatz eines Vergasermotors im Flugzeug zu berücksichtigen hat. Um diese Nachteile zu reduzieren bzw. die Sicherheit der Passagiere zu erhöhen, werden derzeit moderne Motorsteuergeräte bzw. Motorsteuereinheiten (MSE) für eine Benzineinspritzung von Flugmotoren entwickelt. Aufgrund der hohen Komplexität der Steuergeräte ist es notwendig, eine Vielzahl an Diagnosesystemen zur Verfügung zu stellen. Darunter versteht man die Überwachung elektrischer bzw. nicht elektrischer Parameter von Sensoren und Aktuatoren. Diese Arbeit beschreibt eine Diagnosemöglichkeit zur Überwachung der Verbrennungsvorgänge einer Kolbenverbrennungskraftmaschine für Flugmotoren. Ursachen für einen sog. Zylinderausfall bzw. einer schlechten Verbrennung können z.B. sein: Ausfall der Zündung, fehlerhafte Benzinzufuhr, Kompressionsverlust oder auch eine fehlerhafte Berechnung der ECU um nur einige Fehlermöglichkeiten zu nennen. Im Bereich der Diagnose für Verbrennungskraftmaschinen gibt es bereits eine Vielzahl an Publikationen bzw. Systemen mit einem teils sehr theoretischen Ansatz, welche für einen Einsatz in der Serie nur eine bedingte Anwendung finden. Auch der beträchtliche Kostenaufwand mancher Überwachungsmethoden macht es zum Teil aus wirtschaftlichen Gründen nicht sinnvoll, diese zu implementieren. Die in dieser Arbeit beschriebene Betriebsstörungsüberwachung basiert auf der Messung von Schwingungen im unteren Hörschallbereich. Für die Schwingungsaufnahme wird ein Beschleunigungssensor verwendet, welcher am Motor befestigt wird. Dabei werden primär die Bewegungen des Antriebsaggregates analysiert. Auf die Analyse von Körperschallsignalen im klassischen Sinn wird in dieser Arbeit nicht eingegangen. Für die Fehlerdetektion werden die Schwingungssignale als erstes im Frequenzbereich verarbeitet und anschließend für die örtliche Zylinderzuordnung bzw. Lokalisierung in die Zeitdomäne transformiert. Die Zylinderzuordnung erfolgt auf Basis eines mathematischen Modells, welches die Verbrennungskraftmaschine mit den dafür relevanten Bauteilen beschreibt. Das System ermöglicht die Überwachung in einem Drehzahlbereich von 1800 bis ca. 6000 U/min, welches den Bereich vom Leerlauf bis zur Maximaldrehzahl definiert. Um die praktische Anwendung zu demonstrieren, wurde die Motorzustandsüberwachung an einer 6-Zylinder V-Maschine mit 120 Grad Zündwinkelversatz angewendet. Alle simulierten Einzylinderfehler konnten erkannt werden und der gesuchte Zylinder wurde in nur wenigen Motorumdrehungen zugeordnet. Durch die zylinderselktive Fehlerkennung ist es weiters noch möglich, durch aktive Beeinflussung durch die Motorsteuerung, den Motor in einen Betriebszustand zu versetzen, welcher für die internen Bauteile einen unkritischen Zustand darstellt und externe Bauteile vor Schädigung schützt. Durch diese neue Methode können Funktionsstörungen der Verbrennungskraftmaschine für Fluganwendungen sofort erkannt werden. Die daraus abgeleiteten Aktionen können den Motor bzw. Bauteile des Motors vor Überbelastung schützen und erhöhen damit erheblich die Flugsicherheit.

II. ABSTRACT

Small spark ignited engines in the aircraft industry are mainly carburettor versions. Fixed carburettor setups especially at low and high altitude frequently result in too rich or too lean an air-fuel mixture formation and further in high fuel consumption and poor exhaust emissions. Cold start deficiencies and safety rules are some other examples of the disadvantages associated with carburettor equipped aircrafts. These facts result in the use of an electrical fuel injection system. Due to the high complexity of aircraft “*engine management systems*” (EMS) and certification restrictions, aircrafts have to have highly efficient on board diagnostic and monitoring functions. Monitoring means controlling the behaviour of sensors and actuators installed on engines by measuring electrical or non electrical parameters.

This work describes an online diagnostic method for aircraft combustion engines with the objective to detect poor combustion and further locate the faulty cylinder.

Possible failures are missing ignition or injection, excessive blow by and compression irregularities, of the relevant cylinder. Many different methods to detect misfire on combustion engines were published in the past. Most of the described methods are too complex and cannot be applied for different engine types. Thus these concepts are not suitable for serial production.

The described method employs an acceleration sensor, which detects irregular engine block movements. The sensor is located fire wall forward and installed on the engine block. In principle the sensor detects the engine movement and does not pick up structure born sound. This leads to a signal processing chain done in frequency and also in time domains. In order to detect engine misfire a mechanical engine model has been developed. Based on the mechanical engine model the faulty cylinder can be located. The described method monitors the engine movement and allows deriving an engine health level based upon the vibration signal. In case of a failure, which is related to the in-cylinder pressure, the motion of the engine is quite different to the motion without engine failures. This fact is used to distinguish between normal and abnormal engine behaviours. The allocation of the concerned cylinder is performed by developed signal processing algorithm. As soon as the appropriate cylinder is located, different actions to protect the engine against mechanical stress can be processed as well. The method was applied on an aircraft 6-cylinder V-type engine with an ignition angle offset of 120° crank angle. The algorithm was verified on multiple aircrafts with different propeller setups. During the tests the monitoring system detects all simulated failures in a range from 1800 to maximum engine revolutions per minute. Also the appropriated cylinder was found in a few engine revolutions. Due to special actions on the engine which is controlled by e.g. the “*electronic control units*” (ECU), the mechanical stress could be prevented and the engine could be operated without damage or dangerous operating conditions.

This new condition monitoring system shows a better way the aircraft industry can observe combustion engines. The system's efficiency increases with a higher number of cylinders. This system offers one major advantage over other methods. Multi cylinder engines can be observed by measuring the vibration signal employing only one sensor. It detects abnormal engine behaviours, in-cylinder pressure loss and respectively in a few engine revolutions with high detection probability.

TABLE OF CONTENTS

TABLE OF CONTENTS

I. KURZFASSUNG	2
II. ABSTRACT	3
1 INTRODUCTION	6
2 STATE OF THE ART METHODS & MOTIVATION	8
2.1 MISFIRE DETECTION CLASSIFICATION	10
2.2 MISFIRE DETECTION METHODS	11
2.2.1 CRANKSHAFT SPEED FLUCTUATION	11
2.2.2 ION CURRENT OBSERVATION	12
2.2.3 EXHAUST GAS FLOW RATE AND EXHAUST GAS PRESSURE	13
2.2.4 IN-CYLINDER PRESSURE MEASUREMENT	14
2.2.5 INTAKE MANIFOLD PRESSURE OR FLOW RATE	15
2.2.6 VIBRATION MONITORING	15
2.2.7 VIBRATION MONITORING BY MEASURING THE ENGINE BLOCK FLUCTUATION	16
3 ENGINE MODEL	17
3.1 INTRODUCTION	17
3.2 POWER TRAIN SYSTEM AND MODEL ASSUMPTIONS	19
3.2.1 INERTIA TENSOR	20
3.2.2 TORSION BAR	21
3.2.3 TORSION BAR	27
3.2.4 HYDRO DAMPER	32
3.2.5 CRANKSHAFT AND ENGINE CASE	33
3.2.6 SHOCK MOUNTS	34
3.2.7 PROPELLER	36
3.3 EXCITATION	37
3.3.1 PERIODICAL EXCITATION	37
3.3.2 NON-PERIODICAL EXCITATION	37
3.4 ENGINE BOUNDARY CONDITIONS	38
3.4.1 COORDINATE SYSTEM	38
4 POWERTRAIN SYSTEM	43
4.1 CRANK DRIVE	43
4.2 GAS FORCE	46
4.3 GAS TORQUE	51
4.4 MASS EFFECTS ON THE CRANK MOTION	54
4.4.1 ROTATING MASS EFFECTS	56
4.4.2 CRANKSHAFT TORQUE DUE TO MASS EFFECTS	57
4.4.3 OSCILLATING MASS EFFECTS	59
4.4.4 TOTAL MASS TORQUE	61

TABLE OF CONTENTS

4.5	TOTAL ENGINE TORQUE CALCULATION	65
5	MODEL RESULTS AND SIGNAL PROCESSING	67
5.1	ENGINE MODEL DESCRIPTION	67
5.2	ENGINE MODEL DESCRIPTION CONTINUED	70
5.3	SIMULATION RESULTS OF A MISFIRE EVENT	86
6	SIGNAL PROCESSING	101
6.1	FUZZY BASED ENGINE HEALTH CONDITION SYSTEM	101
6.2	MODEL BASED CONDITION MONITORING	104
7	RESULT	119
8	SYSTEM EXTENTION	133
9	SUMMARY	146
10	OUTLOOK	147
11	BIBLIOGRAPHY	148
12	TABLE OF SYMBOLS	151
13	TABLE OF FIGURES	157
14	TABLE OF IDENTIFICATION CODES	163

1 INTRODUCTION

In the middle of the last century most of the common used aircraft technology, especially for small aircraft's had been developed. Current systems in use are for the air-fuel mixture formation, integrated in reciprocating engines, mainly carburettors. Devices like, "*electronic control units*" (ECU's) had not been developed for aircrafts until now or are still in the process of development. Standard avionic equipment with integrated electronic devices are, control units for jet engines, communication boxes, navigation systems and other display units.

Reasons why ECU's for engines are not available for aircrafts maybe due to the result of cost, e.g. certification investments, exposures which result in very high insurance costs and the life cycle of the products. Life cycle in regards to the engine means a minimum required runtime of 2000 hours before overhauling (TBO).

In terms of the ECU the rate of a single failure or a probable double failure leading to a "*loss of power control*" (LOPC) of the aircraft should be better than 4.5^{-5} . Finally with the support of spare parts for more than 20 years could be an argument for old technology.

Fixed carburettor setups for example at low and high altitude result in too rich or too lean air-fuel mixture formation and leads to poor exhaust emissions. Further motivations to convert engines from carburettor driven engines to electronic controlled injection systems are cold start problems and safety reasons. The first approach would be to take a standard automotive system which has been used in the automotive industry for many years. Unfortunately automobile standards and airplane requirements are not comparable. It is almost impossible to copy and paste an automotive system for aircraft application. For example the electromagnetic compatibility (EMC) requirements are defined in the DO-160 [10] and the outcome of the DO-160 further depends on the dimension of the aircraft and the environmental which the engines have to be operated in.

Depending on the size of the aircraft the system is categorized in different certification levels. This means components such as ECU's have to be developed in a way to meet the certification requirements. The most important point designing an electronic control system is the consideration about single failures of the EMS. At a single failure the EMS has to fulfil the requirements in a way to have at least 85% of nominal engine power available. Especially at take-off and landing the system power must be guaranteed for at least 85% of the nominal power. This primary objective drives all the considerations around the control system. This is different compared to the automotive standard for example. There is no requirement in the automotive industry to specify a minimum power target for their engines. In order to meet the demand on weight of the aircraft engine, it is further essential to take lightweight parts. This already has to be considered during the engine design. In an effort to reduce engine irregularities caused by gas and mass torques and increase the comfort, balancer shafts and torsion bars have to be considered in the design. The torsion bar is mainly installed to reduce propeller accelerations and keep constant propeller torque at certain propeller speeds. Further a hydro damper reduces the resonance frequency of the complete power train and decreases the varying torque of the engine.

A new electronic engine control system for an aircraft engine maintains two independent lanes. This independency is not inherently required but a fine approach to reach the required reliability of the whole system. Different devices like intake manifold pressure sensor, intake manifold temperature sensor, knock sensors, cooling water temperature sensors, throttle position sensors, ambient pressure sensors, ambient temperature sensors, exhaust gas temperature sensors, waste gate actuators and engine speed sensors are necessary for controlling the engine.

In order to monitor the condition of sensors and the whole system, it is necessary to implement diagnostic methods commonly used in automotive systems. It is not possible to detect all variations of system failures, i.e. non electrical injector faults caused by a mechanical failure with the standard EMS equipment.

Due to these aspects it is further essential to develop systems which can detect non electrical failures. One of those failure modes is called "misfire". This was the motivation to investigate a method which identifies misfires. It is called "misfire detection".

In order to observe components in the engine compartment which are not accessible, measuring engine body movement has to be executed. Therefore a model which describes the relationship between vibrations and crank shaft torque is necessary.

Based on the developed model, which will be described in the next chapters, the in-cylinder pressure can be derived from the vibration signal acquired from the engine block.

Due to emission regulations in the automotive industry misfire detection is part of the "*on board diagnose*" (OBD). Since the 1980's the OBD functionality has been implemented in standard ECU's used in cars as an example. Misfire detection is one of the most important parts in the OBD II standard.

One of the main focuses of misfire detection is the prediction of increasing exhaust emissions caused by unburned fuel. Unburned fuel may be due to several reasons, e.g. lack of spark, wrong air-fuel mixture formation and mechanical defects of the cylinder or other related components (inlet or outlet valves).

Misfire detection is also important to prevent damage to the exhaust gas purification systems or to reduce the likelihood of an uncontrolled ignition event (back fire) of the air-fuel mixture in the exhaust pipe.

The main goal in the automotive industry is to control exhaust emissions and prevent failures of the EMS. In contrast to the automotive industry there are no restrictions concerning exhaust emissions in the aircraft industry. Aircraft technology focuses on safety and prevention of hazardous engine conditions.

A failure of engine components or the EMS, may lead to minor or major failures of the aircraft and further to undefined flight situations. Those aspects show the importance of the new misfire detection method.

Condition monitoring systems in the avionics are common used systems for structure observation and monitoring the behaviour of jet engines. The observation focus based on vibration signals on combustion engines, are mainly limited to knock control. Failures of the engine caused by misfire lead to high vibrations of the aircraft structure and the engine block as well. Structure vibration at a certain frequency is highly uncomfortable and may be dangerous and should be prevented or reduced as a minimum. In order to prevent structure vibrations, the engine operating point could be changed by varying the engine speed. All possible online engine modifications with the target to prevent undesired flight behaviour might also positively influence vibration levels felt by the passengers and acoustic noise in the cockpit compartment.

2 STATE OF THE ART METHODS & MOTIVATION

Many different analysis methods and physical principles for misfire detection have been published in the past. A rough classification could be concluded by distinguishing between cylinder selective and none cylinder selective measurements. Individual cylinder measurements are very accurate and directly referenced to the observed combustion chamber. These methods are mainly applied on test bench measurements during engine developments [48].

Some disadvantages of these systems or sensors could include the high cost, malfunctions due to engine vibration or the harsh environment and very often for aircraft applications not available.

Examples are exhaust gas pressure measurement, exhaust gas flow rate check, exhaust gas temperature measurements, in-cylinder pressure observation and ion-current observation [38] to [48].

Methods which are not measuring the physical effects directly are called "indirect measurement". These methods need some model assumptions or converter for observations. Advantages of these methods are lower costs compared to the cylinder selective methods due to fewer sensors [46].

Many observation methods use only one sensor, or in best case the sensors from the EMS e.g. knock sensors. All these assumptions are based on models which describe the systems behaviour. The models are more or less accurate and the result of the measurements is dependent on the model quality.

The main problems of some models are the complexity of some systems and the long term consideration, because some systems cannot be assumed as time invariant. One example is an engine which is developed for multiple aircraft types. This means the exhaust pipe and the intake manifold have to be modified based on aircraft installations for example. Or in case of exhaust temperature measurements [46] sensors have drifts during lifetime or deposits on the sensor surface influences the measurements. These are some reasons why models have to be updated.

Systems with non linear behaviours need very complex algorithms or a linearization approximation at the operating point. This results in different signal processing procedures, below are a few exemplary methods listed:

Intake manifold pressure or flow rate measurement [43], crankshaft speed fluctuation [38] and vibration monitoring systems [25].

Some of the systems described as "*direct measurement methods*" could be also used as so called "*non direct measurement*". This depends on the location of the sensor, which is used to observe the engine. Crankshaft speed fluctuation is the most common used method in the automotive industry for misfire detection [38]. Challenging factors of those methods are model assumptions of the mechanical system, accuracy of the standard incremental sensor like magnetic pick ups and the number of cylinders. Especially at high engine speeds in conjunction with high numbers of cylinders, those methods fail or become very imprecise. Neuronal networks, adaptive filters and model based statistical methods are further derivatives of the crankshaft speed fluctuation analysis [49] and [50].

Vibration analysis methods like pressure dynamic models have been published in the past. [7] and [25] publish a method which recalculates the in-cylinder pressure of the related cylinder based on vibration information taken directly from the engine block. This leads to a complex signal processing method to obtain the results.

Measurements from engine block vibrations result in lower kHz frequency [8] and [6]. In fact the monitoring system has to have faster analysis algorithms compared to the method proposed in this thesis.

By monitoring the engine block movement a lot of the disadvantages of the aforementioned methods can be resolved. Due to the analytically described mechanical system of such combustion engines the in-cylinder pressure characteristics can be calculated based on vibration signals coming from an acceleration sensor. The computation of the in-cylinder pressure is based on a consideration of “*linear time invariant*” (LTI) system. Simple signal processing and low system costs regarding implementation in the standard ECU or the EMS are some benefits of the proposed condition monitoring method.

Further advantages are the fast response time of the system and the good signal to noise ratio. These facts make the system robust against external disturbances or possible misinterpretations which maybe found in the same frequency range.

2.1 Misfire detection classification

Figure 2-1 shows different methods to observe engine behaviours. All of the listed appendages realize misfire detection possibilities, based on different physical principles. All these examples are mainly applied in the automotive industry. One of the most used systems in the automotive industry is the measurement of exhaust gas temperatures [46]. For this measurement it is essential to have at least one air temperature sensor installed in the exhaust pipe. Defect sensors caused by vibrations in combination with high temperatures up to 1000°C; high costs and limited durability are some of the disadvantages of this method. A review of condition monitoring systems can be read in [52].

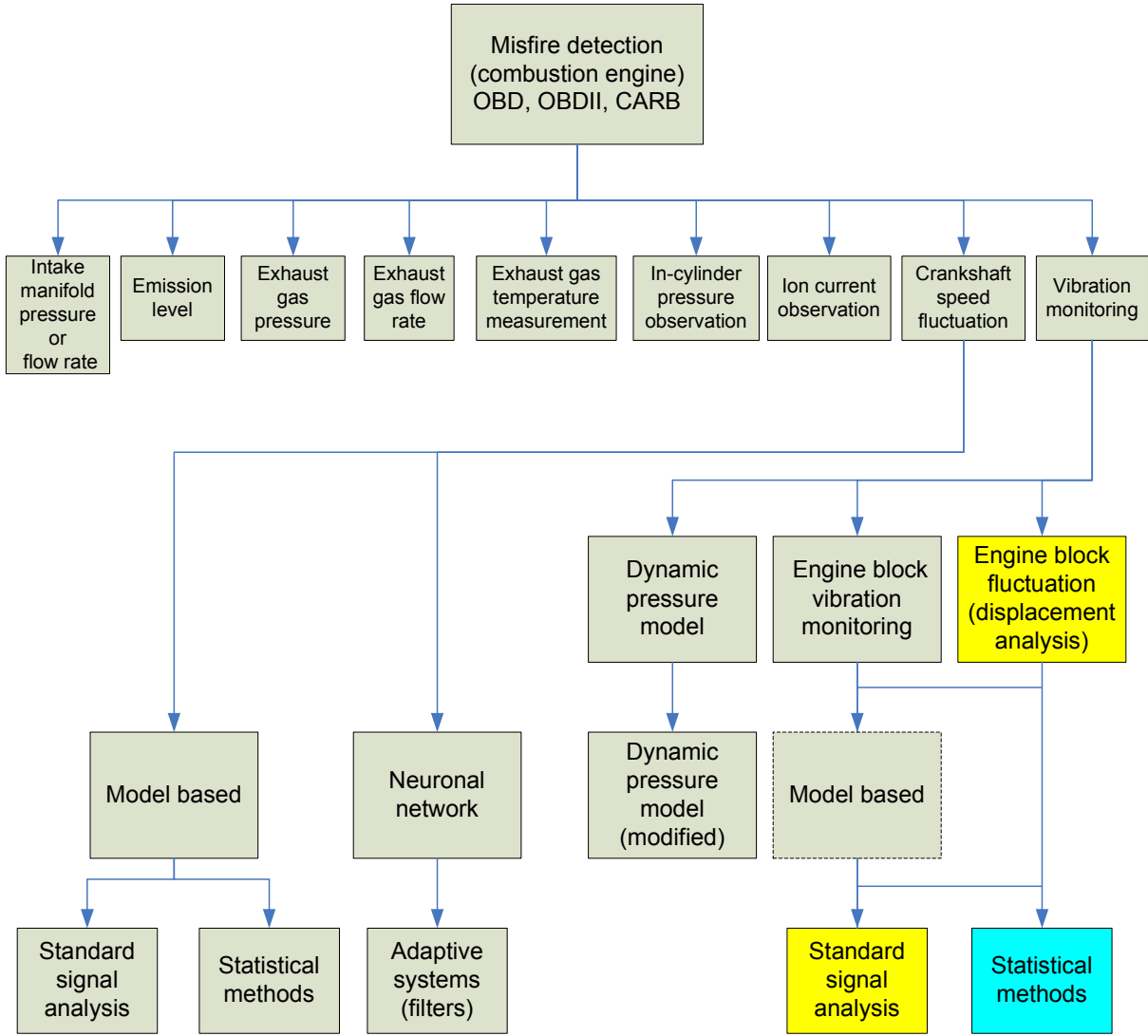


Figure 2-1 Overview of methods for misfire detection.

2.2 Misfire detection methods

2.2.1 Crankshaft speed fluctuation

Making use of Kalman filtering techniques is a new approach to process the crankshaft speed signal. Applying this technique means that misinterpretations or false alarms can easily be avoided.

Automotive Engine Misfire Detection Using Kalman Filtering

"This paper presents a new approach to misfire detection using system parameter estimation techniques. A mathematical model has been developed for the engine firing system. The resulting model contains many unknown parameters or coefficients. A system parameter identification technique employing a Kalman filter is then developed to estimate all the unknown parameters based on actual vehicle test data. The paper shows that the new Kalman filter approach for misfire detection has greatly enhanced the detection accuracy and reduced the false alarm rate of current misfire detection systems" [38].

The "crankshaft speed fluctuation" (CSF) method is based on software algorithms to detect incorrect ignition events. [1], [2], [3], [4] and [5] describes briefly the algorithms and the issues related to the methods. All of the published methods employ additional sensors, i.e. pressure or vibration sensors to avoid misinterpretations. Additional sensors are often used to detect so called "in range" failures of the systems and further increase the likelihood of the detection of poor combustion processes by comparing different sensor signals to each other. An automotive engine normally is fitted with a crank position sensor, a tooth wheel and furthermore other important sensors and actuators for engine management. The tooth wheel is normally mounted on the crankshaft and has a predefined position referenced to a fixed engine point. The position of the flywheel and the number of teeth depends on the designer and the dynamic properties of the engine. A standard wheel for automotive applications has 36-2 teeth. This leads to a physical resolution of 10° crank angle. By using interpolation methods the resolution can be increased within certain limits.

An external electronic device like a speed sensor is wired to the ECU. The sensor picks up the edges of the trigger wheel and transfers the generated signal to the engine control unit. ECU synchronization is triggered upon a certain tooth, which serves as engine reference point. Each calculation of the ECU is referenced to that point. At a given crank angle position the ECU generates an ignition pulse. If an ignition event and furthermore a combustion process is initiated, the crankshaft will be accelerated. In case of a normal engine behaviour the average engine speed (crankshaft rotation speed) over one full engine rotation is quite constant.

A cut out over some crank angle degrees of the crank signal shows the engine behaviour in detail. Under normal operational conditions, the engine shows different widths between crank signal pulses caused by the ignition events. The resolution of the pulse depends on the counts of teeth on the tooth wheel. In case of a failure in the ignition system or a pressure loss of e.g. one cylinder, the crank signal shows significant changes in pulse widths and can be distinguished by comparing the tooth widths of each pulse. A failure caused by misfire, shows instantaneous changes of the crankshaft speed at a related tooth wheel position. Misfire can be located by observing regional distinctions of angular velocities. A closer look to the pulses shows the behaviour of the affected cylinder. An engine fault results in different pulse widths of the crankshaft signal. This can be observed and the faulty cylinder can be recognized.

Cylinder numbers, engine speed, signal magnitude, dynamic mechanical effects of the

crankshaft and other disturbances on the engine are some reasons for using special software algorithms to detect abnormal cylinder conditions.

High cylinder counts combined with high engine speed requires optimized software algorithms. To distinguish between normal and abnormal engine conditions many different signal filter techniques can be used. A common problem of this detection method is the influence of the crankshaft. Any crankshaft vibrations can influence the signal quality, acceleration and deceleration of the crankshaft may also, at normal engine conditions, create ghost failures by the detection algorithms. To prevent misinterpretations most of the published methods implement crankshaft models. The higher the quality of the crankshaft models the lower the likelihood for misinterpretations, which leads to a robust condition monitoring system.

2.2.2 Ion current observation

Herein are some proposed examples of indirect misfire detection methods. Based on measuring ion current flow misfire can be detected. Disadvantages of these methods are additional electronic devices or controllers for measuring the current flow.

Monitoring the Combustion Quality in Internal Combustion Engines Using the Spark Plug as a Plasma Probe

"A method of monitoring the quality of combustion in spark ignition gasoline engines using the spark plug's centre electrode as a plasma probe is presented. Due to the ionized species remaining in the burned gases after combustion, a current is induced in a network attached to the spark plug's centre electrode. The time dependence of this induced current is shown to correlate with the presence or absence and the time of occurrence of the pressure component due to combustion in pressure transducer signals recorded simultaneously. Based on these correlations, three types of burns could be recognized from plasma probe signals: good burns, slow burns, and misfires. The specific correlation between the absence of a pressure component due to combustion and a corresponding absence of a plasma probe signal was used to form the basis for the operation of a one-channel engine misfire monitoring circuit" [39].

A Method of Torque Estimation Utilizing Ionization Sensing Technology in Internal Combustion SI Engines

"This paper describes a method of torque estimation by using in-cylinder ionization sensing technique in an internal combustion SI engine. Through the characterisation of the ion current signal measured across the spark plug electrode with four parameters, two peaks of ionization signal were investigated and used to build the relationship between the net torque of engine and the ion current signal. From the experiment results, a conclusion can be drawn that the averaged ionization signal over 20 consecutive combustion cycles is well correlative with the variation of torque, especially in the case of higher torque conditions. The intensity and position of the second peak of this signal are most sensitive to the change of torque" [40].

2.2.3 Exhaust gas flow rate and exhaust gas pressure

Following is a technique presenting how an exhaust gas pressure can be estimated. Applying this method, additional pressure sensors are no longer necessary, or a monitoring system for observing the pressure sensors is feasible.

Exhaust Pressure Estimation and Its Application to Variable Geometry Turbine and Waste gate Diagnostics

"Exhaust pressure is a critical engine parameter used to calculate engine volumetric efficiency and EGR flow rate. In this paper, exhaust pressure is estimated for an internal combustion engine equipped with a variable geometry turbocharger. A coordinate transformation is applied to generate a turbine map for estimation of the exhaust pressure. This estimation can be used to replace an expensive pressure sensor for cost saving. On the other hand, for internal combustion engines that have already installed exhaust pressure sensors, this estimation can be used to generate residual signals for model-based diagnostics. Based on the residual signals, two diagnostic methods are proposed: one based on cumulative sum algorithms and the other based on pattern recognition and neural networks. The algorithms are able to detect and isolate different failure modes for a turbocharger system" [41].

The paper below describes a sensor to measure the exhaust gas flow rate. High time resolution and precision of the sensor realizes the possibility to monitor in-cylinder pressure losses.

A Capacitance Ultrasonic Transducer with Micro machined Back plate for Fast Flow Measurements in Hot Pulsating Gases

"A novel high-temperature resistant capacitance ultrasonic transducer is presented. It is designed for an ultrasonic transit-time gas flow meter and meets two main requirements not fulfilled by common piezoelectric transducers: First, a special construction based on an oxidized and patterned silicon back plate combined with a metallic membrane enables transducer operation at elevated gas temperatures of up to 600 °C. Second, the geometry and material parameters were chosen to obtain a broadband device that allows high signal slew rates and pulse repetition rates. As proven by measurements in an automotive combustion engine test bed environment, this new transducer suits for internal combustion engine exhaust flow measurements in between the catalytic converter and the end of the exhaust pipe. Preliminary results for the exhaust mass flow (up to 160 kg/h) of a typical automotive engine measured with these novel transducers are given and compared with the mass flow calculated from fuel consumption and air/fuel ratio (λ)" [42].

2.2.4 In-cylinder pressure measurement

In the following outlet a new sensor for measuring the in-cylinder pressure will be presented.

Development of a Fibre-Optic Sensor for the Measurement of Dynamic Cylinder Pressure in Spark Ignition Engine

"This paper describes a new design of in-cylinder pressure sensor for automotive applications using optical technology. The technology has been applied to a spark ignition engine and compared against piezoelectric sensor. The paper presents a fibre-optic interferometric sensor based on highly birefringent side-hole fibres. The sensing part is composed of a side-hole fibre characterized by a very high pressure-to-temperature sensitivity ratio equal to 25°C/bar, which are about two orders of magnitude higher than in the case of other highly birefringent fibres. The research with positive laboratory verification has proven the usefulness of fibre-optic sensor for diagnostics of combustion engine work cycle. Assumptions that the use of interferential fibre-optic sensor shall enable pressure measurements and calculation of indices resulting from these measurements that are based on an obtained data as well as controlling the engine the way have turned out to be true. The research revealed the relation between the track of interferential fibre-optic sensor signal and work cycle parameters of SI engine. Also the thesis that the measurement signal of interferential fibre-optic sensor can be the carrier of data about certain SI engine work cycle parameters had been proven. The initial results from the sensors show good performance against reference sensor. We compared the dynamic characteristics of the fibre-optic sensor, to the responses of a calibrated and temperature-compensated piezoelectric sensor. The dynamic characteristics of the fibre-optic sensor are in good agreement with the reference piezoelectric sensor, which shows the great utility of the side hole fibres in accurate measurements of high dynamic pressures" [48].

2.2.5 Intake manifold pressure or flow rate

Using the method proposed below, exhaust emissions can be reduced dramatically. Applying this method, a misfire due to too rich air-fuel mixtures formation caused by sensor, ECU or injection failures for example, can be avoided by estimating the fuel quantities based on an analytic model. A comparison of calculated (from the ECU) and estimated fuel quantities realizes an applicable condition monitoring system for misfire.

Air-Fuel Ratio Control in Gasoline Engines Based on State Estimation and Prediction Using Dynamic Models

"A highly accurate air-fuel ratio control scheme has been developed for reducing exhaust emissions from gasoline engines. It uses a compensation scheme based on state estimation and prediction to cope with the problems of precisely detecting the amount of air flowing into the cylinder, which is difficult in transition due to air-flow sensor delay, air charging of the intake manifold, and a control structure that requires predicting the air flow one stroke ahead, and the delay in fuel transport caused by the fuel impacting on the wall of the intake manifold. The internal state variables, the manifold pressure, the air flow rate at the inlet port, and the fuel film amount are estimated using a previously adjusted dynamic model; the fuel injection amount is controlled based on these estimated values so that the target air-fuel ratio can be accurately achieved. Experiments showed that the air-fuel ratio control is improved, reducing exhaust emissions from 10% to 35% compared with the conventional method" [43].

2.2.6 Vibration monitoring

Vibration monitoring systems are common used methods to observe the behaviour of combustion engines. The engine noise can be observed by using an acceleration sensor, which is mounted on the engine block. All applications use knock sensors for vibration observations to prevent severe in-cylinder pressures. The knock sensor is a standard sensor for automotive engines. From [7] to [9] some methods are described to observe the in-cylinder pressure by measuring structure born sound. In [6] a method is presented which uses a transfer function to calculate the in-cylinder pressure. The major task to re-calculate the in-cylinder pressure based on vibration signals is to find the transfer function of the engine. Based on this function further calculations can be derived. As explained in [6] and [7], costs and reliability are the main drivers to reduce sensor quantities. Common used methods work with model assumptions. Sound signal models, identification and reconstruction are the main parts to recalculate the cylinder pressure characteristics from an acceleration signal. As mentioned in chapter 2.2.1 a faulty ignition event leads to a change of the crankshaft angular velocity and then to a torque distortion on the crankshaft. The complex signal processing algorithms, the difficulty to find correct parameters for the transfer function of the engine and limitations on the implementation of the algorithm in the ECU are some examples why these methods are not applied to aircraft engines.

Two examples how vibration signals can be used to determine engine faults are listed below.

FAST IN-CYLINDER PRESSURE RECONSTRUCTION FROM STRUCTURE-BORNE SOUND USING THE EM ALGORITHM

"The paper addresses the problem of reconstructing the low-frequency part of in-cylinder pressure of spark ignition engines by analyzing structure-borne sound signals measured on the surface of the engine block. The new pressure trace model proposed yields accurate approximations with a minimal number of parameters. When combined with the EM algorithm, a processing scheme results that provide fast pressure estimates and efficiently exploits the information contained in the sound signal. Experimental results with real measurement data show the potential of the reconstructed signal to perform misfire detection and closed-loop spark ignition timing tasks" [6].

ENGINES CONDITION MONITORING BASED ON SPECTRUM ANALYSIS OF SOUND SIGNALS

"This paper proposes the use of spectrum estimation with cross spectrum correlation to monitor the condition of automotive engine based on their sound signatures. This approach is convenient and economical as it is non intrusive and does not require high precision sensors. The nonparametric spectrum estimation is chosen because the sample available is sufficiently large such that there is no leakage and frequency resolution problem. The methods chosen are periodogram, Bartlett, Welch and Blackman-Tukey" [44].

2.2.7 Vibration monitoring by measuring the engine block fluctuation

The observation of the engine block fluctuation allows measuring the behaviour of the engine, even if the sensor like e.g. an acceleration sensor is not directly attached to the engine block. This means the sensor could be installed on an external engine aggregate as well.

[8] Briefly describes the working principle and the idea of this method. The paper does not include a detailed description how it works and which mechanical parts could influence the quality of the misfire detection. Unfortunately [8] does not describe the relation between the measured vibration signal and the mechanical system. There is no information about the signal processing algorithm and the expected frequencies in case of an engine ignition fault. Later on this thesis will explain why these parameters are essential for a model based misfire detection method.

The paper illustrates that in case of misfire the vibration signal shows a peak approximately 90° crank angle after the missing ignition event. This is an invariant parameter of the engine and constant across the entire engine speed range. If this parameter is referenced to an e.g. crankshaft signal the affected cylinder can be located.

The main purpose of this invention is to prevent the destruction of the exhaust gas purification system. As mentioned in the paper the biggest advantage of the detection method is the rapid response of the engine block caused by an ignition event failure. If a malfunction is detected, the related injector will be switched off and the catalyst can be protected. The paper does not describe dynamic effects which must be considered describing combustion engines as published in this thesis.

3 ENGINE MODEL

3.1 Introduction

In chapter 2.2.7 a method to detect an abnormal cylinder firing event was mentioned. The method is based on measurements of engine block fluctuation [8].

This thesis employs the knowledge presented in 2.2.7 and describes an extended model based diagnostic method for aircraft combustion engines with more than one cylinder.

This chapter describes the mechanical model for the investigated engine type.

The engine design requirements for aircraft engines are quite different to automotive engines. For aircraft engines it is essential to use mainly lightweight materials to reduce weight of the aircraft. A further design requirement concerning engine vibrations relates to the comfort in the passenger compartment. It is not acceptable that a lot of disturbances produced by the engine are transferred to the cockpit compartment and produce unpleasant noise there. Torque of engines e.g. cars is transmitted to the wheels via power train systems. Power train system means the joints between crankshaft-gear box, gear box-differential gear and further to the wheels. The moment of inertia and effects on the engine due to the moment of inertia of the propeller is generally underestimated. It must be considered that the moment of inertia of the propeller \mathcal{S}_p related to the driving side (crankshaft must be divided by the squared gear ratio).

In order to reduce torque distortions on the engine due to the moment of inertia of the propeller \mathcal{S}_p it is necessary to uncouple the engine from the propeller. This can be achieved by using a special damped clutch or a torsion bar. In [12] an alternative method to reduce vibrations by using a switch able torsion bar is presented. With this method the torsion stiffness of the power train system can be switched between two spring parameters. It can be chosen if the propeller connected to the crankshaft is stiff or flexible. During the starting phase the propeller is directly connected to the crankshaft via a bar with a high spring constant. At a predefined engine revolution the torsion bar with lower spring constant will be engaged. If the propeller is directly connected to the crankshaft meaning without gear box no clutches or torsion bars are necessary. Figure 3-1 shows the working principle of the system.

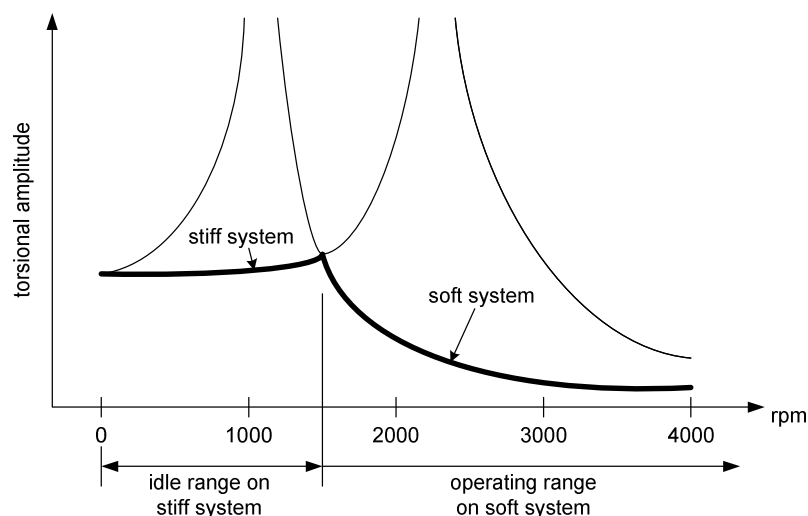


Figure 3-1 Torsional amplitude versus engine speed –Dual frequency system.

Following the state of the art aircraft design it is recommended to have a decoupled arrangement between the engine and the propeller by using e.g. a torsion bar. This helps to decrease crankshaft vibrations and keeps a smooth and stable engine torque at the propeller. Engineers are challenged to find a very flexible torsion bar with the purpose to reduce engine vibrations and withstand the maximum engine torque without any restrictions.

This means the torsion bar has to operate in a predefined range of the Hooke's law [11]. Overstressing the torsion bar could result in damages or a complete breakdown. In this case the mechanical joint, meaning the power train system between the engine and the propeller, is lost and no engine torque can be transmitted.

Effects such as bearing friction or piston friction are not included in the mathematical model and therefore not considered in the representation of the misfire event.

Figure 3-2 represents an overview of the mechanical model. For the simulation of the engine behaviour a mathematical model was developed based on the picture below. This block diagram briefly describes the engine and the mechanisms. Due to the chosen method, monitoring the engine movement, only high power effects like a missing firing event of the engine will be recognized. A tooth crack or pitting of a tooth wheel for example will not excite the engine in a manner such as caused by failure of the ignition or injection system. The structure possesses a low pass filter characteristic without additional damping elements.

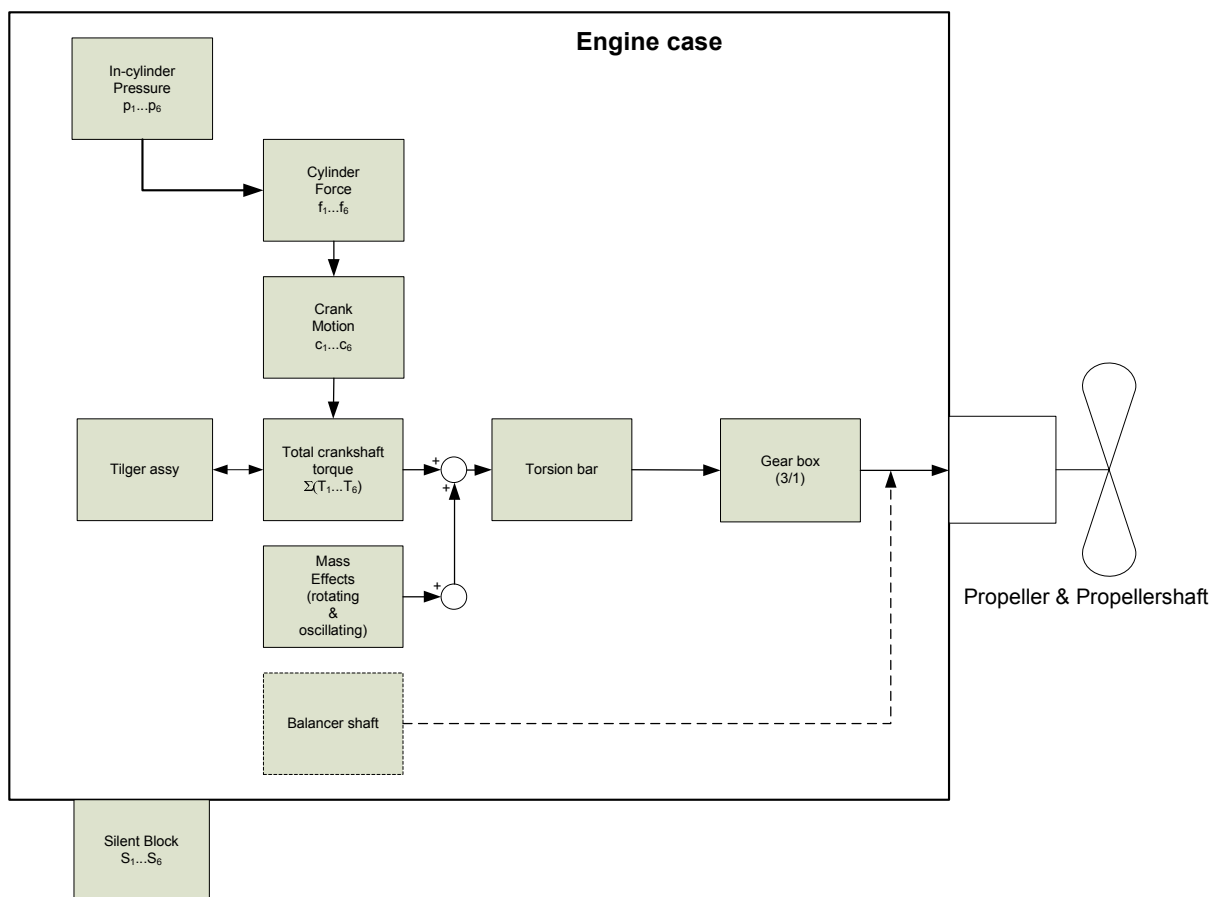


Figure 3-2 Engine model overview.

3.2 Power train system and model assumptions

In an effort to describe the physical behaviours of real systems it is mostly necessary and helpful to reduce the complexity of a system with multiple degrees of freedom (MDOF) to a system with fewer degrees of freedom [13]. For the analytic description and simulation of behaviours of a 6-cylinder, 4-stroke combustion engine, including a gearbox and a propeller, some model restrictions must be assumed.

If the engine mounts for example must be considered too, linearization approximations around the operating point of the silent blocks are recommended. Without the linearization the model cannot be described as an LTI system and must be calculated as a non linear system. [13] distinguishes between three system levels for the model assumptions and describes how mechanical systems can be expressed in an analytic way and which level has to be applied for the system description. The system levels are called “level one”, “level two” and “level three”.

Stage one is based on a rigid body type and it is called “level one”. It can be applied if the excitation is quite slow. This means the natural frequency of the system is higher than the highest excitation frequency.

$$f_{excitation} \ll \omega_1 \quad (3.1)$$

In case of a transient excitation the model “level two” can be assumed if the time of the force transition t_a is much higher than the cycle duration T_{real} of the real physical phenomena.

$$\frac{1}{f_{real}} = T_{real} \ll t_a \quad (3.2)$$

“Level three” approaches can be assumed if non linear problems have to be investigated. In this thesis the restrictions to “level one” and “level two” are assumed. Non linear effects will not be considered or converted to LTI systems. Based on the fact that a silent block for example is a non linear system, it will be transferred to a LTI system for further assignments.

3.2.1 Inertia tensor

In a homogeneous gravitation field the centre of mass is the same as the centre of gravity [14]. Due to the fact that the influence of an inhomogeneous gravitation field is less compared to the phenomena described in this thesis, it will be ignored. If the centre of the coordinate system is located at the centre of gravity, the static mass moments of area will be zero. For the description of dynamic systems it is necessary to work with the moment of inertia and the product of inertia. The moment of inertia \mathfrak{S}_a and the product of inertia \mathfrak{S}_{pq} are given by

$$\mathfrak{S}_a = \int_m s^2 dm \quad (3.3)$$

and

$$\mathfrak{S}_{pq} = \int_m pq dm. \quad (3.4)$$

Where a is the reference axis, s the distance from the axis to the points of the bodies and p and q represent the axis of the reference plane.

The engine block including all internal and external components, such as the external generator, the air conditioning compressor, is considered in the engine model. The design of the engine was done by the program Pro-Engineer [22] and also the moment of inertia tensor was calculated by this program. The formula listed below is referenced to the centre of mass \mathfrak{S}_c of the whole engine.

$$\mathfrak{S}_c = \begin{bmatrix} \mathfrak{S}_{xx} & \mathfrak{S}_{xy} & \mathfrak{S}_{xz} \\ \mathfrak{S}_{xy} & \mathfrak{S}_{yy} & \mathfrak{S}_{yz} \\ \mathfrak{S}_{xz} & \mathfrak{S}_{yz} & \mathfrak{S}_{zz} \end{bmatrix} \quad (3.5)$$

The moment of inertia of mass are defined by

$$\mathfrak{S}_{xx} = \int (y^2 + z^2) dm \quad (3.6)$$

$$\mathfrak{S}_{yy} = \int (x^2 + z^2) dm \quad (3.7)$$

$$\mathfrak{S}_{zz} = \int (x^2 + y^2) dm \quad (3.8)$$

and the products of inertia

$$\mathfrak{S}_{xy} = \mathfrak{S}_{yx} = -\int xy dm \quad (3.9)$$

$$\mathfrak{S}_{zx} = \mathfrak{S}_{xz} = -\int zx dm \quad (3.10)$$

$$\mathfrak{S}_{yz} = \mathfrak{S}_{zy} = -\int yz dm. \quad (3.11)$$

3.2.2 Torsion bar

As mentioned above, the design objective of aircraft combustion engines should allow stable torque delivery, which ultimately reduces the level of engine block movement.

Due to angular velocity irregularities caused by mass and gas effects, it is proposed to counteract by means of a torsion bar. In order to realize a stable output torque, the engineers either integrate a torsion spring between the crankshaft and the power train or use the power train system as spring. Aircraft engines mostly use clutches with elastic spring elements to reduce mechanical stress caused by mechanical clearance in the power train system.

Due to teeth clearance in the gear box it is strongly recommended to install a torsion bar for example or other spring elements in addition. If the propeller is connected to the engine via a gear box without damping components, engine vibrations increase caused by the mass moment of inertia of the propeller in combination with teeth backlash. This leads to excessive noise and gear wear. Worn gears are also cause for torque fluctuations that are transmitted by the crankshaft and ultimately result in elevated engine block movement.

The engine described in this thesis was equipped with a torsion bar. Figure 3-3 shows a sectional representation of the hydro damper (1) on the left hand side, followed to the right by the crankshaft (2), the pistons (3), the torsion bar (4), the pinion shaft (5), the gearbox (6), and the propeller shaft (7). On the bottom the silent block (8) with the fixation is drawn as well. Before a computation can be done, the torsion bar and all other parts of the engine have to be investigated in which model level they can be expressed. As mentioned in 3.2 model “level one” could be applied if the excitation frequency is much lower than the natural frequency of the part. If model “level one” is not applicable, the model “level two” or “level three” must be applied. For the classification it is necessary to have the information of the natural frequency of the investigated part. For the categorization the eigen-modes have to be calculated. This was done by the program MATLAB-Simulink [18].

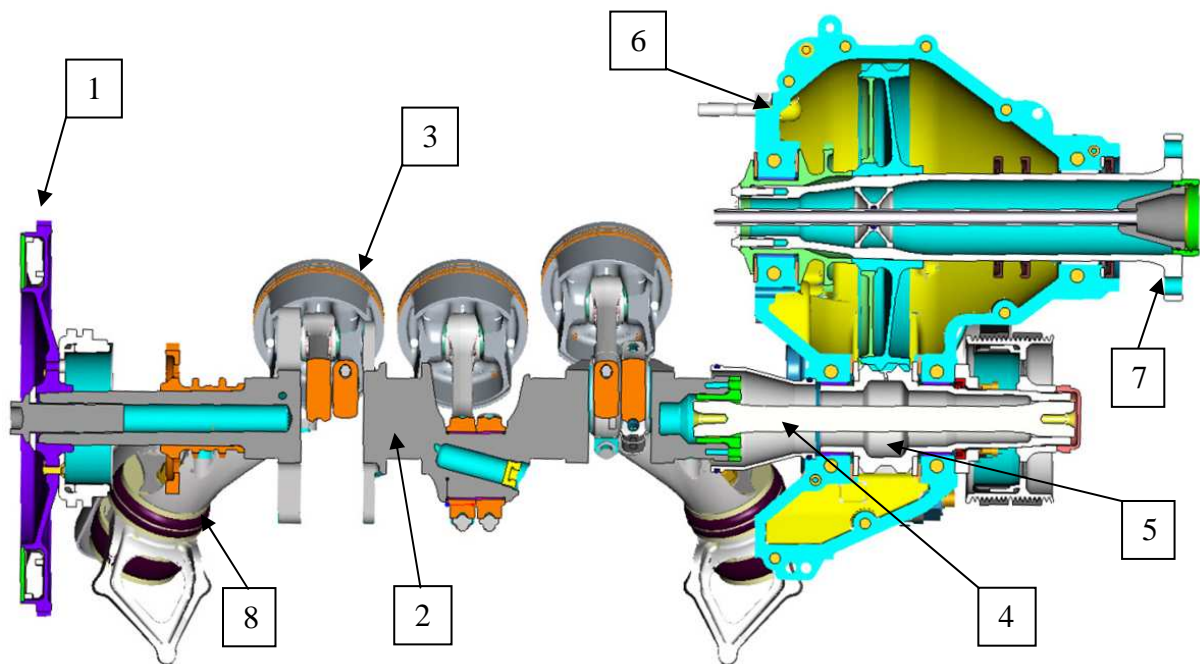


Figure 3-3 Sectional representation of the power train system. (1) hydro damper, (8) silent block, (2) crankshaft, (3) piston, (4) torsion bar, (5) pinion shaft, (6) gear box and propeller shaft (7).

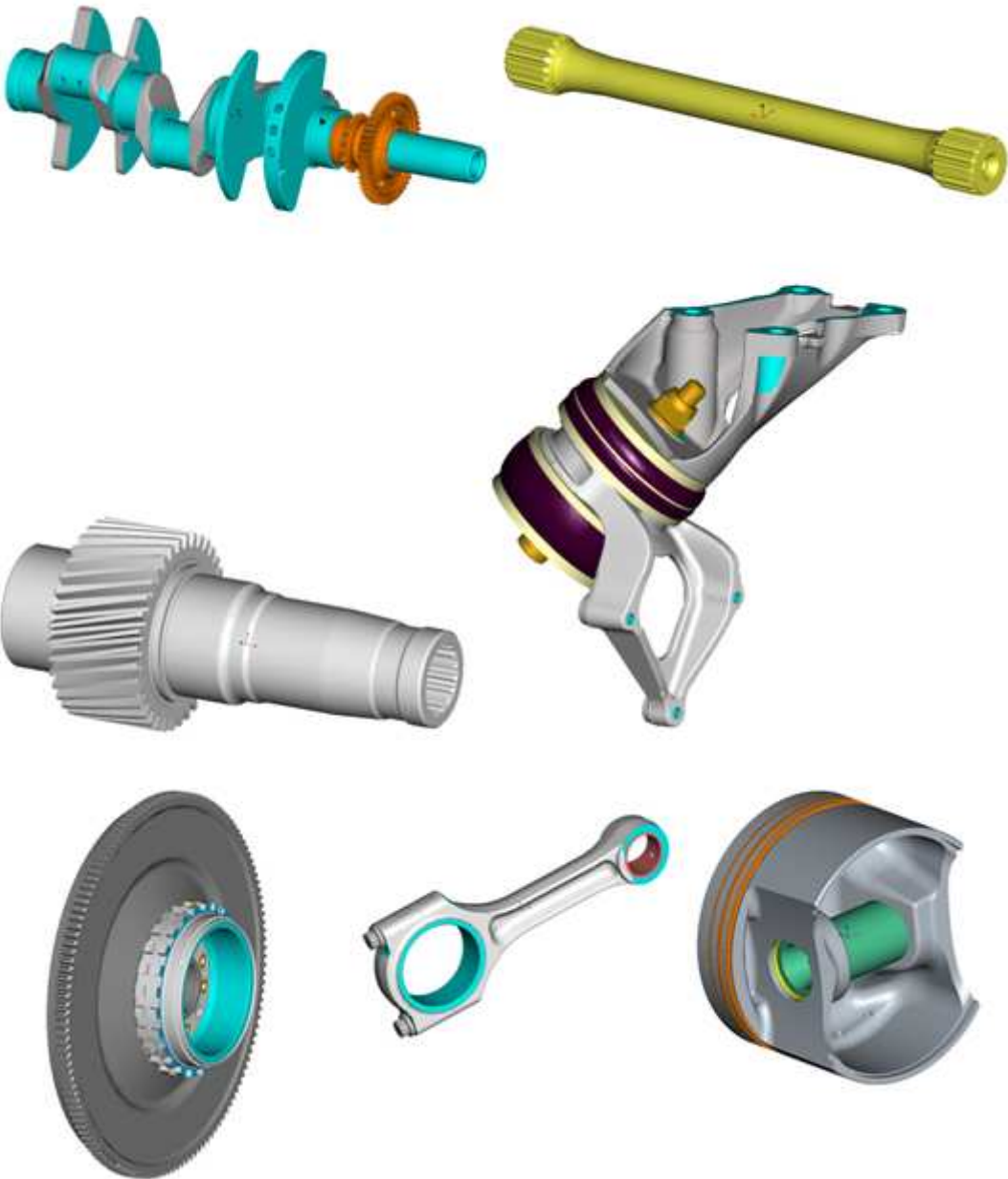


Figure 3-4 Overview of engine parts of the power train system. Top: Crankshaft left hand side and torsion bar right. Middle: Pinion shaft left hand side and silent block with fixation to the right. Bottom: Hydro damper with tooth wheel left hand side, to the right the connecting rod and the piston.

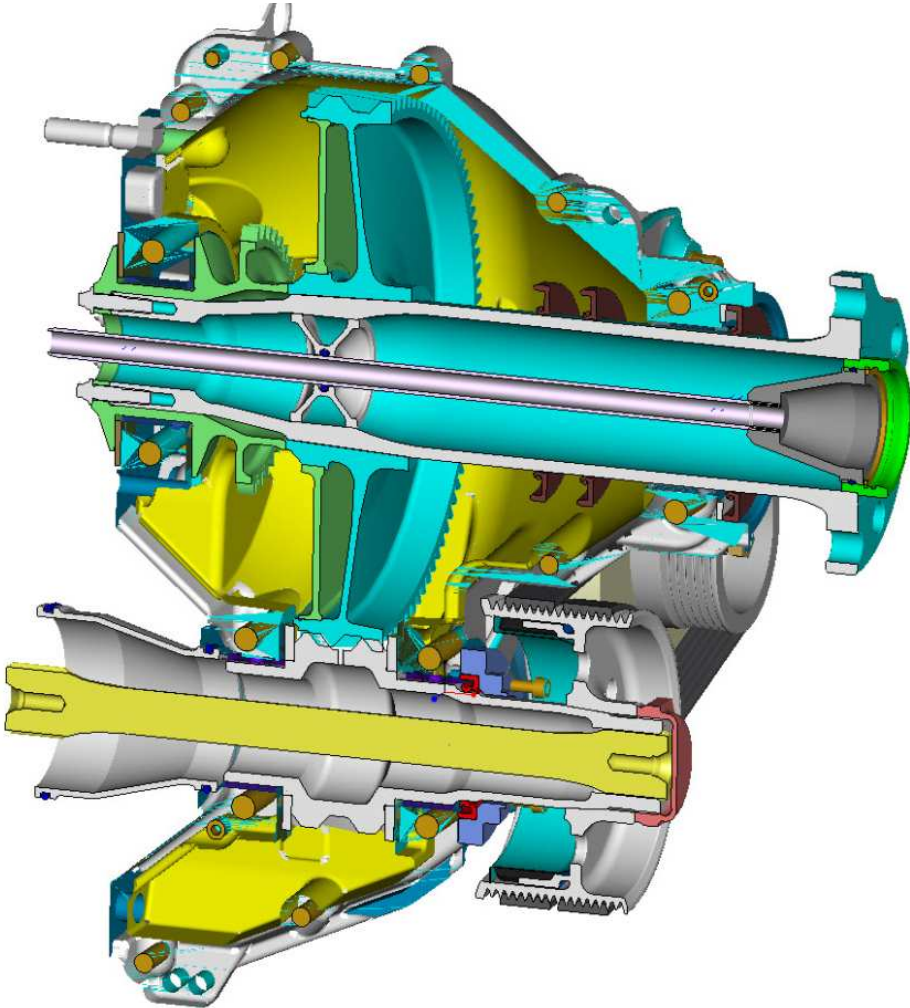


Figure 3-5 Sectional representation of the gear box.

Below the equations for the power train system shown in Figure 3-6 are listed. For the calculation of the natural frequency $f_{1,2} = \frac{\omega_{1,2}}{2\pi}$ a non excited system (excitation = 0) must be formulated. \mathfrak{S}_{16} denotes the moment of inertia of the crankshaft and the hydro damper. $\ddot{\varphi}_1$ Represents the angular acceleration and φ_1 the angular displacement of the crankshaft, as well as the hydro damper. The spring constant of the torsion bar is denoted by ct_4 . φ_2 describes the angular displacement of the tooth wheel with the radius r_5 (on crankshaft). The moment of inertia of the propeller and the propeller shaft is described by \mathfrak{S}_5 and \mathfrak{S}_4 denotes the moment of inertia of the tooth wheel with the radius r_6 . ct_6 describes the spring constant of the propeller shaft and the parameter r_5 and r_6 describe the wheel diameter of the gear box. A more detailed description will follow in section 3.2.3.

$$\mathfrak{S}_{16}\ddot{\varphi}_1 = -ct_4(\varphi_2 - \varphi_1) \quad (3.12)$$

$$\mathfrak{S}_{16}\ddot{\varphi}_1 + ct_4(\varphi_1 - \varphi_2) = 0 \quad (3.13)$$

$$\left(\mathfrak{S}_2 + \mathfrak{S}_4 \left(\frac{r_5}{r_6} \right)^2 \right) \ddot{\varphi}_2 - ct_4(\varphi_1 - \varphi_2) + ct_6 \left(\frac{r_5}{r_6} \right)^2 \left(\varphi_2 - \varphi_5 \left(\frac{r_6}{r_5} \right) \right) = 0 \quad (3.14)$$

$$\mathfrak{S}_5 \left(\frac{r_5}{r_6} \right)^2 \ddot{\varphi}_5 - ct_6 \left(\frac{r_5}{r_6} \right)^2 \left(\varphi_2 - \varphi_5 \left(\frac{r_6}{r_5} \right) \right) = 0 \quad (3.15)$$

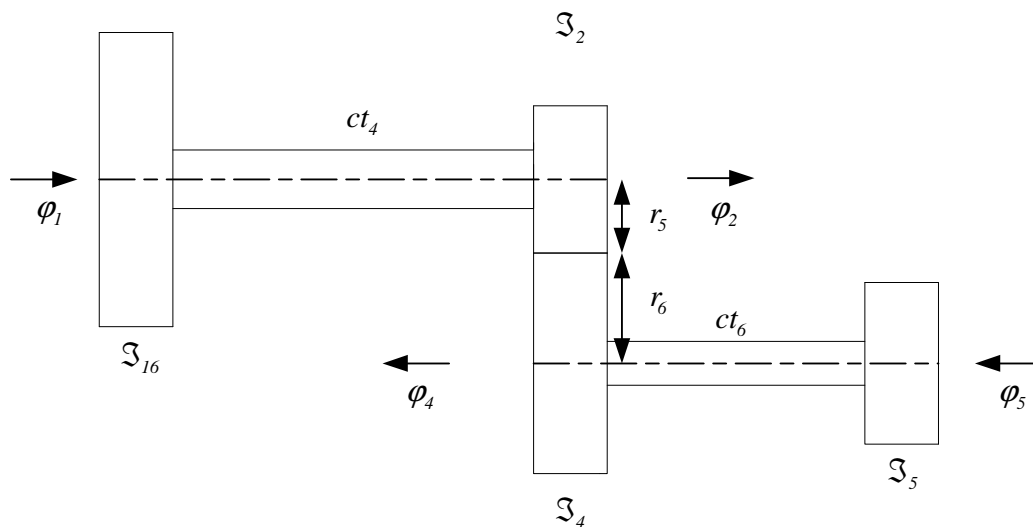


Figure 3-6 Rigid body type model of the power train system.

The angular rate is given by [13]:

$$\omega_0 = 0 \text{ Hz} \quad (3.16)$$

$$\omega_{1,2} = \frac{1}{2} \left(\omega_*^2 \pm \sqrt{\omega_*^4 - \frac{4ct_4ct_6 \left(\frac{r_5}{r_6}\right)^2}{\mathfrak{S}_{16} \left(\mathfrak{S}_2 + \mathfrak{S}_4 \left(\frac{r_5}{r_6}\right)^2\right)} \left(\frac{\mathfrak{S}_{16} + \left(\mathfrak{S}_2 + \mathfrak{S}_4 \left(\frac{r_5}{r_6}\right)^2\right)}{\mathfrak{S}_5 \left(\frac{r_5}{r_6}\right)^2} + 1 \right)} \right) \quad (3.17)$$

with the reference angular rate

$$\omega_*^2 = \frac{ct_4}{\mathfrak{S}_{16}} + \frac{ct_4 + ct_6 \left(\frac{r_5}{r_6}\right)^2}{\mathfrak{S}_2 + \mathfrak{S}_4 \left(\frac{r_5}{r_6}\right)^2} + \frac{ct_6 \left(\frac{r_5}{r_6}\right)^2}{\mathfrak{S}_5 \left(\frac{r_5}{r_6}\right)^2}. \quad (3.18)$$

The calculated angular rate ω_l (3.17) of the torsion bar is 34.11 Hz. If the operating range of the engine is considered, the maximum value of the first order frequency of the engine is 100 Hz (equivalent to 6000 rpm).

Since the natural frequency of the torsion bar is close to the operating frequency of the engine a description of the torsion bar by a dynamic model is required.

This means the power train system must be described with model "level two" or "level three". In this thesis model "level two" was chosen for the system description.

Figure 3-8 shows the torque characteristics of the torsion bar (top), of the gearbox (middle) and the propeller shaft (bottom) versus engine speeds. The simulation was done with an excitation magnitude of one.

The maximum torque fluctuation occurs at an engine speed of around 4200 rpm, equivalent to 35 Hz (based on a 4-stroke cycle). The reason for the torque fluctuation is the distance being closer to the natural frequency of the torsion bar. This behaviour must be considered for the misfire detection model.

Due to the fact that the investigated engine was a 4-stroke engine one engine cycle needs two full engine rotations (720° crank angle). If an order analyses will be done the lowest possible oscillation mode starts at the 0.5th engine oscillation mode.

Figure 3-7 represents the calculated magnitude of the eigen-modes. The horizontal axis represents the position on the power train system. The system was calculated at 3 positions. The magnitude of the eigen-modes was calculated in positions "hydro damper", "gear box" and the "propeller".

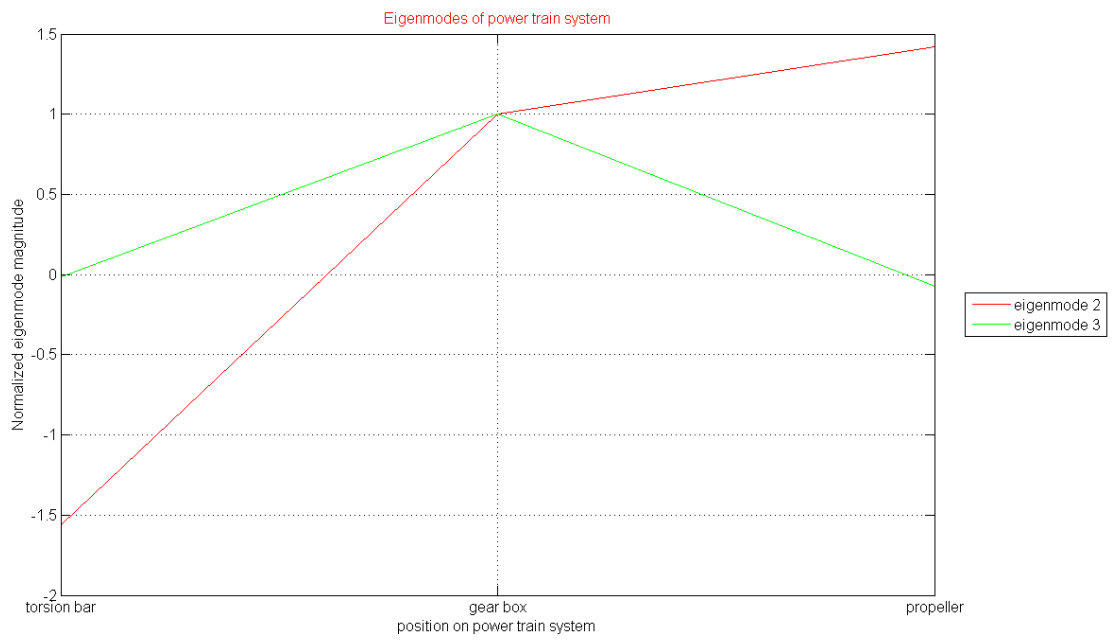


Figure 3-7 Normalized eigen-mode magnitude of the power train system.

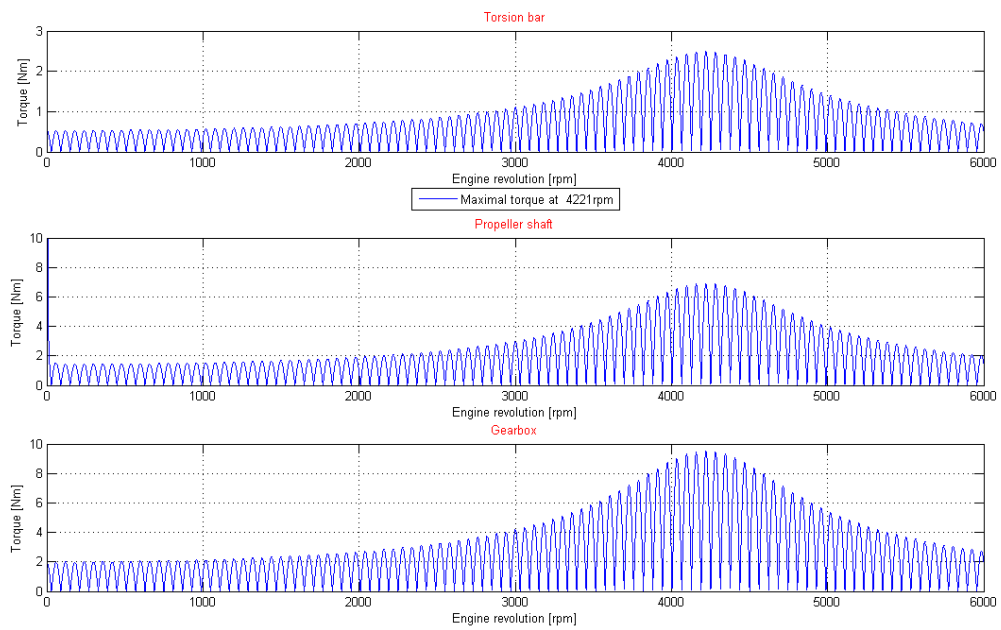


Figure 3-8 Torques on parts of the transmission system versus engine speed. Top torsion bar, middle propeller shaft and bottom gear box.

3.2.3 Torsion bar

As mentioned in section 3.2.2 due to the natural frequency of the power train system, it is necessary to assume a dynamic model of the crank mechanism. The new dynamic model includes additionally the spring and the damping factors.

The description of the power train system with the dynamic behaviours included will be shown in Figure 3-9.

The moment of inertia \mathfrak{S}_6 represents the hydro damper, \mathfrak{S}_1 the crankshaft, \mathfrak{S}_2 and \mathfrak{S}_4 the tooth wheels of the gear box and \mathfrak{S}_5 the moment of inertia of the propeller. $d_{1,4,6}$ describes the damping and $c_{1,4}$ the spring constants of the system. The degrees of freedoms are described by the angular displacement $\varphi_{1,2,4,5,6}$. The angular displacements are denoted by φ_6 (hydro damper), φ_1 (crankshaft), φ_2 (tooth wheel on crankshaft), φ_4 (tooth wheel on propeller shaft) and φ_5 (propeller). The angular velocities and the angular acceleration of the system are defined by $\dot{\varphi}_6, \ddot{\varphi}_6$ (hydro damper), $\dot{\varphi}_1, \ddot{\varphi}_1$ (crankshaft), $\dot{\varphi}_2, \ddot{\varphi}_2$ (tooth wheel on crankshaft), $\dot{\varphi}_4, \ddot{\varphi}_4$ (tooth wheel on propeller shaft) and $\dot{\varphi}_5, \ddot{\varphi}_5$ (propeller). For the tooth force description at the gear box the variable F was selected and for the tooth wheel radius r_2 and r_4 were defined. The torque variables are formulated as followed: T_6 (hydro damper), T_1 (crankshaft), T_2 and T_4 (tooth wheel torque gear box) and T_5 at the propeller.

The system is specified by the following equations:

1. Hydro damper :

$$\mathfrak{S}_6 \cdot \ddot{\varphi}_6 + d_6 \cdot (\dot{\varphi}_6 - \dot{\varphi}_1) = T_6 \quad (3.19)$$

2. Crankshaft:

$$\mathfrak{S}_1 \cdot \ddot{\varphi}_1 + d_1 \cdot (\dot{\varphi}_1 - \dot{\varphi}_2) + c_1 \cdot (\varphi_1 - \varphi_2) - d_6 \cdot (\dot{\varphi}_6 - \dot{\varphi}_1) = T_1 \quad (3.20)$$

3. Torsion shaft and gear box:

$$\mathfrak{S}_2 \cdot \ddot{\varphi}_2 - d_1 \cdot (\dot{\varphi}_1 - \dot{\varphi}_2) - c_1 \cdot (\varphi_1 - \varphi_2) + F \cdot r_2 = T_2 \quad (3.21)$$

4. Gearbox and propeller:

$$\mathfrak{S}_4 \cdot \ddot{\varphi}_4 + d_4 \cdot (\dot{\varphi}_4 - \dot{\varphi}_5) + c_4 \cdot (\varphi_4 - \varphi_5) + F \cdot r_4 = T_4 \quad (3.22)$$

$$-\frac{I}{r_4} \left[\mathfrak{S}_4 \cdot \ddot{\varphi}_4 + d_4 \cdot (\dot{\varphi}_4 - \dot{\varphi}_5) + c_4 \cdot (\varphi_4 - \varphi_5) - T_4 \right] = F \quad (3.23)$$

With the relation of

$$\varphi_4 = -\frac{r_2}{r_4} \cdot \varphi_2 \quad (3.24)$$

the equation (3.23) changes to

$$-\frac{I}{r_4} \left[\mathfrak{S}_4 \cdot \frac{r_2}{r_4} \ddot{\varphi}_2 + d_4 \cdot \left(-\frac{r_2}{r_4} \dot{\varphi}_2 - \dot{\varphi}_5 \right) + c_4 \cdot \left(-\frac{r_2}{r_4} \varphi_2 - \varphi_5 \right) - T_4 \right] = F . \quad (3.25)$$

5. Propeller:

$$\mathfrak{S}_5 \cdot \ddot{\varphi}_5 - d_4 \cdot (\dot{\varphi}_4 - \dot{\varphi}_5) - c_4 \cdot (\varphi_4 - \varphi_5) = T_5 \quad (3.26)$$

By a substitution of φ_4 in (3.26) the equations changes to

$$\mathfrak{S}_5 \cdot \ddot{\varphi}_5 - d_4 \cdot \left(-\frac{r_2}{r_4} \dot{\varphi}_2 - \dot{\varphi}_5 \right) - c_4 \cdot \left(-\frac{r_2}{r_4} \varphi_2 - \varphi_5 \right) = T_5 \quad (3.27)$$

and by a substitution of F in (3.21) the system of equation results in

$$\begin{aligned} & \mathfrak{S}_2 \cdot \ddot{\varphi}_2 - d_1 \cdot (\dot{\varphi}_1 - \dot{\varphi}_2) - c_1 \cdot (\varphi_1 - \varphi_2) - \frac{r_2}{r_4} \cdot \\ & \left[\mathfrak{S}_4 \cdot \left(-\frac{r_2}{r_4} \ddot{\varphi}_2 \right) + d_4 \cdot \left(-\frac{r_2}{r_4} \dot{\varphi}_2 - \dot{\varphi}_5 \right) + c_4 \cdot \left(-\frac{r_2}{r_4} \varphi_2 - \varphi_5 \right) - T_4 \right] = T_2 \cdot \end{aligned} \quad (3.28)$$

The equation expressed by matrices can be written as

$$\underbrace{\begin{pmatrix} \mathfrak{S}_1 & 0 & 0 \\ 0 & \mathfrak{S}_2^* & 0 \\ 0 & 0 & \mathfrak{S}_5 \end{pmatrix}}_{\underline{\mathfrak{S}}} \cdot \underbrace{\begin{pmatrix} \ddot{\phi}_1 \\ \ddot{\phi}_2 \\ \ddot{\phi}_5 \end{pmatrix}}_{\underline{\ddot{\phi}}} + \underbrace{\begin{pmatrix} d_1 & -d_1 & 0 \\ -d_1 & d_1 + \left(\frac{r_2}{r_4}\right) \cdot d_4 & \frac{r_2}{r_4} \cdot d_4 \\ 0 & \frac{r_2}{r_4} \cdot d_4 & d_4 \end{pmatrix}}_{\underline{d}} \cdot \underbrace{\begin{pmatrix} \dot{\phi}_1 \\ \dot{\phi}_2 \\ \dot{\phi}_5 \end{pmatrix}}_{\underline{\dot{\phi}}} + \underbrace{\begin{pmatrix} c_1 & -c_1 & 0 \\ -c_1 & c_1 + \left(\frac{r_2}{r_4}\right)^2 \cdot c_4 & \frac{r_2}{r_4} \cdot c_4 \\ 0 & c_4 \cdot \frac{r_2}{r_4} & c_4 \end{pmatrix}}_{\underline{c}} \cdot \underbrace{\begin{pmatrix} \phi_1 \\ \phi_2 \\ \phi_5 \end{pmatrix}}_{\underline{\phi}} = \underbrace{\begin{pmatrix} T_1 \\ T_2^* \\ T_5 \end{pmatrix}}_{\underline{T}}. \quad (3.29)$$

With the assumption

$$\mathfrak{S}_2^* = \mathfrak{S}_2 + \left(\frac{r_2}{r_4}\right)^2 \cdot \mathfrak{S}_4 \quad (3.30)$$

and

$$T_2^* = T_2 - \frac{r_2}{r_4} \cdot T_4 \quad (3.31)$$

the matrices set of linear equation is denoted by

$$\underline{\mathfrak{S}} \cdot \underline{\ddot{\phi}} + \underline{d} \cdot \underline{\dot{\phi}} + \underline{c} \cdot \underline{\phi} = \underline{T}. \quad (3.32)$$

The solution of (3.32) can be found by using the approaches

$$\underline{T} = \underline{T}_a \cdot \cos(\omega \cdot t) \quad (3.33)$$

$$\underline{\phi} = \underline{x} \cdot e^{j \cdot \omega t} \quad (3.34)$$

$$\underline{\dot{\phi}} = j \cdot \omega \cdot \underline{x} \cdot e^{j \cdot \omega t} \quad (3.35)$$

$$\underline{\ddot{\phi}} = -\omega^2 \cdot \underline{x} \cdot e^{j \cdot \omega t}. \quad (3.36)$$

By a consideration of (3.33), (3.34), (3.35) and using (3.36) in (3.32) we obtain

$$\underline{T}, \underline{\varphi}, \underline{\dot{\varphi}}, \underline{\ddot{\varphi}} \rightarrow \underline{\mathfrak{S}} \cdot \underline{\dot{\varphi}} + \underline{d} \cdot \underline{\ddot{\varphi}} + \underline{c} \cdot \underline{\varphi} = \underline{T}. \quad (3.37)$$

The differential equation changes to

$$\left(-\omega^2 \cdot \underline{\mathfrak{S}} + j \cdot \underline{d} \cdot \omega + c\right) \cdot \underline{x} = \underline{T}. \quad (3.38)$$

The imaginary and the real part of the equation must be separated

$$\underline{x} = \underline{x}_{real} + j \cdot \underline{x}_{imag} \quad (3.39)$$

and by an insertion of (3.39) in (3.38) the equation can be expressed by

$$\begin{aligned} -\omega^2 \cdot \underline{\mathfrak{S}} \cdot \underline{x}_{real} + j \cdot \omega \cdot \underline{d} \cdot \underline{x}_{real} + \underline{c} \cdot \underline{x}_{real} - j \cdot \omega^2 \cdot \underline{\mathfrak{S}} \cdot \underline{x}_{imag} + \\ j^2 \cdot \omega \cdot \underline{d} \cdot \underline{x}_{imag} + j \cdot \underline{c} \cdot \underline{x}_{imag} = \underline{T}_a + 0 \cdot j. \end{aligned} \quad (3.40)$$

Using

$$\underline{A} = -\omega^2 \cdot \underline{\mathfrak{S}} + \underline{c} \quad (3.41)$$

and

$$\underline{B} = \omega \cdot \underline{d} \quad (3.42)$$

the equation changes to

$$\underline{A} \cdot \underline{x}_{real} - \underline{B} \cdot \underline{x}_{imag} + \left[\underline{B} \cdot \underline{x}_{real} + \underline{A} \cdot \underline{x}_{imag} \right] \cdot j = \underline{T}_a + 0 \cdot j \quad (3.43)$$

and further to

$$\begin{bmatrix} \underline{A} & -\underline{B} \\ \underline{B} & \underline{A} \end{bmatrix} \cdot \begin{pmatrix} \underline{x}_{real} \\ \underline{x}_{imag} \end{pmatrix} = \begin{pmatrix} \underline{T}_a \\ 0 \end{pmatrix}. \quad (3.44)$$

The real part of the equation describes the system behaviour.

$$\underline{\varphi}_{real} = Re[\underline{x} \cdot e^{j\omega t}] = Re\{\underline{x} \cdot [\cos(\omega \cdot t) + j \cdot \sin(\omega \cdot t)]\} \quad (3.45)$$

$$Re\{[\underline{x}_{real} + j \cdot \underline{x}_{imag}] \cdot [\cos(\omega \cdot t) + j \cdot \sin(\omega \cdot t)]\} = \underline{x}_{real} \cdot \cos(\omega \cdot t) - \underline{x}_{imag} \cdot \sin(\omega \cdot t) \quad (3.46)$$

Expressed in the Euler equation form (3.45) can be written as

$$\underline{\varphi}_{real} = \underline{C}_a \cdot \cos(\omega \cdot t + \underline{\phi}). \quad (3.47)$$

The signal amplitude can be expressed by

$$C_{a,n} = \sqrt{x_{n,real}^2 + x_{n,imag}^2} \quad (3.48)$$

and the angular offset is denoted by

$$\phi_n = \arctan\left(\frac{x_{n,imag}}{x_{n,real}}\right). \quad (3.49)$$

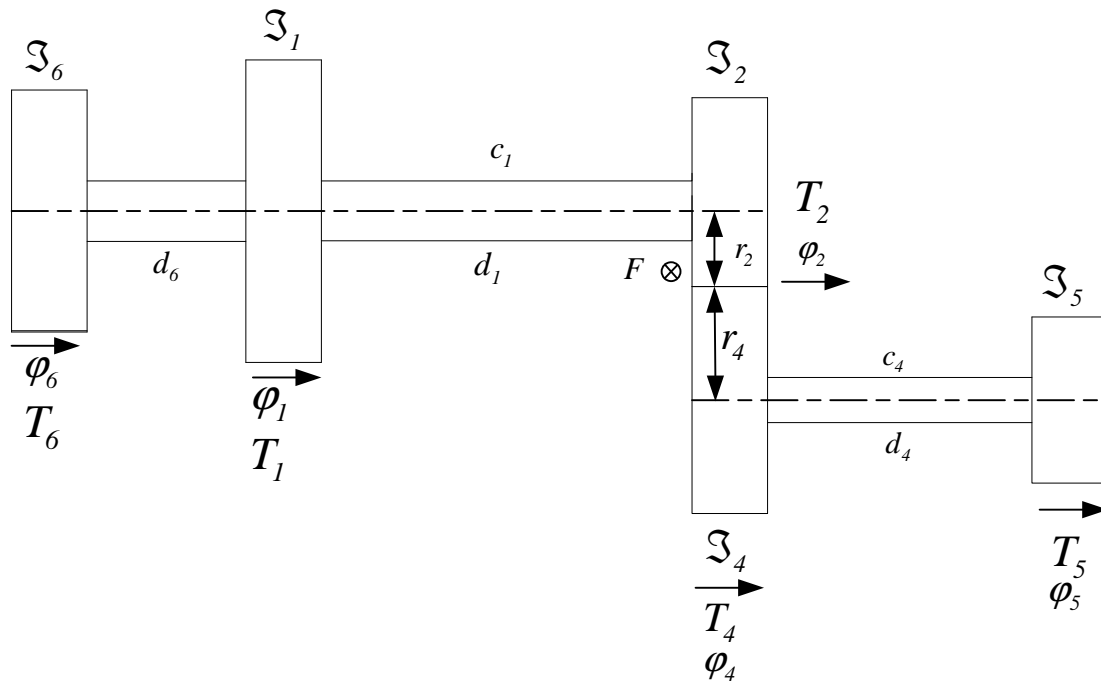


Figure 3-9 Dynamic model overview of the power train system.

3.2.4 *Hydro damper*

Hydro dampers are used for smooth engine torque delivery. Due to gas forces, rotating and oscillating masses of the crankshaft the engine torque varies over one full engine cycle. In order to achieve smooth torque characteristics additional masses fitted to the crankshaft can be used. Using heavy flywheels on the crankshaft helps smoothing engine torque characteristics.

Due to the fluctuation of the angular velocity $\dot{\phi}$ the torque variation is often not acceptable. To mitigate engine torque fluctuations heavy masses can be applied. The working principle is easy to understand. In phases during which the instantaneous torque exceeds the average torque the flywheel absorbs energy. In phases during which the instantaneous torque is lower than the average torque the flywheel releases energy. By changing the mass of the hydro damper the smoothing characteristic can be optimised.

On the left hand side of Figure 3-3 the hydro damper is shown. This arrangement of the damping systems realizes the best size weight ratio of the investigated engine with desired system characteristics. This part was designed to have variable damping factors over a wide engine speed range. In fact the resonance frequency of the whole crank motion becomes lower by using a heavy hydro damper. In order to achieve good results special fluid similar to oil was filled into the hydro damper. The oil represents the damping factor in a spring mass system.

Due to the complexity of this part it is not possible to derive an analytic equation. The values for the spring constant and also for the damping characteristics were not known and had to be estimated. The behaviour of the whole hydro damper was tested and measured on the test rig. The model parameters were optimised in a manner to get the best correlation between test results and simulation. Detailed hydro damper designs can be looked up in [13] and will not be further investigated in this paper.

In this thesis the starting procedure (engine speed range is defined from 0 to idle rpm) of the engine was not considered and there was no focus on it. If the starting phase should be considered too, the steady state system does not have to be applied and the linear differential equation can be solved by calculating the homogenous and the particular parts.

Due to the facts which are mentioned above, the hydro damper can be described as a rigid body system and dynamic effects will not be considered.

3.2.5 Crankshaft and engine case

The model of the crankshaft and the associated parts were done by the "level one" assumption (see page 19). Also the engine case was assumed as a rigid body type. It is known that crankshaft vibrations (torsional vibrations) are in a range of 300 Hz upwards depending on the crankshaft design. This can be proven by a "*finite element method*" (FEM) simulation (with a spring mass model assumption of the crankshaft) and was done by the design engineers during the design process.

This thesis describes the engine behaviour in audio frequencies up to 100 Hz. This means the maximum estimated frequency is the first order frequency of the engine. Due to that fact it is allowed to describe the crankshaft in a "level one" model.

Also the engine case behaviour was investigated via a FEM calculation. It is also a common understanding that the eigen-values of the engine case are higher than the observed frequency range for this application. This means the engine case can be assumed as a rigid body part as well and therefore treated as a "level one" model.

3.2.6 Shock mounts

Four silent blocks were installed on the engine. Figure 3-3 shows two of the silent blocks below the crankshaft connected to the engine case. Figure 3-4 represents details of the power train system and shows the silent block orientation with the fixation.

Silent blocks are necessary for a flexible installation in the aircraft. If the design does not foresee flexible elements between the engine and the engine mount or the aircraft, the engine will stiffly be connected to the aircraft hull. All vibrations coming from the engine will be transmitted to the aircraft chassis.

By using silent blocks there are a few considerations with regards to installation requirements such as stiffness, engine position, engine speed and the resonance frequency of the whole system and the exposure temperature to be made.

In case of using a silent block for the engine fixation, the part should fix the engine in the right position and should decouple the engine from the airframe of parasitic audio sound. The silent block must withstand forces and torque created by the engine e.g. gas forces, mass forces, mass torques and non periodical effects due to misfire. To prevent damages or disturbances of the engine mount and the aircraft all the malicious influences must be reduced to an acceptable level.

By using a silent block with sufficient characteristic higher engine vibrations will be damped and the negative effect upon the engine mount will be limited to acceptable levels.

Quality of the silent blocks, frequency behaviour and resistance against shear stress, the geometry and aging are parameters which have to be considered.

The silent block is highly non linear and it is sufficient to use linear approximation for the calculation and the analytic simulation. Because of the robustness of the detection method it can be shown later on that the linearization approach of the silent block is in good agreement with the measured test results.

Due to the position of the silent blocks, stress occurs in two directions of the silent block. The compression spring rate and the shear spring rate are parameters which describe the system behaviour of the silent block. These parameters were given by the supplier and are not directly measurable on the engine test bench.

It can be shown that all peak values are in a frequency range lower than 850 Hz which is equivalent to an engine speed of 14 rpm.

Due to the reason that the detection method proposed in this thesis works in a frequency range from 30 Hz to 100 Hz and the fact that the maximum peak values of the silent blocks are lower than 850 Hz the transfer behaviour does not have to be considered.

If a system from zero engine speed to maximum engine speed should be described, the behaviour of the silent blocks must be considered in the same manner as by the hydro damper.

With the assumption of a linear approximation of the silent block it can be modelled by

$$-m \cdot \hat{x} \cdot \omega^2 + j \cdot b \cdot \hat{x} \cdot \omega + c \cdot \hat{x} = \hat{F} . \quad (3.50)$$

Using

$$\hat{F} = A_* \cdot e^{(j\varphi)} = A \cdot [\cos(\varphi) + j \cdot \sin(\varphi)] \quad (3.51)$$

$$\hat{x} = A \cdot \cos(\omega \cdot t) + B \cdot \sin(\omega \cdot t) \quad (3.52)$$

$$\hat{x}' = \omega \cdot (-A \cdot \sin(\omega \cdot t) + B \cdot \cos(\omega \cdot t)) \quad (3.53)$$

$$\hat{x}'' = -\omega^2 \cdot (A \cdot \cos(\omega \cdot t) + B \cdot \sin(\omega \cdot t)) \quad (3.54)$$

3.2.7 Propeller

The analytic model of the propeller was described by one parameter, the moment of inertia \mathfrak{I}_{xx} .

In this thesis a three blade propeller was considered. The investigated aircraft was equipped with a three and a four blade propeller. A comparison of the measurement data acquired with the three and the four blade propeller shows similar engine results. Performing an order analyses the 0.5th engine oscillation mode shows higher magnitudes by using a four blade propeller compared to a three blade propeller. Reason for is the higher moment of inertia of the four plate propeller.

Also the measurements shown in this paper were done with a three blade propeller. Due to the high moment of inertia \mathfrak{I}_p of the propeller and the assumption of a constant propeller rotation speed a general plane motion for the propeller and the associated engine can be assumed. Movement in y and z directions are not considered.

Only movements around the x-axis are expected. This agreement allows observing the engine movement using an acceleration sensor only around the x-axis (see coordinate plane "CSYS centre of gravity"). Three dimensional measurements do not have to be applied. Furthermore an acceleration sensor with sensitivity in one direction is sufficient for the application.

Equation (3.55) denotes the moment of inertia of the propeller. Due to the symmetrical contour of the propeller the parameters around the main diagonal of the matrix are zero and the moment of inertia can be described by \mathfrak{I}_{xx} , \mathfrak{I}_{yy} and \mathfrak{I}_{zz} .

$$\mathfrak{I}_p = \begin{bmatrix} \mathfrak{I}_{xx} & \mathfrak{I}_{xy} & \mathfrak{I}_{xz} \\ \mathfrak{I}_{xy} & \mathfrak{I}_{yy} & \mathfrak{I}_{yz} \\ \mathfrak{I}_{xz} & \mathfrak{I}_{yz} & \mathfrak{I}_{zz} \end{bmatrix} \quad (3.55)$$

3.3 Excitation

The excitation of a system can be distinguished between two types. One is the periodical and the second one the non-periodical excitation. The first represents the standard excitation of the engine. The second one could also be a standard phenomenon of a system or it could be a type or a parameter for abnormal engine behaviours like misfire. In this thesis only periodical excitations will be investigated.

3.3.1 Periodical excitation

Common used methods for the description of mechanical behaviours and effects of combustion engines are Fourier analyses techniques. Each periodic signal $f_{(x)}$ e.g. forces or torques can be described with the Fourier theorem. In the following chapters the system behaviour will be described and explained by using this method. This helps to understand the working principle of a combustion engine and is a useful tool for analysing the system in the frequency domain.

$$f_{(x)} = a_0 + \sum_{i=1}^{\infty} a_i \cos(ix) + \sum_{i=1}^{\infty} b_i \sin(ix) \quad i = 1, 2, \dots \quad (3.56)$$

By a substitution of x with ψ the equation (3.56) can be expressed versus crank angle.

$$f_{(\psi)} = a_0 + \sum_{h=1}^Z a_h \cos(h\psi) + \sum_{h=1}^Z b_h \sin(h\psi) \quad h = 1, 2, \dots \quad (3.57)$$

The parameter h denotes the harmonic number, a_0 the average value, ψ the crank angle (from 0 to 360°) and the parameters a_h and b_h are coefficients of the equation (3.57) [19].

The first oscillation mode is related to a single engine rotation, which is only half of a combustion cycle. This means one full 4-stroke engine cycle results in the 0.5th oscillation mode.

3.3.2 Non-periodical excitation

As mentioned in [13], non-periodical excitations are e.g. run up procedures, clutch mechanisms and changes of the engine speed. This means all the effects listed above are limited in time.

3.4 Engine boundary conditions

3.4.1 Coordinate system

For the description of the engine movements it is necessary to define at least one coordinate system, introduced at a reference point. Since the body movement of the engine case is measured by means of a one axis acceleration sensor, a system with an absolute reference and a system which is referenced to the body can be assumed.

For the simulation and the comparison of the aircraft measurements, the system "CSYS engine centre" was used. In order to describe the engine system two different coordinate planes were defined. The coordinate system "CSYS engine centre" is shown in Figure 3-12 and Figure 3-13 and "CSYS centre of gravity" is drawn in Figure 3-14, Figure 3-15 and Figure 3-16.

For the calculation of the total gas and mass torque the reference system "CSYS engine centre" was used.

For the engine inertia calculation "CSYS centre of gravity" was defined.

The analytic model assumes that the engine case moves around the centre of gravity of the engine block (see "CSYS centre of gravity"). As mentioned above it can be assumed that the engine block will remain in one plane. This leads to a movement around the x-axis referenced to "CSYS centre of gravity". Good correlation between simulation and measurement in terms of amplitudes and frequencies proof the assumption.

The cylinder selective gas and mass forces and also the gas and mass torques computation can be done in the cylinder coordinate system "CSYS cylinder coordinate" (see Figure 3-11).

In this case the crank drive can be described with the standard formulas found in the literature and coordinate transformation or other calculations do not have to be done. The total engine torque for example can be computed by a superposition of the cylinder selective torques by adding the correct cylinder offset angle.

The engine torque referenced to cylinder 1 must be shifted to the reference point "CSYS engine centre" using the correct angle offset. This leads to an engine torque computation referenced to the "CSYS engine centre" coordinate system.

Since the engine model was described in two different reference systems it is essential to take care in which reference system the model description and the calculation will be computed.

Data from the engine design program have to be transferred into the appropriate reference system before they can be used for the engine simulation.

All calculated results of the power train system are referenced to "CSYS engine centre". This allows implementing the simulation results coming from the engine design tool in the MATLAB model without any restrictions.

The coordinate plane for the design tool is defined in the middle of cylinder 1 and 2 (reference point of "CSYS engine centre"). This means 60 degree crank angle offset after the top dead centre (TDC) of cylinder one.

The negative x-axis is defined in flight direction and the positive y-axis represents the vertical direction. The z-axis is the Cartesian product of the y and x-axis.

Looking out of the cockpit in flight direction, the propeller rotates counter clockwise. Due to the one stage gear box, the crankshaft rotates clockwise. The physical location, their firing order in brackets and the coordinate system "CSYS engine centre" of the 6 cylinders, featuring 120° crank angle offset, are defined as per Figure 3-10.

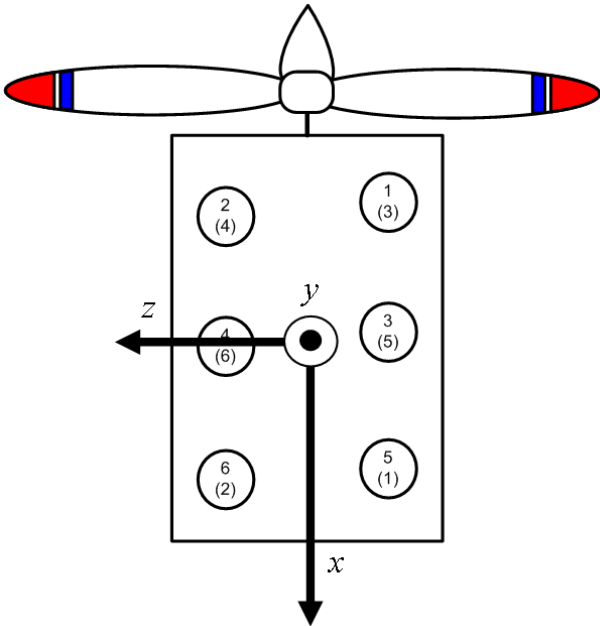


Figure 3-10 Cylinder location, bracketed the firing order and coordinate plane "CSYS engine centre".

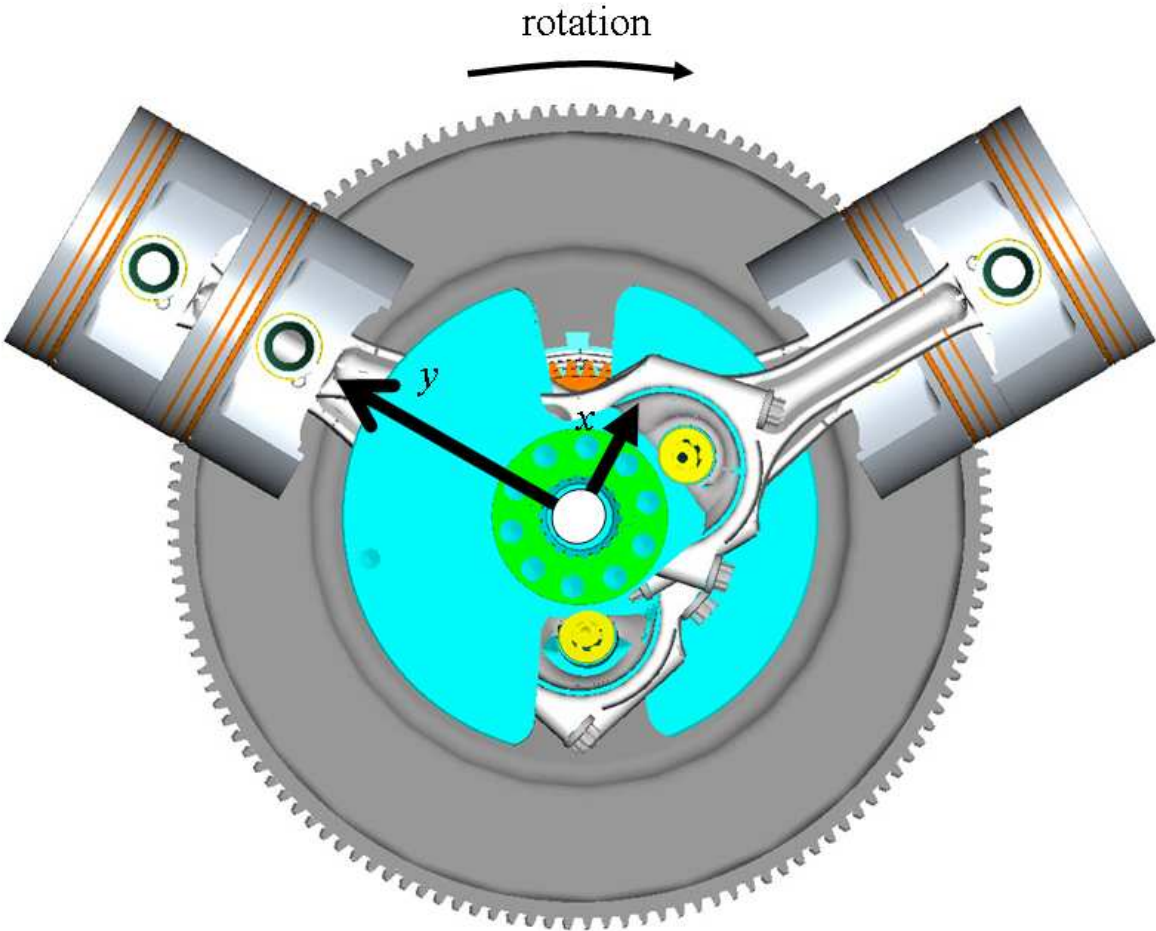


Figure 3-11 Cylinder coordinate system "CSYS cylinder coordinate" for cylinder 1 and rotation direction of crankshaft.

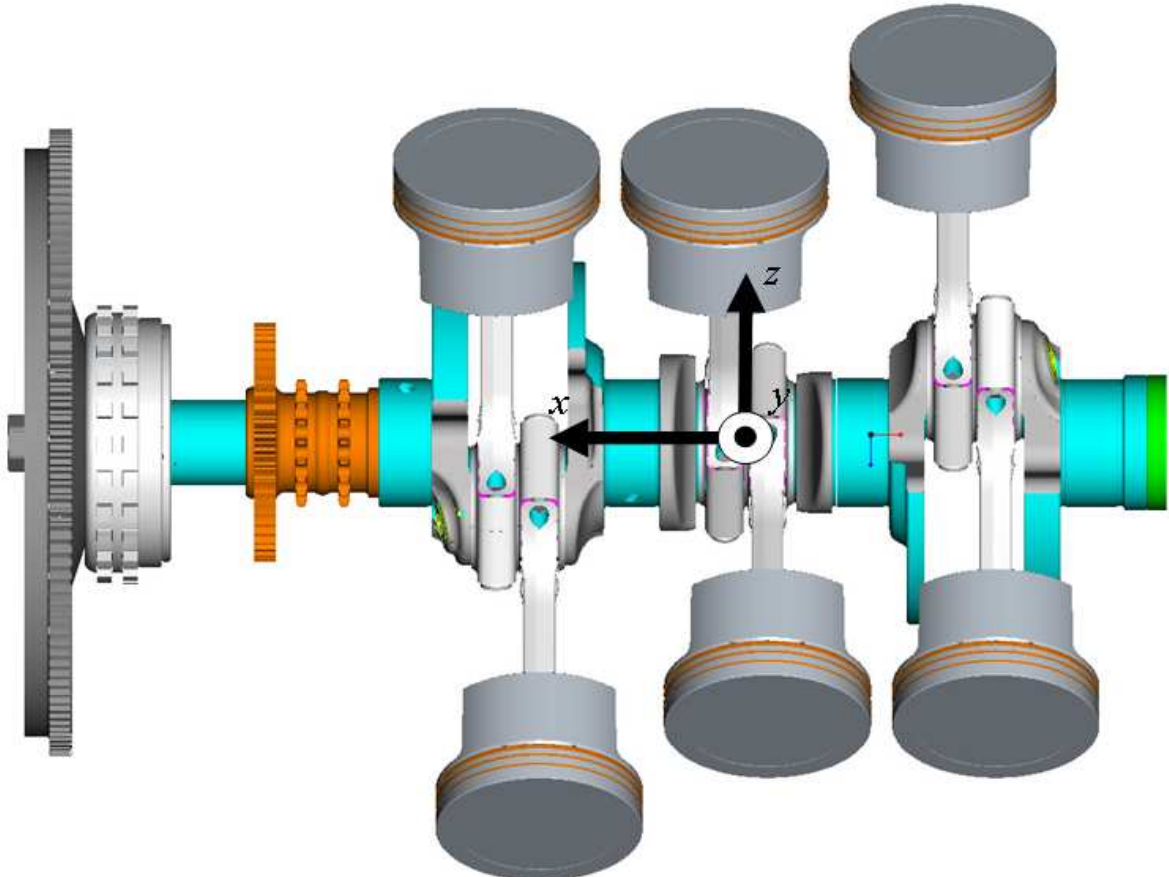


Figure 3-12 Coordinate planes "CSYS engine centre" top view.

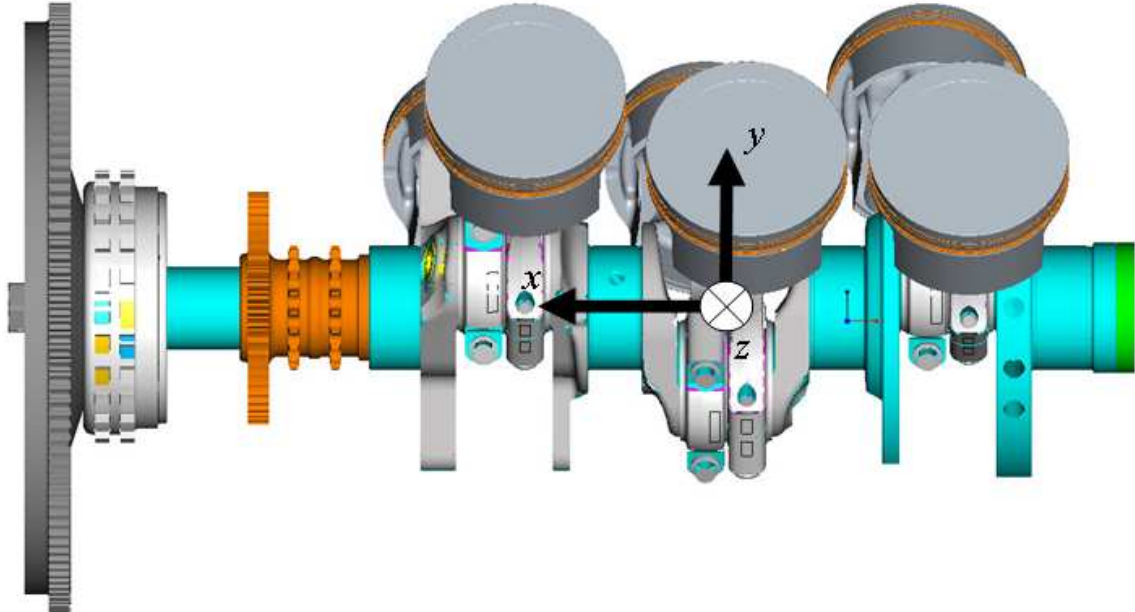


Figure 3-13 Coordinate planes "CSYS engine centre".

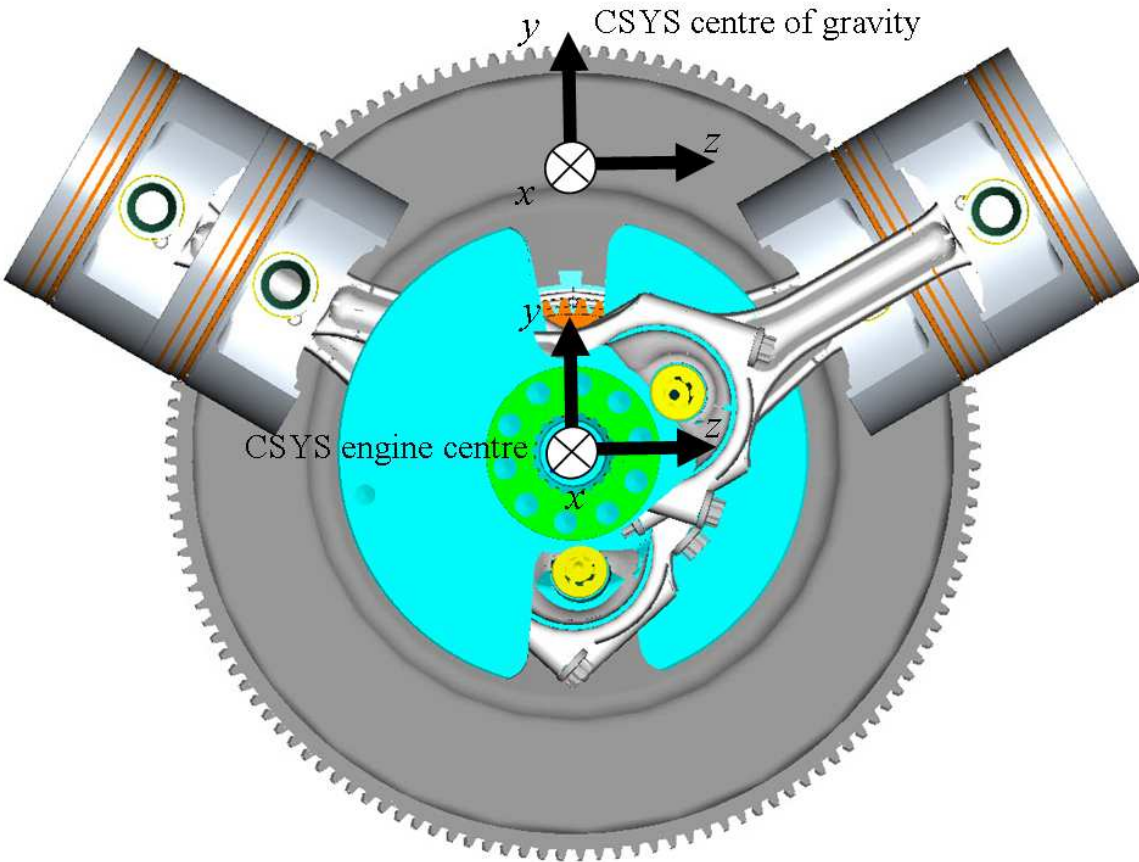


Figure 3-14 Coordinate planes "CSYS centre of gravity" calculated of the whole engine and "CSYS engine centre".

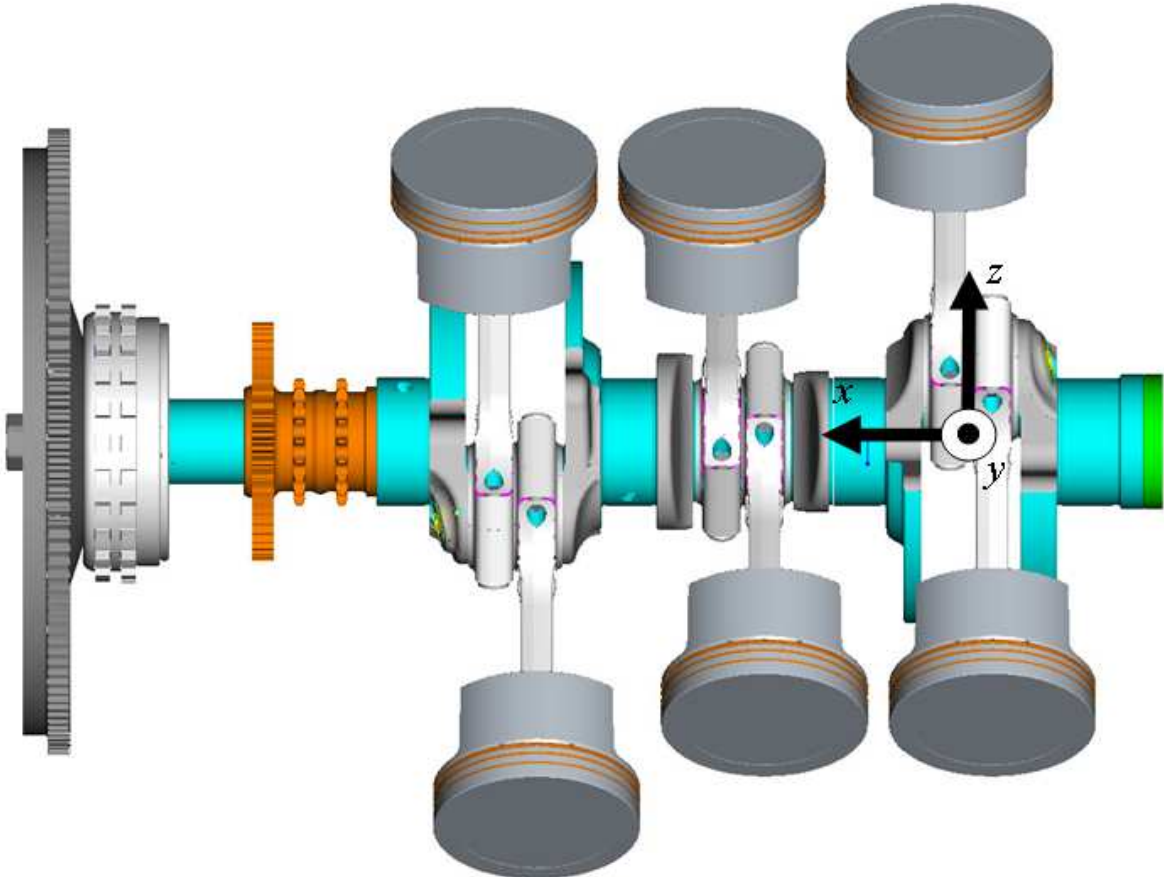


Figure 3-15 Coordinate planes "CSYS centre of gravity" calculated of the whole engine (top view).

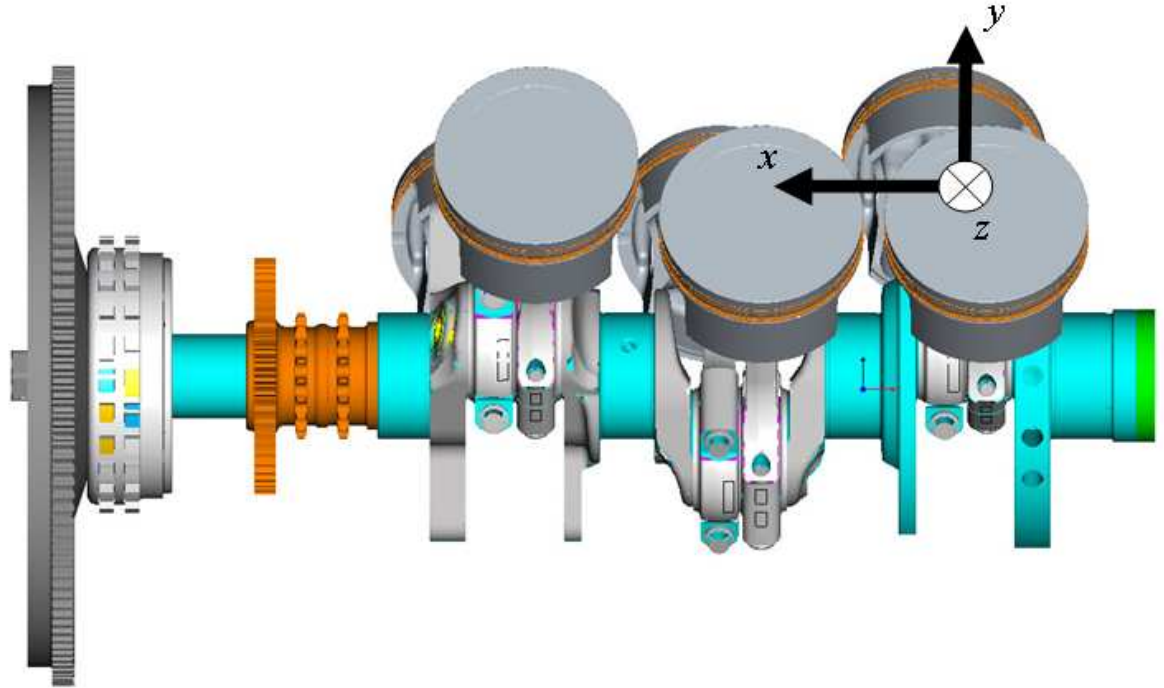


Figure 3-16 Coordinate planes "CSYS centre of gravity" of the whole engine.

4 POWERTRAIN SYSTEM

4.1 Crank drive

Due to the cyclic changes of the gas forces, the piston and associated parts such as the crankshaft, will be accelerated and decelerated which results in a non uniform engine torque characteristic. Engine torque changes can be reduced or smoothed by adding levelling components. It can be assumed that the rotation speed of the crankshaft is uniform by connecting sufficient additional masses to the crankshaft [19]. In this case the angular velocity $\dot{\psi}$ can be assumed as constant. Due to minor impact upon the system behaviour effects of relative motion like piston and engine block movements are not considered in this thesis.

$\dot{\psi}$ can be calculated using $\dot{\psi} = \omega$ and further $\omega \left[\frac{1}{s} \right] = \frac{n [rpm] \cdot \pi}{30}$.

Where n denotes the constant engine speed [rpm].

Hence the derivation of the angular velocity is zero.

$$\frac{d\dot{\psi}}{dt} = \ddot{\psi} = 0 \quad (4.1)$$

Figure 4-1 shows the crank drive system and in Figure 4-2 the forces are shown. Based on this the model description and the mathematical equations were derived.

In cylinder coordinates the position of the related piston is calculated by

$$s + R \cdot \cos(\psi) + l \cdot \cos(\beta) = R + l. \quad (4.2)$$

With the abbreviation

$$\lambda = \frac{R}{l} \quad (4.3)$$

$$\sin(\beta) = \frac{R}{l} \cdot \sin(\psi) = \lambda \cdot \sin(\psi) \quad (4.4)$$

$$\cos(\beta) = \sqrt{1 - \lambda^2 \cdot \sin^2(\psi)}. \quad (4.5)$$

The outcome of the equation is the position of the piston with the “*top dead centre*” (TDC) as reference in relation to the crankshaft radius:

$$x = \frac{s}{R} = 1 - \cos(\psi) + \frac{l}{\lambda} - \frac{l}{\lambda} \cdot \sqrt{1 - \lambda^2 \cdot \sin^2(\psi)}. \quad (4.6)$$

The piston speed can be calculated by

$$\dot{s} = \frac{ds}{dt} = \frac{ds}{d\psi} \cdot \frac{d\psi}{dt}. \quad (4.7)$$

With the assumption of a constant angular velocity

$$\frac{d\psi}{dt} = \dot{\psi} = \omega = const \quad (4.8)$$

The velocity (dimensionless) of the piston is given by

$$x' = \frac{\dot{s}}{R \cdot \omega} = \sin(\psi) + \frac{\lambda \cdot \sin(\psi) \cdot \cos(\psi)}{\sqrt{1 - \lambda^2 \cdot \sin^2(\psi)}}. \quad (4.9)$$

For practical aspects it can be simplified if $\lambda \ll 1$ to

$$x' \approx \sin(\psi) + \frac{\lambda}{2} \cdot \sin(2\psi). \quad (4.10)$$

Deriving piston velocity provides piston acceleration (dimensionless) [19].

$$x'' = \frac{\ddot{s}}{R \cdot \omega^2} = \cos(\psi) + \frac{\lambda \cdot \cos^2(\psi) - \lambda \cdot \sin^2(\psi) + \lambda^3 \cdot \sin^4(\psi)}{\left(\sqrt{1 - \lambda^2 \cdot \sin^2(\psi)}\right)^3} \quad (4.11)$$

If the angular velocity is not constant then the equation of the acceleration changes to

$$\ddot{s} = R \cdot (x' \cdot \dot{\psi} + x'' \cdot \dot{\psi}^2) \quad (4.12)$$

with

$$x'' \approx \cos(\psi) + \lambda \cdot \cos(2\psi) \quad (4.13)$$

if $\lambda \ll 1$.

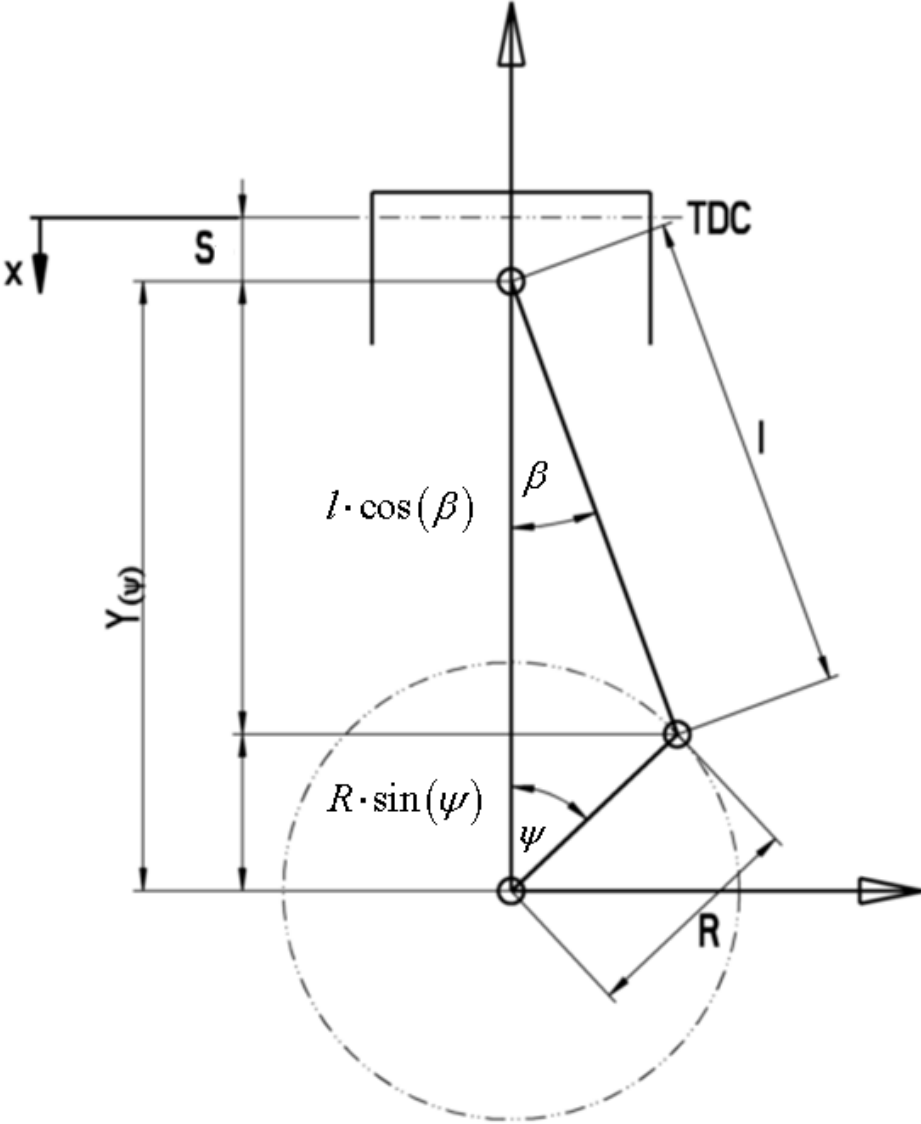


Figure 4-1 Overview of the crank drive system.

4.2 Gas force

The combustion process depends on parameters like engine load, air and engine temperature, ignition angle and fuel injection quantity for example.

The cylinder head, the piston and the associated parts and finally the cylinder wall are affected by the gas force.

The internal force F_G cannot be measured by means of externally located measuring devices but it stresses the engine case and all associated parts. A common used name for this internal force is called "closed force" and will not be included in the model for the misfire detection.

The transversal force F_N of the gas force F_G is the result of the kinematics. Forces of the crank motion system can be seen in Figure 4-2. It is not constant and varies with the position of the piston $F_{N(\psi)}$. The gas force can be calculated by

$$F_{G(\psi)} = p_c \cdot A_p \cdot \quad (4.14)$$

Where p_c denotes the in-cylinder pressure and A_p the piston area.

The torque around the x-axis of the coordinate plane can be measured by using e.g. an acceleration sensor.

The engine torque can be expressed by

$$M_{engine} = -M_{case} \quad (4.15)$$

with

$$M_{engine} = F_T \cdot R \quad (4.16)$$

and

$$M_{case} = -F_N \cdot y_{(\psi)} \cdot \quad (4.17)$$

The engine torque stresses the engine mounts. By using silent blocks the stress level and also the noise pollution can be reduced and the absolute vibration level mitigated. Due to the engine torque the engine case makes moderate movements at normal engine condition. This represents the desired engine behaviour.

The forces of the crank motion can be expressed by

$$\sin(\beta) \cdot l = R \cdot \sin(\psi) \quad (4.18)$$

with

$$\lambda = \frac{R}{l}$$

the equation (4.18) changes to

$$\sin(\beta) = \lambda \cdot \sin(\psi). \quad (4.19)$$

By using the law of cosines the equation (4.19) can be written as

$$\cos(\beta) = \sqrt{1 - \sin^2(\beta)} = \sqrt{1 - \lambda^2 \cdot \sin^2(\psi)}. \quad (4.20)$$

To calculate the connecting rod force F_{con} the cosines law was applied.

Based on the drawing Figure 4-2 the connecting rod force F_{con} is calculated by

$$F_{con} = F_G \cdot \frac{l}{\cos(\beta)} = F_G \cdot \frac{l}{\sqrt{1 - \lambda^2 \cdot \sin^2(\psi)}}. \quad (4.21)$$

The transversal force F_N of the piston force F_G is given by

$$F_N = F_G \cdot \tan(\beta) = F_G \cdot \frac{\lambda \cdot \sin(\psi)}{\sqrt{1 - \lambda^2 \cdot \sin^2(\psi)}}. \quad (4.22)$$

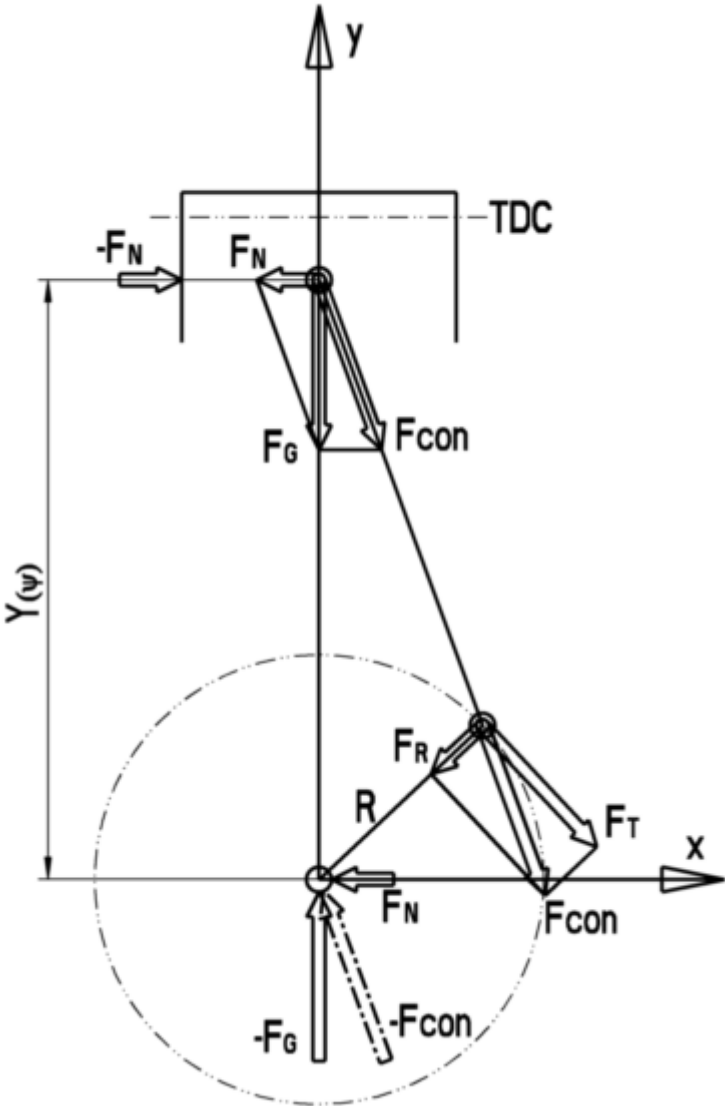


Figure 4-2 Overview of forces on the crank drive system.

Figure 4-3 shows a typical gas force progression of a turbo charged combustion engine over 720° crank angle. This diagram symbolises a measured gas pressure of the investigated 6-cylinder 4-stroke V-type engine. It shows the pressure maximum after TDC. The reason for the delay is the combustion process and depends on the ignition angle offset. Without combustion, the peak pressure can be seen at TDC (refer to Figure 4-4). The temperature rise due to the increase of pressure during the combustion process was not considered. This pressure characteristic will be assumed for the analytic model if a cylinder fails and thus a regular combustion cannot take place.

Figure 4-5 illustrates the transversal force of the gas force of one cylinder. This transversal force excites the engine case and can be measured for example by an acceleration sensor

$$U_{sensor} = f(a).$$

The engine case will be moved around the centre of gravity as mentioned in section 3.4.

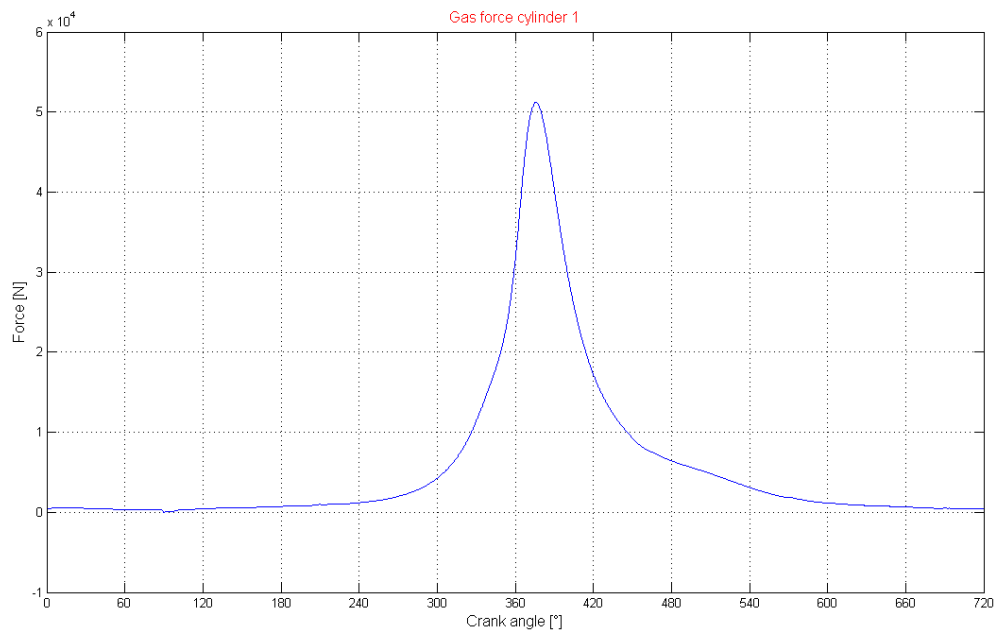


Figure 4-3 Typical characteristics of gas force F_G of a turbo charged combustion engine.

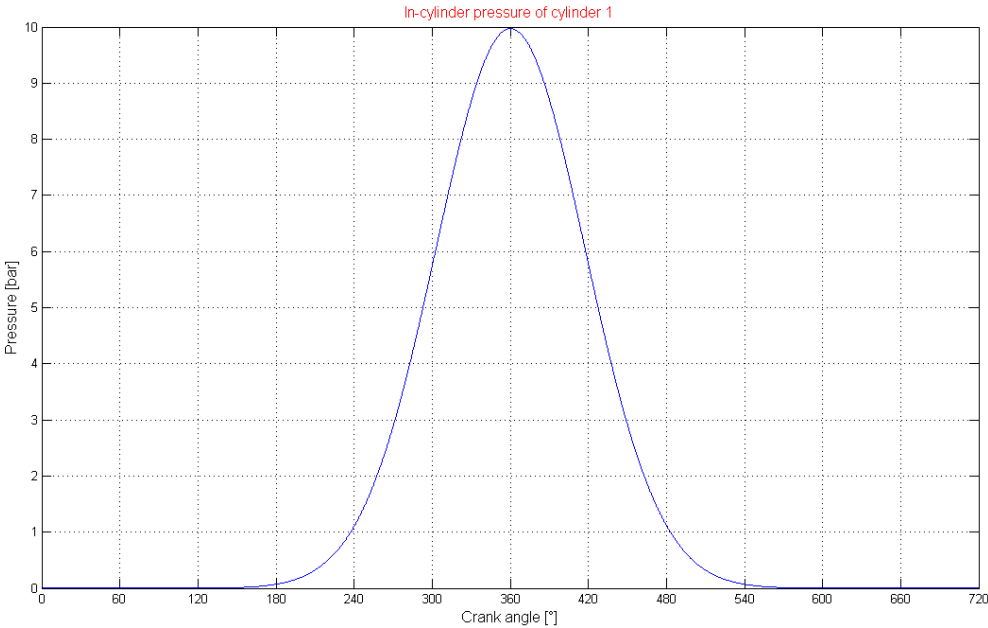


Figure 4-4 Pressure curve without ignition (no combustion process). In case of a total cylinder shut down this pressure characteristic will be applied in the analytic mode.

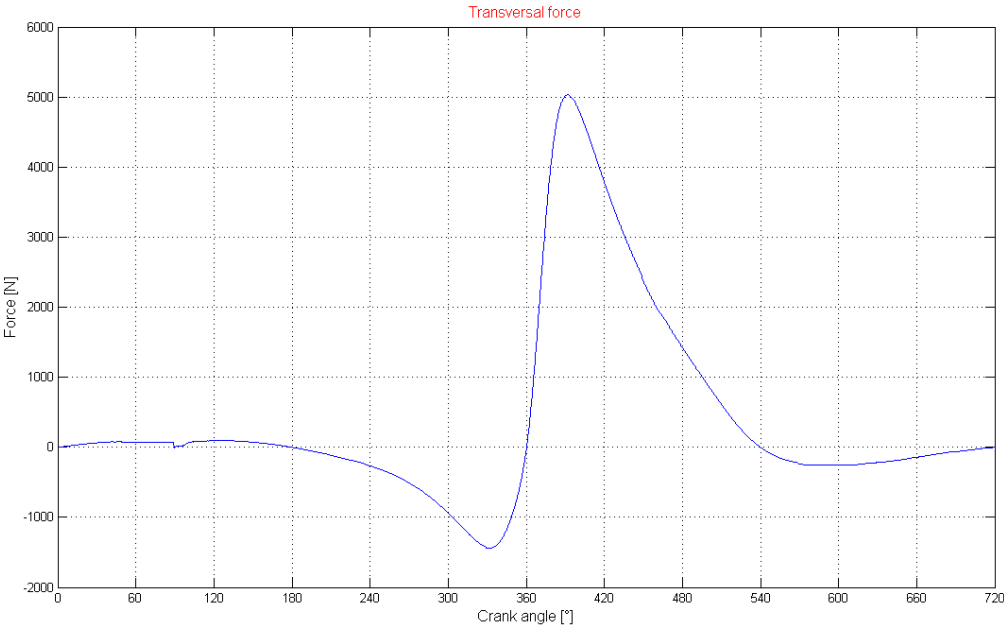


Figure 4-5 Characteristic of the transversal force calculated from the gas force.

4.3 Gas torque

As described in equation (4.15) the torque transmitted to the engine case is equal to the crankshaft torque. By observing the transversal gas force, misfire events can be detected. The engine case movement is directly linked to it and will be monitored by using an acceleration sensor.

The engine torque can be calculated by multiplying the transversal force component of the gas force F_N with the distance $y_{(\psi)}$ from the piston pin to the centre of rotation of the crankshaft.

The piston position (distance to the centre of rotation of the crankshaft) can be calculated by

$$y_{(\psi)} = R \cdot \cos(\psi) + l \cdot \cos(\beta). \quad (4.23)$$

The torque of the engine case is denoted by following equations:

$$M_{case} = -F_N \cdot R \cdot \left(\cos(\psi) + \frac{l}{R} \cdot \cos(\beta) \right) \quad (4.24)$$

$$M_{case} = -F_G \cdot R \cdot \left(\cos(\psi) \frac{\sin(\beta)}{\cos(\beta)} + \frac{l}{R} \cdot \sin(\beta) \right) \quad (4.25)$$

and

$$M_{case} = -F_G \cdot R \cdot \left(\frac{\lambda \cdot \sin(\psi) \cdot \cos(\psi)}{\sqrt{1 - \lambda^2 \cdot \sin^2(\psi)}} + \sin(\psi) \right). \quad (4.26)$$

Figure 4-6 shows an overview of the simulated crank motion movement at the top, the cylinder force in the middle and the crankshaft torque of one cylinder at the end.

In order to calculate the total gas torque of the crankshaft, the cylinder individual torques must be added with the cylinder angle offset before superposing them.

At the top of Figure 4-7 the individual gas torques of the 6 cylinders and below the total crankshaft torque are drawn. The x-axis represents one full engine cycle meaning 720° crank angle.

In Figure 4-8 an example of the gas torque of one cylinder is shown.

The total gas torque amount can be calculated by

$$M_{g_tot} = \sum_{i=0}^{N-1} -F_{G_i} \cdot R \cdot \left(\frac{\lambda \cdot \sin\left(\psi + i \cdot \frac{2 \cdot \pi}{3}\right) \cdot \cos\left(\psi + i \cdot \frac{2 \cdot \pi}{3}\right)}{\sqrt{1 - \lambda^2 \cdot \sin^2\left(\psi + i \cdot \frac{2 \cdot \pi}{3}\right)}} + \sin\left(\psi + i \cdot \frac{2 \cdot \pi}{3}\right) \right). \quad (4.27)$$

The negative sign represents the torque transmitted to the engine case and $N = 6$ is the number of the corresponding cylinder in physical order.

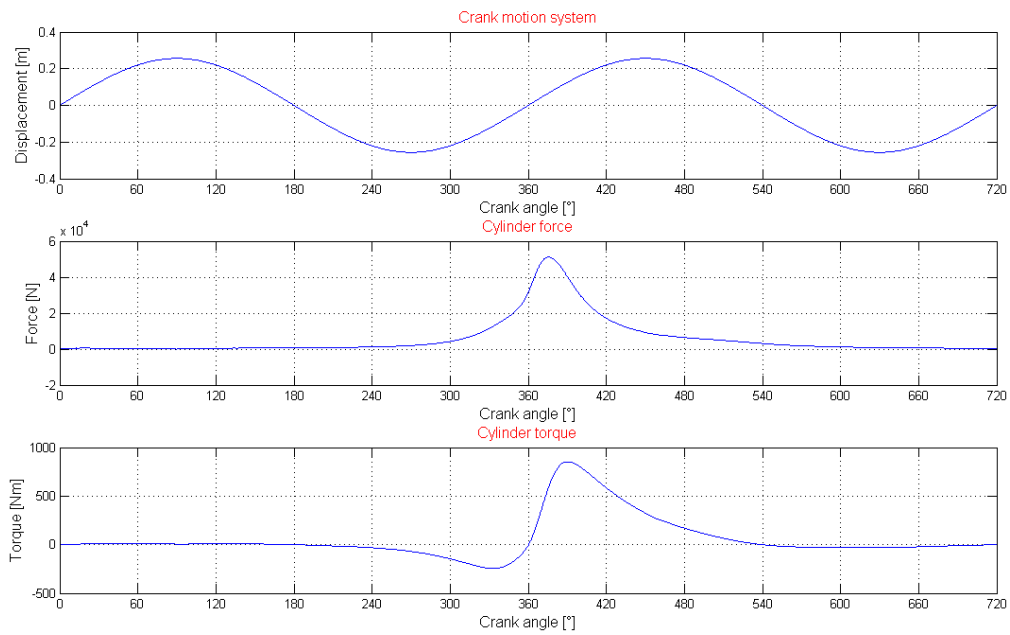


Figure 4-6 Computed crank motion system (top). Calculated cylinder force (middle) and cylinder torque (bottom) based on measured in-cylinder pressure characteristics.

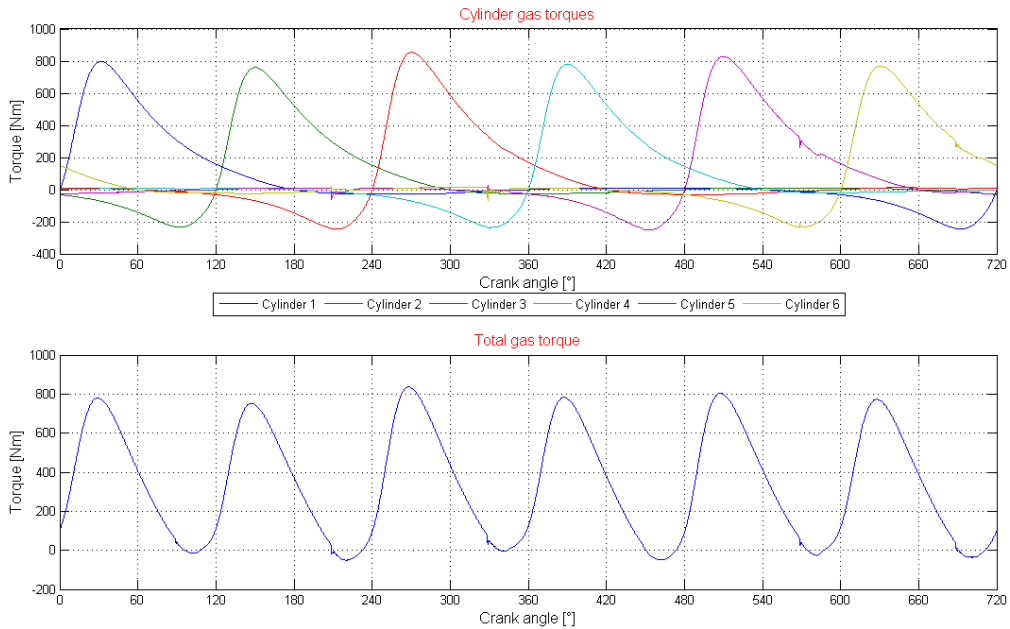


Figure 4-7 Calculated gas torques of the individual cylinders (top graph) and the calculated total gas torque on the crankshaft based on measured in-cylinder pressure characteristics (bottom graph).

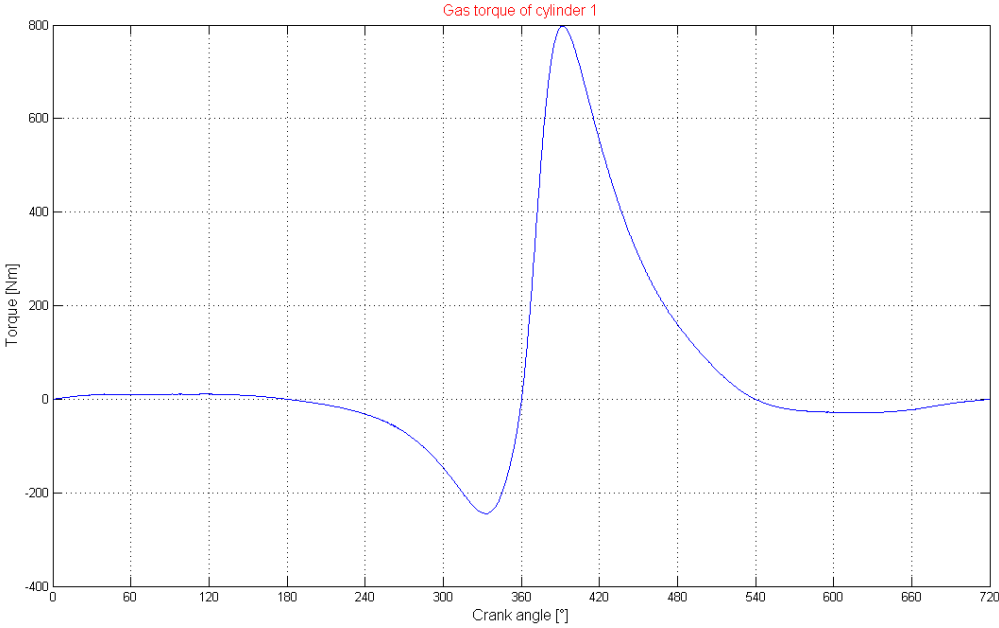


Figure 4-8 Typical calculated gas torque curve of one cylinder based on measured in-cylinder pressure characteristics of a turbo charged combustion engine.

4.4 Mass effects on the crank motion

The relation between force and acceleration and torque and angular acceleration can be expressed in a form of

$$\vec{F} = m \cdot \vec{a} \quad (4.28)$$

and

$$\mathfrak{S} \ddot{\psi} = M. \quad (4.29)$$

If the movement of a mass should be described in a general plane motion, the inertia effect can be denoted by the acceleration of the centre of mass. One example for this is the connecting rod movement of the crank motion. For the calculation and the analysis of the mass effects of the engine, the given system masses must be separated into a rotating and oscillating component. A general declaration of a movement can be accomplished by the specification of the tangential force F_{Tm} and the transversal force F_N [15].

A special case is the rotation of the crankshaft. Due to the assumption of a constant crankshaft rotation speed $\dot{\psi}$ the derivation of $\dot{\psi}$ is zero and the tangential force F_{Tm} (see Figure 4-9) is zero as well. The residual part is the radial force F_{Rs} (see Figure 4-9).

The inertia force of the crankshaft can be denoted by

$$F_{Rs} = m \cdot R_s \cdot \omega^2 = m \cdot \frac{v^2}{R_s}. \quad (4.30)$$

For theoretical aspects the connecting rod can be separated in single mass points. Figure 4-11 shows the two mass point model of the connecting rod.

The mass points are called "rotating mass point" m_{pr} and "oscillating mass point" m_{po} . The "oscillating mass point" m_{po} can be assumed in piston pin axis and the "rotating mass point" m_{pr} at the position in crank pin axis.

With special masses on the crankshaft the centrifugal force F_{Rs} can be balanced.

At this engine type the oscillating force F_o of the connecting rod is not balanced. The result is a torque around the x-axis of "CSYS engine centre" (see Figure 3-12 and Figure 3-13).

Due to the mass torque the engine case will be moved around the x-axis. This mass torque influences the simulation result and must be considered in the model as well.

On top of the aforementioned gas force and additionally the gas torque, the mass torque due to rotating and oscillating masses must be superposed with the gas torque.

For the theoretical investigation of the torque effects on the engine case all involved parts were assumed as a rigid body type and reduced to a mass point model.

The centre of rotation of the crankshaft will be assumed as reference point for the calculation. As mentioned in [19] for the analytical calculations of the mass torque the information about the crank angular ψ , the crank angular velocity $\dot{\psi}$ and further the crank angular acceleration $\ddot{\psi}$ are essential. By the assumption of a constant engine speed due to heavy masses on the crank shaft, i.e. a hydro damper the angular acceleration $\ddot{\psi}$ can be assumed as zero.

Figure 3-14 shows the reference system ("CSYS engine centre") for calculating the mass effects on the crank drive system.

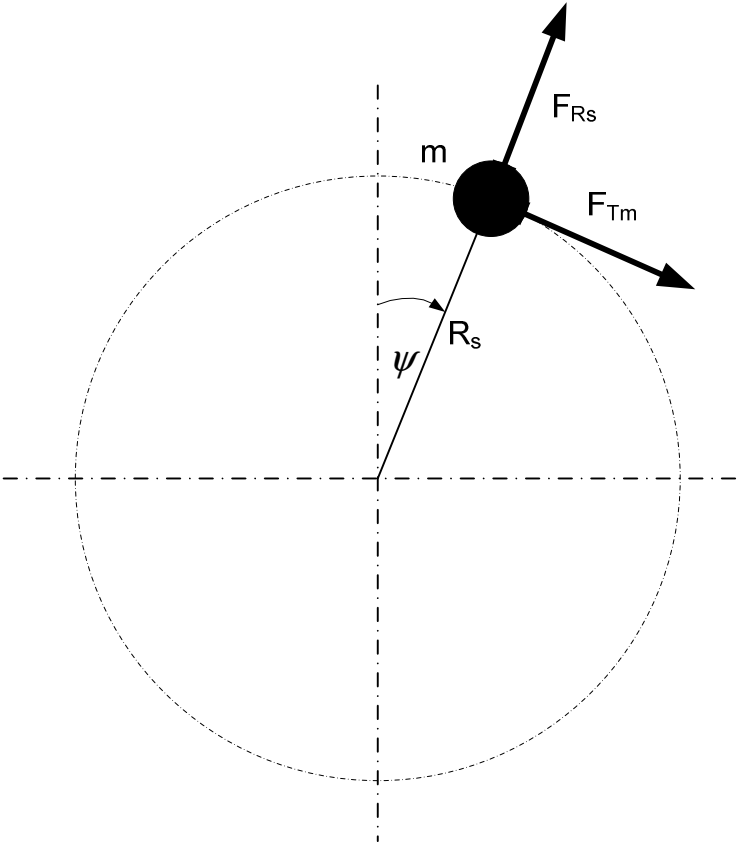


Figure 4-9 Model of forces of a rotating single mass point. The force is split to the tangential force F_{Tm} and centrifugal force F_{Rs} .

4.4.1 Rotating mass effects

The total rotating masses on the drive system of a combustion engine are the mass of the connecting rod m_{pr} and the crankshaft mass with all associated masses like the crank pin with bearing for example.

Based on equation (4.30) and considering a constant angular velocity $\dot{\psi}$ of the crankshaft the rotating mass force F_{Rs} can be calculated as followed

$$F_{Rs} = -m \cdot R_s \cdot \dot{\psi}^2 . \quad (4.31)$$

If the angular velocity $\dot{\psi}$ is not constant and the tangential force F_{Tm} is not zero, torque will be produced.

For the detection method described in this thesis it was assumed that the angular velocity $\dot{\psi}$ is constant. The reason for this approach is a heavy mass on the crankshaft, like the mass of the hydro damper, helps to smooth the engine torque and keep a constant engine speed.

4.4.2 Crankshaft torque due to mass effects

As mentioned above, by an assumption of a constant engine speed the parts in all equations associated to the angular acceleration are zero.

A torque effective upon the crankshaft will be generated caused by the oscillating masses like the connecting rod for example. This periodical event produces a torque on the crankshaft similar to the gas force torque and will depend on the engine speed. It must be considered that the gas force correlates to the engine load. On the other hand the mass torque M_m depends upon the engine speed $M_m = f(n_{engine})$.

The calculation of the crankshaft torque M for one cylinder is denoted by [19]

$$p \cdot A_p \cdot R = M = -R \cdot \omega^2 \left[(m_2 + m_p) \cdot x' \cdot x'' + m_3 \cdot (u' \cdot u'' + w' \cdot w'') \right]. \quad (4.32)$$

Where m_2 and m_3 are the connecting rod masses, m_p represents the piston mass and u', u'' w' and w'' are geometrical parameters of the connecting rod.

Figure 4-10 represents the three mass model of the connecting rod and the equations (4.33) to (4.36) describe the parameter u', u'', w' and w'' .

Equation (4.32) describes the crankshaft torque based on a three mass model of the connecting rod [19]. The connecting rod can be approximated by using the two mass model, in which the mass m_3 must be set to zero and the mass m_2 represents the oscillating parts of the connecting rod $m_2 = m_o$.

The total mass torque of the engine can be calculated by a superposition and a consideration of the correct cylinder angle offset of the individual cylinder torques.

$$u' = \frac{l_1}{l} \cdot x' + \frac{l_2}{l} \cdot \sin(\psi) - \frac{e}{l} \cdot \cos(\psi) \quad (4.33)$$

$$u'' = \frac{l_1}{l} \cdot x'' + \frac{l_2}{l} \cdot \cos(\psi) + \frac{e}{l} \cdot \sin(\psi) \quad (4.34)$$

$$w' = \frac{l_2}{l} \cdot \cos(\psi) + \frac{e}{l} \cdot \sin(\psi) - \frac{e}{l} \cdot x' \quad (4.35)$$

$$w'' = -\frac{l_2}{l} \cdot \sin(\psi) + \frac{e}{l} \cdot \cos(\psi) - \frac{e}{l} \cdot x'' \quad (4.36)$$

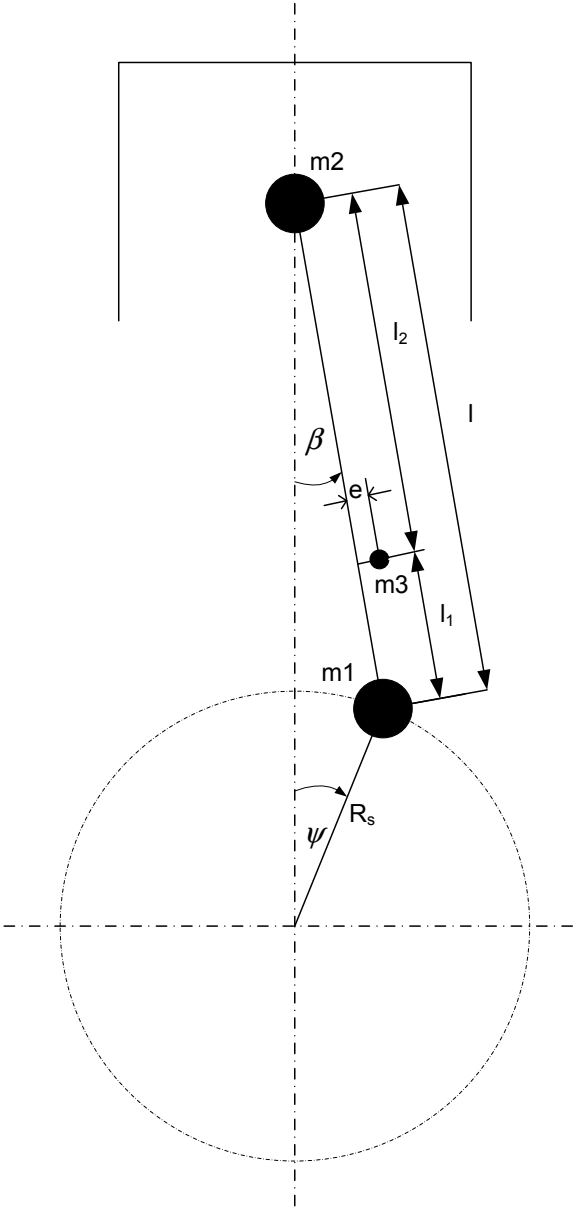


Figure 4-10 Three mass model of the connecting rod. Oscillating mass m_2 , rotating mass m_1 and the centre of gravity m_3 of the connecting rod.

4.4.3 Oscillating mass effects

The oscillating parts of the crank motion are the piston with all associated components and the mass m_{po} of the connecting rod (by a two mass assumption of the connecting rod like in Figure 4-11 presented). For an analytic formulation of the connecting rod it must be separated into two or three independent masses as mentioned in chapter 4.4.1. The calculation of the moment of inertia was conducted during the design process by the program PTC Wildfire [22].

The total mass force F_o of the oscillating parts (up and down movements) referenced to cylinder coordinate system "CSYS cylinder coordinate" drawn in Figure 3-11 can be calculated by

$$F_o = -m_o \cdot R \cdot (x' \cdot \ddot{\psi} + x'' \cdot \dot{\psi}^2). \quad (4.37)$$

Where m_o represents the oscillating parts of the drive system, x' the piston velocity, x'' the piston acceleration, $\ddot{\psi}$ the angular acceleration and $\dot{\psi}$ the angular velocity [19].

The crankshaft torque M_o caused by the oscillating masses can be denoted by

$$M_o = -m_o \cdot R^2 \cdot (x'^2 \cdot \ddot{\psi} + x' \cdot x'' \cdot \dot{\psi}^2) \quad (4.38)$$

The total mass torque M_{mass} of the crankshaft drive can be calculated by [19]

$$M_{mass} = \mathfrak{S}_{(\psi)} \cdot \ddot{\psi} + \frac{I}{2} \cdot \mathfrak{S}'_{(\psi)} \cdot \dot{\psi}^2. \quad (4.39)$$

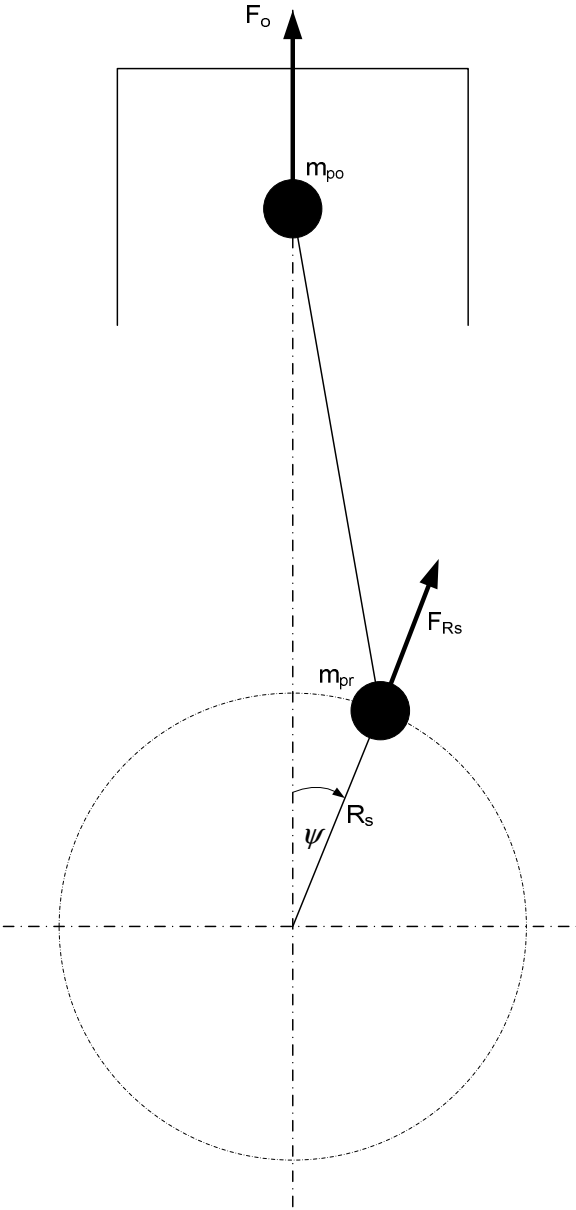


Figure 4-11 Mass model of the connecting rod. Separation of the connecting rod to oscillating mass point m_{po} and rotating mass point m_{pr} .

4.4.4 Total mass torque

In order to reduce so called free engine torques, some engines will be equipped with additional mass balancers. The engine which was investigated for this thesis was designed with one balancing shaft.

As mentioned in chapter 4.4.2, often it is not achievable to reduce the whole mass torques caused by the oscillating parts. It is also not possible to reduce the gas torque occurring around the x-axis by means of balancer weights added to the crankshaft.

In Figure 4-14 an arrangement of a balancer shaft is shown. If the balancer shaft is installed with an offset (see distance "d" in Figure 4-14) and rotated an additional torque will be produced.

The effects, which can be eliminated by using a balancing shaft, are the forces on the x, y and z-axis.

If the balancer shaft is offset to the cylinder coordinate system (see Figure 4-14), some unwanted effects will be reduced or eliminated. But due to the asymmetrical position of the balancer shaft an engine torque around the x-axis referenced to "CSYS engine centre" due to the centrifugal force F_b , multiplied by the distance d will be produced. [19] Describes the formalism and the effects for a combustion engine in more details.

Due to the small influence on the engine behaviour and based on the reason to observe mainly the gas torque which is considered around the x-direction of the coordinate plane "CSYS engine centre" the reactions caused by mass effects in the y and z-axis are not considered in the model.

The total engine case torque caused by to the total mass torque was calculated with the program PTC-Wildfire [22].

The engine case torque around the x, y and z-axis are denoted by

$$M_{m_x_total} [Nm] = -475 \cdot \left(\frac{n_{engine}}{6125}\right)^2 \cdot \sin(3 \cdot \psi - \pi), \quad (4.40)$$

$$M_{b_y_total} [Nm] = 831,7 \cdot \left(\frac{n_{engine}}{6125}\right)^2 \cdot \sin\left(2 \cdot \psi - \frac{\pi}{6}\right) + 13,2 \cdot \left(\frac{n_{engine}}{6125}\right)^2 \cdot \sin\left(4 \cdot \psi - \frac{\pi}{6}\right) \quad (4.41)$$

and

$$M_{b_z_total} [Nm] = 277,2 \cdot \left(\frac{n_{engine}}{6125}\right)^2 \cdot \sin\left(2 \cdot \psi - \frac{\pi}{6}\right) + 4,4 \cdot \left(\frac{n_{engine}}{6125}\right)^2 \cdot \sin\left(4 \cdot \psi - \frac{\pi}{6}\right). \quad (4.42)$$

The equation (4.40) shows the torque of all cylinders on the crankshaft which was not balanced and consequently influences the engine case movement. The equation is referenced to the highest engine speed at 6125 rpm. The equations (4.41) and (4.42) were not considered in the model but mentioned in an effort to be thorough. It describes the influence on the engine case coming from the balancer shaft. An appropriate system description can be formulated with equation (4.40) only. It describes the engine case movement which can be measured with a one axis acceleration sensor installed on the engine block.

The position of the sensor can be seen in Figure 4-13. With the sensor sensitivity in only one axis (see Figure 4-13) the acceleration signal coming from the engine movement in y and z directions (see Figure 4-13) are small and can be ignored.

At low engine speed the influence of $M_{m_x_total}$ is quite low and can also be ignored. But at higher engine speed the influence to the engine case due to rotating masses gets higher and has to be considered. Figure 4-12 shows the torque characteristic versus the engine speed caused by the unbalanced mass effects.

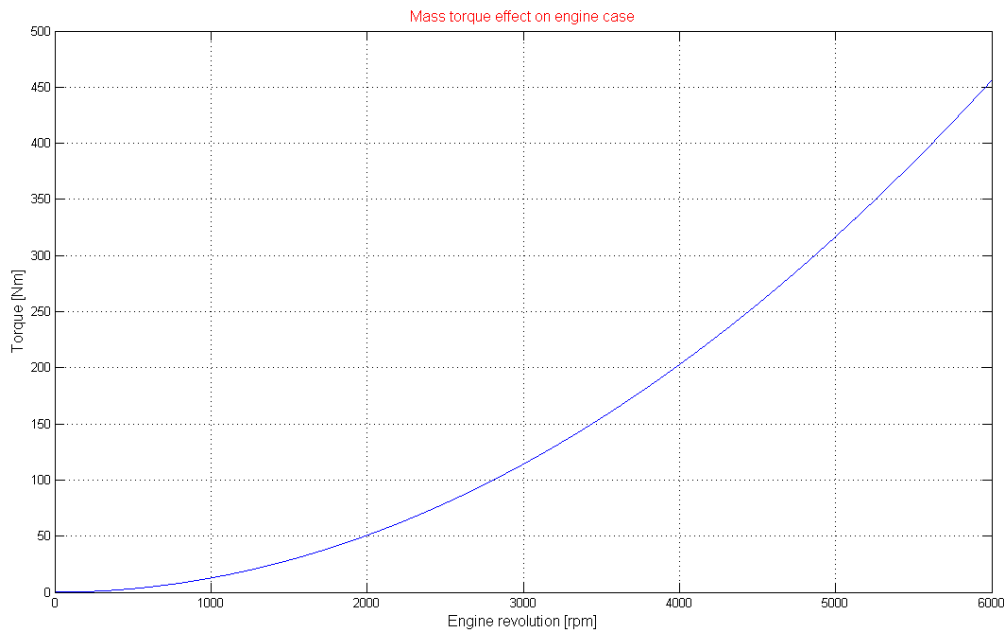


Figure 4-12 Characteristic of the mass torque effect on engine case versus engine speed

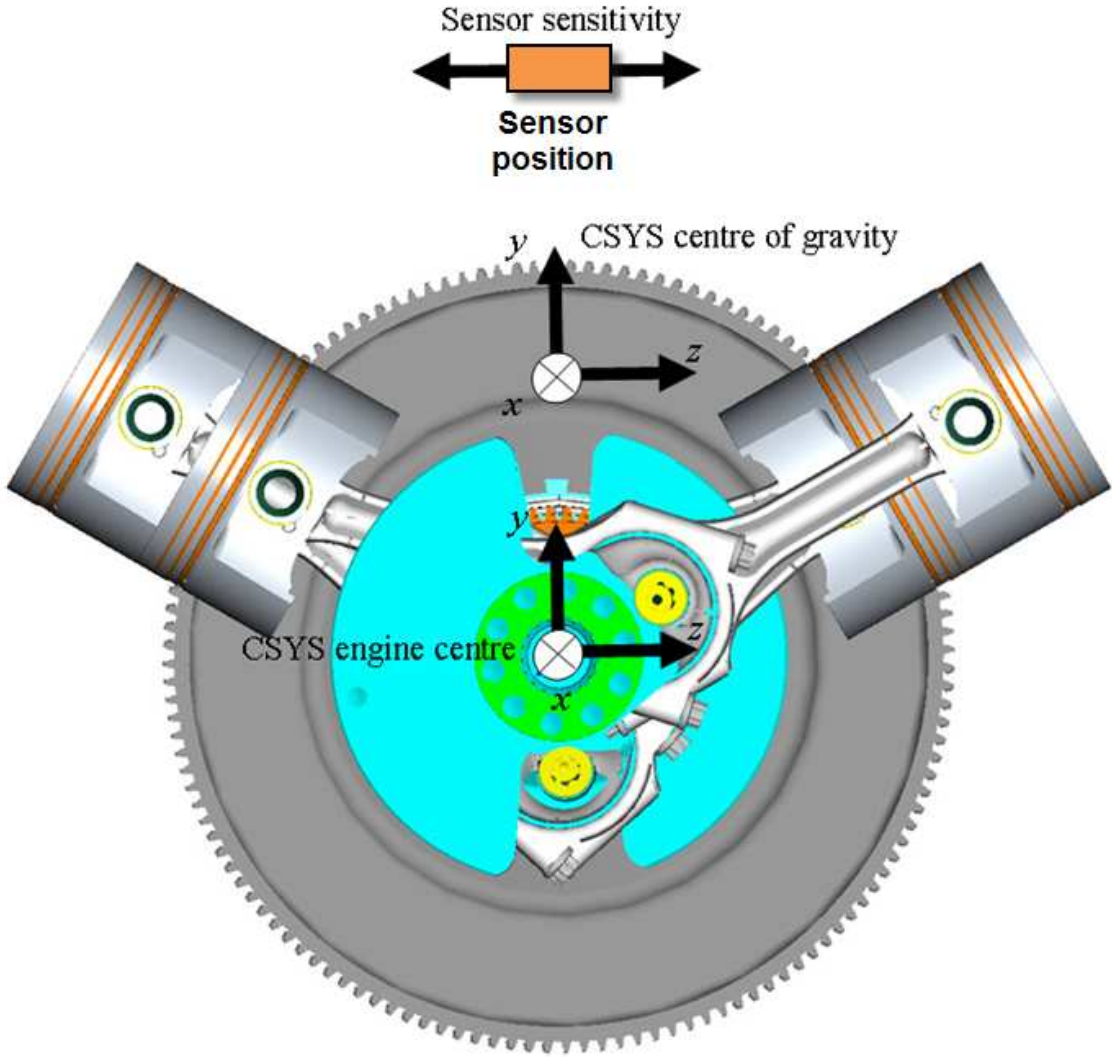


Figure 4-13 Overviews of coordinate planes with the position of the acceleration sensor and direction of sensitivity.

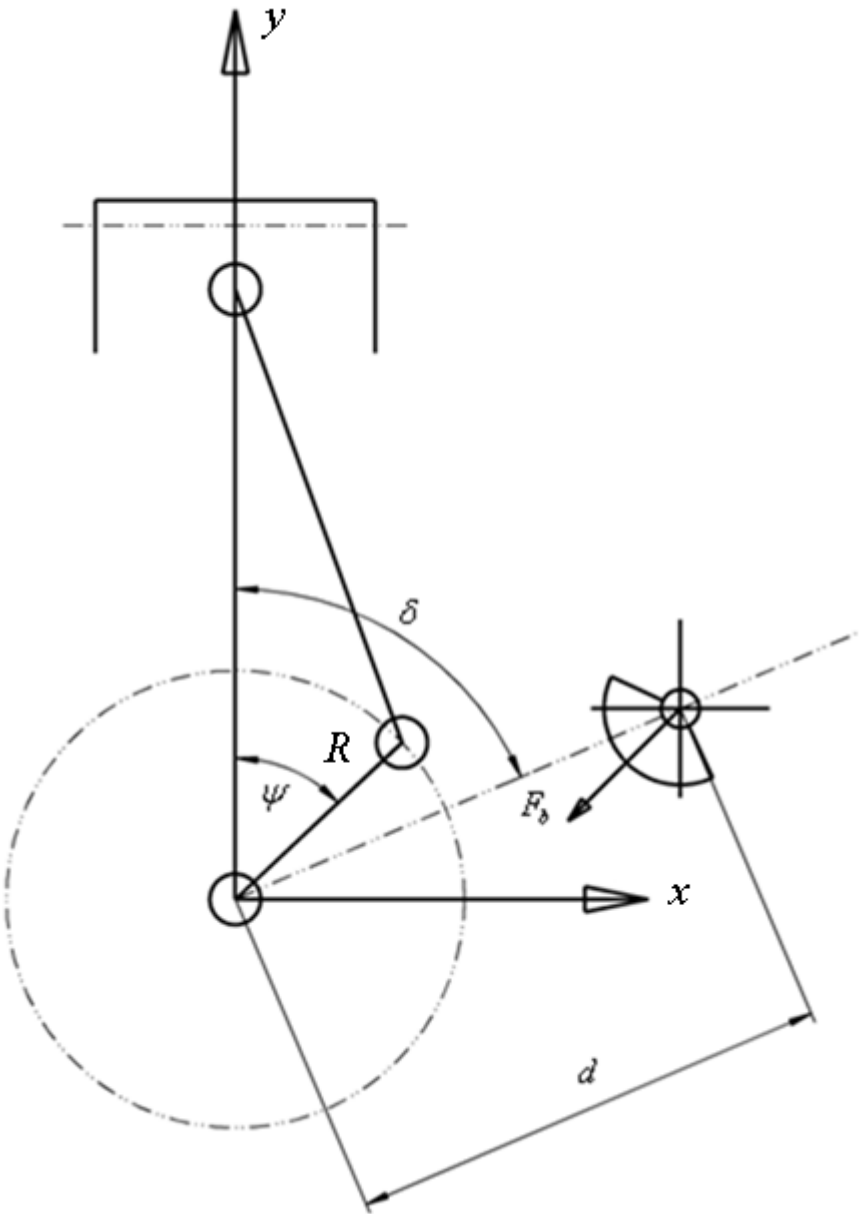


Figure 4-14 Arrangement of a balancer shaft referenced to coordinate plane "CSYS cylinder coordinate".

4.5 Total engine torque calculation

The total engine torque or crankshaft torque can be calculated by the superposition of the individual cylinder gas and mass torques. The equation (4.43) describes the sum of all considered torques.

$$M_{case_total} = -\sum_i^N (M_{g_tot_i} + M_{m_total_i}) \quad (4.43)$$

The result presented in Figure 4-16 was calculated at an engine speed of 5000 rpm and shows in the mid range the total crankshaft torque. It includes all gas and mass phenomena. On the top of the chart the gas (green line) and mass torques (blue curve) are drawn. The third graph represents the engine case torque. It can be seen that the mass torque at high engine revolutions due to the oscillating masses is not insignificant. This leads to a torque influence around the x-axis that cannot be ignored. Some disturbances in Figure 4-16 (are seen in some other Figures as well), the blue curves are reasonable given the measurements of the in-cylinder pressure. Figure 4-15 shows the measured in-cylinder pressure of cylinder 5 for example. Each simulation is based on measured in-cylinder pressure characteristics of the individual cylinders. Disturbances on the measured pressure curve leads to break-down in simulation results. The disturbances in the next two Figures are marked by arrows.

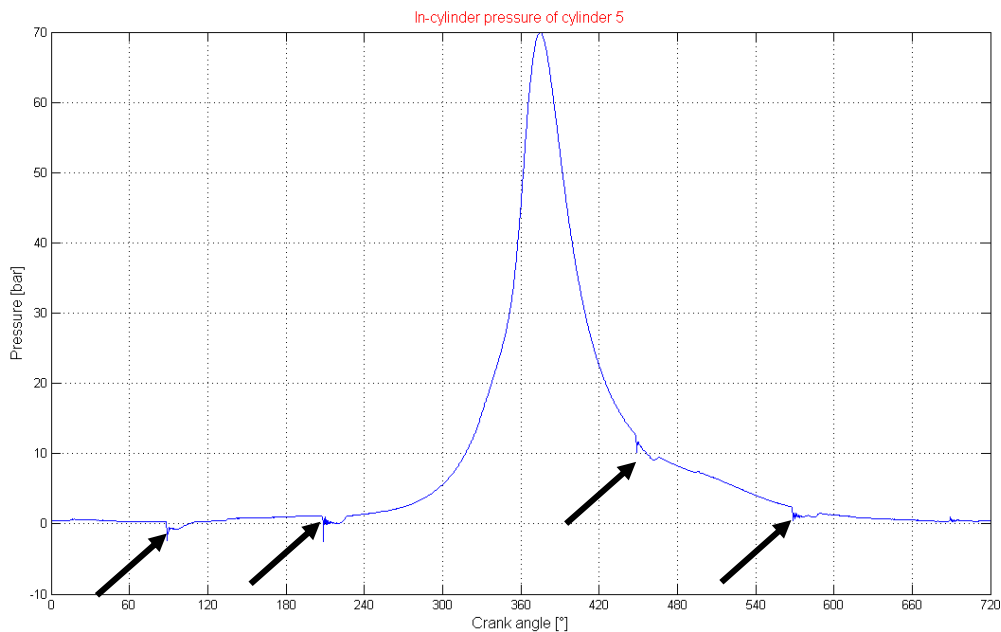


Figure 4-15 Measured in-cylinder pressure curve of cylinder 5.

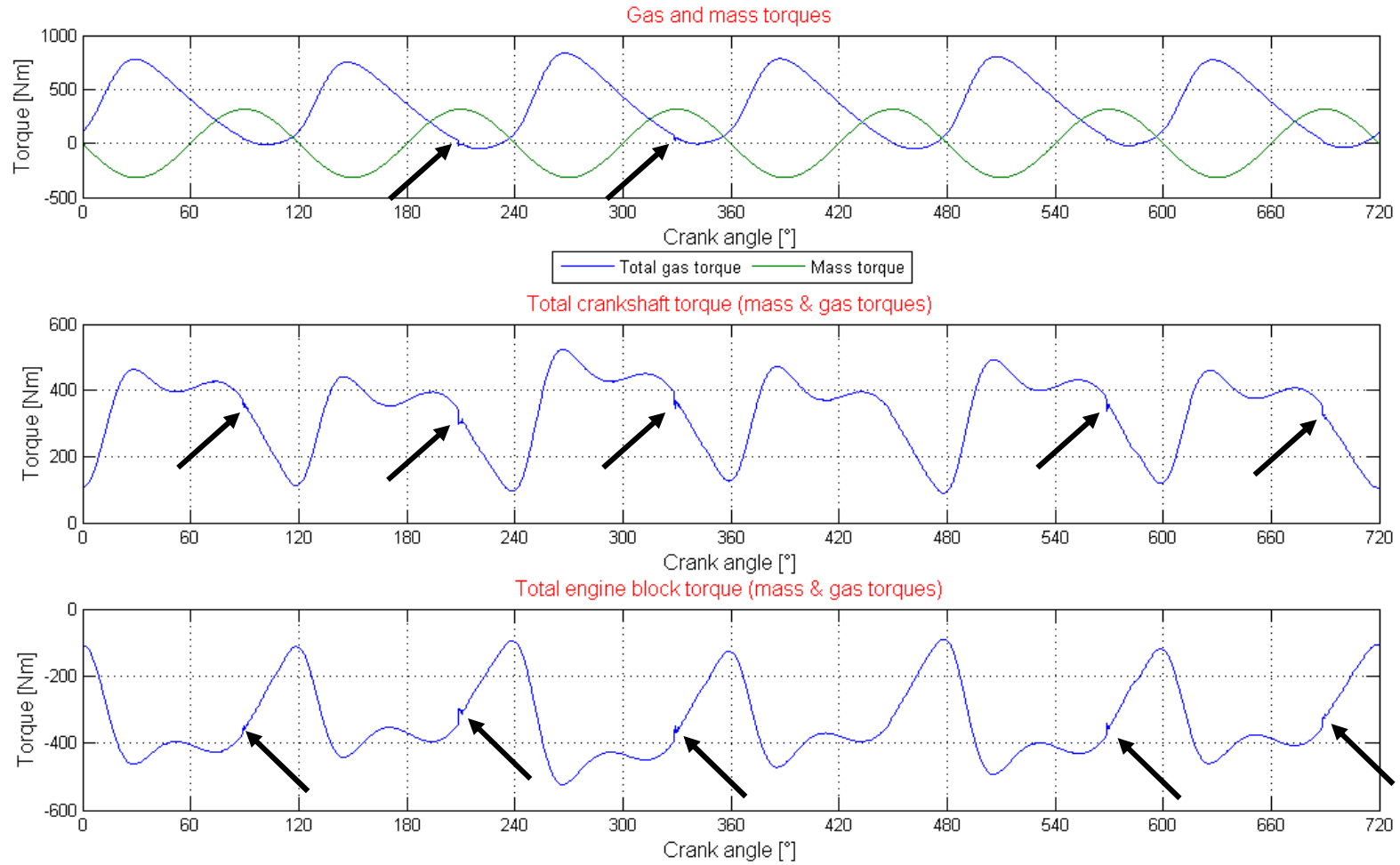


Figure 4-16 Simulated gas and mass torques based on measured in-cylinder pressure curves at 5000 rpm

5 MODEL RESULTS AND SIGNAL PROCESSING

Chapter 5.1 describes all mechanical relevant parts of the investigated reciprocating aircraft engine which are also included in the analytic model. The model approximates the engine in a good manner and shows simulation results in compliance to the real world measurements.

5.1 Engine model description

Figure 5-1 shows the mechanism of the analytic engine model.

The model structure was done in a way to split the mechanical system into certain blocks. After a simulation each model block can be independently investigated. If this is completed consecutively the working principle of the whole system can be understood easily by a visualisation of the calculated model blocks.

The software algorithm starts first with the import of measured in-cylinder pressure data. Based on the individual pressure curves the cylinder force can be calculated. All mechanical parameters of the engine, i.e. piston diameter, masses etc, are included in a special data file. Before the calculation can be made the parameters must be loaded from this file.

After the in-cylinder pressure data is loaded, it then can be modified online by a scaling factor. A floating point number between 0 and 1 can be chosen for each cylinder. This means the in-cylinder pressure can be modified between 0 (total pressure loss) and maximum pressure magnitude which comes from the measured data and depends on the engine load condition. It would also be possible to increase the pressure by applying scaling factors greater than 1. In this case engine behaviours at high in-cylinder pressure amounts can be investigated.

By playing with the cylinder selective scaling parameters, different engine conditions can be simulated. For example a total cylinder shut down can be simulated by a factor 0 for the related cylinder. In this case a standard pressure curve is loaded and all further simulations of the related cylinder will be done with the standard curve aforementioned in Figure 4-4. The standard pressure curve represents a working cycle without an ignition, giving a compression and an expansion cycle. As mentioned before there were no considerations given to the temperature and pressure rises during the combustion.

The in-cylinder pressure correction factor can be further used to simulate different engine load conditions by varying the scaling factor. This leads to selective controllable in-cylinder pressures. After the individual pressure correction and force calculation, the cylinder selective crankshaft torque can be computed. If this step is completed for all cylinders the total crankshaft torque can be estimated. Before then however, the individual ignition angle offset of this engine type must be applied, this will be done automatically by the mathematical model. Figure 4-8 shows a typical gas torque characteristic of one cylinder. The total crankshaft torque (due to gas forces) was shown in Figure 4-16 on the top, blue coloured. If the total gas torque is known, the unbalanced mass torque effects can be applied. Before a superposition of both torque signals can be done the mass torque has to be corrected by the right angle offset. As mentioned in chapter 3.4.1 the coordinate plane "CSYS engine centre" must be considered for this calculation. The outcome of this calculation is the total gas and mass torque on the crankshaft. Next the signal path has to be split. The total torque (gas and mass) calculated at the end of the crank shaft stimulates the hydro damper, the torsion bar, the

gear box and the propeller shaft with the associated propeller. Due to the interactions of the pistons and the gear box to the engine block the engine will be stimulated as well.

By inverting the gas and mass torque the engine case torque can be calculated and represents one of the measurable signals by using an acceleration sensor located on the engine block.

The second signal path is fed to the torsion bar. Before a calculation of the torsion bar can be applied the total crankshaft torque signal has to be converted into several spectral frequencies. By a consideration of a LTI system of the torsion bar, the calculation can be done with derived spectral components. If all of the components are calculated, the output signal of the torsion bar is the sum of all computed partial results. Torque correction due to the tooth wheel force of the gear box and further the engine case torque has to be calculated. To calculate the total torque, the engine block caused by the gas and mass torques and the gear box case torque have to be superposed.

The total amount of the engine case torque is dumped by the engine mounts. The engine mounts behaviour is frequency dependent and shows a frequency-response characteristic like a low pass filter. This will finally change the signal bandwidth of the engine torque which causes the engine motion.

The engine movement around the x-axis is the outcome of all the calculation steps and can be measured by a one axis acceleration sensor.

MODEL RESULTS AND SIGNAL PROCESSING

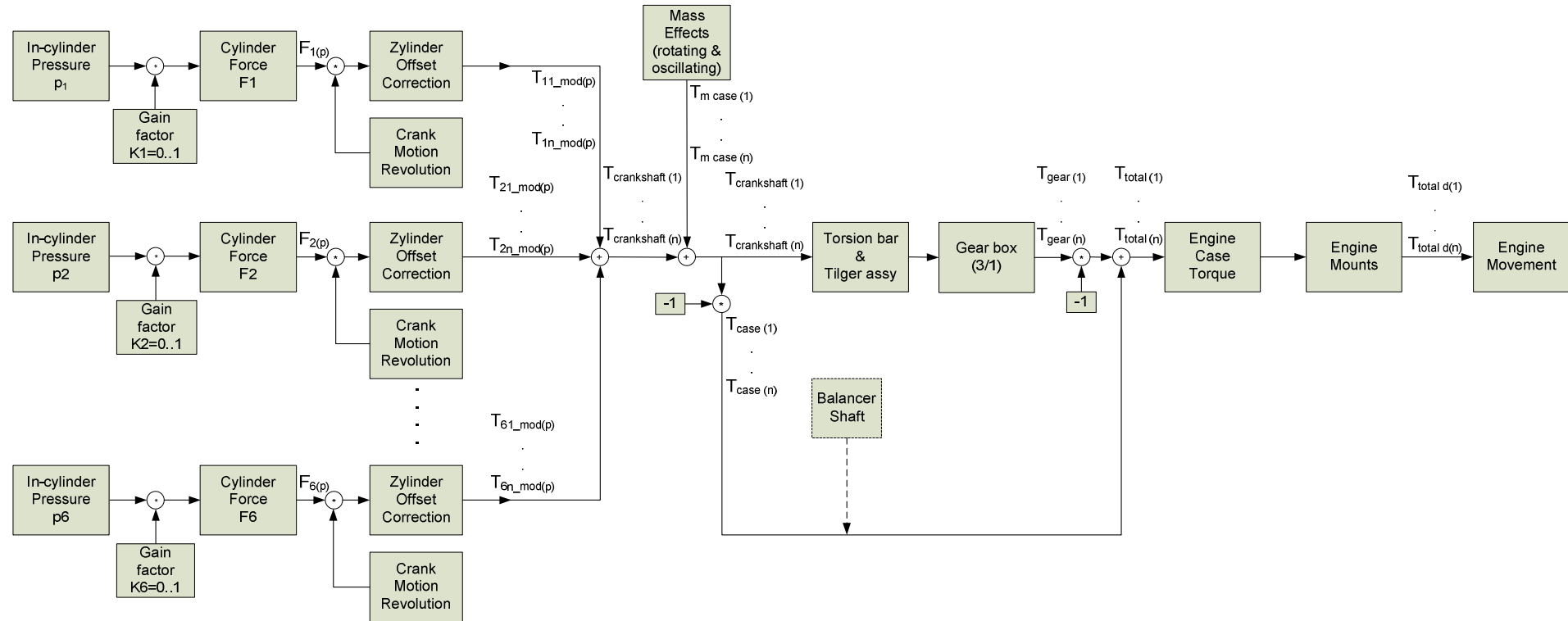


Figure 5-1 Model overview of the mechanical system and the torque mechanism

5.2 Engine model description continued

A closer inspection of the system blocks shown in Figure 5-1, explains the working principle of the detection method. The investigated engine was a 6-cylinder V-type engine with 120° crank angle offset. This means every 120° degree crank angle a firing event occurs and in case of a good engine the air-fuel mixture formation will be ignited and a crankshaft torque will be produced. With this consideration it is quite clear if one cylinder is on the TDC that the corresponding has a 360° crank angle offset, is on the BDC. This is important as the reaction of the engine by a misfire event should be kept in mind. The corresponding cylinders are

1 and 4

2 and 5

3 and 6

Figure 5-2 shows the spectral components of each cylinder versus crank angle. A 720° crank angle represents one 4-stroke cycle. It can be seen that the 0.5^{th} (blue line) the 1.5^{th} (red line) and the 1^{st} (green line) engine oscillation modes are dominant compared to the other frequencies.

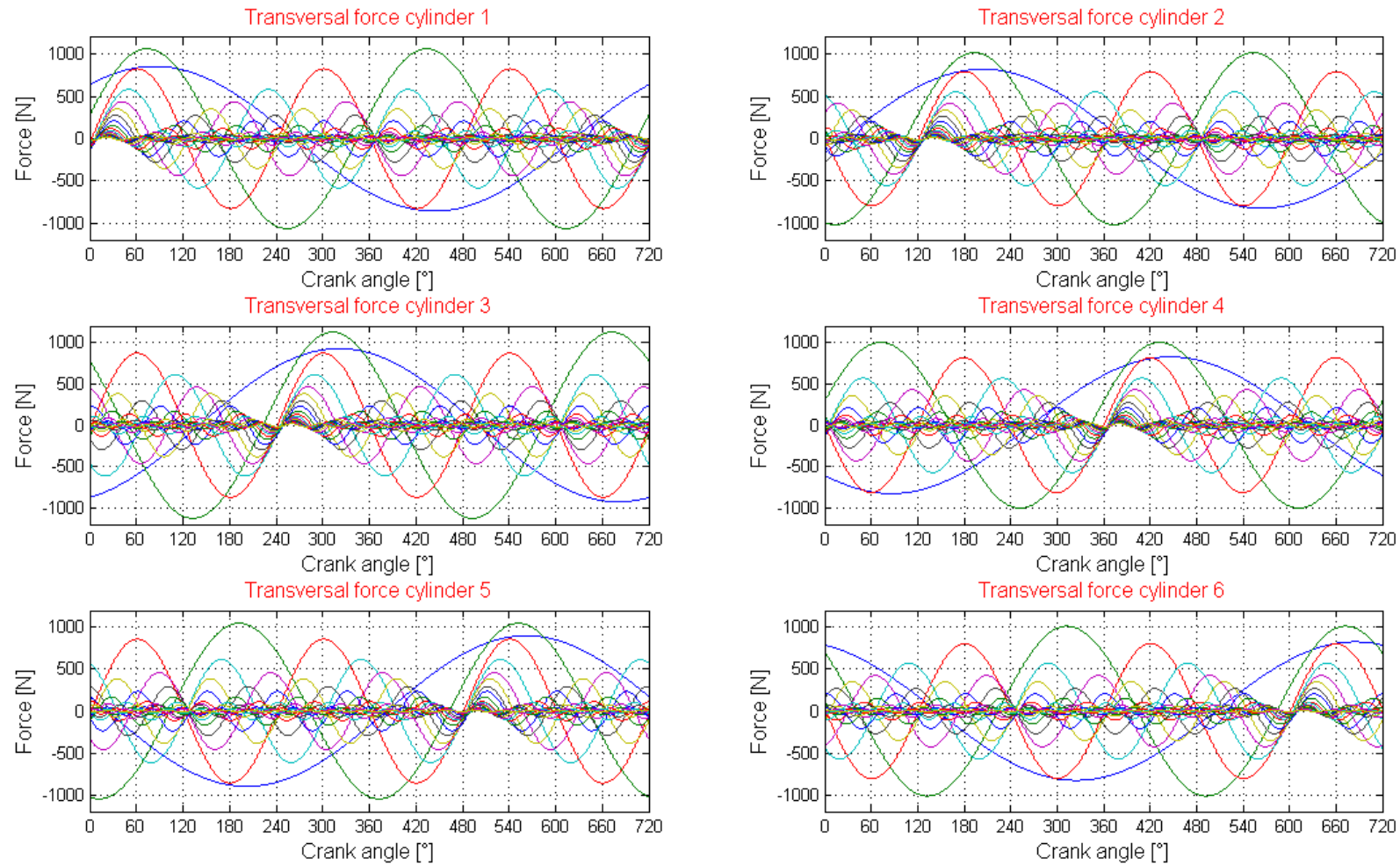


Figure 5-2 Overview of the cylinder selective spectral components drawn versus crank angle

MODEL RESULTS AND SIGNAL PROCESSING

The main power is concentrated in these three oscillation modes and they are mainly responsible for the engine power. Figure 5-3 represents the typical spectral components (bar diagram) of the transversal force of the gas force.

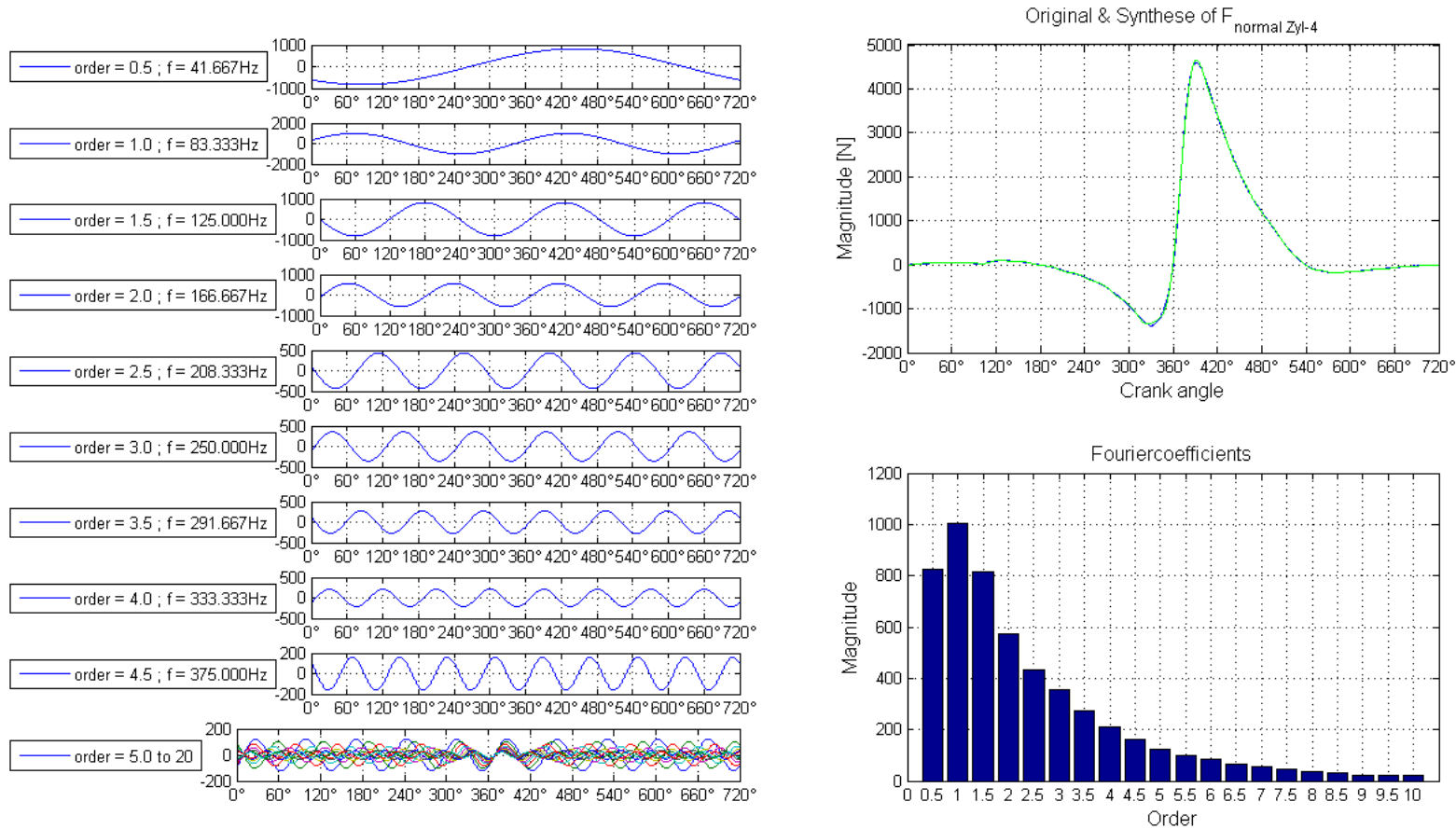


Figure 5-3 Spectral analyses of the transversal force of the gas force

MODEL RESULTS AND SIGNAL PROCESSING

The graph down the right-side shows the amplitude of the certain frequency based on engine oscillation modes. In Figure 5-4 an order analysis of the crankshaft torque of one cylinder is printed. As explained above the main power is located in the lower three engine oscillation modes.

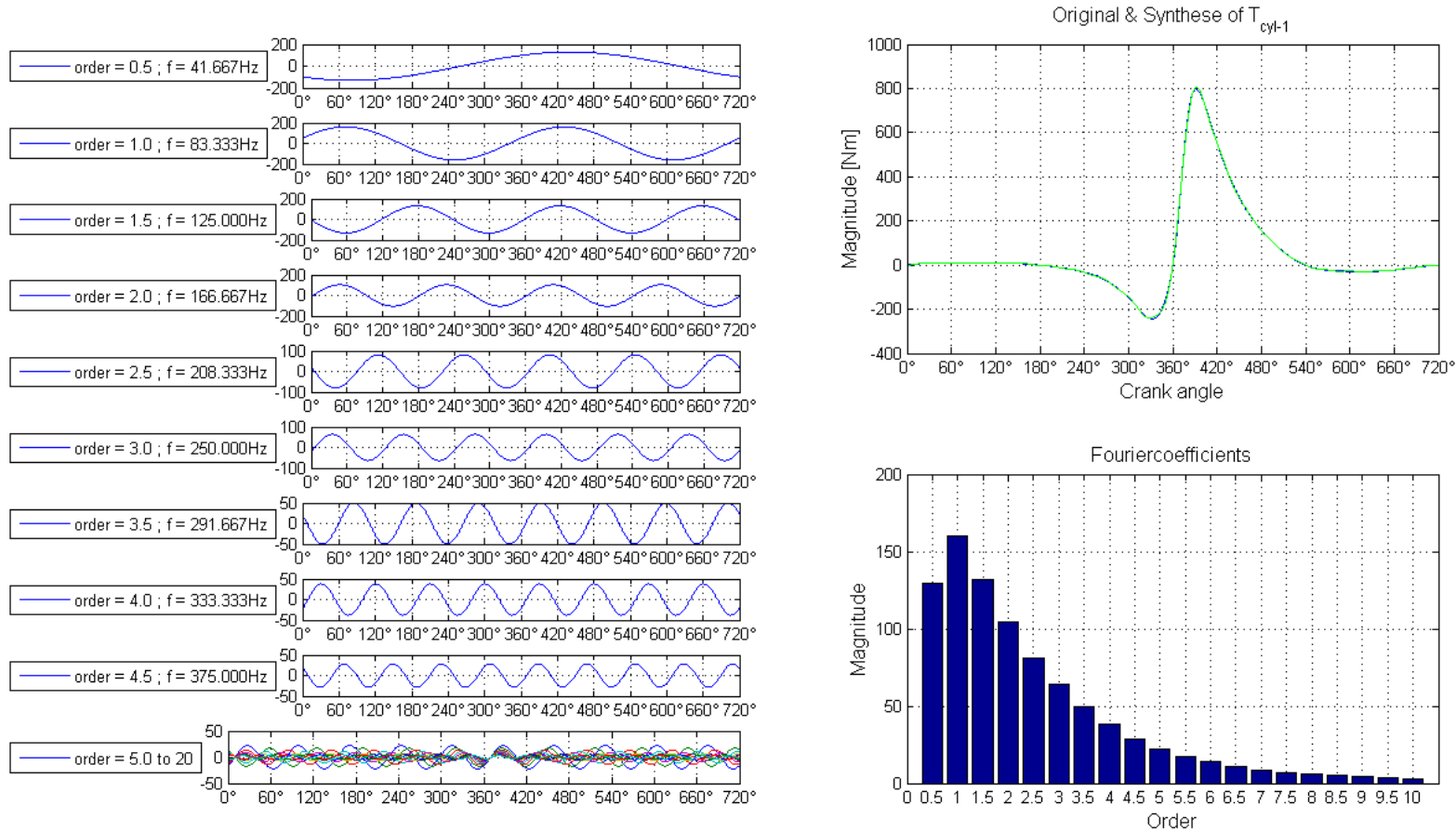


Figure 5-4 Spectral analyses of the crankshaft torque of cylinder 1. Watch the different scales used for higher engine orders.

MODEL RESULTS AND SIGNAL PROCESSING

In Figure 5-5 the upper three plots present the sum of transversal forces of the corresponding cylinders and at the bottom plot the total sum of the transversal force of all cylinders of the crankshaft is shown.

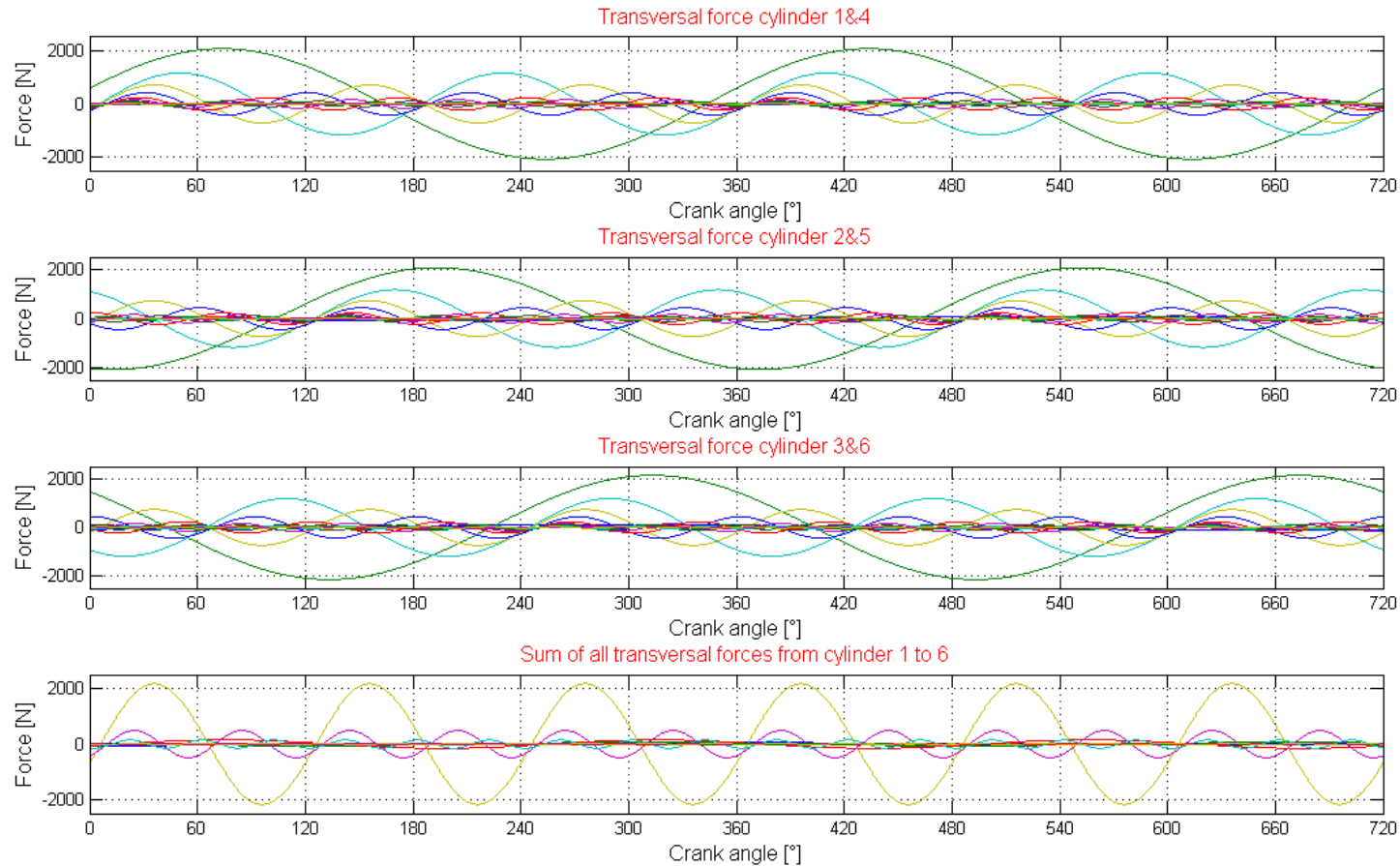


Figure 5-5 Simulated spectral components of transversal forces of the corresponding cylinder pairs and the total calculated sum of the transversal force on the crankshaft

As you can see the main torque will be produced by the engine oscillation mode one and two. Any other frequencies will be compensated or reduced to a low torque value. In the bottom chart the crankshaft torque versus engine oscillation modes can be seen. The 3rd engine oscillation mode based on 360° crank angle analyses window produces the main engine torque in the case of a normal engine condition.

The next step as shown the simulation model (see Figure 5-1) is the computation of the mass torque on the crankshaft.

The upper chart in Figure 5-6 shows the torque due to ignited air-fuel mixture (blue) and the mass torque (green) simulated on the crankshaft.

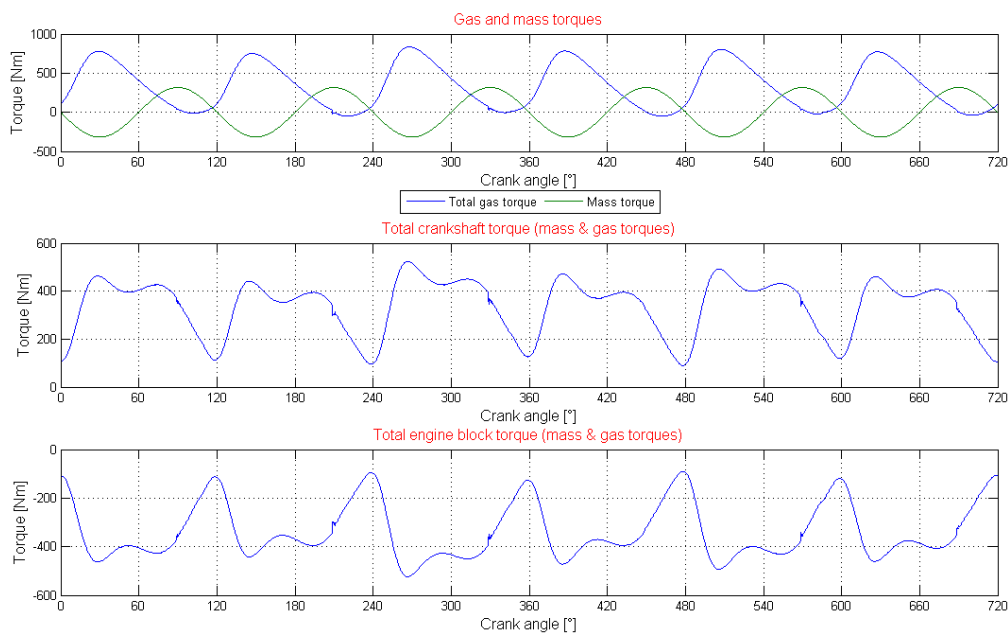


Figure 5-6 Simulated gas and mass torques. Upper plot gas (blue) and mass torque (green). Middle plot: Total torque on crankshaft and bottom plot engine block torque.

The total crankshaft torque is calculated by adding the gas and mass torques. The result on the crankshaft is presented in the middle and the simulated effect on the engine case is shown on the bottom plot. It must be considered that the engine case effect has to be added later on to the gear box output as shown in the model overview Figure 5-1.

The gas and mass effects on the engine block bypass the torsion bar and the gear box stage. As previously mentioned the engine block torque is equal to the crankshaft torque but has no joint to the torsion bar. In fact the torsion bar cannot be accelerated from the engine block but it must be considered that the engine block is already excited.

In parallel the crankshaft torque signal appears at the torsion bar stage and further on the gear box. This means the engine torque passes the torsion bar and the gear box. Due to the gear box an additional engine block torque is produced, which has a frequency dependency (coming from the torsion bar) and has to be added to the engine block torque coming from the transversal forces of the pistons.

Before the torsion bar can be calculated the crankshaft torque signal has to be split into certain spectral components. This can be done by an assumption of an LTI system of the torsion bar. Before the mass effects on the crankshaft will be calculated the signal is independent from

engine speed. This means that the crankshaft signal only depends on the in-cylinder pressure or in other words on the engine load condition $p_{cylinder} = f(engine_load)$.

Due to the frequency response of the torsion bar as shown in Figure 3-8 the spectral components of the crankshaft torque signal will have different phase angles and magnitudes after passing the torsion bar. This behaviour is important for the misfire detection method and must be considered in the signal analyses.

If all cylinders work fine, most of the produced frequencies will be compensated as during the engine design specified. Only the oscillation mode 6, based on 4π analyses window (equals to oscillation mode 3 based 2π analyses window) is dominant with a high magnitude as shown in Figure 5-5 4th plot.

This oscillation mode will be filtered and the magnitude is reduced by passing the torsion bar. Using silent blocks normal engine vibration can be measured on the engine block.

The signal output of the crankshaft then passes through the gear box stage. The green line in Figure 5-7 shows the torque on the engine case due to the gear box. The significant oscillation mode is mainly oscillation mode 0.5th but with low magnitude compared to the crankshaft torque. A magnitude comparison of the torque signals shows, that a torque amount with approx. 60 Nm can be neglected and does not dramatically effect the engine motion.

MODEL RESULTS AND SIGNAL PROCESSING

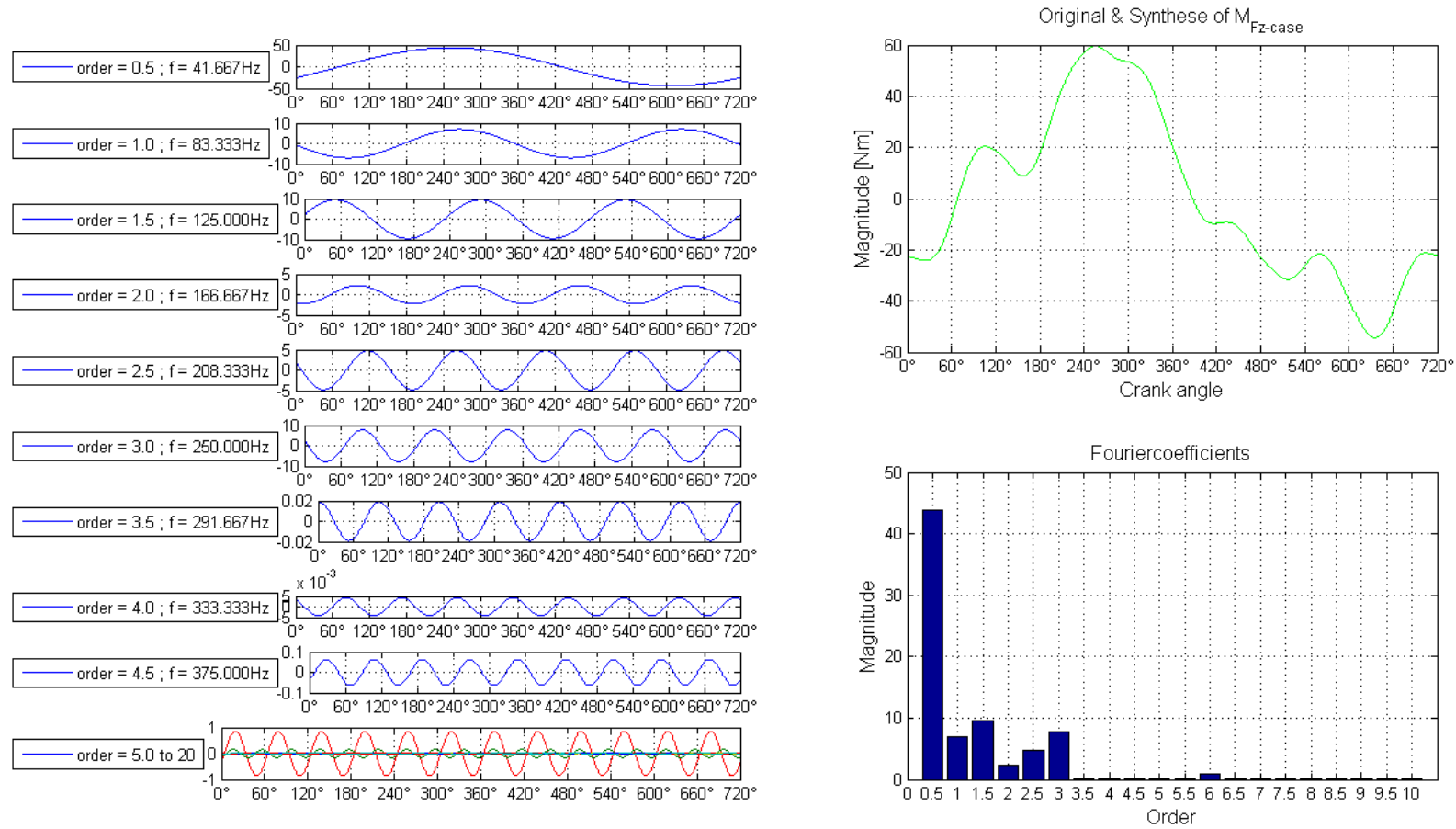


Figure 5-7 Spectral analyses of the gear box torque appearing on the engine block.

MODEL RESULTS AND SIGNAL PROCESSING

In Figure 5-8 the total engine case torque amount (green line) is plotted versus crank. Below the spectral components are shown. It can be seen that the influence of the torsion bar is quite low and the frequency spectrum is similar to the crankshaft signal.

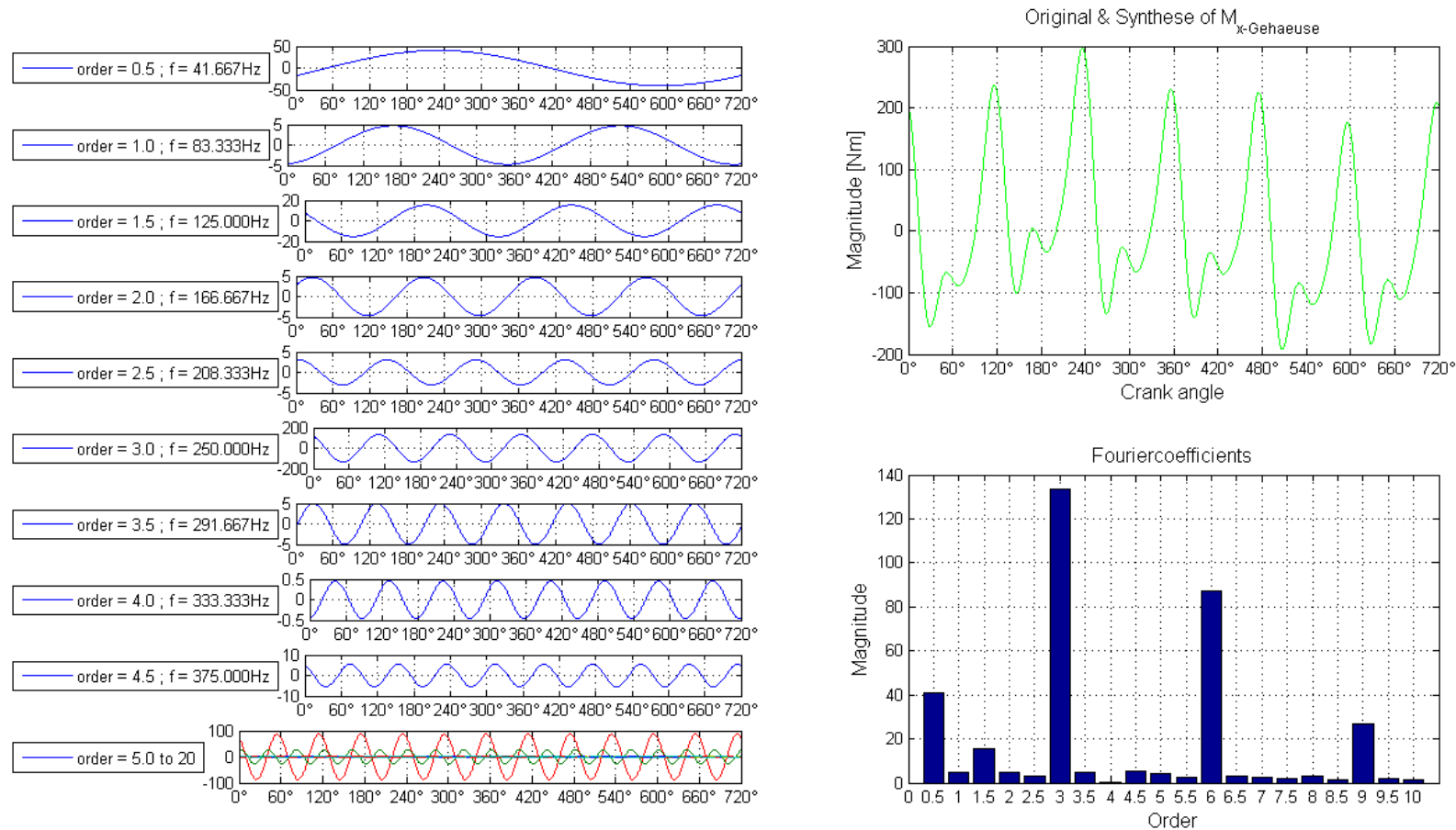


Figure 5-8 Spectral analyses of the engine case torque around x-axis.

The next charts in Figure 5-9 show a summary of different model blocks. On the left hand side order analyses are plotted off the graphs listed down the right column. On the top of this the total engine case torque due to gas and mass effects is plotted. In the middle the gear box torque is printed and on the bottom the total engine case torque around the x-direction is listed. It can be seen in the last diagram in the right hand column, that the individual cylinder torques are dominant and no low engine oscillation modes with high magnitude are present.

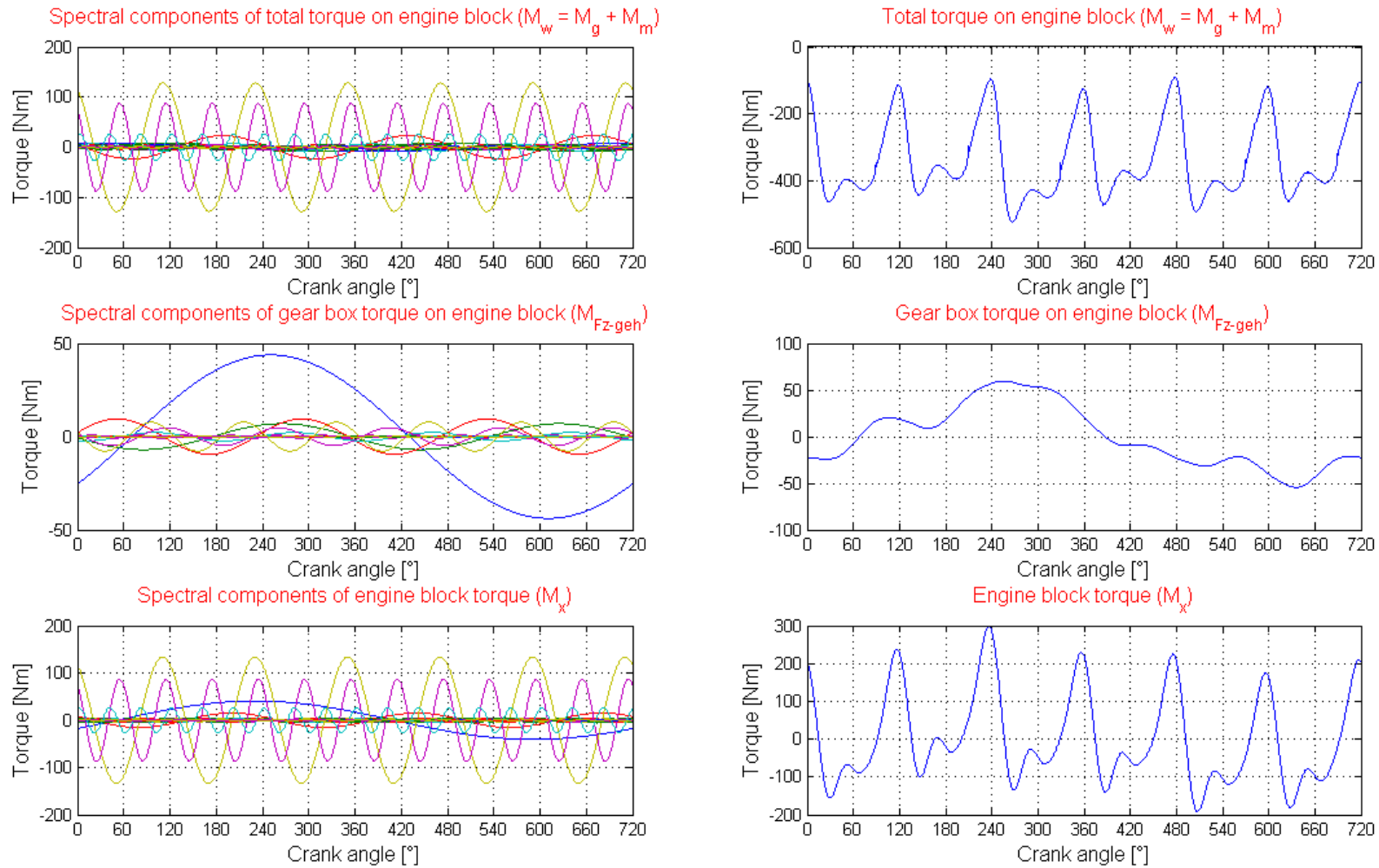


Figure 5-9 Frequency overview of total crankshaft torque, gear box torque and engine case torque simulated around x-axis.

Figure 5-10 shows an overview of the main torque sources means the power chain of the system can be observed. At normal operational conditions the green line (represents the 0.5th oscillation mode of the engine) are calculated at the gear box and show the torque on it. The amount of the 0.5th oscillation mode depends on the in-cylinder pressure differences. As above mentioned this oscillation mode is theoretically compensated if the in-cylinder pressure characteristics of all cylinders are 100 % equal. Due to small differences of the cylinders caused by mechanical tolerances or thermodynamic reasons, this oscillation mode is normally not totally compensated as shown in the diagram below. As revealed later, the gear box torque amount is mainly responsible for the engine case movement.

In the next chart (Figure 5-11) the expected engine case behaviour is simulated. This calculation shows the acceleration in units of [g] at normal engine operation. This calculation includes the distance from the acceleration sensor to the centre of rotation of the complete engine (see "CSYS centre of gravity"). For the online analyses the exact sensor location is not necessary and also not included in the observation method. The magnitudes of the spectral frequencies are not the most important information. For further engine analysis of the power train system i.e. torque analyses of the torsion bar or a force calculation of the tooth wheels installed in the gear box, it is also necessary to have the information of the sensor position. This information is important because the mechanical stress calculation is based on the amount of the engine movement as well.

The distance from the sensor to the centre of rotation of the engine ("CSYS centre of gravity") is only an assumption and not known exactly but a fine approach for acceleration estimations, as it can be seen the acceleration amount of 0.5th engine oscillation mode is little and has no impact on the case movement. This means the engine case excitation is mostly driven by the 6th engine oscillation mode based on 4π crank angle.

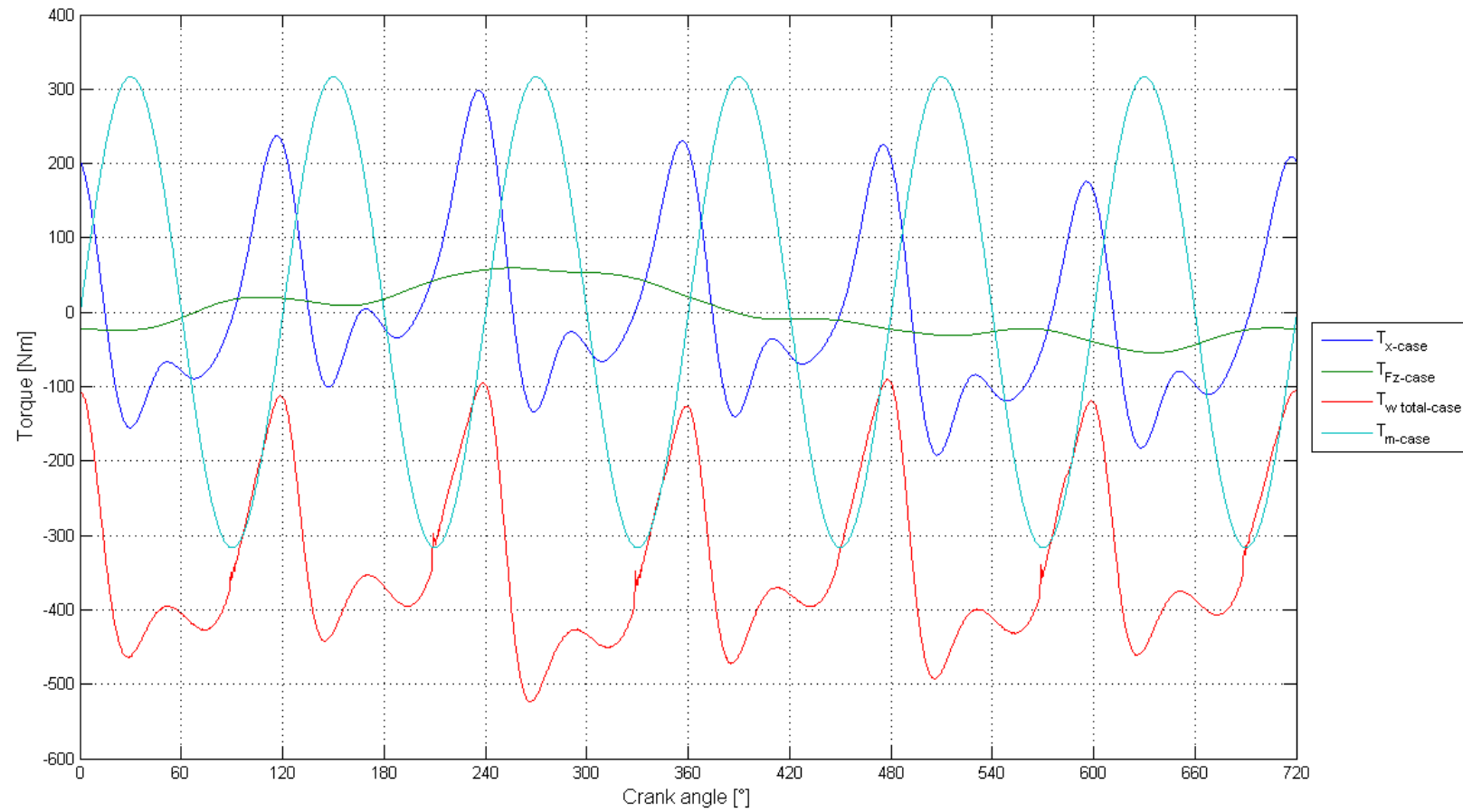


Figure 5-10 Simulated torque signals on engine case around x -direction. Gear box torque (green), total crankshaft torque on case (red), mass torque (turquoise) and total engine block torque (blue).

MODEL RESULTS AND SIGNAL PROCESSING

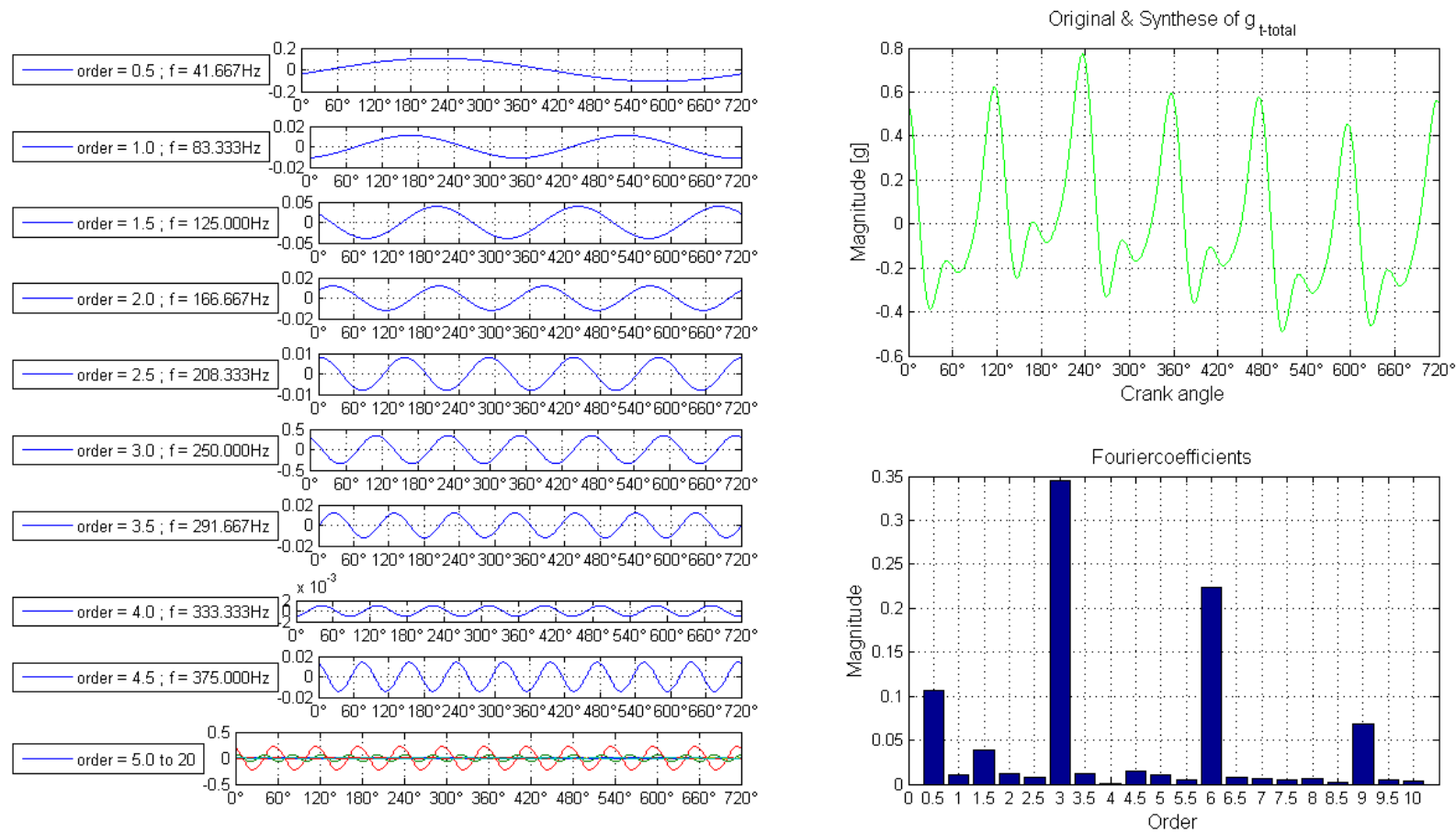


Figure 5-11 Spectral analyses of the engine case excitation.

In the next Figure (Figure 5-12) a summary of the most important calculation steps is drawn. This simulation was done at 5000 rpm.

The upper plot on the left hand side represents the piston forces of the 6 cylinders. On the right hand side the alternated gas torque (blue line) and the average crankshaft torque is plotted. In the middle left hand side, the total crankshaft torque including gas and mass effects are drawn and on the right hand side (same row) some important torque signals like gear box torque (red), gas torque (green) and engine case torque (pink) are printed. The last plot on the bottom shows the simulated acceleration signal on the predefined sensor position on the engine block. The total acceleration magnitude is lower than 1 g. This magnitude is in the expected normal operating range.

MODEL RESULTS AND SIGNAL PROCESSING

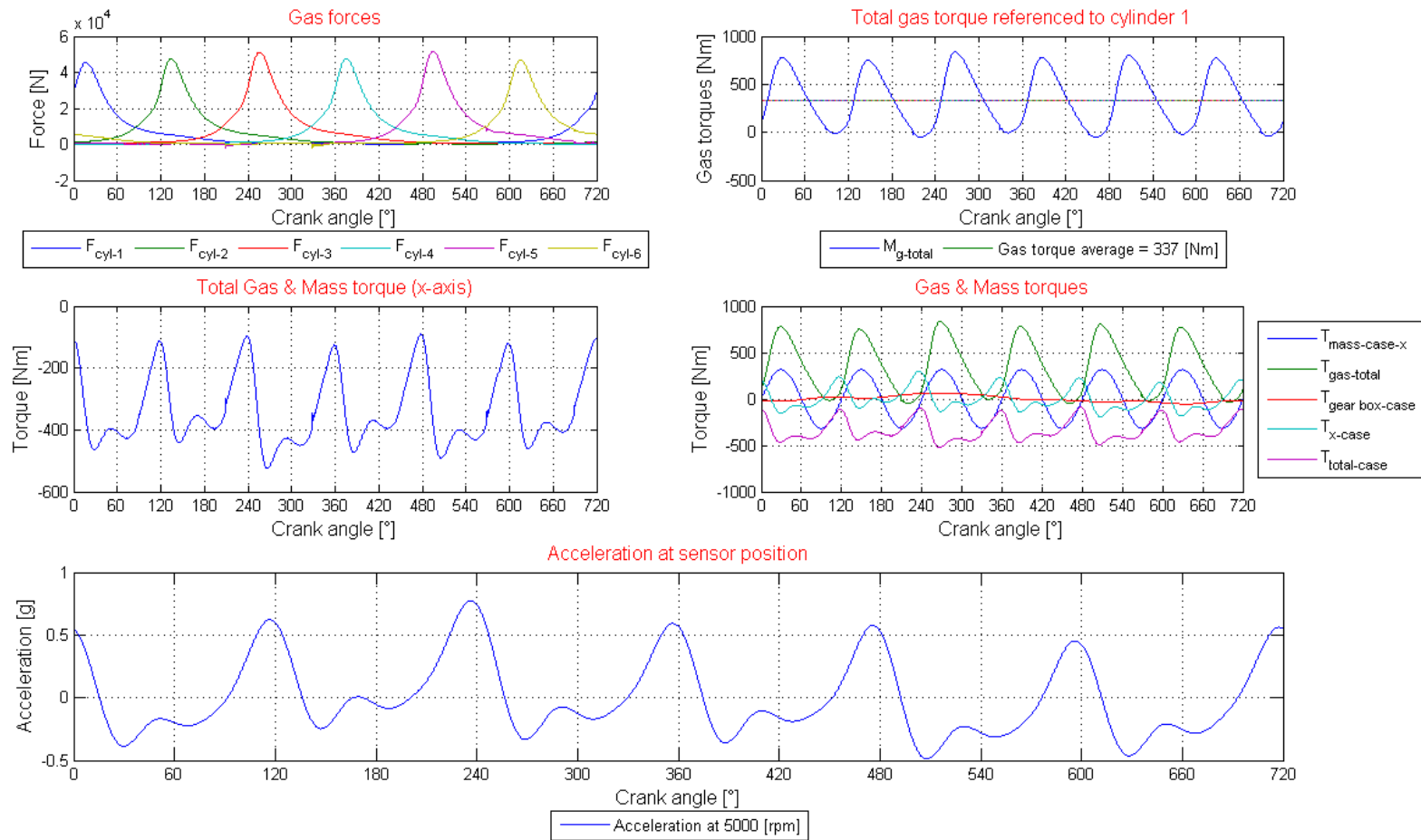


Figure 5-12 Overview of calculation steps from gas force to engine case acceleration if all cylinder work fine. Simulation was done at 5000 rpm.

5.3 Simulation results of a misfire event

In case of a poor burn process of one cylinder due to misfire certain signal components which are compensated in normal operation conditions will not further be compensated and uncompensated frequencies appear at the crankshaft. Misfire at one of the cylinder leads to a distorted waveform of the torque appearing at engine case.

This can be seen in Figure 5-14 and Figure 5-15.

However in Figure 5-14 it shows spectral components of the cylinder selective transversal forces versus 720° crank angle (one full 4-stroke cycle).

At cylinder 3 for example it can be seen that the signal magnitude is lower than that of the other cylinders with standard in cylinder pressures. For simulating a complete cylinder shut down the scaling factor for the in-cylinder pressure used in the analytic model was set to zero. As in this example, a complete cylinder shut down, the cylinder torque drawn below in Figure 5-13 (green line) will be applied for a proper cylinder torque characteristic. If this torque curve is applied instead of zero torque, a better system description which is similar to the engine will be reached.

In Figure 5-15 the third plot shows the result of the superposed signals from cylinder 3 and 6, which represents the corresponding pair of cylinders. It can be seen that more spectral components are present on the crankshaft compared to Figure 5-5. The most important spectral component for the misfire detection is the 0.5th engine oscillation mode. Later on it will be demonstrated that only the 0.5th engine oscillation mode is usable for the misfire detection and no other frequency can be used for that detection method, using an acceleration sensor.

The 0.5th oscillation mode is not compensated and shows very dominant signal power. Compared to the waveforms in Figure 5-5 (last plot) the spectral components show significant differences (number of oscillation modes and magnitude) which effect the engine case movement.

MODEL RESULTS AND SIGNAL PROCESSING

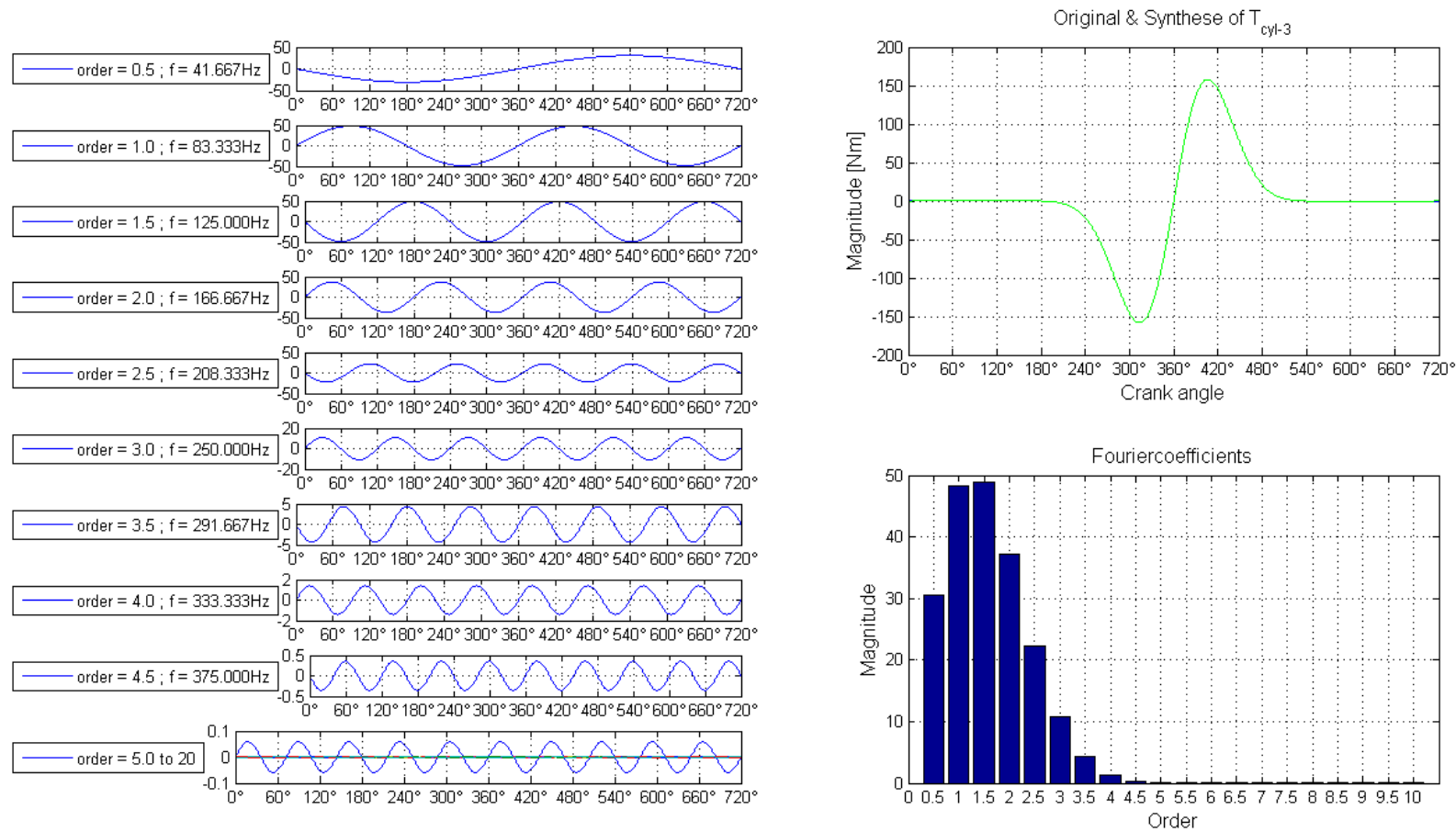


Figure 5-13 Spectral analyses of the crankshaft torque (green line) based on an analytic in-cylinder pressure characteristic.

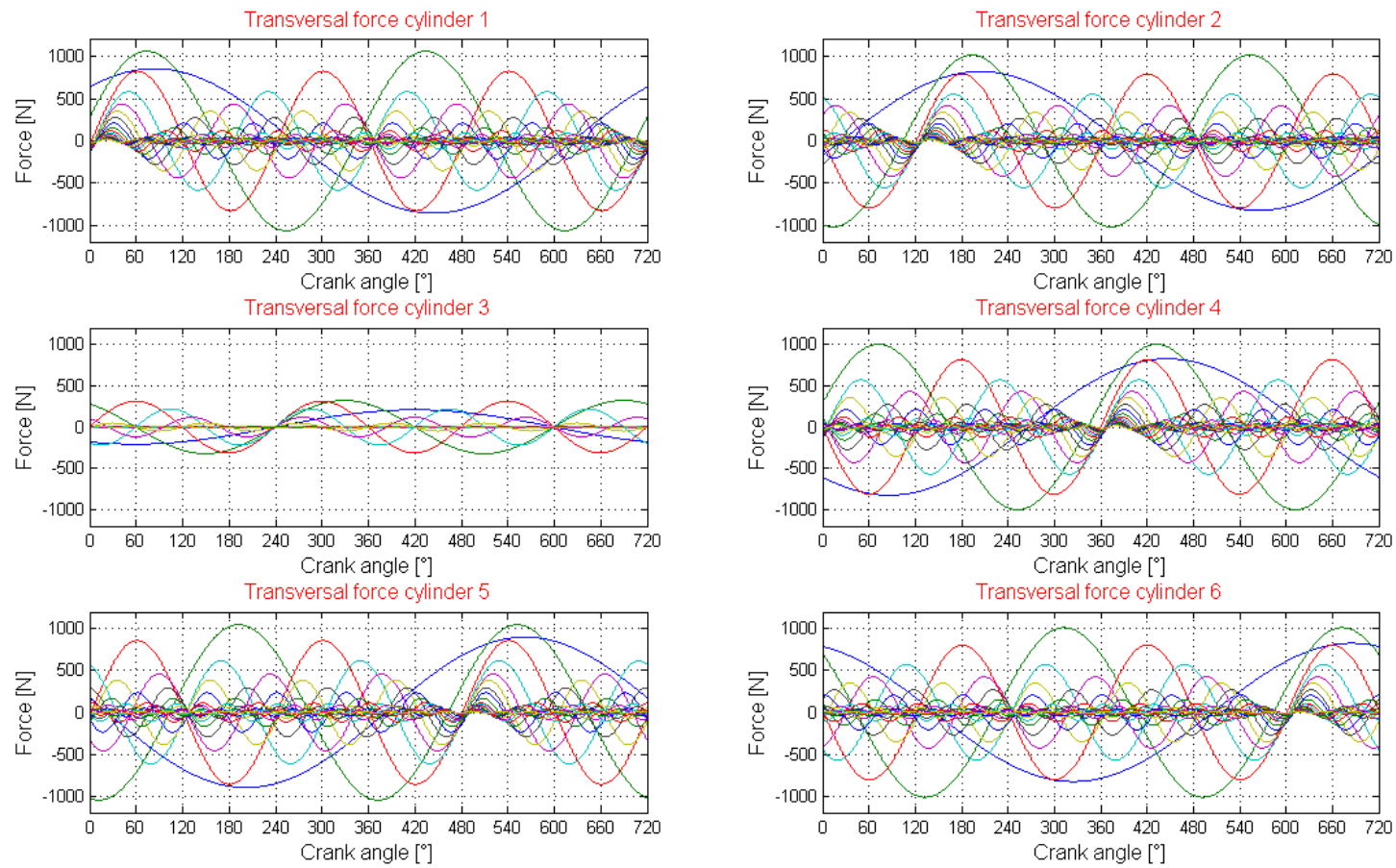


Figure 5-14 Overview of the cylinder selective spectral components with a simulated failure at cylinder 3.

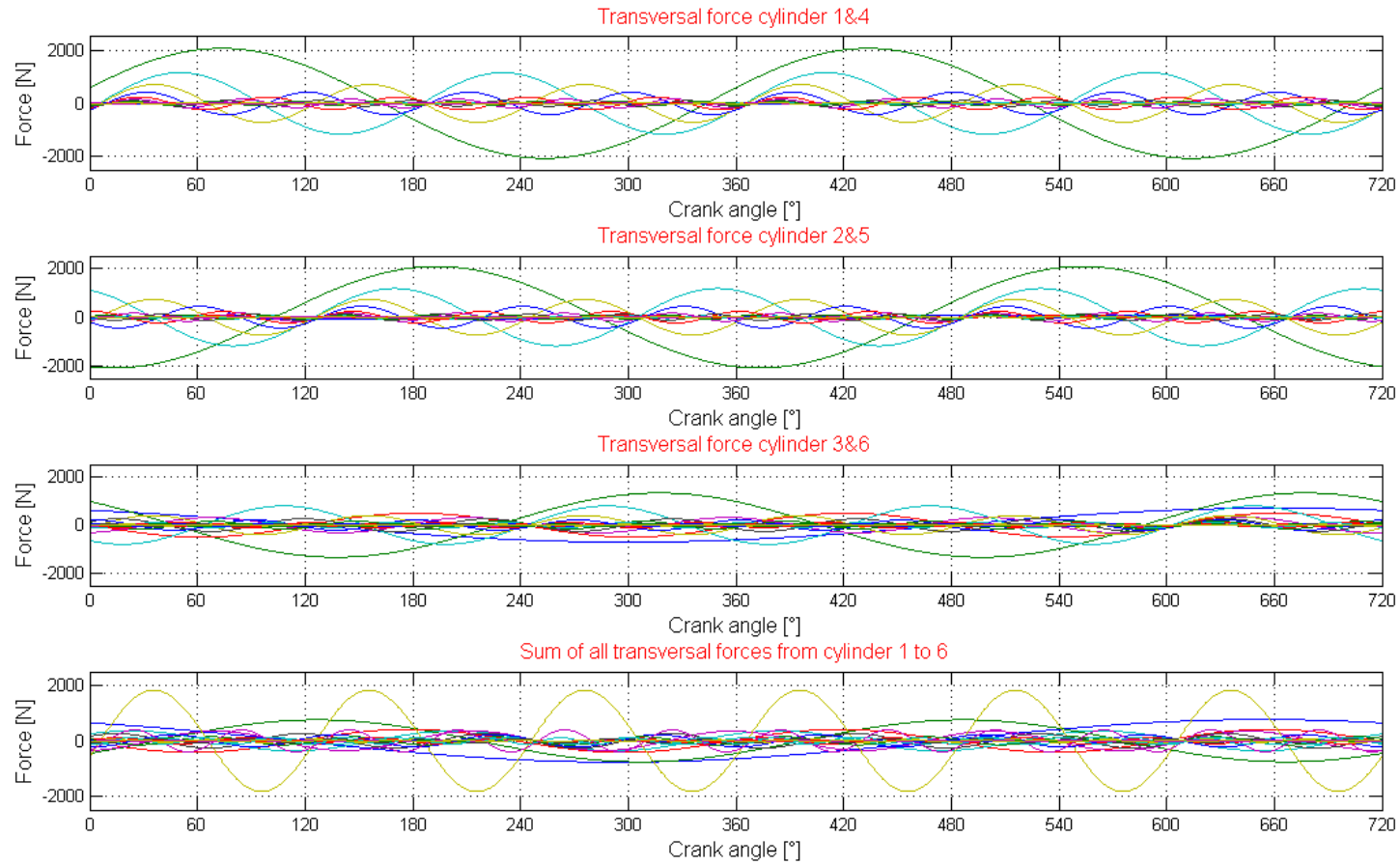


Figure 5-15 Spectral components of transversal forces of the corresponding cylinder pairs and the total sum at the crankshaft.

As mentioned above the next analytic step is to add the mass torque effects of the crank motion. The mass torque has to be added to the torques produced from the ignited air-fuel mixture.

The next calculation is the computation of the gear box torque. Before the proceedings of this step can be taken the system behaviour of the torsion bar has to be calculated.

The total crankshaft torque signal passes the torsion bar and in parallel the crankshaft torque appears on the engine block with negative algebraic sign (represents the engine block torque). The implementation of this system behaviour in the model was achieved by computing a spectral analysis of the crankshaft torque signal before passing the torsion bar.

The calculation of the torsion bar behaviour is completed in an away that for each spectral component of the crankshaft signal, the system behaviour of the torsion bar will be simulated. In the next step a superposition of the signal components will be ready. This leads to the total torsion bar output signal. Due to the frequency behaviour of the torsion bar the frequencies and further the whole engine behaviour will be affected dramatically especially at different engine revolutions.

The outcome of the torsion bar has completely different spectral components and signal amounts compared to the input. These frequencies appear as tooth force and further as gear box torque on the engine case and influence the engine case as explained above.

In Figure 5-16 the gas and mass torques are drawn. This chart shows the simulation result, in the case of cylinder 3, it is de-powered which is similar to an injector fault of this cylinder. The first chart (blue) represents the crankshaft torque coming from the gas force. The graph shows only 5 peaks over a torque of 500 Nm, as opposed to the six peaks an engine without failures would expect. The third peak is missing due to the simulated misfire event. By adding the mass torque to the crankshaft torque the total crankshaft torque is calculated. The result is printed in the middle. Also here the missing torque peak can be found. The last plot draws the engine case torque. It is equal to the total crankshaft torque but with negative algebraic sign. Figure 5-17 shows the result of the spectral analysis done at the total crankshaft torque. As mentioned in the chapters before, the spectral analysis shows a huge amount at the 0.5th engine oscillation mode. This can be seen at the bar diagram and also on the left hand side which represents the spectral components in magnitude and phase angle.

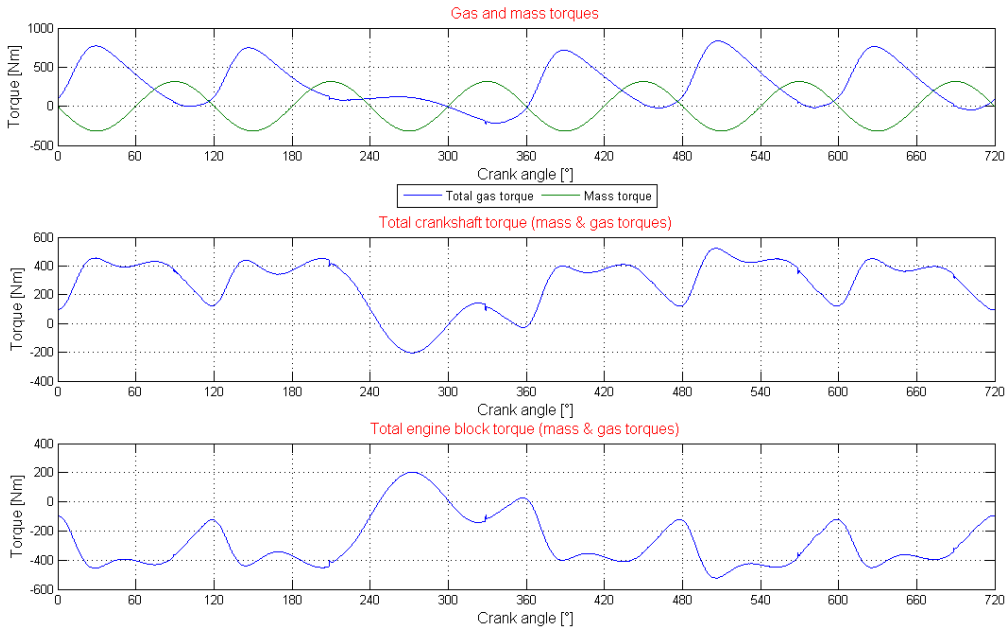


Figure 5-16 Gas and mass torques with simulated engine failure at cylinder 3.

MODEL RESULTS AND SIGNAL PROCESSING

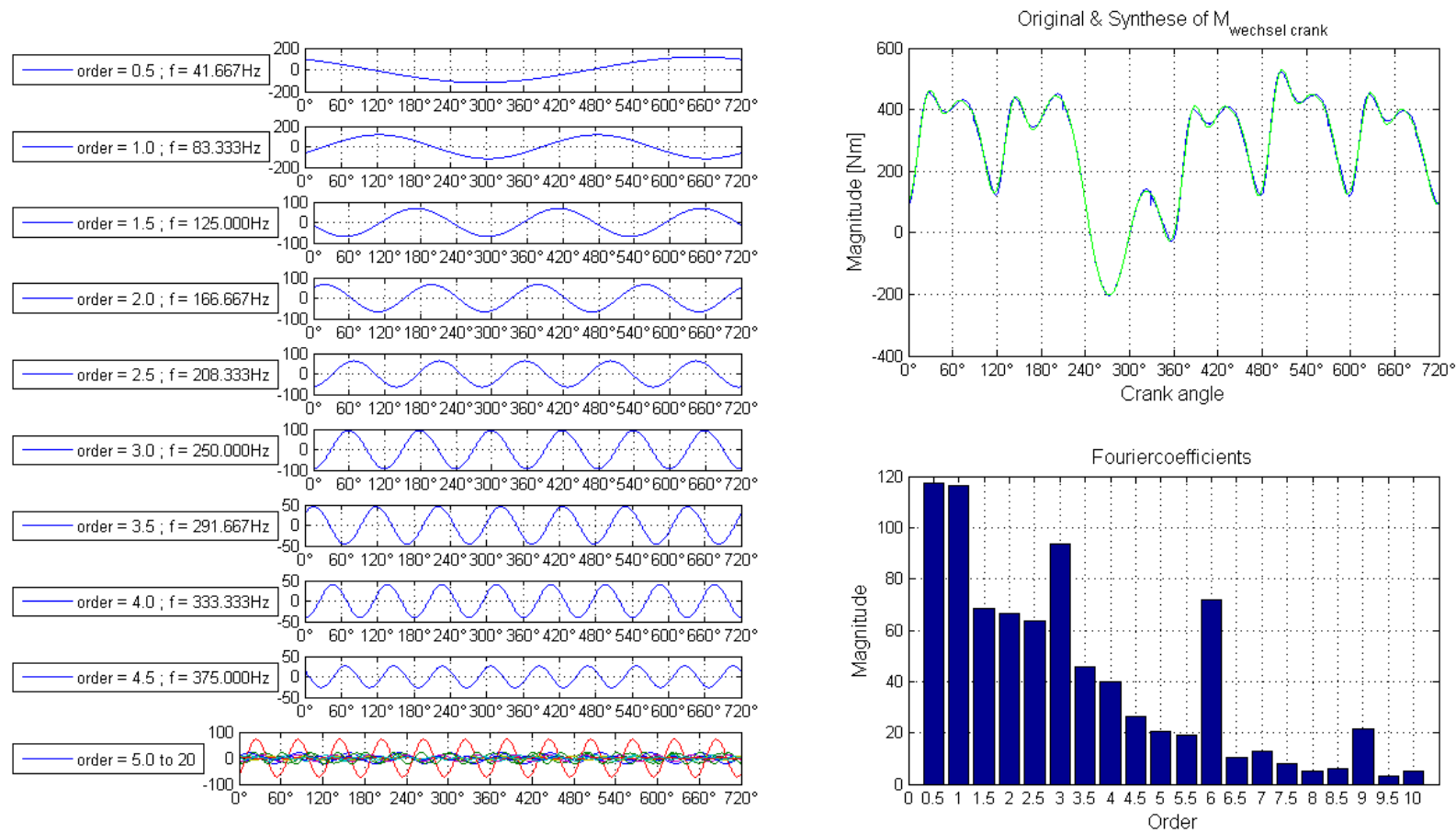


Figure 5-17 Spectral analyses of the total crankshaft torque with poor combustion process at cylinder 3.

In the next analytic model block the gear box torque is calculated. Figure 5-18 shows the simulation result of this calculation. Compared to Figure 5-7 the torque amount drawn in the chart below is quite high and rises up to about 700 Nm. At normal operation conditions the gear box torque was calculated of approximate 60 Nm.

This is the result of the non compensated spectral components in case of a poor burn process of one cylinder, which will be amplified by the torsion bar in combination with the gear box. A comparison of the torques at this stage between good and bad engine condition (no misfire or misfire) leads to a ratio of approximate by 1:10.

In Figure 5-18 the reaction on the engine case due to the gear box torque is drawn (green line). The spectral analysis shows that the main power of the frequency is concentrated in the 0.5th engine oscillation mode. It also shows the same result as mentioned above by having a good engine condition. All other signal components are quite low in magnitude which will not excite the heavy motor. But a comparison with Figure 5-7 shows differences in magnitudes especially at the 0.5th engine oscillation mode. The maximum torque value is also approximately 10 times higher compared to an engine without ignition failures. This is mainly driven by the gear box torque.

This torque magnitude at the 0.5th engine oscillation mode must not be ignored. Figure 5-19 shows the total engine case torque. It can be seen that the 0.5th engine oscillation mode is now dominant and contains the main signal power. A comparison with Figure 5-8 (good engine condition) results in a completely different analysis. The torque and the frequencies changed dramatically and the engine behaviour is affected by this change as well.

MODEL RESULTS AND SIGNAL PROCESSING

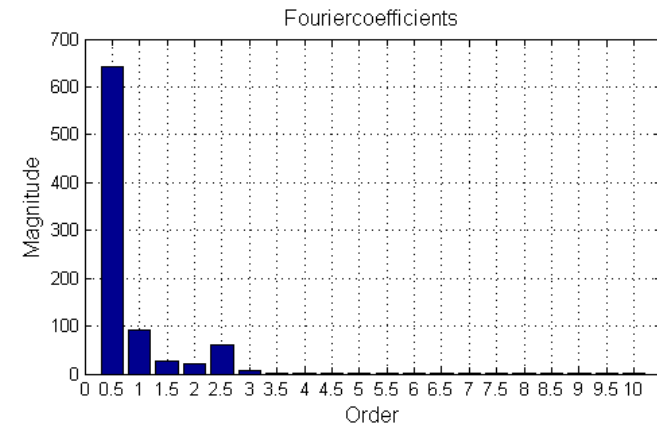
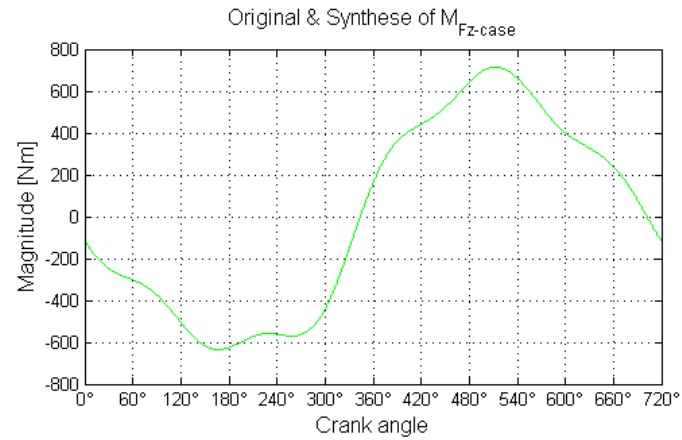
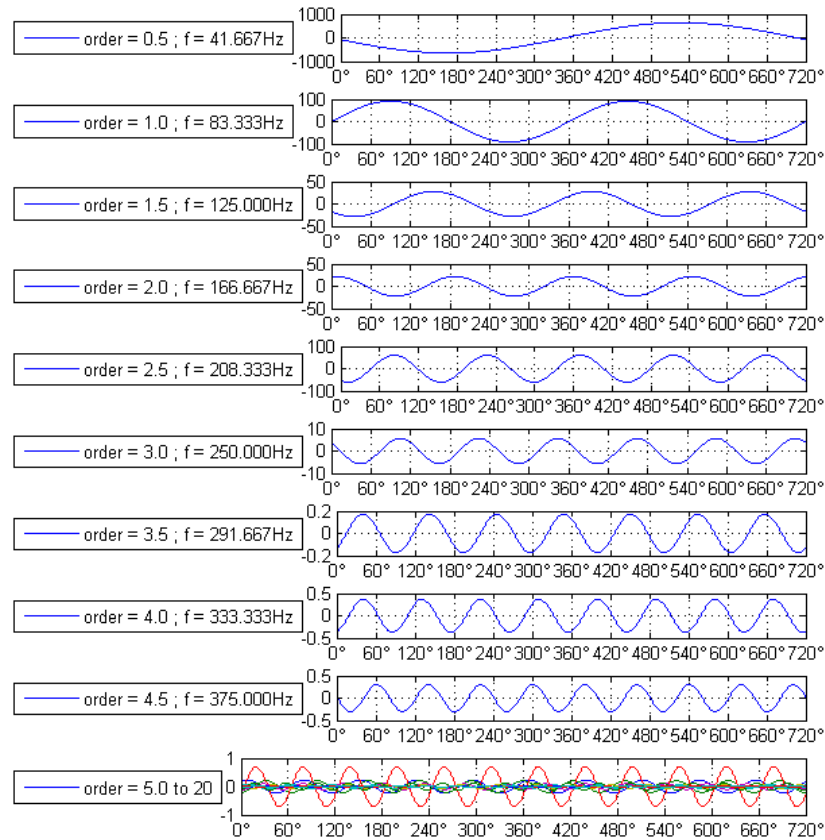


Figure 5-18 Spectral analyses of the influence to engine case due to gear box torque.

MODEL RESULTS AND SIGNAL PROCESSING

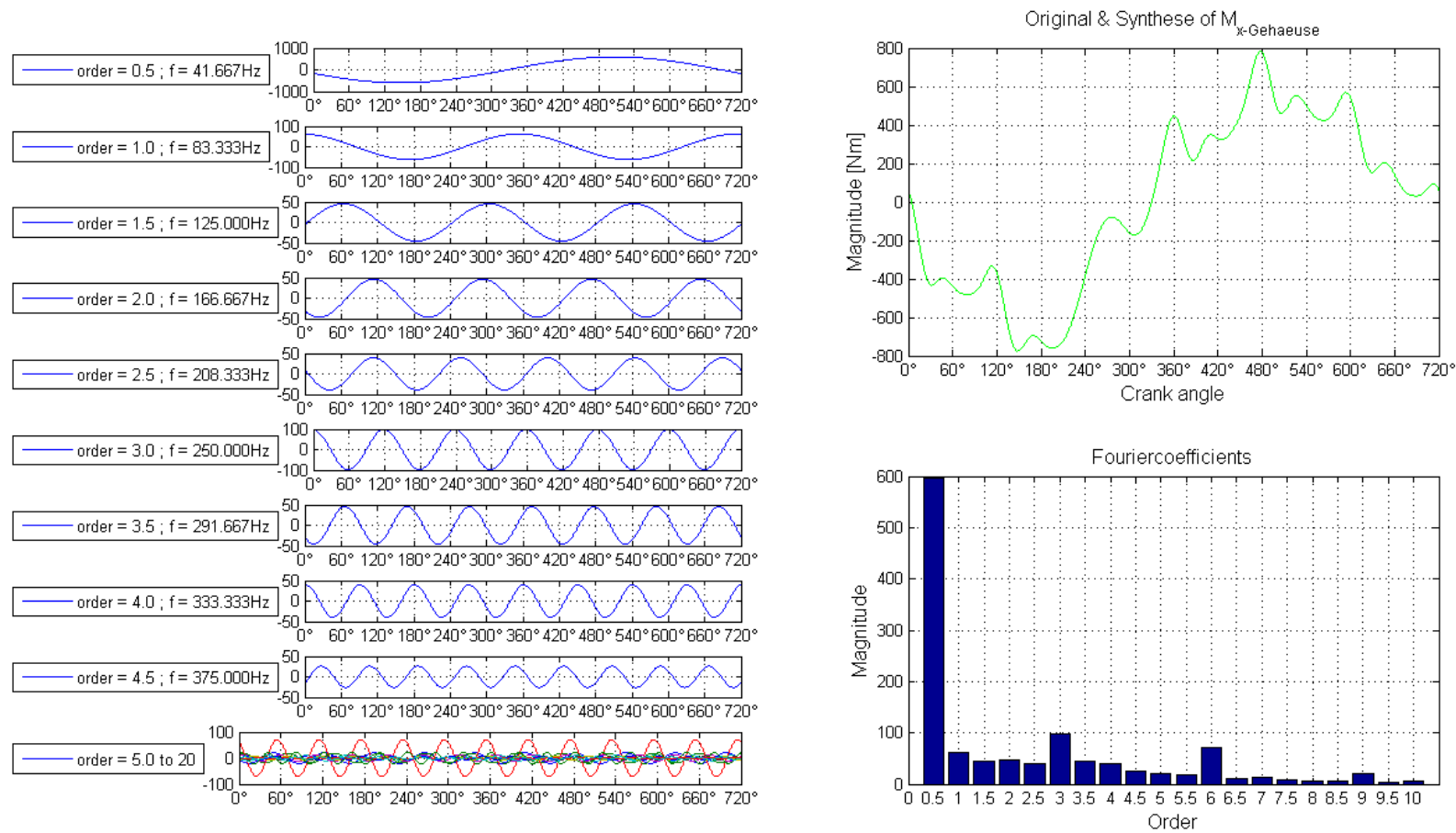


Figure 5-19 Spectral analyses of the engine case torque around the x-axis referenced to coordinate plane "CSYS centre of gravity".

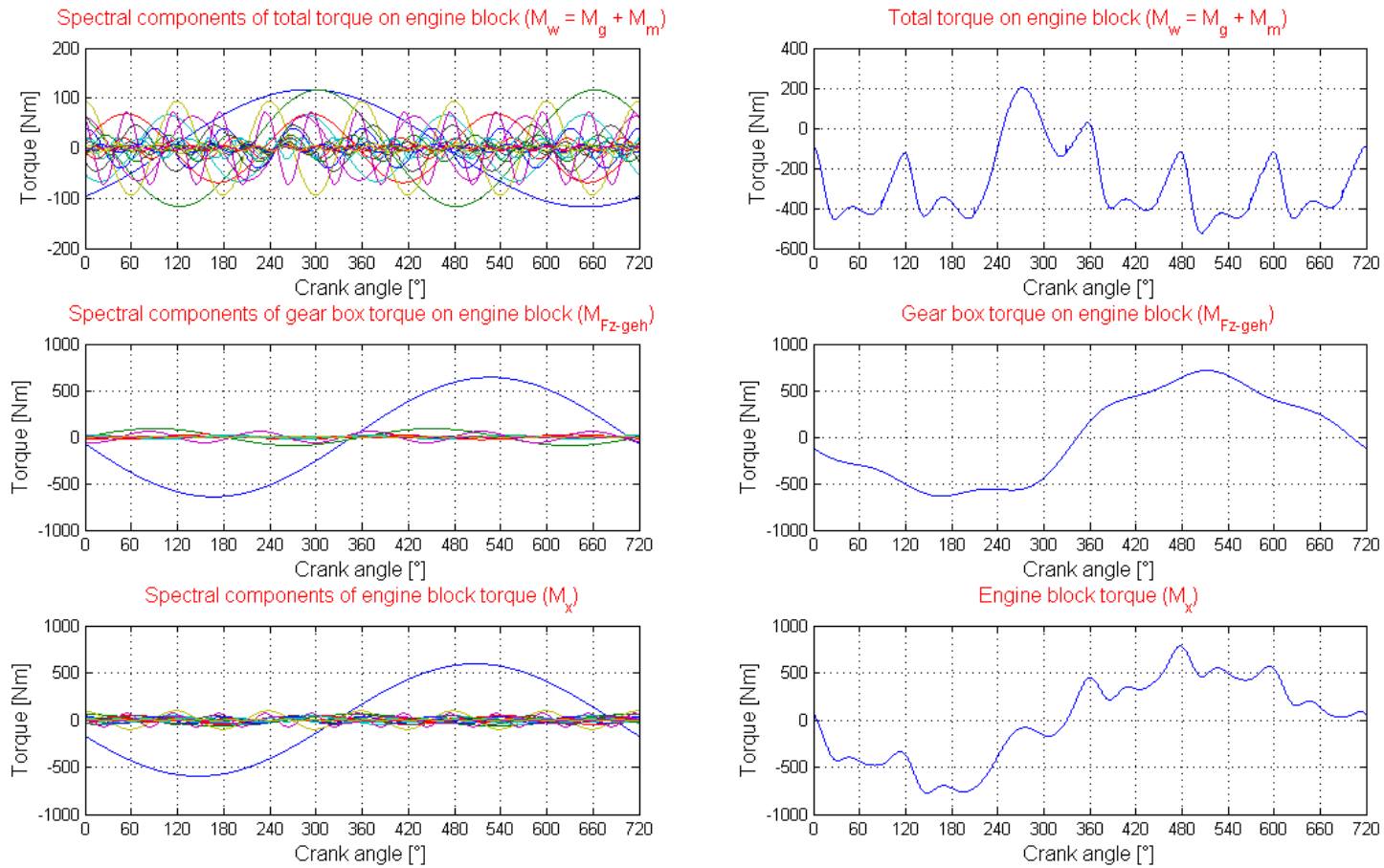


Figure 5-20 Frequency overview of the total crankshaft torque, the gear box torque and the engine case torque simulated around x-axis with the reference to "CSYS centre of gravity".

In the Figure above the most important calculation stages of the power train system are drawn. On the top the torque on the engine case is presented, in the middle the torque on the gear box and finally at the bottom the total engine case torque.

The left hand side represents all spectral components of the engine case. One of the most dominant engine oscillation modes is the 0.5th. This oscillation mode includes a lot of the signal power compared to that of a good engine (Figure 5-9). With the engines without misfire, this oscillation mode is more or less not present because of the compensation of the cylinder pairs. In the middle, left hand side, the result of the spectral analysis of the gear box torque is shown versus crank angle. Also on the left hand side at the bottom the analysis result of the whole engine case movement (torque) is printed. The 0.5th engine oscillation mode is dominant as well. A slight phase shift compared to the gear box torque can be seen.

Next the most important signals of the power train system are represented. Same signal as mentioned in Figure 5-10 but under closer inspection of the 0.5th oscillation mode big differences can be found. The torque on the gear box (green line) shows a complete different picture as that of the torque of an engine without failures. Also the abnormal peak of the red signal which represents the torque on the engine case is significant for the misfire event.

As explained before it is not necessary to know the exact position of the acceleration sensor on the engine block. To have a common understanding of all simulation results, additional the expected acceleration of the engine case with consideration to the sensor position is printed. The result can be seen in Figure 5-22. The peak magnitude of the 0.5th oscillation mode of the acceleration signal is at least 15 times higher compared to a good engine (see Figure 5-11).

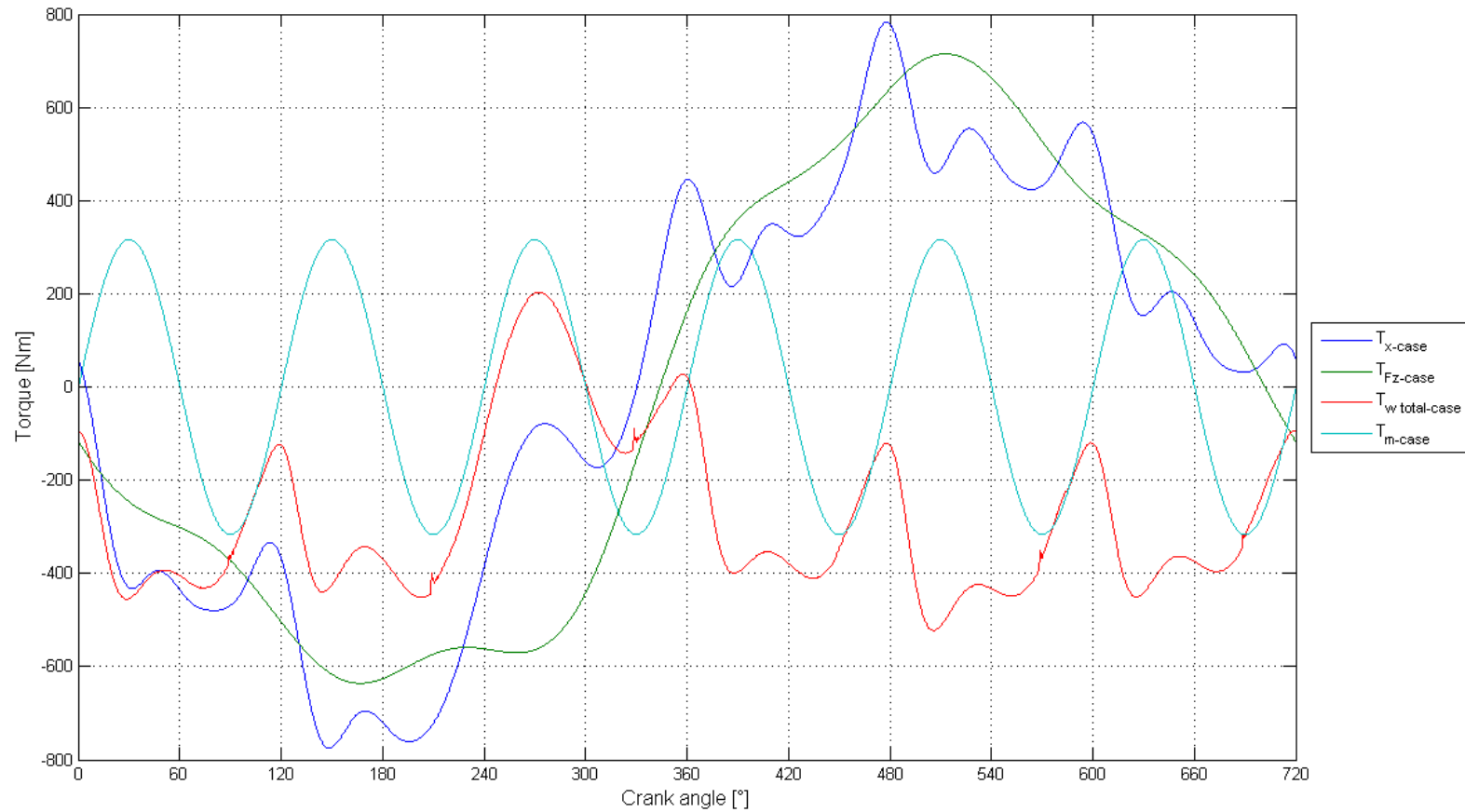


Figure 5-21 Torque signals on the engine case in x-direction referenced to coordinate plane "CSYS centre of gravity". Gear box torque, total crankshaft torque simulated on the engine case and mass torques on engine block.

MODEL RESULTS AND SIGNAL PROCESSING

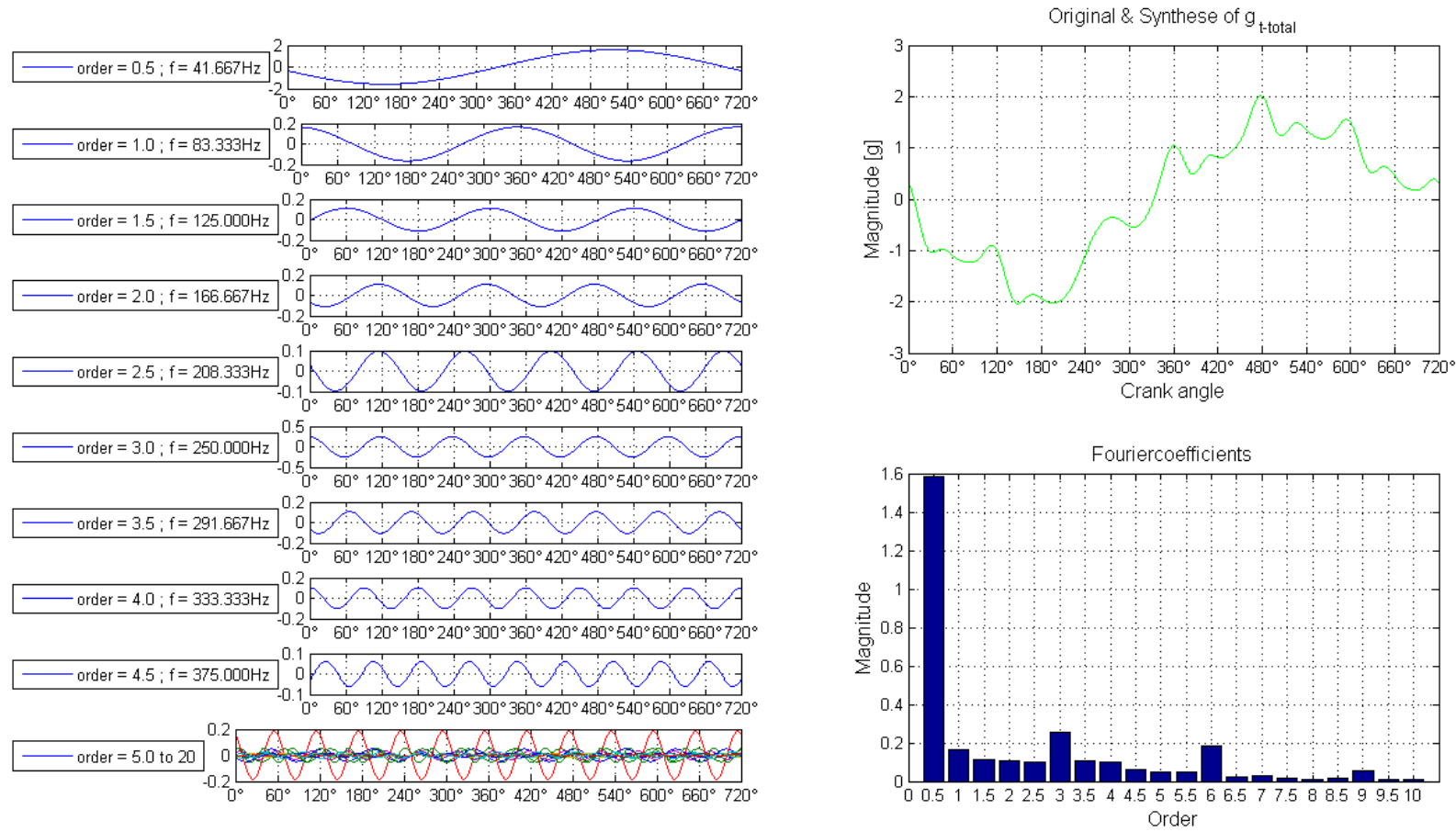


Figure 5-22 Spectral analyses of the engine block excitation in case of misfire.

In the next figure (Figure 5-23) the influence of a faulty cylinder on the engine case movement will be explained step by step. As mentioned in the model overview the calculation of the simulation starts with the in-cylinder pressure. This can be seen on the left hand side first column.

This chart shows missing in-cylinder pressure at cylinder 3. Only the compression pressure (red line) of the cylinder is applied.

Over to the right the gas torque and the average torque are printed. Also on this graph the missing firing event can be noted.

The next picture, in the middle left hand side, shows the calculated total gas and mass torques on the engine case. The peak on the third cylinder represents the misfire event. If a spectral analysis of the inverted engine block signal (representing the crankshaft torque) is completed, the gear box input signal and the total engine block torque can be calculated. This leads to the signals represented in the middle right hand side.

Finally the last plot shows the result simulated on the acceleration sensor positioned on the engine block. At 5000 rpm the acceleration peak is approximately 2g compared to the acceleration signal without cylinder failures which results in 0.5 g. Due to the frequency behaviour of the system the acceleration peak changes by changing the engine speed. This behaviour is mainly driven by the torsion bar and can be seen in Figure 3-8.

This simulation peaks at an approximate maximum of 4200 rpm; this means the maximum torque on the torsion bar will be expected at this engine speed. This knowledge is important for further engine analyses and the observation or predictive maintenance of the mechanical parts installed inside the engine.

MODEL RESULTS AND SIGNAL PROCESSING

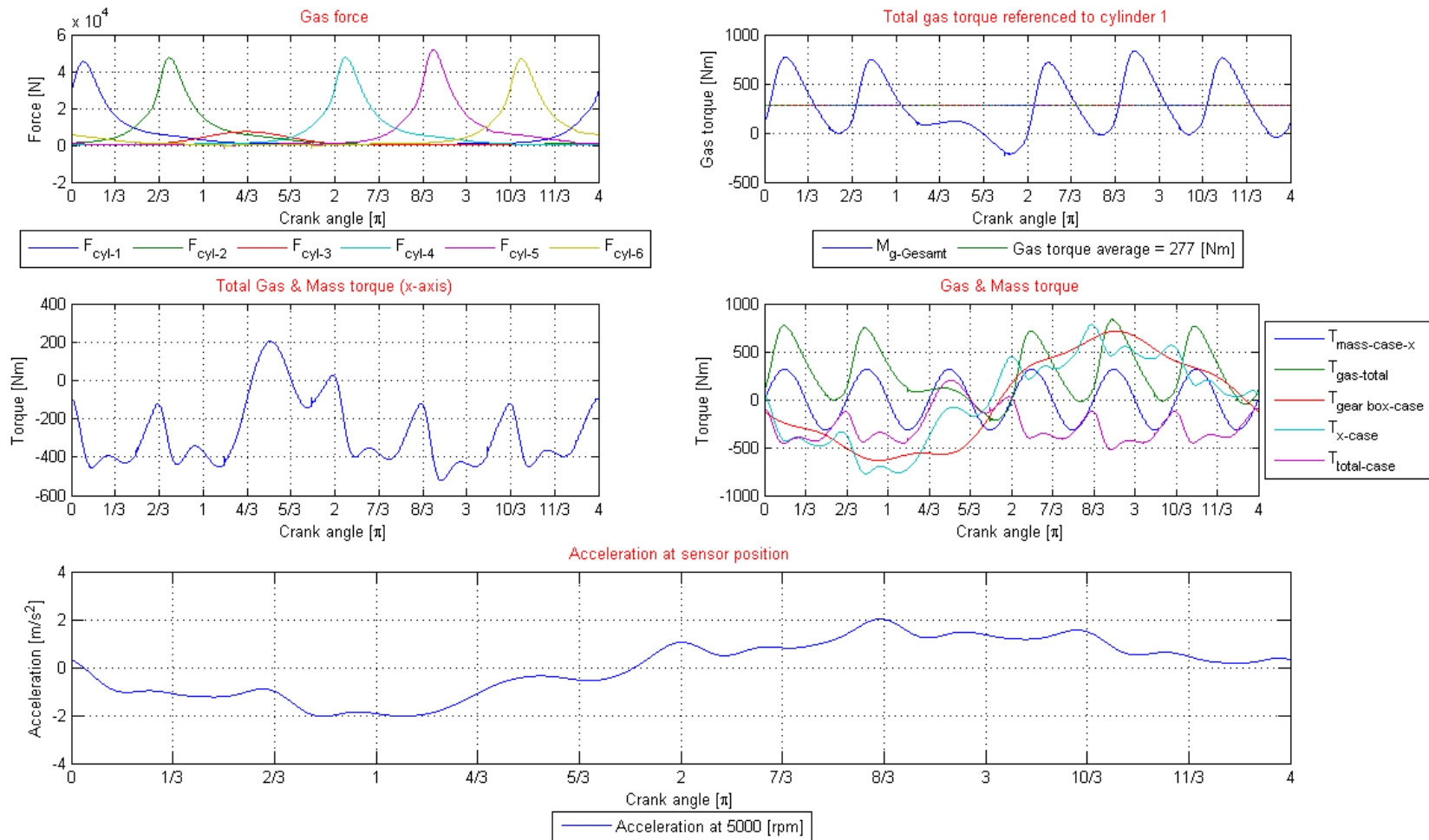


Figure 5-23 Overview of calculation steps from gas force to engine case acceleration if cylinder 3 is switched off.

6 SIGNAL PROCESSING

6.1 Fuzzy based engine health condition system

[51] Describes fuzzy based fault diagnosis for aircraft applications. An extension of this existing method with an additional acceleration sensor was described in [23].

"This paper describes a method for monitoring the condition of reciprocating aircraft engines. In contrast to existing solutions our method is based on information from a single acceleration sensor attached onto the motor block. Model based signal processing using modal analysis and fuzzy logic in a hierarchical estimation scheme enables the possibility to observe engine health level. For each cylinder of the reciprocating system misfire detection and the identification of combustion failures on a per cylinder basis is possible."

The condition monitoring system is based on information of engine case movement delivered by a single possibly low-cost acceleration sensor attached to the motor block. The exact location of the sensor with respect to the engine case is not essential for the monitoring process – only the sensor orientation with respect to the centre of gravity of the engine is important.

In addition to the information of the engine case torque delivered by the acceleration sensor, the signal processing chain also needs information about the actual crankshaft angle as provided by the built-in crankshaft sensor. Since crankshaft angle information is essential for engine operation, controlled by the “*engine control unit*” (ECU) in modern combustion aircraft engines, such sensor data is always available for free.

The first step in the hierarchical data processing chain as sketched in Figure 6-1 is the change of the sensor signals to the digital domain by anti-aliasing filtering followed by A/D-conversion. The useful bandwidth of the engine acceleration sensor signal is between 0...400Hz leading to a sampling frequency of 1 kHz for practical aircraft drive scenarios. The digitized acceleration signal $[n]$ is then fed into FFT-based order analysis, where the acceleration signal is analysed in terms of power estimation for relevant engine orders using the available crankshaft angle information.

Since the most important engine oscillation mode to be evaluated for estimating cylinder health condition is order 0.5, the smallest window length is given by the duration of two full engine turns (i.e. a full combustion cycle of the 4-stroke engine).

The last step in the signal processing chain is the evaluation of the time evolution of signal power in certain engine orders. These expert step is carried out in the Fuzzy based health estimation process, leading to a cylinder health condition in arbitrary units and binary misfire conditions “OK” and “NOT OK” for each monitored cylinder.

The Fuzzy system uses overall signal power and the signal power of 0.5th engine order from order analysis step as input variables. After fuzzification to linguistic variables using triangular and sigmoid membership functions, six rules are used to estimate the cylinder health condition linguistic output variable. Defuzzification based on centre of area leads to the output value quantizing engine health condition between values from ‘0’ for ‘NOT OK’ to ‘1’ for ‘OK’. The obtained characteristic input-output field for the developed fuzzy system is shown in Figure 6-2.

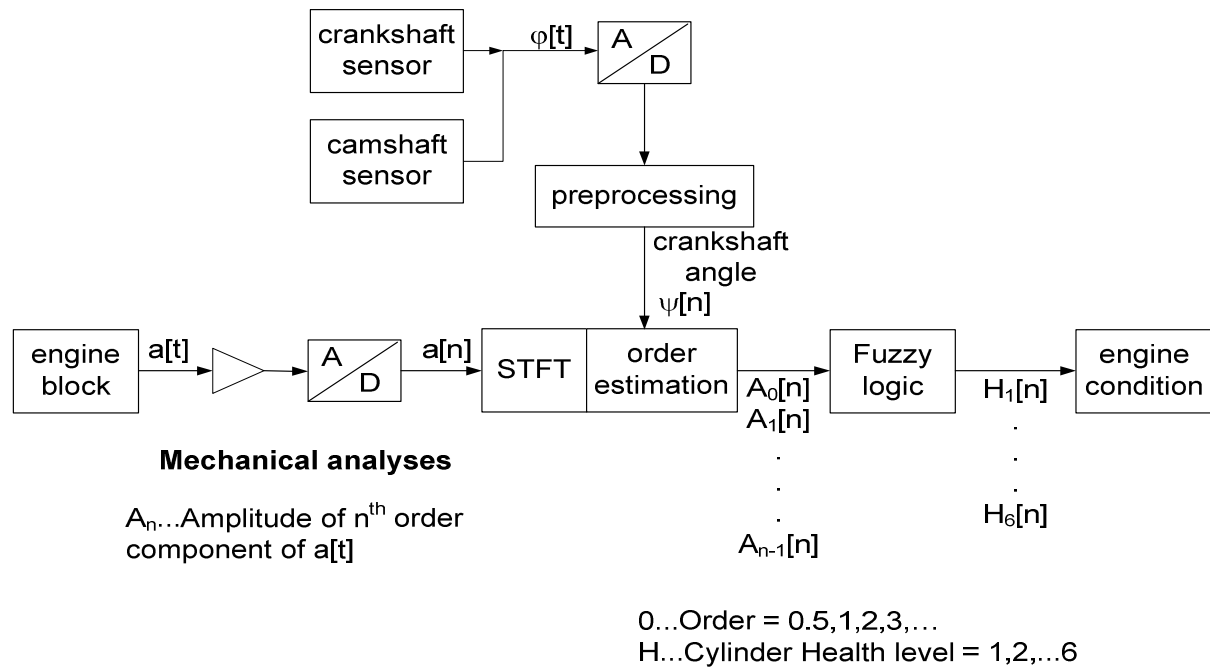


Figure 6-1 Hierarchical data processing chain of a fuzzy based condition monitoring system.

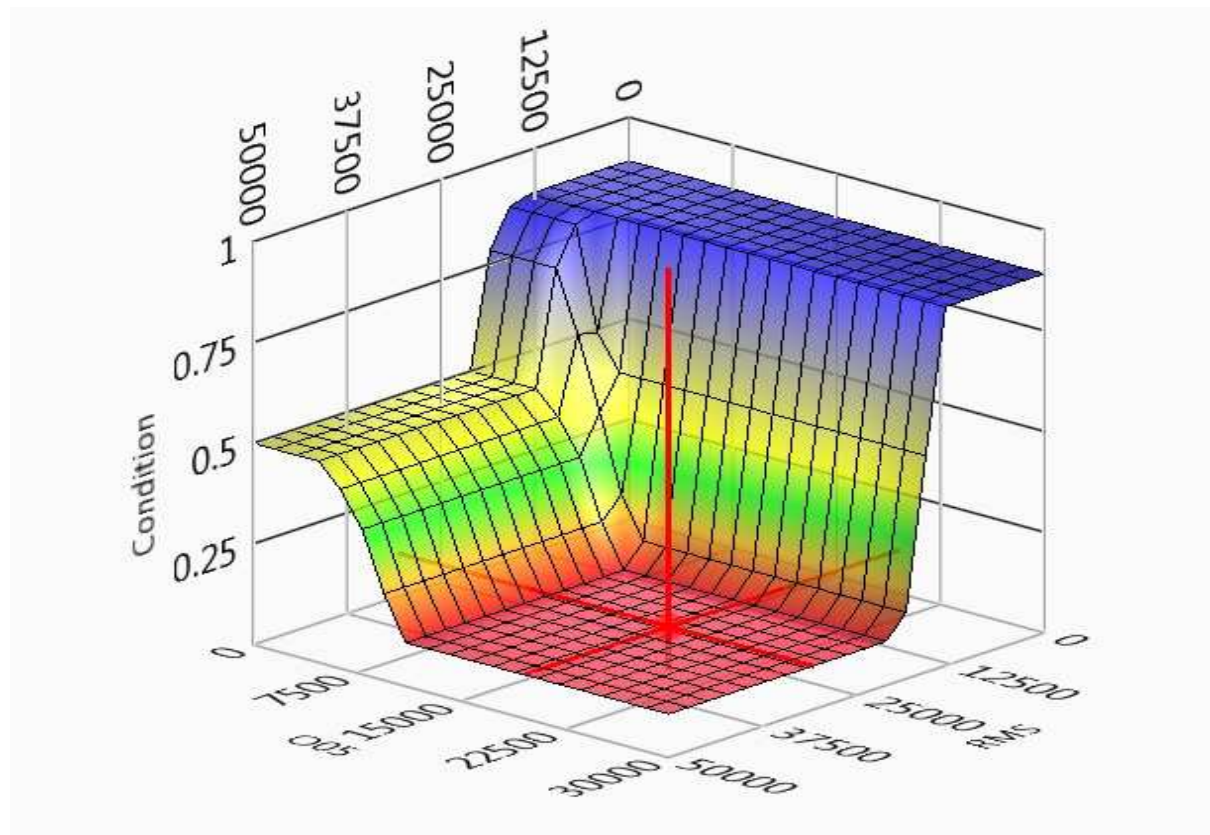


Figure 6-2 Fuzzy map for health level estimation.

Figure 6-3 shows condition monitoring results from a real world field test. During this test a single cylinder failure has been simulated by disabling and enabling the injector associated to a single cylinder. A shut down of an injector results in a very lean fuel-air mixture formation and the combustion process for the corresponding cylinder is stopped. The upper plot in Figure 6-3 shows the evolution of the overall signal power and the signal power in engine oscillation mode 0.5 over the test cycle. Using the Fuzzy based estimation scheme, the engine health condition can be estimated in a very robust and fast manner. During all field tests the simulated failures have been detected immediately and robustly. If the manipulated injector has been switched on again, the engine works in normal operation condition and the calculated health level switched back to the normal level (lower plot in Figure 6-3).

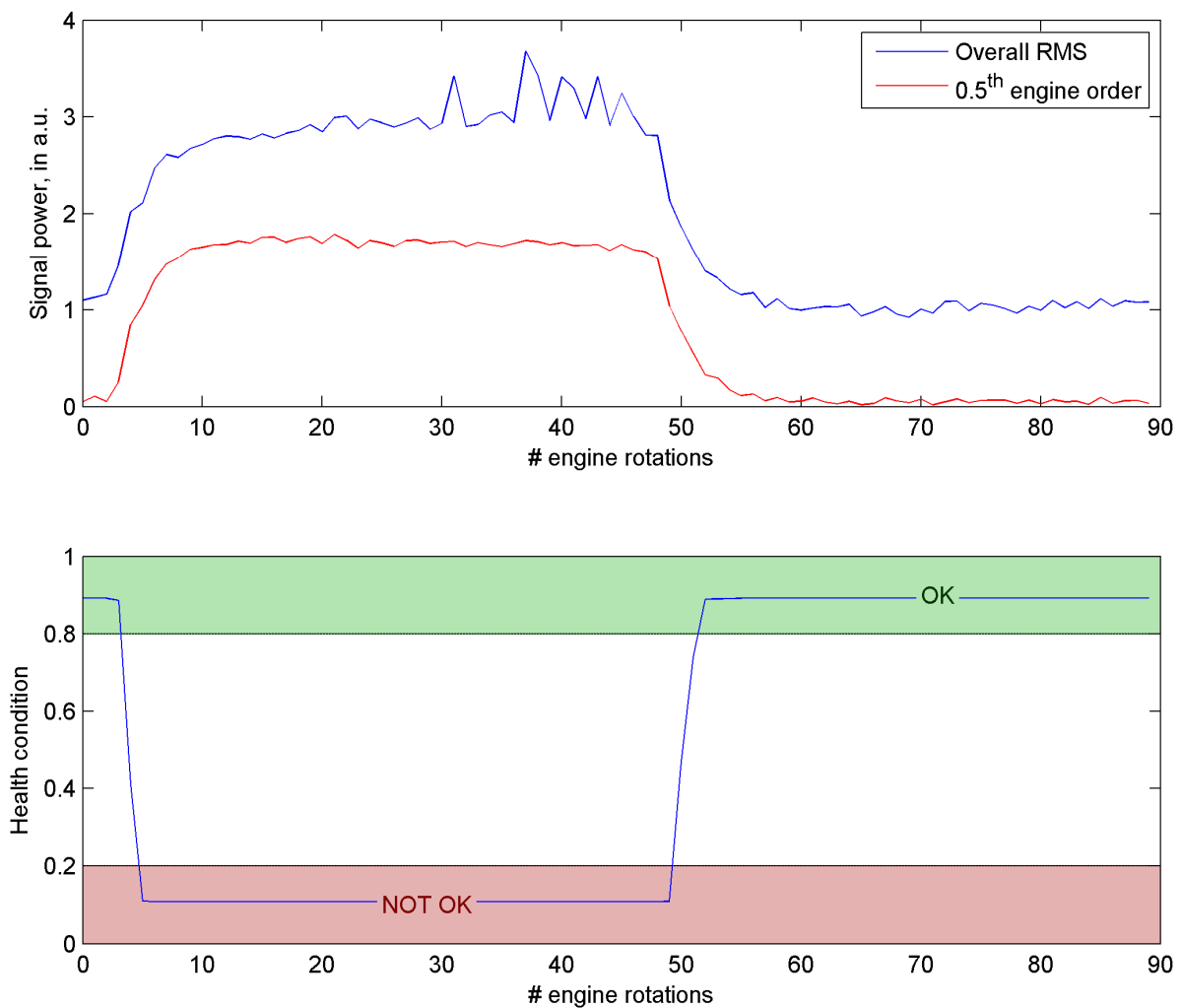


Figure 6-3 Condition monitoring results from a real world field test. Upper plot: Acceleration signal power from real world experiment: time evolution of overall signal power and signal power in order 0.5 for cylinder 1 being disabled and enabled. Lower plot: Engine condition health level from Fuzzy-based engine condition estimation.

6.2 Model based condition monitoring

Due to the analytic model, simple signal processing algorithm can be applied. It can be shown that only the 0.5th engine oscillation mode is usable to detect in-cylinder pressure losses and locate the faulty cylinder by using the proposed detection method. This can be seen later on in Figure 6-8 to Figure 6-12.

One proposed detection algorithm to discover a reduced engine health level, which means a pressure loss in one of the cylinders, was published in [23]. In this paper a method was described how a failure on the engine, which is related to an in-cylinder pressure failure, can be found.

A second tested signal processing method was the “*empirical mode decomposition*” (EMD) algorithm [27]. This algorithm was developed for non stationary signals and it is applicable on LTI system, which this thesis assumes. The EMD algorithm splits the signal in a set of oscillating modes called “*intrinsic mode functions*” (IMF). In the next analysis the Hilbert transformation will be calculated. The amplitude and the phase angle information are the output of the Hilbert transformation. This would be exactly the information which is needed to detect misfire and to locate a defect cylinder.

In order to investigate the performance of different signal processing methods the EMD algorithm was applied on a vibration signal coming from a faulty engine with misfire. Analysing the vibration signal with the EMD algorithm could indicate an in-cylinder pressure loss.

Using the EMD algorithm (without modifications) for misfire detection, signal acquisition length and sampling rate have to be considered. Simulations showed differences in results coming from changes as mentioned above.

In order to prevent misinterpretations expert knowledge of the EMD algorithm and detailed system information are required.

Figure 6-4 and Figure 6-5 show the calculated results by applying the EMD algorithm on a measured vibration signal with a simulated in-cylinder pressure loss at cylinder 1.

Figure 6-4 represents the calculated signals (imf 1 to 11) with a signal length of 10000 sampling points.

In Figure 6-5 the computed results of the same vibration signal but with different signal length (15000 sampling points) can be seen. The signal imf 7 shows signal changes (magnitude and frequency) in a range between sampling point 12000 and 14000 which leads to possible misinterpretations. With expert knowledge a failure indicator for misfire events could be derived by observing the effected intrinsic mode function.

At this example (see Figure 6-4) the misfire event can be discovered by monitoring the signal imf 7. As soon as an in-cylinder pressure loss was simulated by deactivating the associated injector the waveform of the signal imf 7 changes to the 0.5th engine oscillation mode.

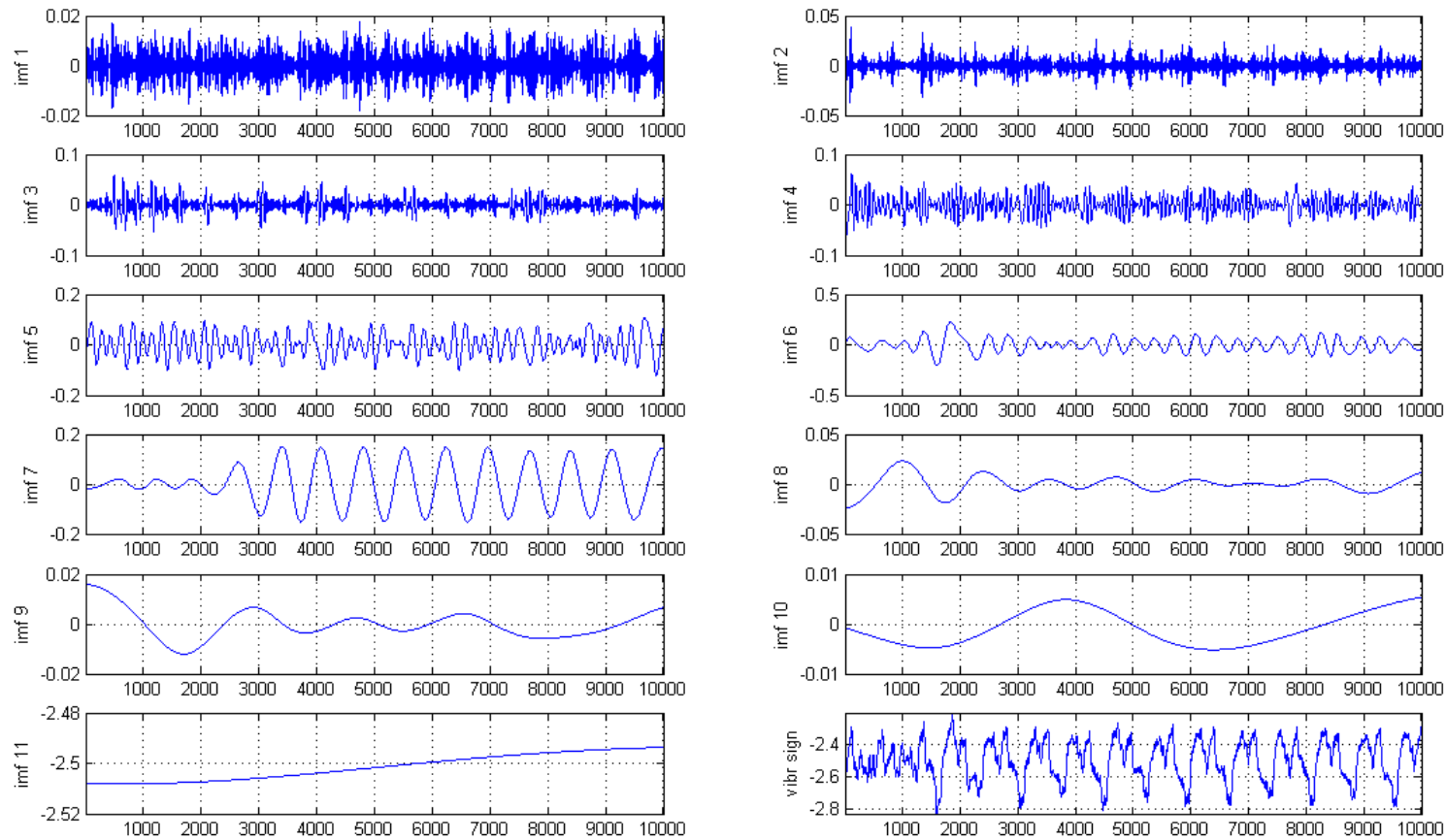


Figure 6-4 EMD results. Calculated intrinsic mode function (IMF) and measured vibration signal coming from engine tests with cylinder 1 deactivated. Engine was operated at 2500 rpm. Bottom right hand side the vibration signal is shown. Imf 1 to imf 11 represents the intrinsic mode functions derived from the vibration signal (vibr sign) with a signal length of 10000 sampling points.

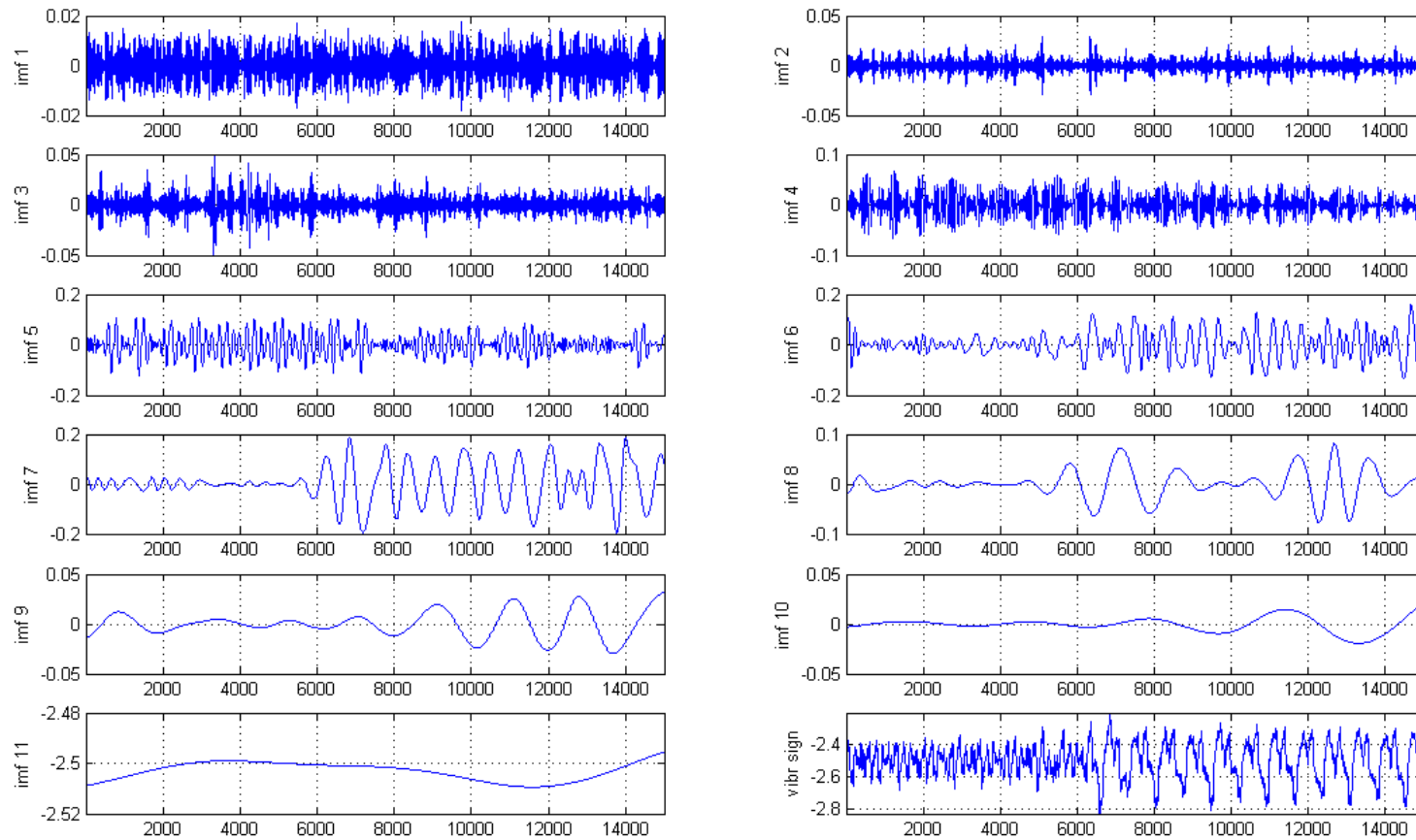


Figure 6-5 *EMD results. Calculated intrinsic mode function (IMF) and measured vibration signal coming from engine tests with cylinder 1 deactivated. Engine was operated at 2500 rpm. Bottom right hand side the vibration signal is shown. Imf 1 to imf 11 represents the intrinsic mode functions derived from the vibration signal (vibr sign) with a signal length of 15000 sampling points.*

A simple observation method is to calculate the magnitude of the signal power of the 0.5th oscillation mode and the sum from oscillation mode one up to the 10th.

By calculating a failure indicator $m_{(failure)}$ via computing the ratio of both signals a bad engine condition can be detected.

The magnitude of the failure indicator can be calculated as followed.

$$m_{(failure)} = \frac{T_{(0.5^{th})}}{\sum_1^{10} T_{(i)}} \quad (6.1)$$

Proposed decision rules:

If the failure indicator $m_{(failure)}$ is lower or equal one $m_{(failure)} \leq 1$ the engine works well.

If the failure indicator $m_{(failure)}$ is greater than 1 $m_{(failure)} > 1$ misfire will be detected.

The results of the proposed algorithm are shown in Figure 6-6 and Figure 6-7.

The first picture represents a normal engine condition without failures on cylinders and the second shows a simulated cylinder failure. As mentioned in previous chapters it can be seen that the signal power in the 0.5th engine oscillation mode is quite low at normal engine conditions. The differences in magnitudes of oscillation mode one and the sum of the others are significant.

The magnitude of the signal power of oscillation modes one to the 10th is at least 4 times higher than the magnitude of the 0.5th oscillation mode.

In Figure 6-7 the magnitudes are completely different to the picture below. The peaks of the oscillation modes 1 to 10 are higher compared to the normal engine condition. This behaviour is also affected by a misfire event but cannot be used for the misfire detection algorithm because there is no relation traceable to the in-cylinder pressure.

In case of in-cylinder pressure loss the 0.5th oscillation mode rises higher than the sum of the other oscillation modes. Most of the signal power is located in this engine oscillation mode. This makes it possible to distinguish between a normal engine condition and a faulty engine with a failure on one of the cylinders.

The variable $m_{(failure)}$ can be used for the health level calculation of the engine. A healthy engine has a level lower than one. If this indicator changes the probability of a failure on the engine which is related to an in-cylinder pressure loss increases.

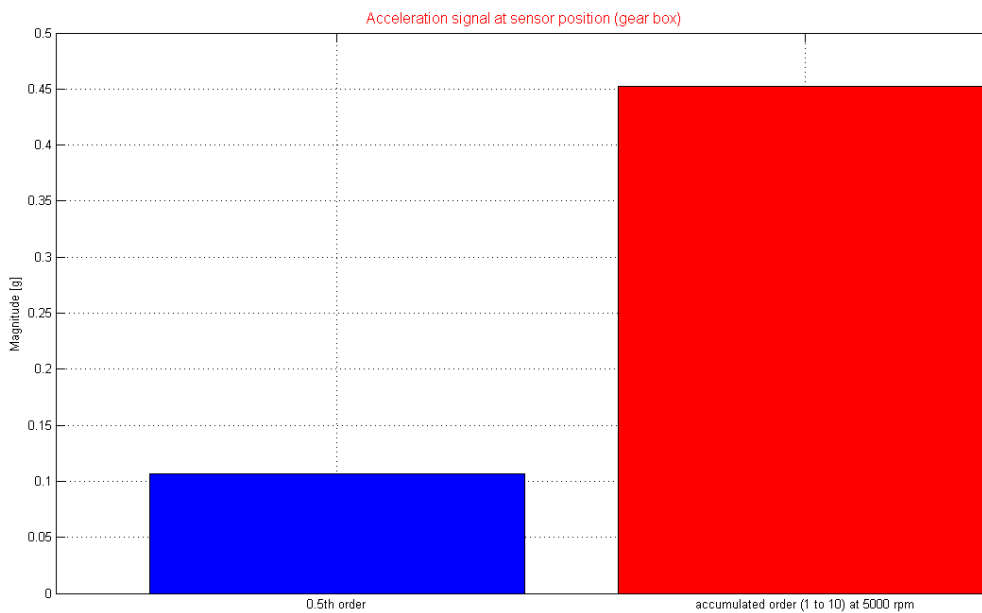


Figure 6-6 Computation of the signal power with no engine faults. The blue bar represents the 0.5th engine oscillation mode and the red the sum from 1st to 10th.

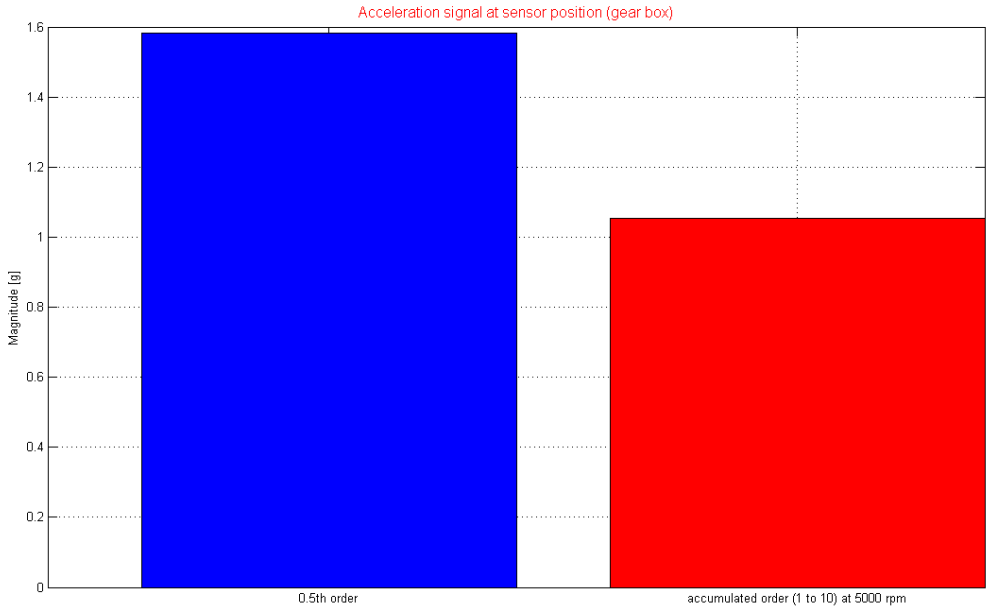


Figure 6-7 Computation of the signal power with engine faults (misfire). The blue bar represents the 0.5th engine oscillation mode and the red the sum from 1st to 10th.

In Figure 6-8 the magnitudes of certain engine oscillation modes of all cylinders are plotted versus engine speed. It can be seen that all cylinders have more or less the same peak value at one engine oscillation mode. Due to this fact a failure on a cylinder can't only be detected by a computation of the magnitude information. It would be quite impossible to explain a cylinder by an observation of the disturbance magnitude. But the peak signal information can be used as a pre-indicator for a faulty engine. Which cylinder fails must be calculated by a further signal processing step. This will be covered later on.

For example in Figure 6-9 the amplitude of the 0.5th engine oscillation mode is printed. It can be seen that the differences on the vibration amount is too low for a robust detection method with high probability rate to find a faulty cylinder. In the drawings it can be seen that the first peak at approximate 1000 rpm is not in the normal operation range and occurs during the starting transition phase. The maximum peak shown at approximate 1800 rpm represents the detection limit of this detection method. This can be seen in Figure 6-12 as well.

As already explained the peak values of certain engine oscillation modes related to cylinders are more or less equal.

Figure 6-10 represents the 0.5th oscillation mode of all cylinders in case of a failure. Due to the similar vibration curves it is not possible to find the affected cylinder which is responsible for the engine fault. This behaviour can be measured and simulated at the other engine oscillation modes as well.

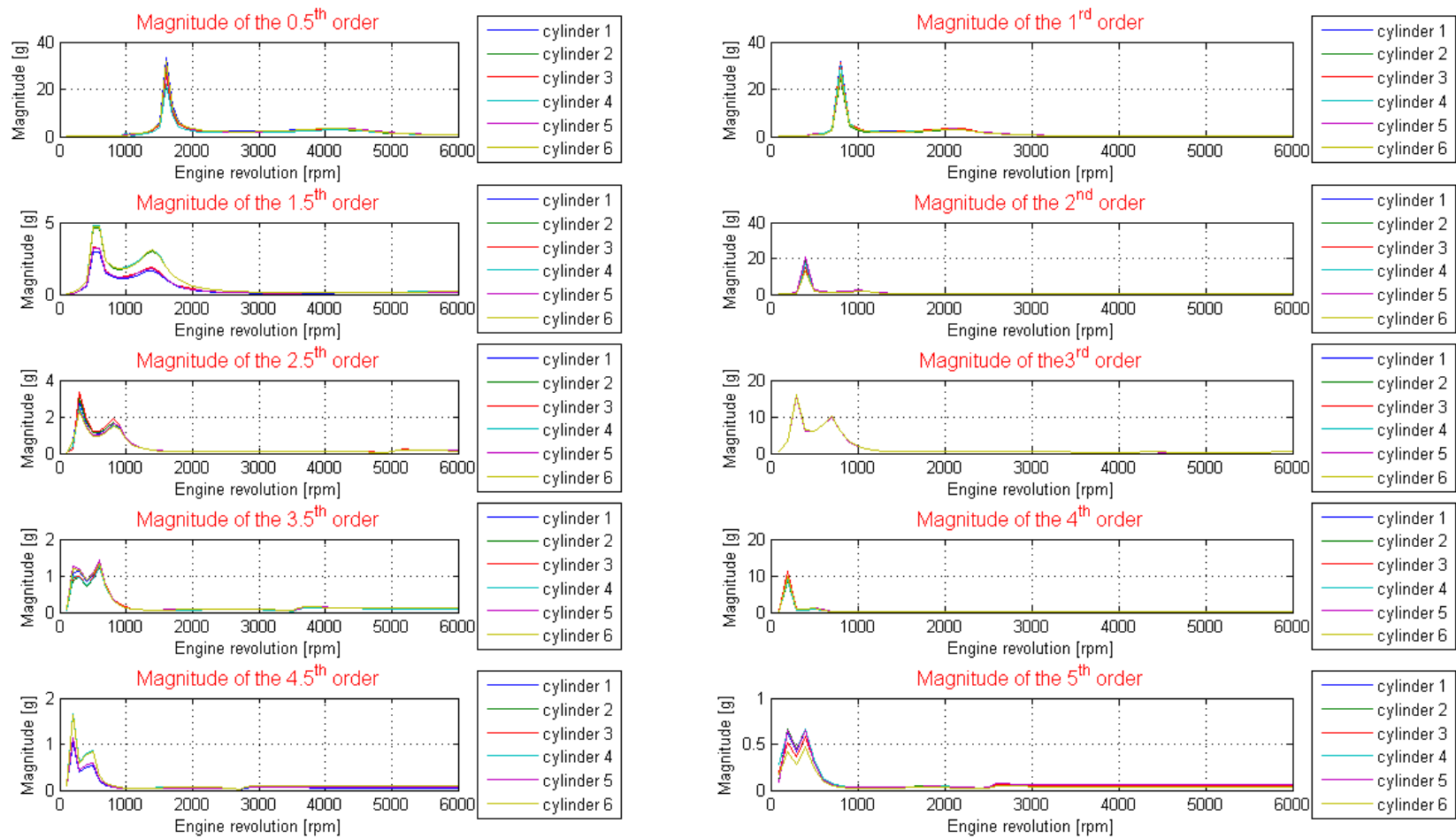


Figure 6-8 Magnitude characteristics of the 0.5th to 5th engine oscillation mode of each cylinders.

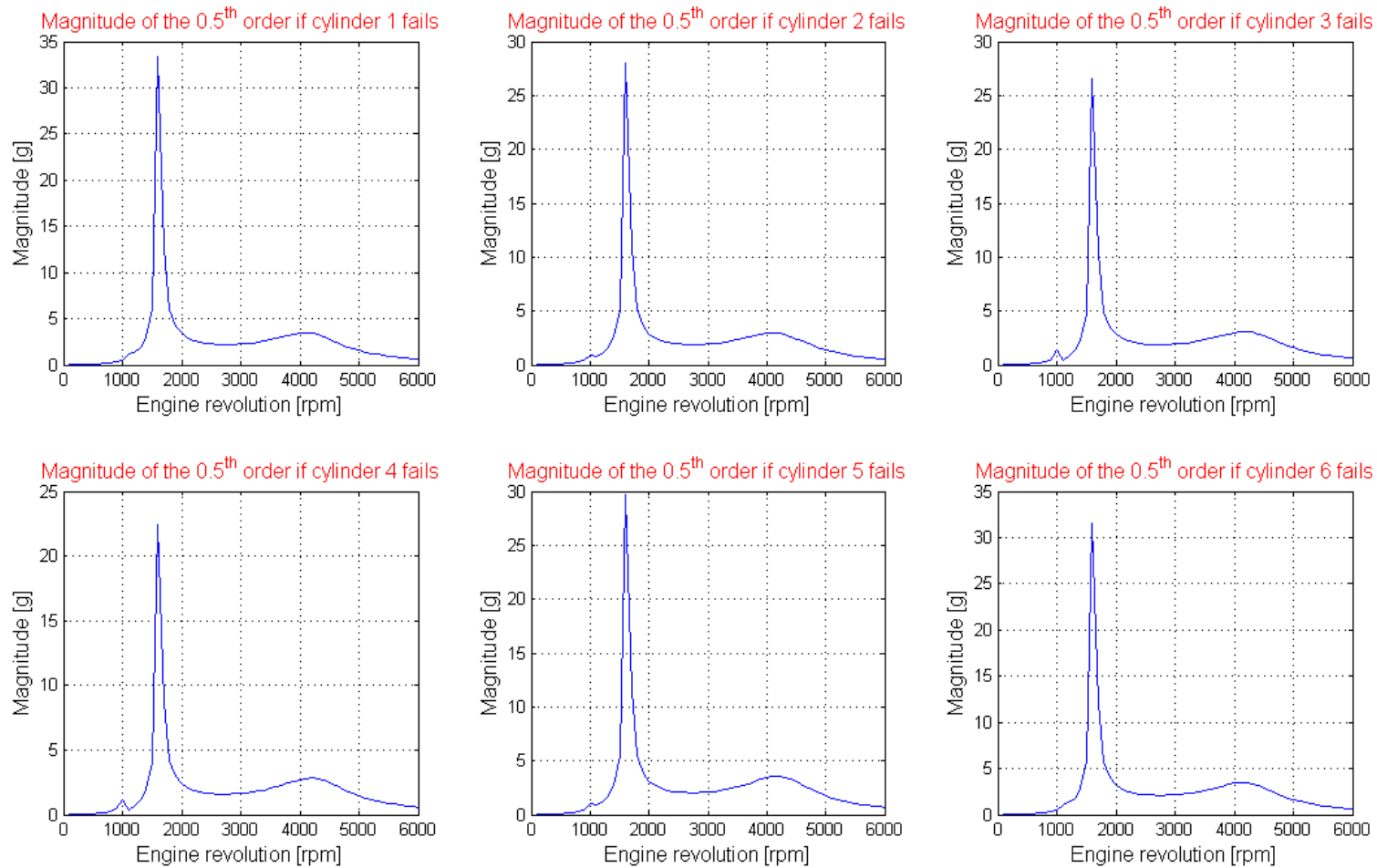


Figure 6-9 Overview of the computed 0.5th engine oscillation mode for each cylinder by simulating misfire events.

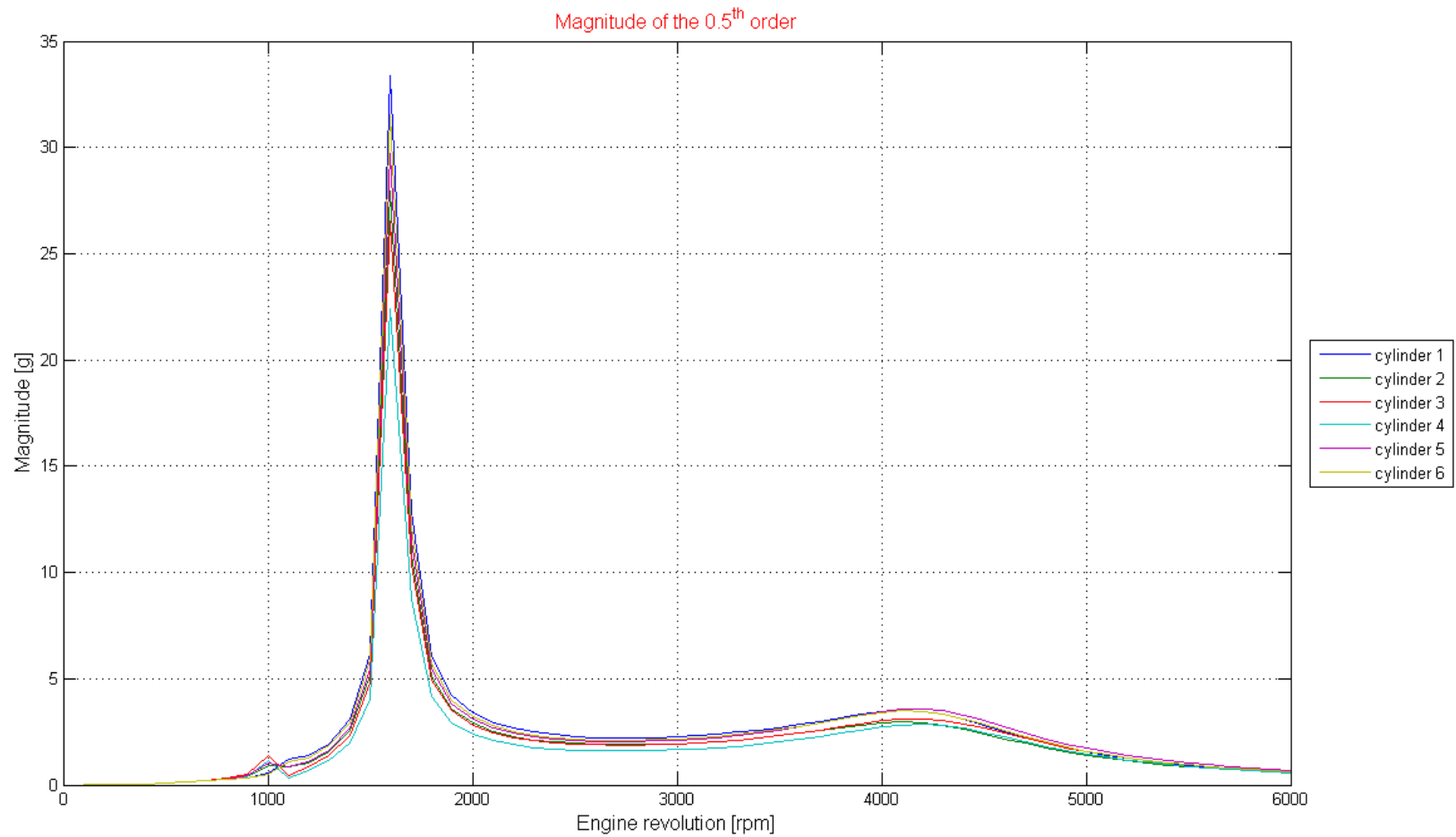


Figure 6-10 Magnitude curve of the 0.5th engine oscillation mode versus engine speed. The picture represents results of simulated misfire events of each cylinder.

As mentioned above by using only the magnitude information of the acceleration signals, it is not possible to find the faulty cylinder. Next a proposed method on how the cylinder can be found will be explained.

A signal can be described with the frequency f , the amplitude A and the phase angle φ . The frequency and the vibration amount are generally used to find a faulty engine. To work out the cylinder responsible for the misfire event, the phase angle information has to be calculated. As mentioned in previous chapters a signal can be described by using the Fourier theorem as well. With a misfire event, the related cylinder does not produce a high in-cylinder pressure due to the burn process and either no or less engine torque is produced from this cylinder. This means if no torque is produced no disturbances can be generated from this cylinder.

But as mentioned above each cylinder has a corresponding cylinder which has 360 degree crank angle offset. In an ideal engine condition both cylinders produce the same torque, meaning they have the same signal power and the summation of both signals is zero. This can be described by a summation of two periodical signals with 180 degree offset.

$$T_{(cyl1\&cyl4)} = T_{(cyl1)} + T_{(cyl4+180^\circ)} = T_{(cyl1)} \cdot \sin(\omega t) + T_{(cyl4)} \cdot \sin(\omega t + 180^\circ) = 0 \quad (6.2)$$

$$T_{(cyl2\&cyl5)} = T_{(cyl2)} + T_{(cyl5+180^\circ)} = T_{(cyl2)} \cdot \sin(\omega t) + T_{(cyl5)} \cdot \sin(\omega t + 180^\circ) = 0 \quad (6.3)$$

$$T_{(cyl3\&cyl6)} = T_{(cyl3)} + T_{(cyl6+180^\circ)} = T_{(cyl3)} \cdot \sin(\omega t) + T_{(cyl6)} \cdot \sin(\omega t + 180^\circ) = 0 \quad (6.4)$$

With

$$T_{(cyl1)} = T_{(cyl4+180^\circ)} \quad (6.5)$$

$$T_{(cyl2)} = T_{(cyl5+180^\circ)} \quad (6.6)$$

$$T_{(cyl3)} = T_{(cyl6+180^\circ)} \quad (6.7)$$

In case of unbalanced in-cylinder pressures characteristics the torques are not equal.

$$T_{(cyl1)} \neq T_{(cyl4+180^\circ)} \quad (6.8)$$

$$T_{(cyl2)} \neq T_{(cyl5+180^\circ)} \quad (6.9)$$

$$T_{(cyl3)} \neq T_{(cyl6+180^\circ)} \quad (6.10)$$

The summation of two periodical signals with 180 degree offset is no longer zero. This means in case of a misfire event, a spectral frequency which is not compensated, can be measured on the engine case. This can be done because the power of one cylinder is missing. It must be considered that the detected signal is not the signal coming from the faulty cylinder because this cylinder does not produce frequencies, but it is the signal from the corresponding cylinder which has 360 degree crank angle offset. In the next diagrams (Figure 6-11) the phase angle versus engine speed of all oscillation modes and all cylinders are shown. To detect the faulty cylinder it is necessary to have different phase angles at each cylinder over the whole engine speed. As in the graph below taken at the engine oscillation modes 1, 1.5, 2, 3, 4, 4.5 and 5th the phase angles are equal at some engine speeds and it is not possible to distinguish between the cylinders. To figure out the related cylinder the phase angles must be different for each cylinder over the whole engine speed range. This target is given by the oscillation modes 0.5th, 2.5th and 3.5th.

As in the graphs shown, sometimes a phase angle shift can be found. The reason for this is the 360 degree angle limit of the analyses method. If a signal raises the limit and an overflow occurs and the angle starts next at -360 degree.

Now the signal power must also be considered, because for the signal analyses a proper signal to noise ratio must be given. This target is only given at the 0.5th engine oscillation mode. All other frequencies have too little signal power to work with it for analyses using an acceleration sensor. This means for the proposed misfire detection method only one spectral frequency must be monitored. To find a misfire event by using an acceleration sensor the 0.5th engine oscillation mode must be observed.

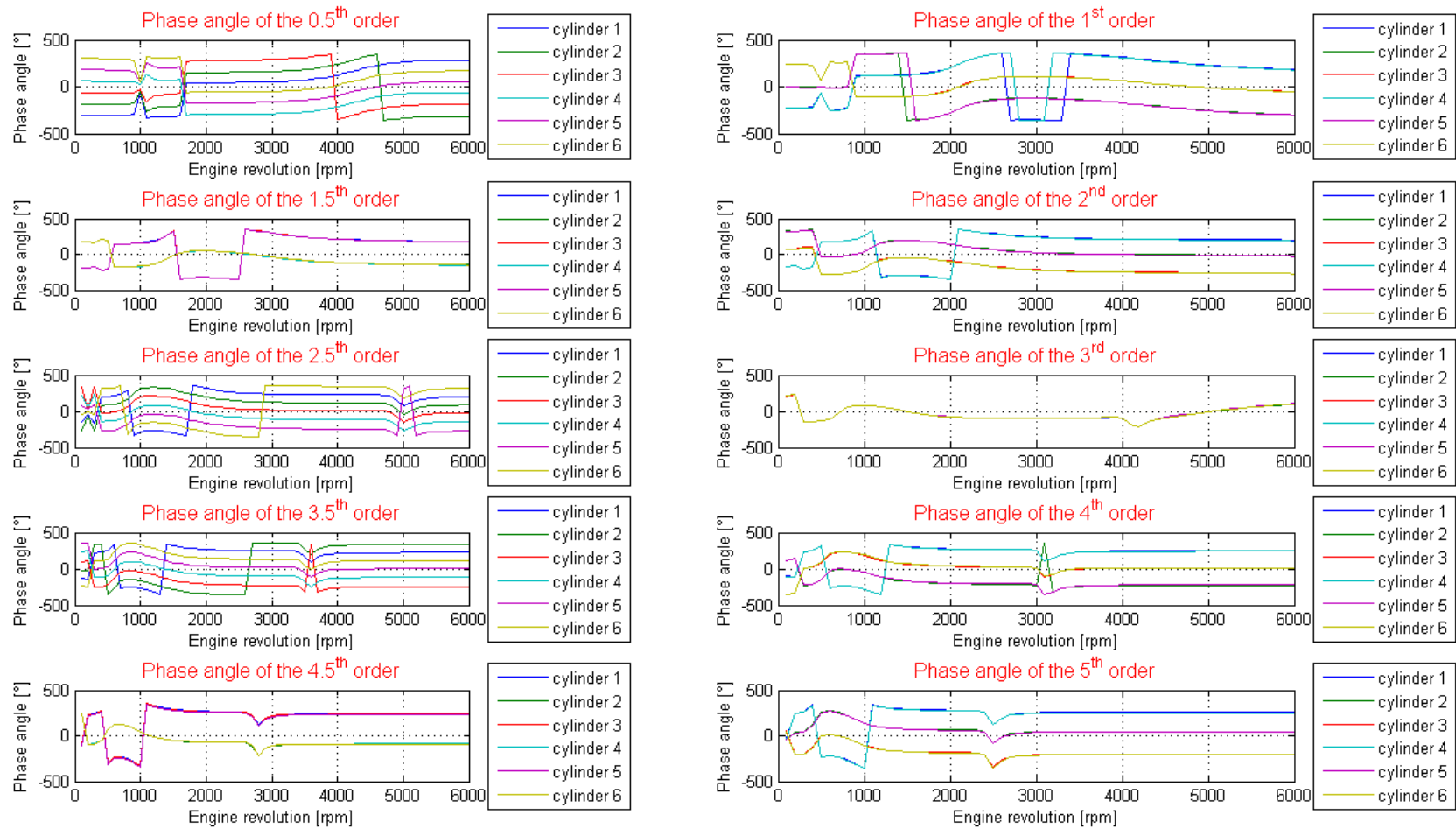


Figure 6-11 Angle offsets of certain engine oscillation modes (referenced to cylinder one) simulated at torsion bar and drawn versus engine speed.

In Figure 6-12 the phase angles of the six cylinders versus engine speed are drawn. The affected cylinder due to a misfire event can be found by a computation of the phase angle based on the 0.5th engine oscillation mode.

As in the simulation proofed, the detection method works from approximated 1800 rpm's up to the maximum attainable engine speed. The reason for the limitation of the lower engine speed is a resonance frequency of the system. At certain engine speeds the phase angles have equal values. This makes it impossible to allocate the affected cylinder. Same behaviour can be seen on torques (see Figure 6-8).

It has to be further considered that the idle speed of this engine type is also in this engine speed range. Below 1800 rpm there is no guarantee to have a controlled idle speed. This may lead to an unwelcome engine shut down.

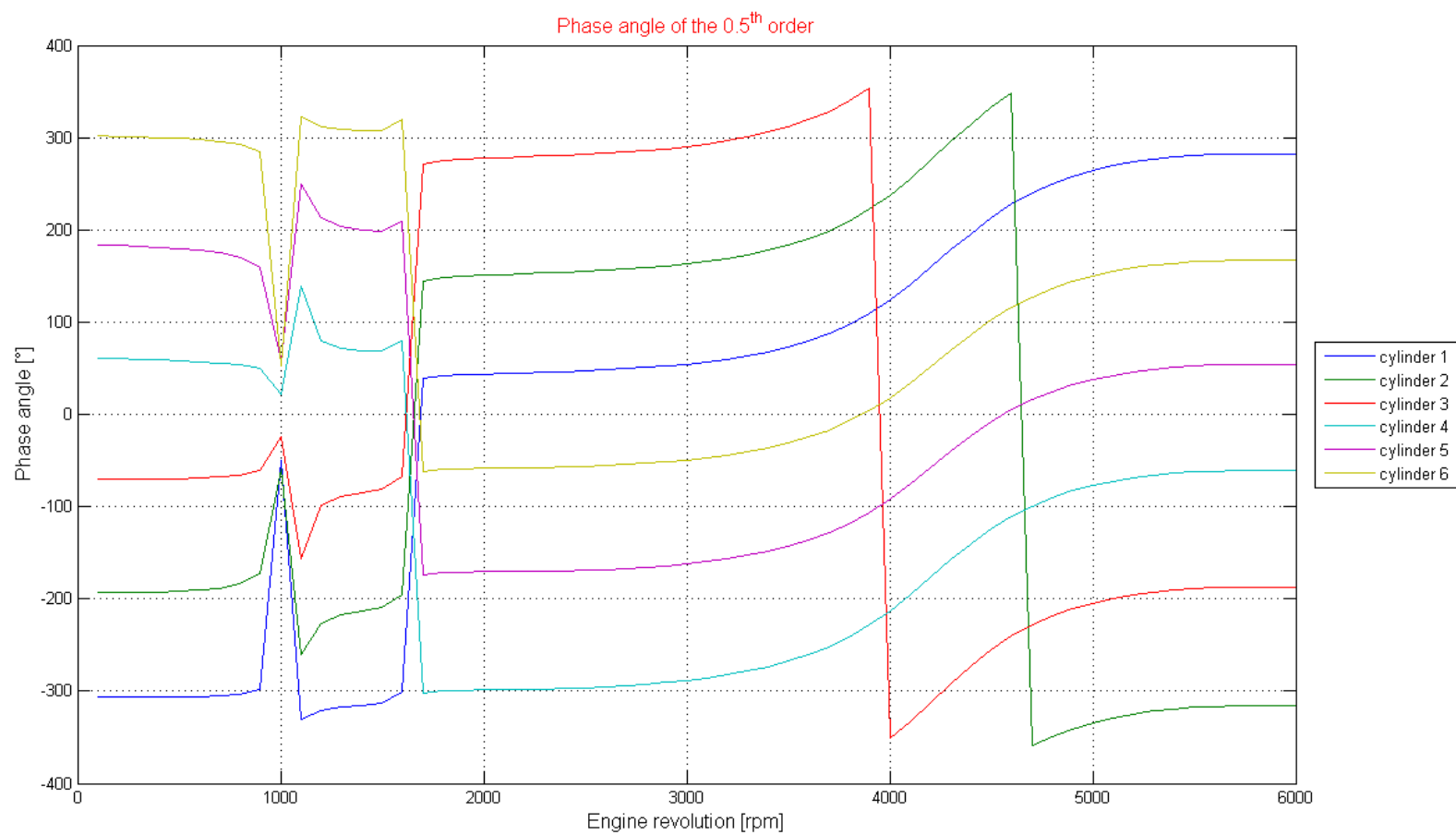


Figure 6-12 Angle offset of the 0.5th oscillation mode (referenced to cylinder one) simulated at the torsion bar versus engine speed.

7 RESULT

To proof the analytic model and the results from the simulation, real world measurements were done on an aircraft. For the tests an engine was equipped with a one axis acceleration sensor. The sensor position was chosen on the gear box but it is not limited to this position. The measurement direction of the acceleration sensor was based on the coordinate plane "CSYS engine centre" described in chapter 3. The engine vibrations were measured in z-direction of the coordinate plane. To simulate misfire events, the engine was equipped with a modified harness which allows disconnecting the injector via a switch. All the tests were done in this way because no modified software for this kind of test was available.

If an injector is switched off, the related cylinder is immediately switched off and no torque is produced. This test setup is exactly the same as simulated in the analytic model. First the aircraft was started in normal engine condition. As soon as idle speed was reached and the engine was stable on, the predefined injector was switched off and the engine was accelerated to maximum engine speed. For the signal processing the engine speed signal, the camshaft signal and the vibration signal were monitored. The camshaft signal was used to have trigger marks which are in relation to an engine cycle and represents one full engine burn process of 720° crank angle. The engine speed was calculated from the camshaft signal. The crankshaft signal which represents 36-2 pulses per revolution was used to have an engine speed signal with higher signal resolution for detailed signal analyses. This signal can be used to measure the engine speed in between the camshaft pulses and has a resolution of 10 degree crank angle. The vibration signal was monitored electrical single ended with engine ground as reference. After the tests a program for the signal analyses was developed. The whole signal analyses were done with the program Flex Pro [24].

As explained before in the analytic model, the first step at the condition monitoring system is to observe the gradients or the progression of the 0.5th engine oscillation mode.

Figure 7-3 shows the result after the signal analysing process.

The black bar diagram represents the characteristic of the 0.5th engine oscillation mode. The x-axis represents the engine cycles in all three pictures. This means every 720° crank angle a new signal was calculated and equates to one engine 4-stroke cycle. The middle diagram shows the characteristic of the phase angle of the 0.5th engine oscillation mode referenced to the camshaft signal and in the last chart the engine speed is plotted. As it can be seen in the first plot below, the magnitude of the 0.5th engine oscillation mode rises dramatically as soon as the injector was switched off. This was done after approximate 173 engine cycles. The phase angle first shows a random signal until the injector was deactivated. After de-powering the injector the phase angle shows very smooth signal characteristic with a slightly positive rise. The change of the phase angle can be explained by the moderate engine speed loss due to less engine power.

Figure 7-4 shows a zoom of the first picture drawn in Figure 7-3. It can be seen that the engine works well until the 172nd engine cycle. At the next engine cycle the magnitude grows up to 6000 units. Already after 4 cycles, after the injector was switched off, the signal value reaches a value which is 14 times higher than at normal engine condition. This means by an engine speed of 4000 rpm's the misfire event can be detected after 120 ms time delay.

As soon as the failure is detected by the observation system the phase angle will be computed and based on the analytic model the cylinder can be found.

Figure 7-4 shows how accurate the system works.

RESULT

Figure 7-5 to Figure 7-10 presents test results of simulated misfire events of each cylinder. The tests were carried out as explained above.

The engine was started with all cylinders. As soon as idle speed was reached one cylinder was switched off and the engine speed was increased. This was done sequentially for all cylinders. Before the injector is de-powered the phase angle shows a stochastic behaviour. As soon as the injection is switched off the phase angles follow as expected and in the analytic model calculated characteristics. This unique engine behaviour makes it possible to locate the faulty cylinder by analysing the phase angles versus engine speed. For a comparison a test was done with good engine conditions. The result of this test is shown in the next figure (Figure 7-2). It can be seen that the 0.5th engine oscillation mode is lower than the magnitude during a test with an in-cylinder pressure loss. The phase angle curve shows random behaviour without any tendencies.

Figure 7-1 shows the results of a simulation of an engine without failures related to an in-cylinder pressure loss. The calculated phase angle progressions of the vibration signal, shows no tendency as Figure 7-2 presented. As long as the engine works fine the phase angle of the 0.5th engine oscillation mode shows stochastic signal behaviours with less signal power. This behaviour comes from the combustion process and it must be considered that the phase angle calculation was taken from a signal with low magnitude, like an engine without failures expected. It must be also considered that due to a "standard" combustion process the 0.5th engine oscillation mode is not perfectly compensated. This leads to stochastic waveforms of the 0.5th engine oscillation mode.

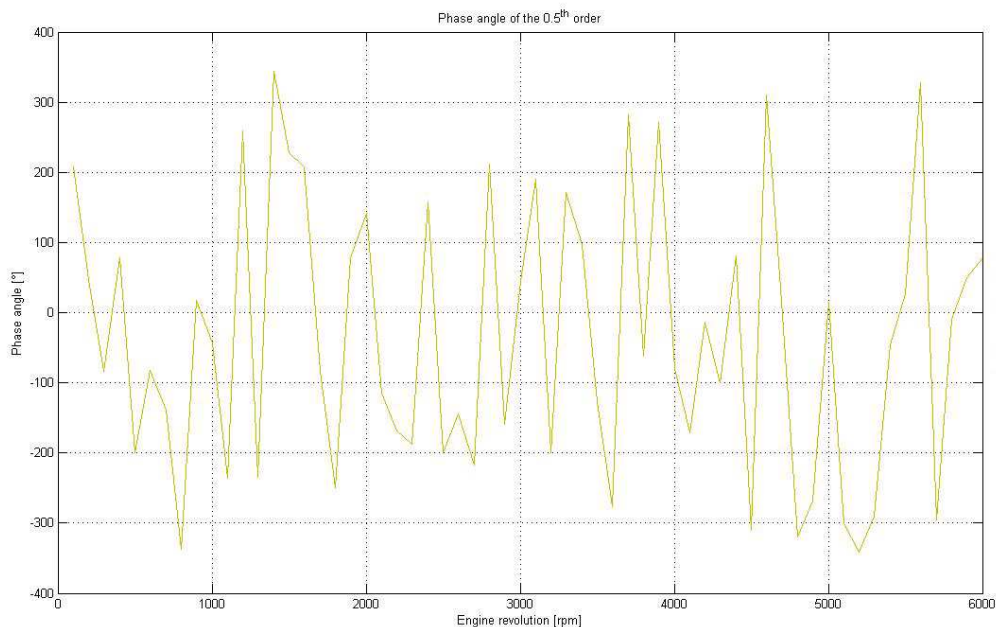


Figure 7-1 Simulated phase angle curve of the 0.5th engine oscillation mode versus engine speed referenced to cylinder one with good engine behaviour.

RESULT

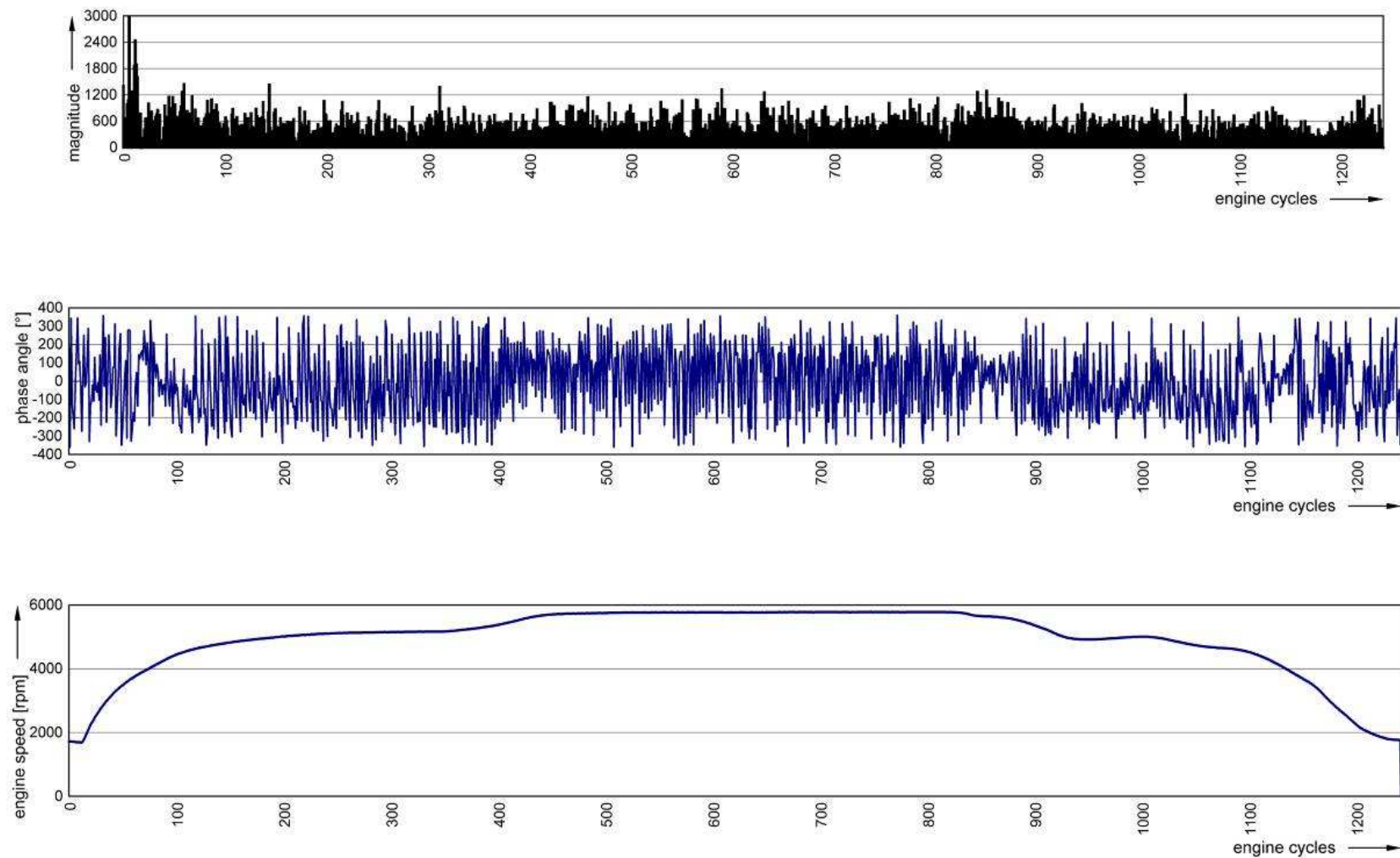


Figure 7-2 Engine test without failures. Acceleration of the engine from idle speed to maximum engine speed. Each plot shows the behaviour over engine cycles First plot 0.5th engine oscillation mode, second plot phase angle referenced to cam shaft signal of the monitored vibration signal and last plot engine speed.

RESULT

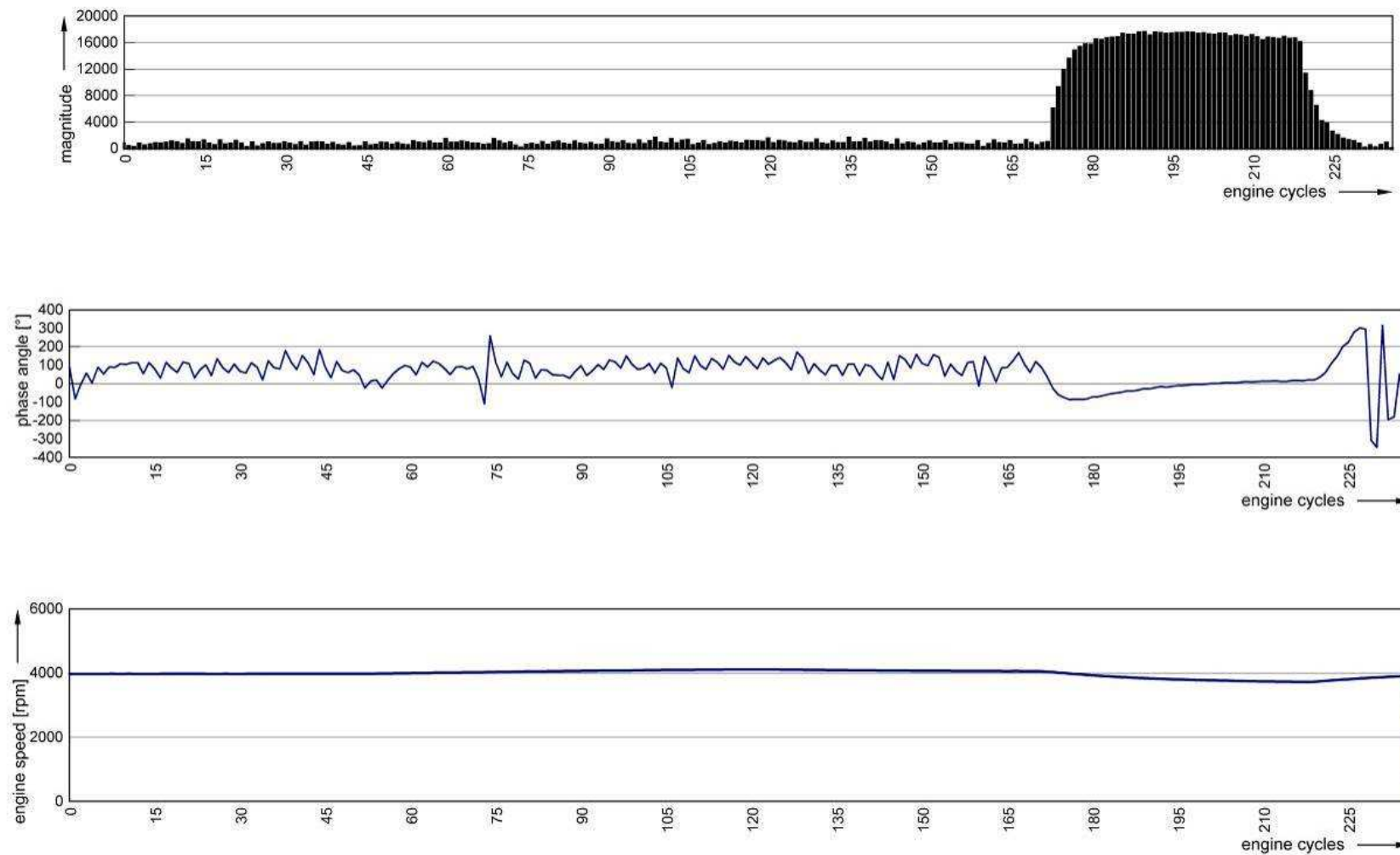


Figure 7-3 Cylinder failure on cylinder 3 at 4000 rpm. The misfiring event occurs approx. after 175 engine cycles. First plot 0.5th engine oscillation mode, second plot phase angle referenced to cam shaft signal and last plot engine speed versus engine cycles.

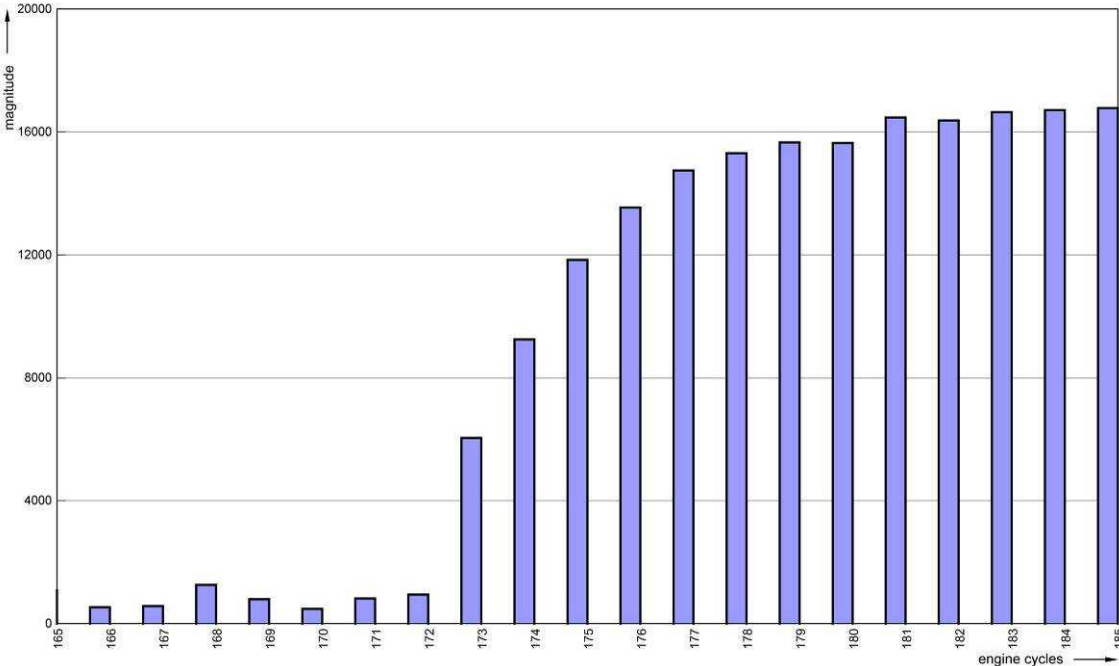


Figure 7-4 Amplitude curve of the 0.5th engine oscillation mode at 4000 rpm after deactivating (172nd engine cycle) an injector.

RESULT

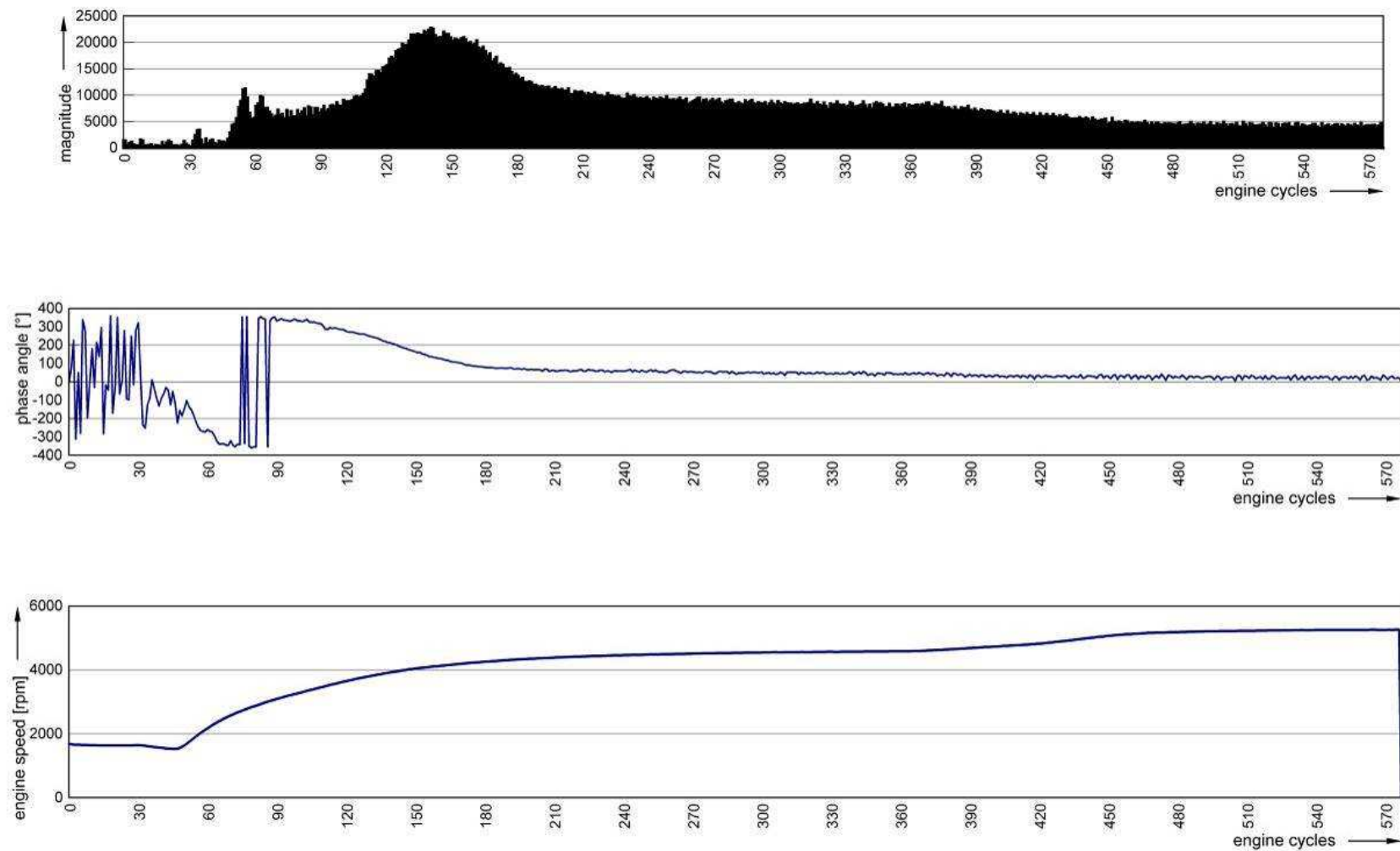


Figure 7-5 *Cylinder 1 was switched off after reaching idle speed and engine was accelerated to maximum engine speed. First plot 0.5th engine oscillation mode, second plot phase angle referenced to cam shaft signal and last plot engine speed versus engine cycles.*

RESULT

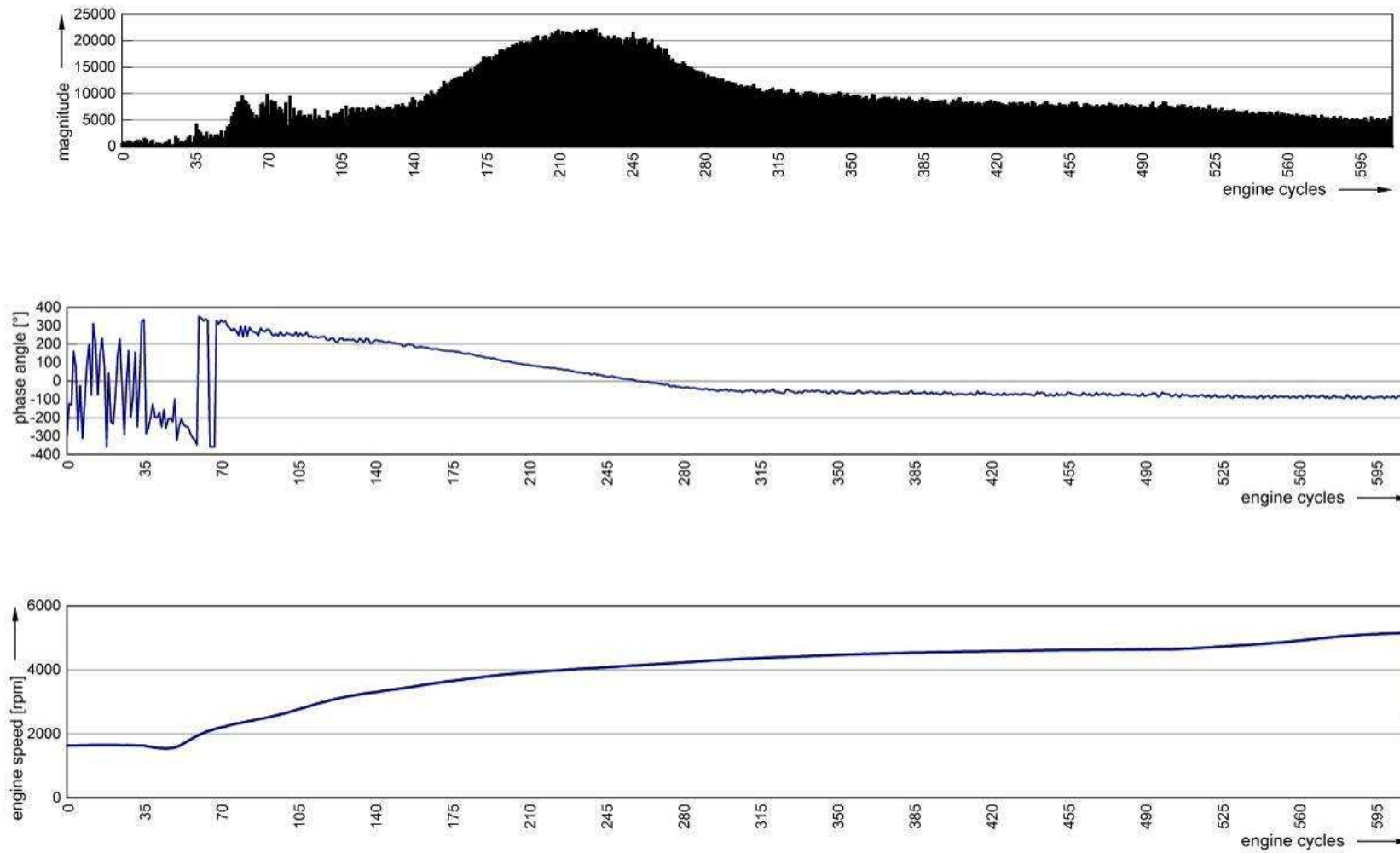


Figure 7-6 Cylinder 2 was switched off after reaching idle speed and engine was accelerated to maximum engine speed. First plot 0.5th engine oscillation mode, second plot phase angle referenced to cam shaft signal and last plot engine speed versus engine cycles.

RESULT

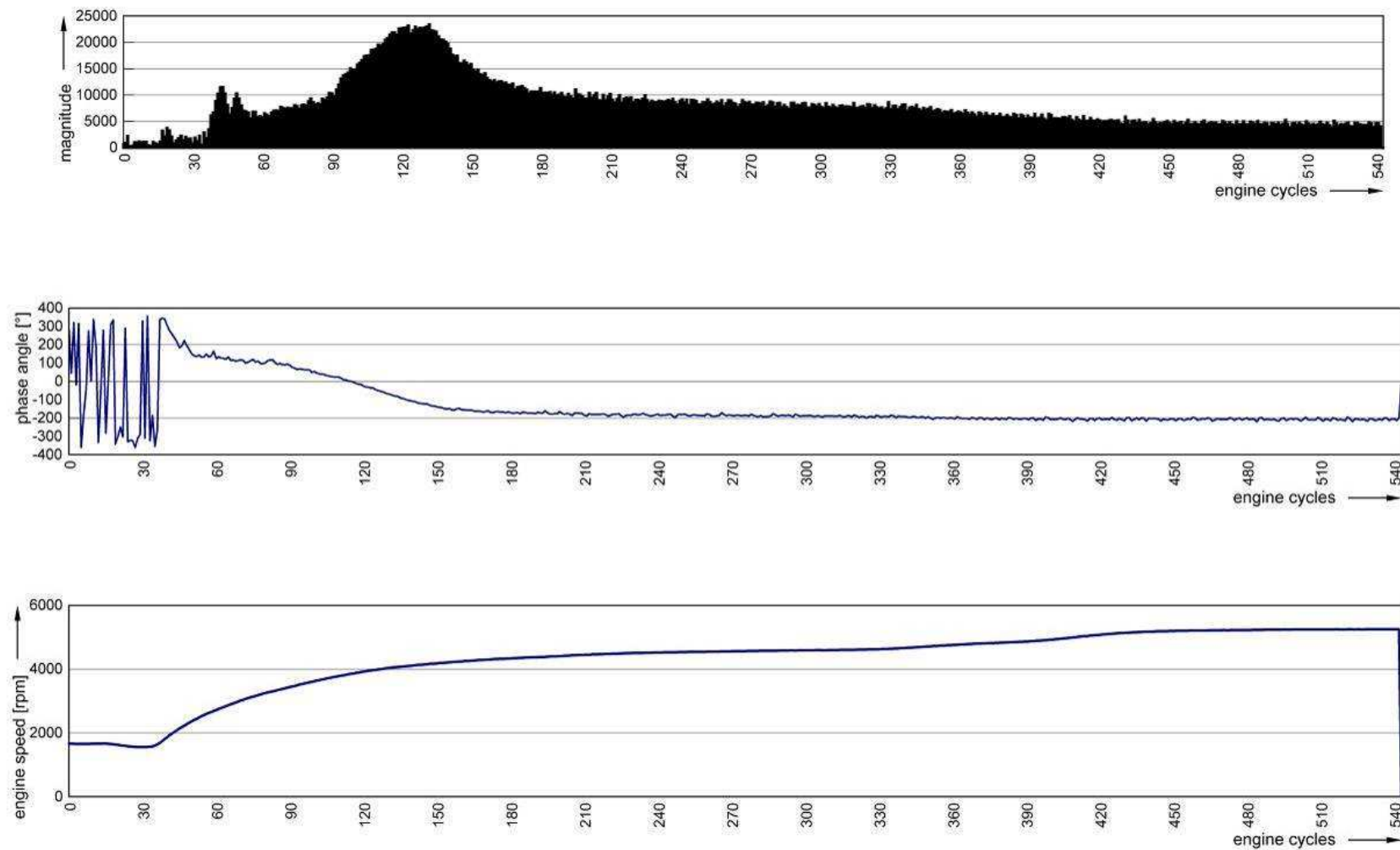


Figure 7-7 *Cylinder 3 was switched off after reaching idle speed and engine was accelerated to maximum engine speed. First plot 0.5th engine oscillation mode, second plot phase angle referenced to cam shaft signal and last plot engine speed versus engine cycles.*

RESULT

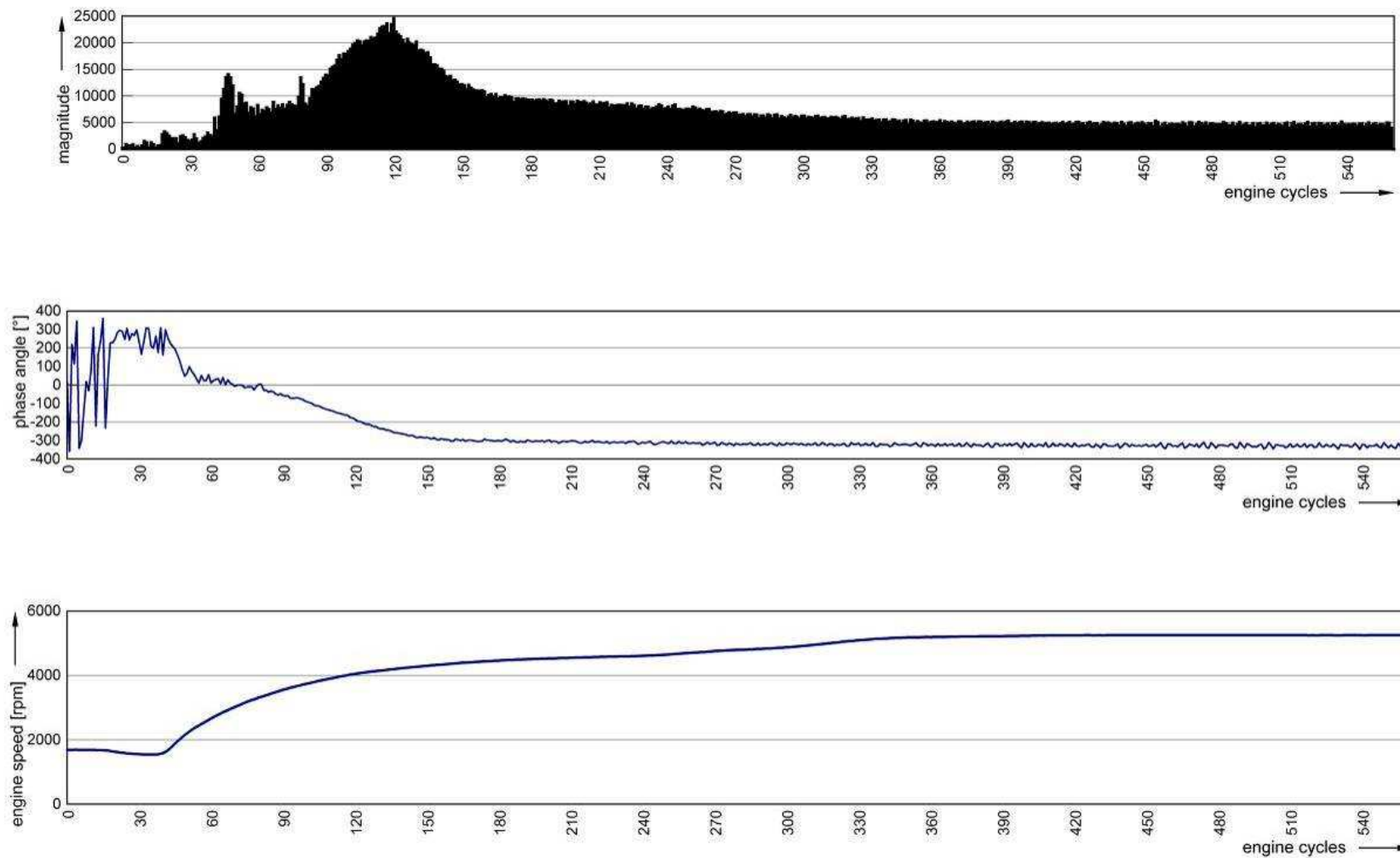


Figure 7-8 *Cylinder 4 was switched off after reaching idle speed and engine was accelerated to maximum engine speed. First plot 0.5th engine oscillation mode, second plot phase angle referenced to cam shaft signal and last plot engine speed versus engine cycles.*

RESULT

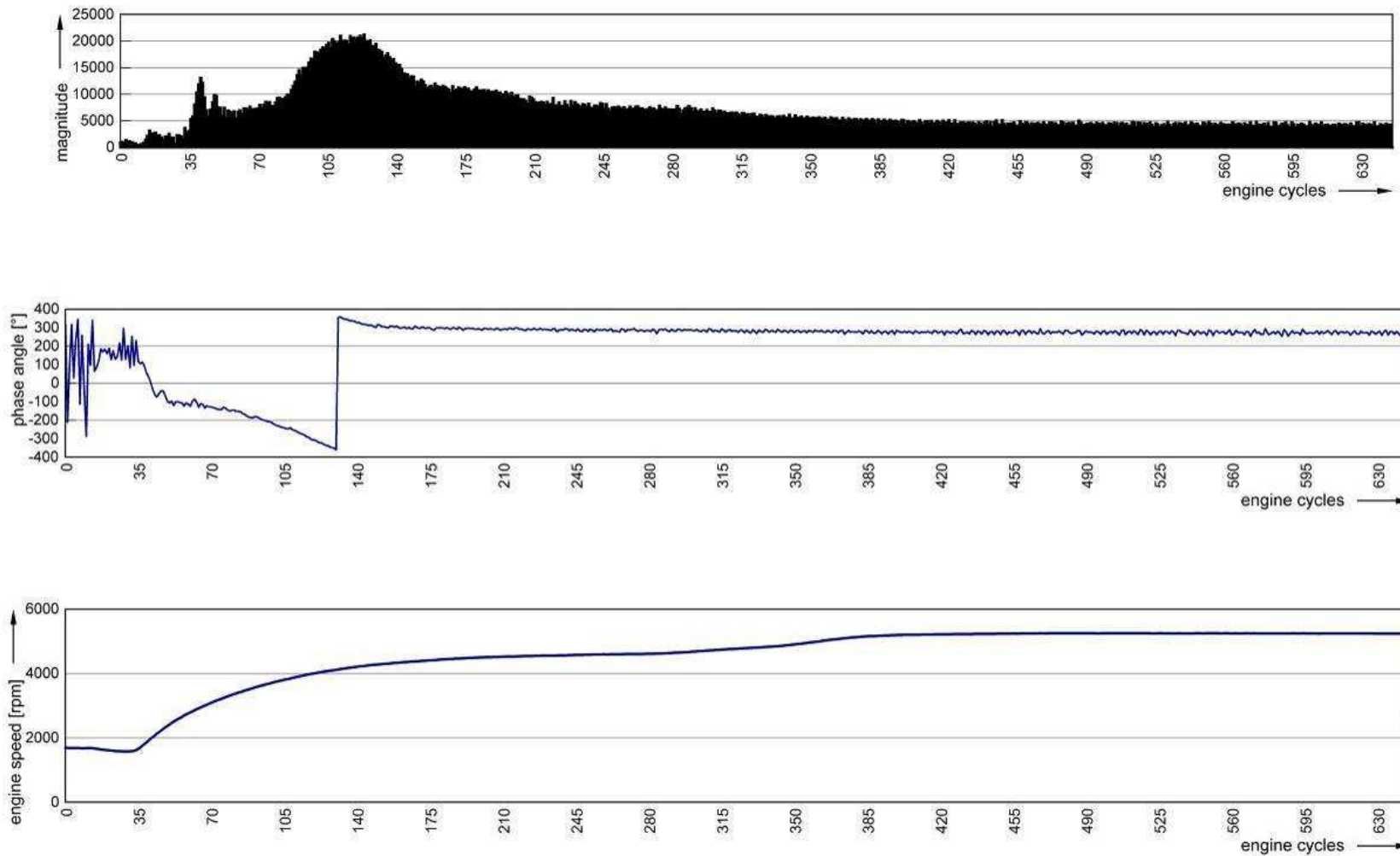


Figure 7-9 *Cylinder 5 was switched off after reaching idle speed and engine was accelerated to maximum engine speed. First plot 0.5th engine oscillation mode, second plot phase angle referenced to cam shaft signal and last plot engine speed versus engine cycles.*

RESULT

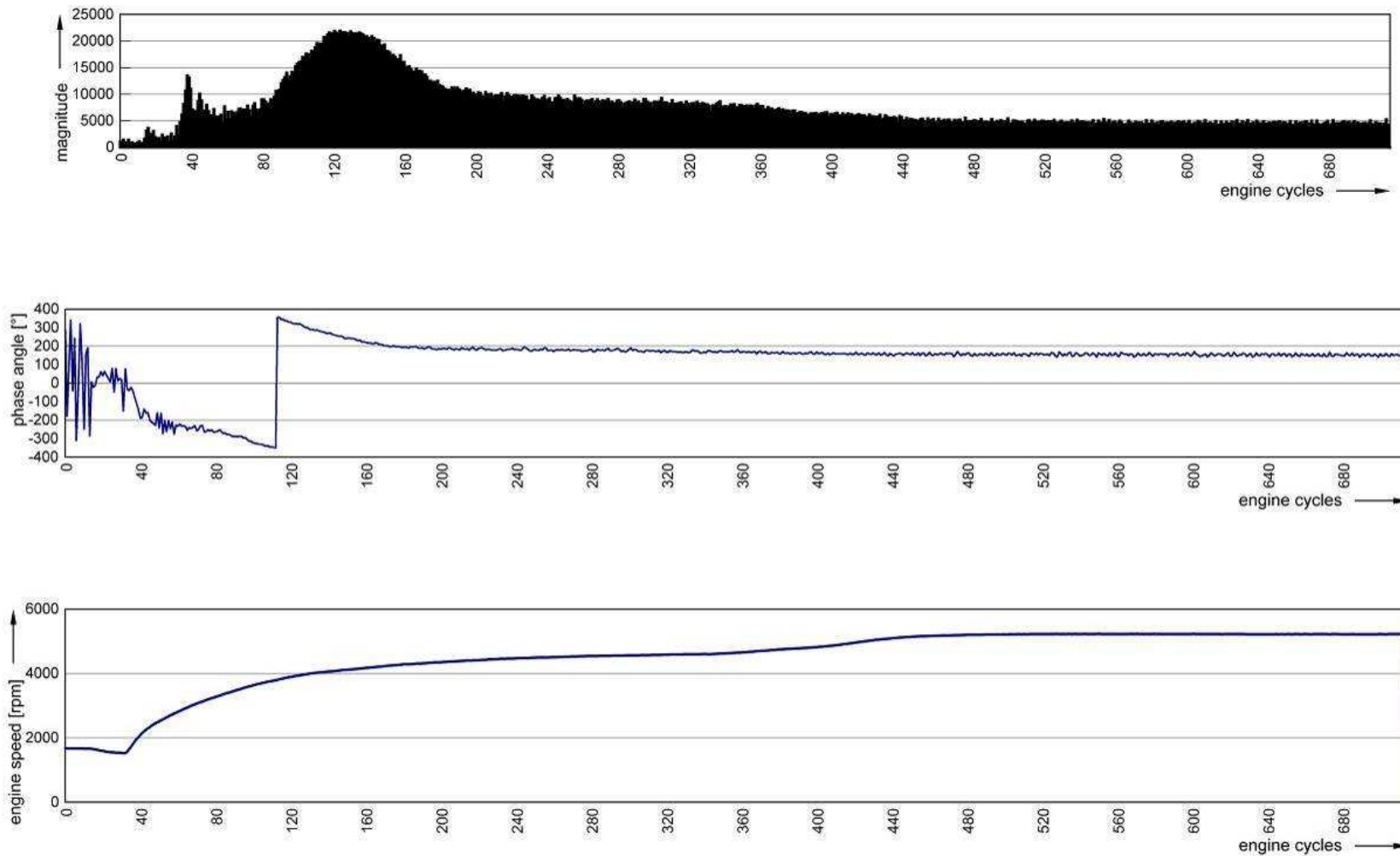


Figure 7-10 Cylinder 6 was switched off after reaching idle speed and engine was accelerated to maximum engine speed. First plot 0.5th engine oscillation mode, second plot phase angle referenced to cam shaft signal and last plot engine speed versus engine cycles.

RESULT

The next charts (Figure 7-11 and Figure 7-12) show a comparison of the cylinders. This was calculated from real world measurements. The first plot below represents the magnitude progression versus engine speed of each cylinder. As already mentioned it is quite impossible to locate the faulty cylinder by only calculating the magnitude information. The magnitude of the cylinders shows insufficient differences in curve progression. The second chart below draws the phase angles of each cylinder of a faulty engine versus engine speed. To locate the faulty cylinder it is essential to have differences in phase angles over the whole engine revolution. If an overlap of the curves occurs at a certain engine speed, the faulty cylinder cannot be found at this operating point of the engine.

As drawn in the chart an inaccurate working cylinder can be found in between 1800 rpm up to maximum engine speed. This is exactly the same result as simulated and proves the theoretical aspects and simulation results. At this application misfire detection below 1800 rpm makes no sense because idle speed is in a range about 1800 rpm and below there is no possibility of a controlled engine working range. The upper engine speed limit of the proposed detection method is given by the maximum engine power which leads to a maximum engine speed.

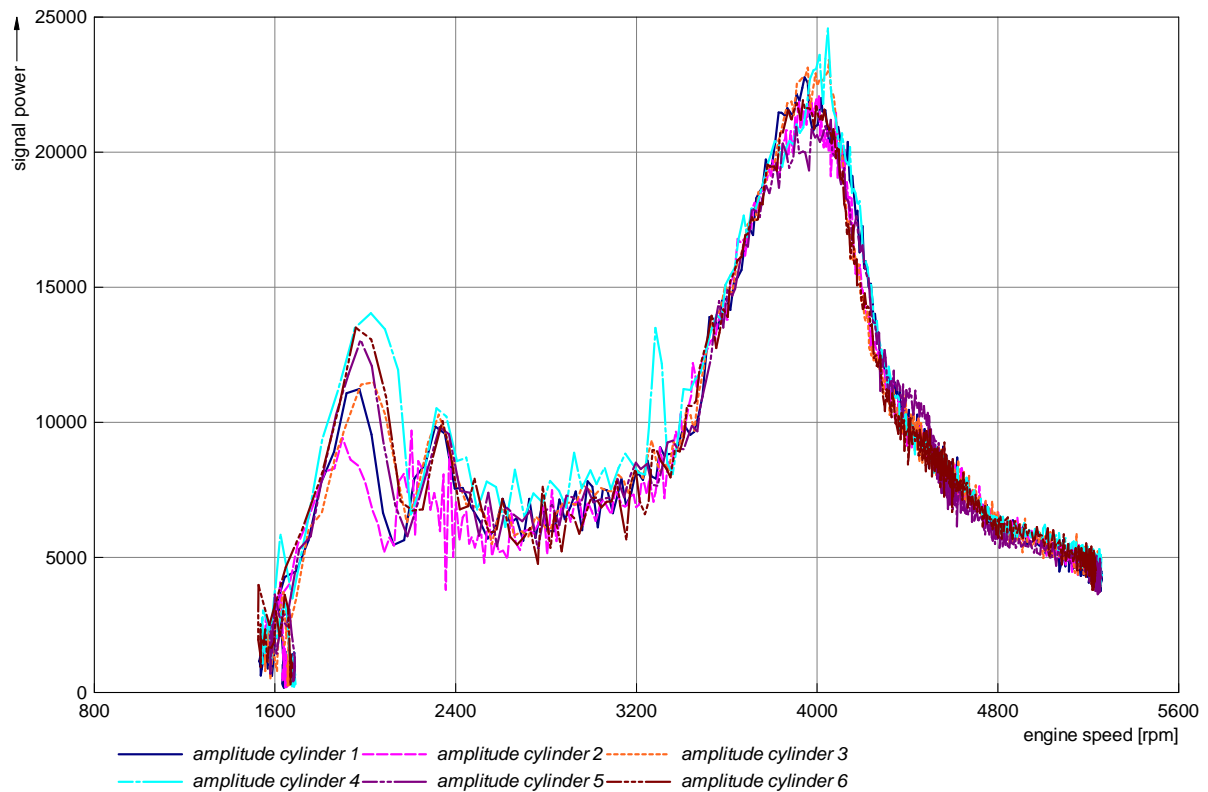


Figure 7-11 Measured magnitude of the 0.5th engine oscillation mode during misfire events of the individual cylinders (cylinder 1 to 6) drawn versus engine speed.

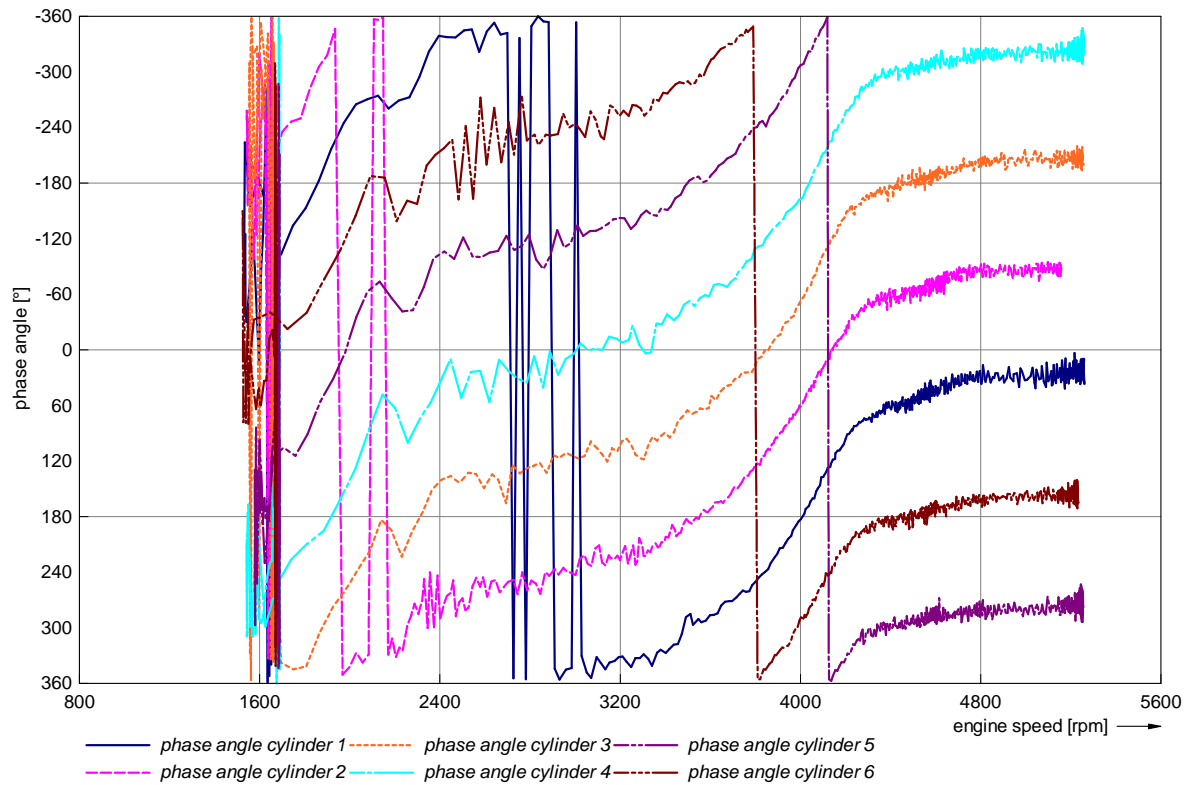


Figure 7-12 Measured cylinder selective phase angle curve of the 0.5th engine oscillation mode versus engine speed referenced to cam shaft signal.

For test reasons a test with only 4 operating cylinders was carried out on the test bench. The test was done in the same way as the test at the aircraft for a 5 cylinder operation mode investigation. Figure 7-13 shows the test result on a propeller test bench. The total average engine power is less compared to engines operated with single cylinder failure. Compared to a 5 cylinder engine operation mode the signal magnitude of the 0.5th engine oscillation mode is quite a bit higher.

The phase angle curve referenced to the cam shaft signal shows also a unique phase angle characteristic. It can be seen that the phase angle curve is different to 5 cylinder operation.

RESULT

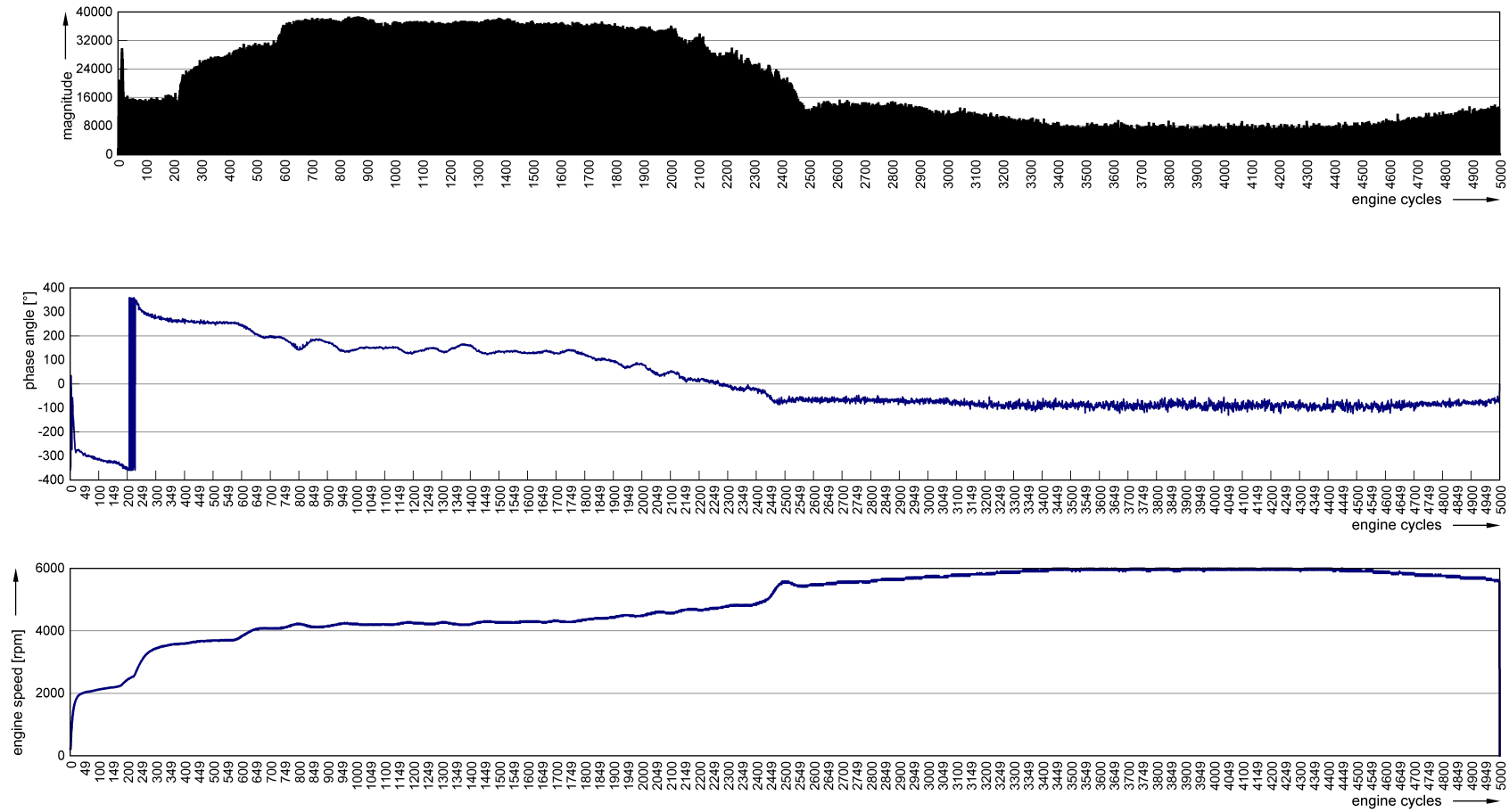


Figure 7-13 Engine operated with 4 cylinder. Cylinder 1 and 2 were de-powered. Upper Plot: Magnitude of the 0.5th engine oscillation mode versus engine cycle. Middle plot: phase angle of the 0.5th engine oscillation mode referenced to cam shaft signal versus engine cycle. Last plot: engine speed versus engine cycle.

8 SYSTEM EXTENTION

In the chapters one to seven the misfire detection method was described from theoretical point of view up to tests results. Due to the engine model, which was developed for the misfire detection method, further important information can be derived.

The analytic model makes it possible to have a look into the engine by using an acceleration sensor mounted on the engine block. This realizes the possibility to get additional information about the mechanical parts which are installed inside the engine and which are not accessible during engine operation. This information can be used as a preventive maintenance tool. In the case of a misfire event, maybe a mechanical part is overstressed and the stress limit of the torsion bar, as an example, will be exceeded. The presented monitor system can analyse the poor engine conditions and the failure information can be transmitted to the pilot. If the stress limits of, e.g. the torsion bar are critical or reaches a critical range, the pilot can be informed by the system. To reduce mechanical stress an engine speed change can be suggested from the monitoring system for example. This action will help to be furthest away from the critical natural frequency of the torsion bar. A change in engine speed can reduce the mechanical stress and the probability of a mechanical fault can be reduced.

In the Figure 8-1 and Figure 8-2 the simulation result of a good and a poor engine is presented. On the right hand side different torques are shown and on the left hand side the torsion angles are drawn. A proper engine condition leads to expected torsion angles which are not critical for the parts. A bad engine condition leads to an abnormal angle displacements and torsion stress. This can be seen in Figure 8-2.

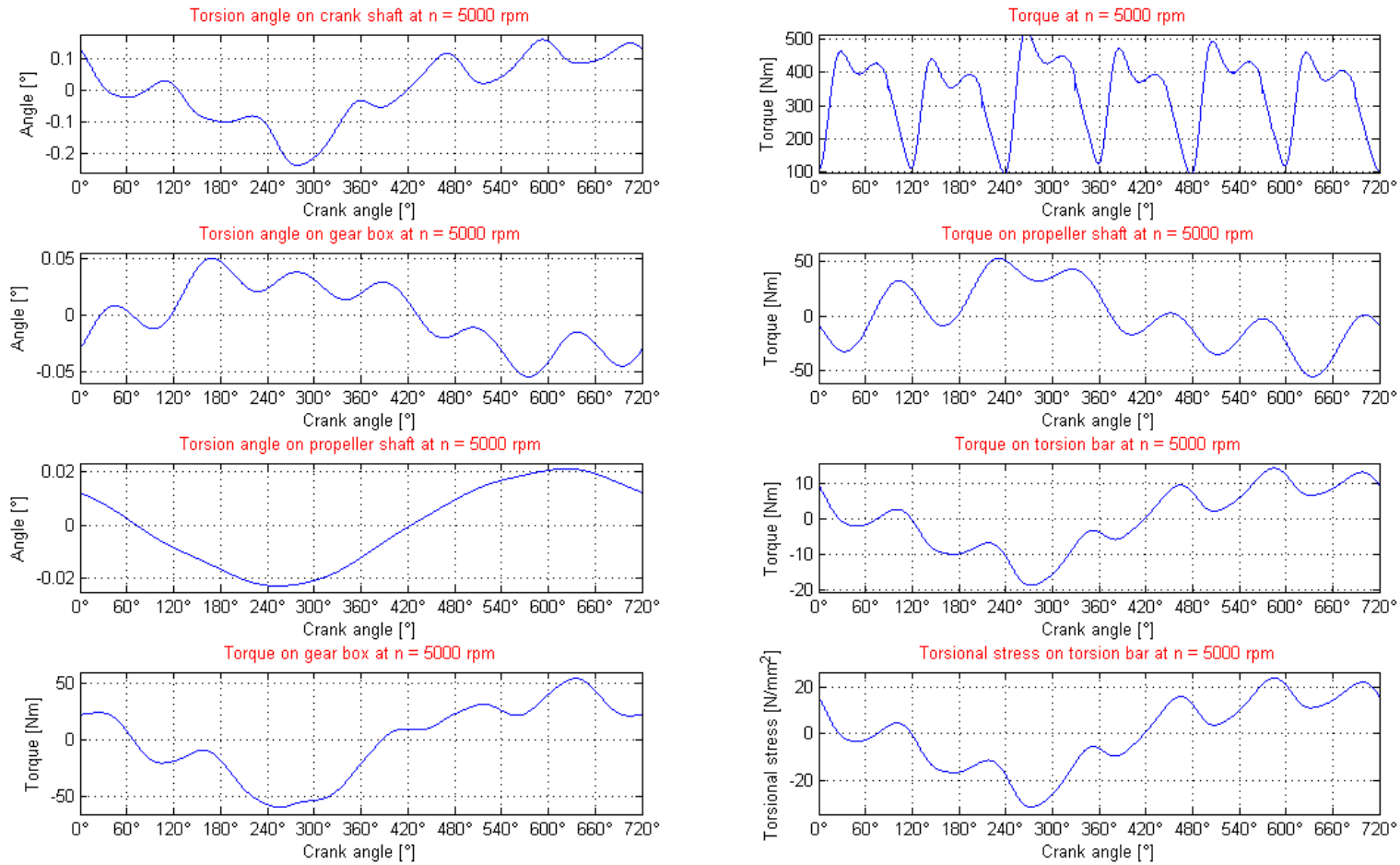


Figure 8-1 Overview of simulated stress analyses of the mechanical components of the power train system. Drawn are crankshaft angle displacement, torsion angel at gear box, torsion angle at propeller shaft and torque at torsion bar. Simulation was done with good engine condition.

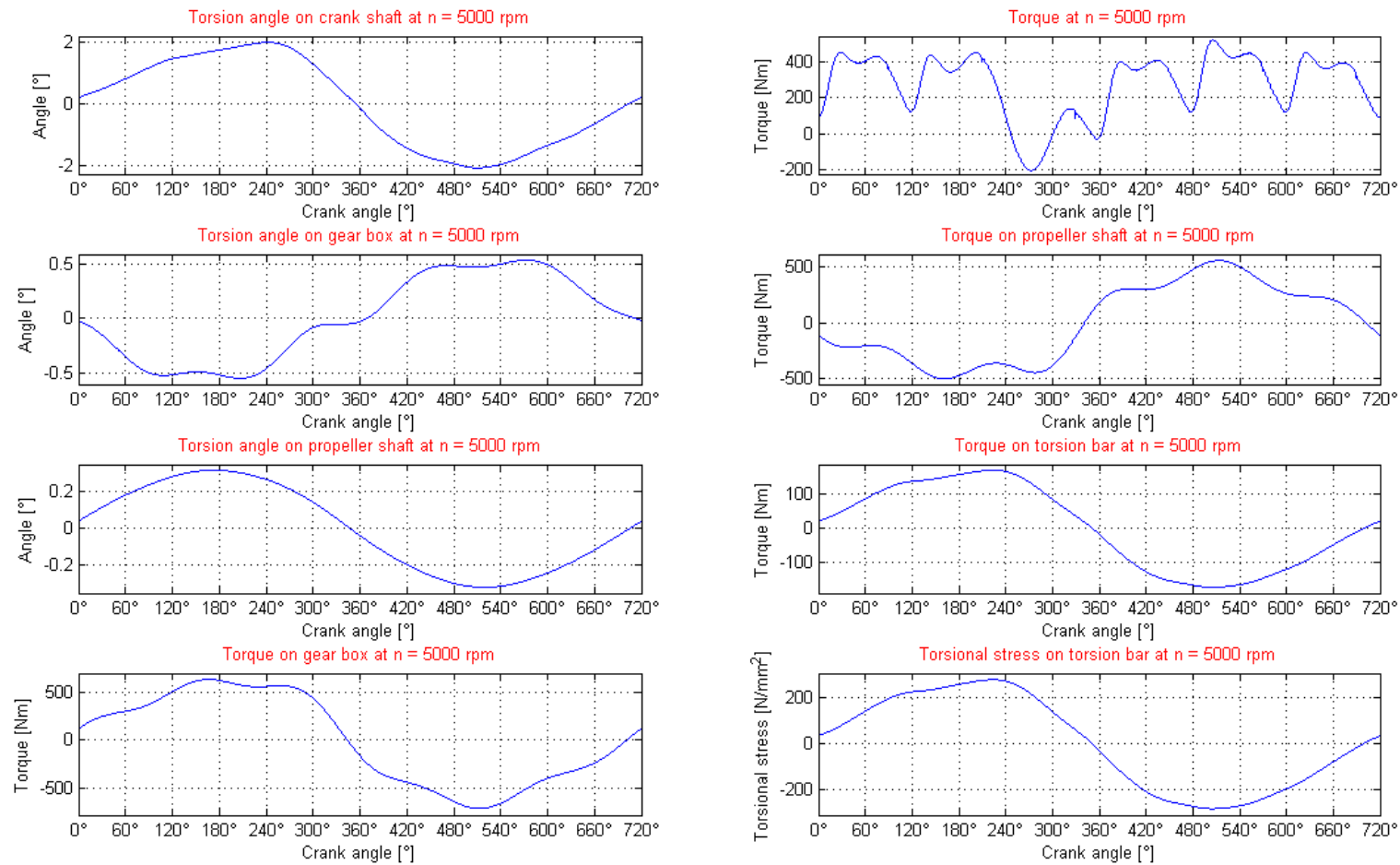


Figure 8-2 Overview of simulated the stress analyses of the mechanical components of the powertrain system. Drawn are crankshaft angle displacement, torsion angle at the gear box, torsion angle at propeller shaft and torque at torsion bar. Simulation was carried out with bad engine condition.

A second good idea is an automatic burn process observation of the engine. In case of a power tolerance of the cylinders the engine leads to a distorted movement which can be detected as well. In principle the working algorithm is the same as at the misfire detection used, but in cooperation with the ECU which controls the engine. If a rise of the 0.5th engine oscillation mode is detected and the faulty cylinder is located the disturbance can be eliminated by a change of the cylinder parameters. To do this the corresponding cylinder which has 360° crank angle offset must be switched off completely or the power of the corresponding cylinder must be reduced to at least the same level of the other cylinder. This can be done by reducing the fuel amount which results in a lean air-fuel mixture formation. A second possibility is to change the ignition angles; it must be considered that the exhaust gas temperature will be affected by changing the fuel quantity and the ignition angle. In case of a total malfunction of one cylinder the corresponding must be also switched off. This reduces the engine vibration to a normal level but with reduced engine power. In case of mechanical or electrical tolerances on the system the engine can be balanced by using this proposed observation method. This can reduce nasty disturbances in the cockpit compartment and increases the passenger comfort as well.

The next view pictures show how the result of such a disturbance can be compensated by a completely shut off of the corresponding cylinder.

Figure 8-3 shows the spectral components of the transversal gas force of each cylinder. In this example cylinder 2 is defect and cylinder 5 is de-activated.

The effect of the controlled power reduction of one cylinder on the crankshaft is drawn in the in Figure 8-4. The first three pictures show the frequency components of the corresponding cylinder pairs of the transversal gas force. The 4th plot represents the spectral components of the transversal gas force on the crankshaft. The crankshaft signal is the sum of all three signals of the corresponding cylinder pairs.

In Figure 8-6 the torques acting on the engine case due to the crankshaft interaction, the gear box and the engine block are drawn. As a comparison with a poor engine, this means one cylinder is defect and shows significant lower torque magnitudes.

SYSTEM EXTENTION

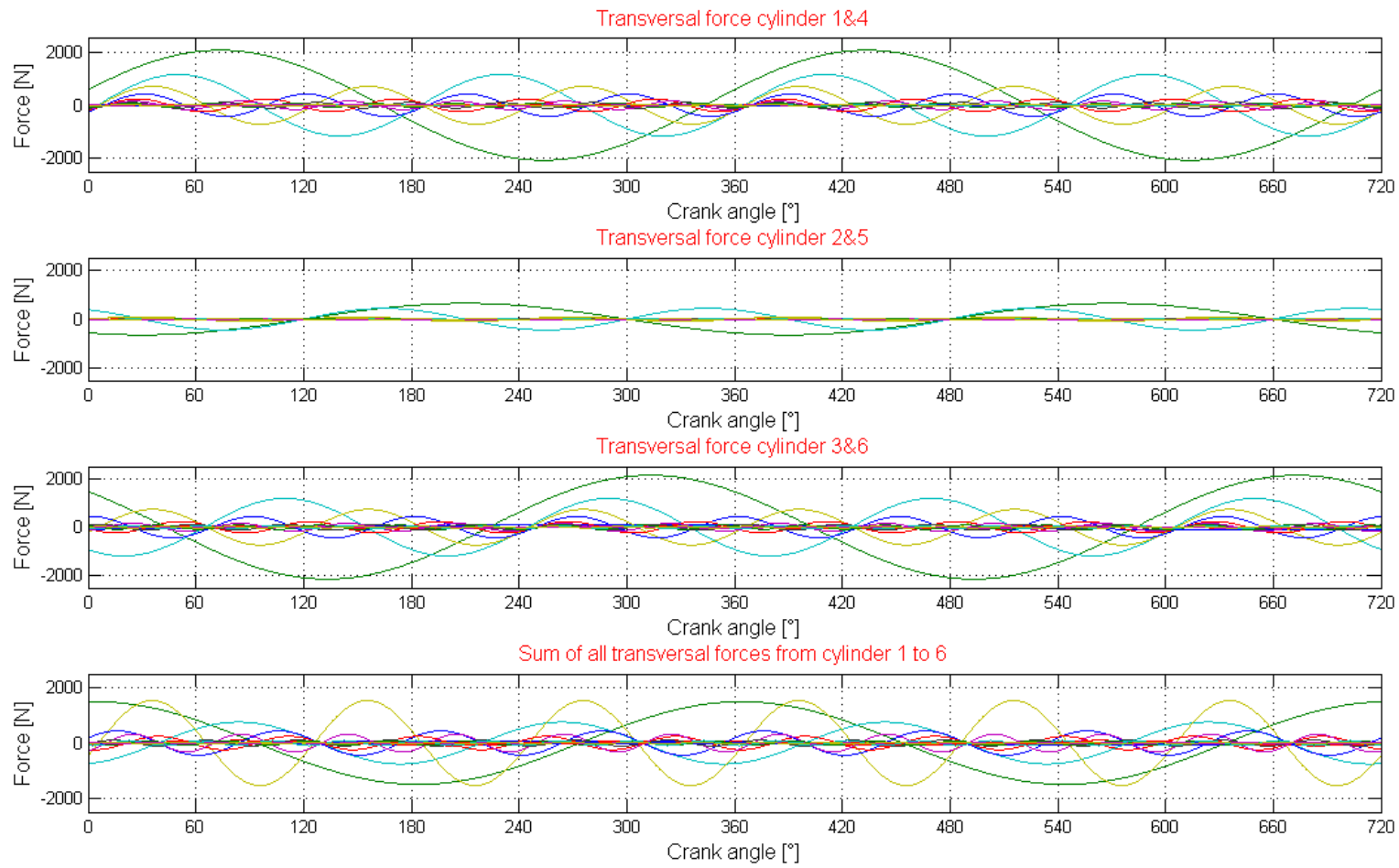


Figure 8-3 Overview of the cylinder selective spectral components with a simulated failure at cylinder 2 and controlled cylinder shut off of cylinder 5.

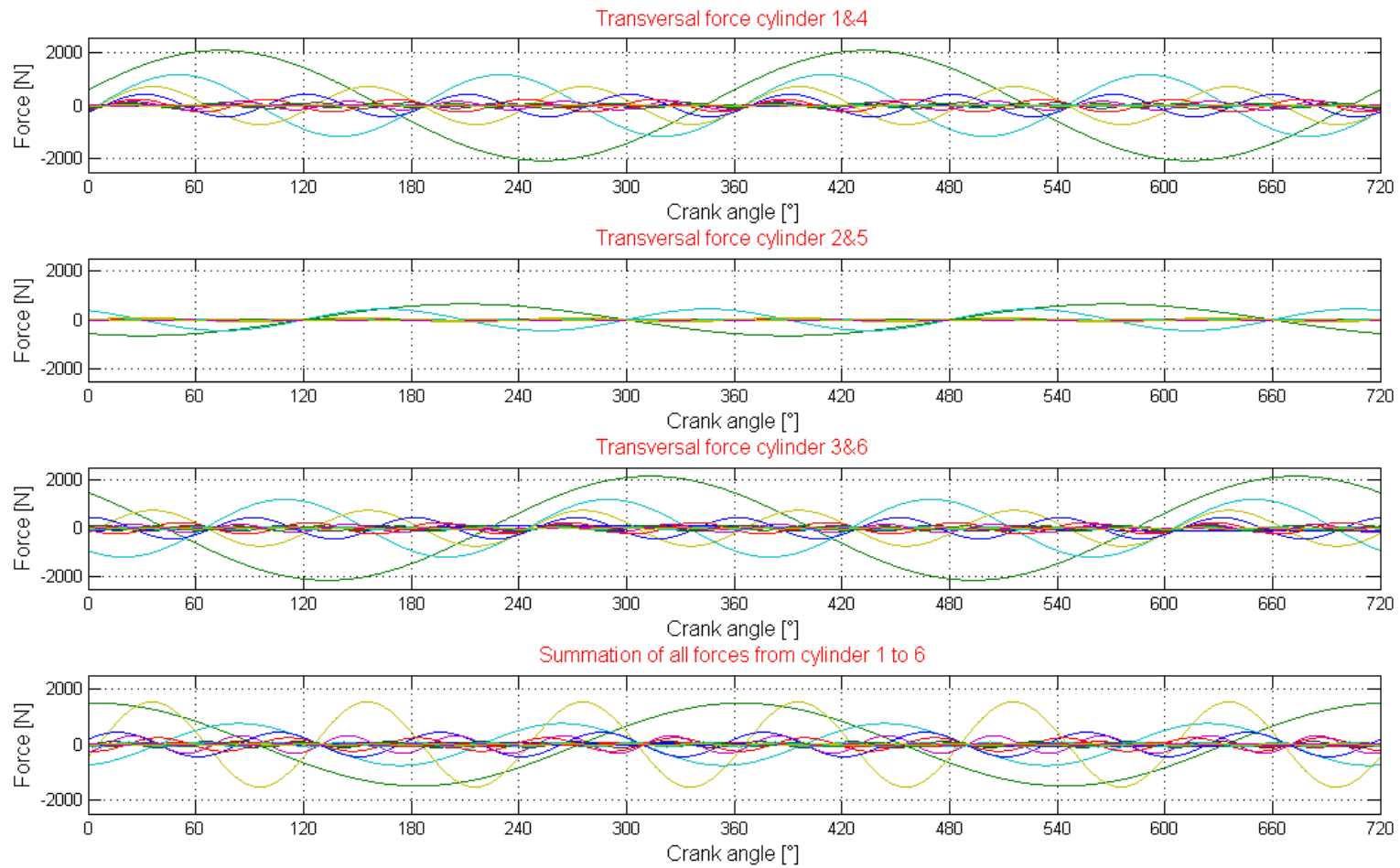


Figure 8-4 Spectral components of transversal gas force of the corresponding cylinder pairs and the total sum at the crankshaft.

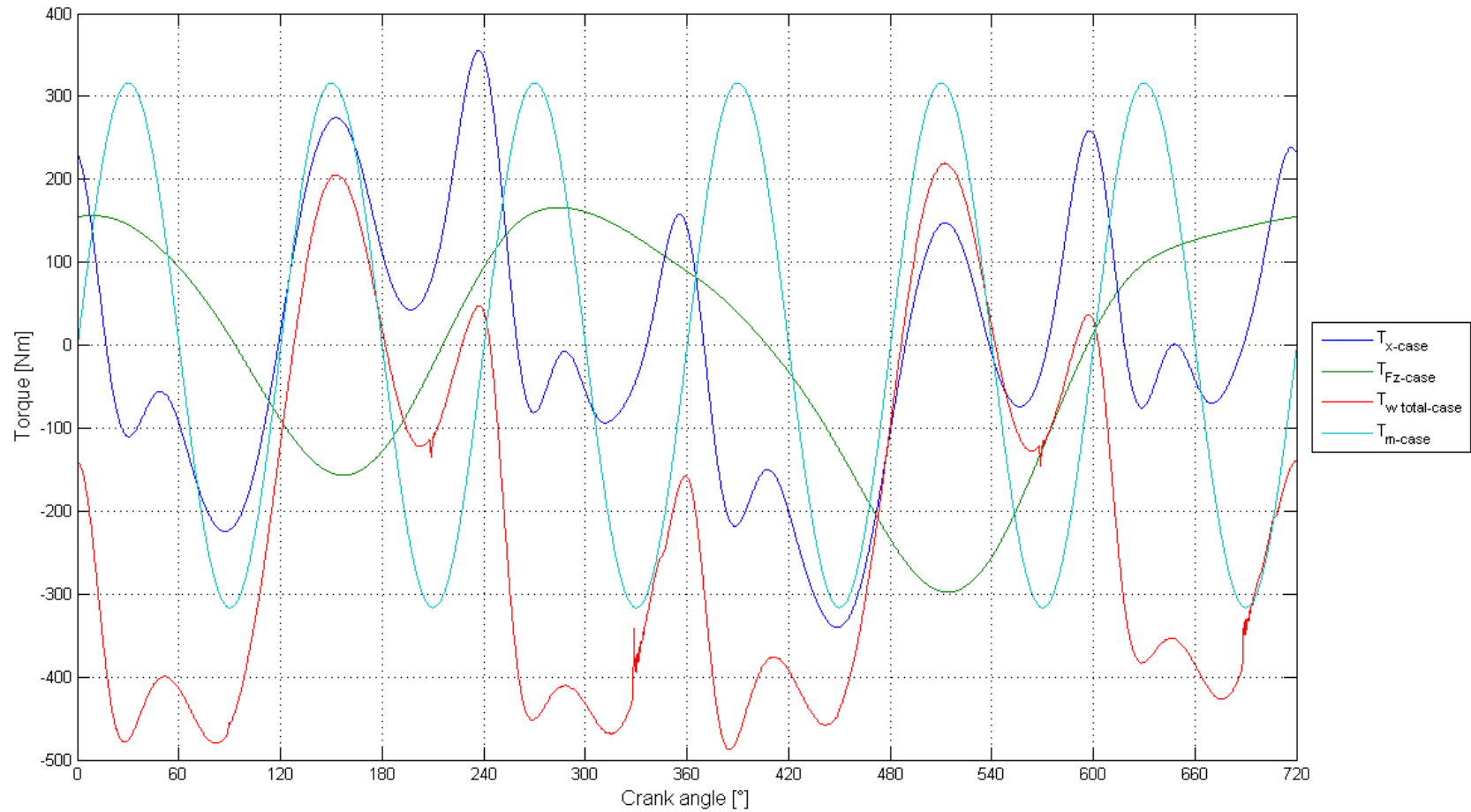


Figure 8-5 Torque signals on the engine case in x -direction referenced to coordinate plane "CSYS centre of gravity". Gear box torque, total crankshaft torque simulated on the engine case and mass torques on engine block by a faulty cylinder 2 and deactivated cylinder 5.

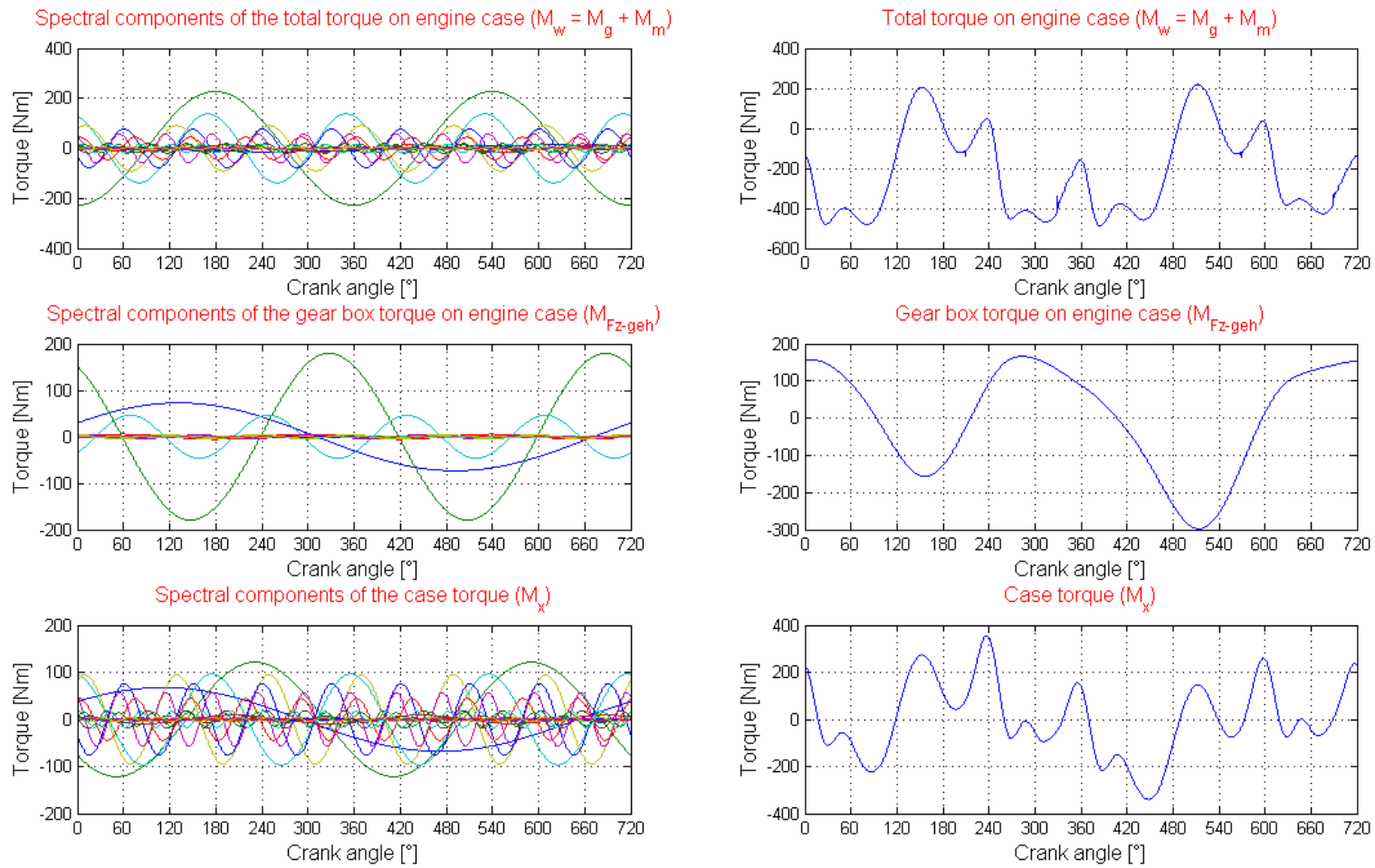


Figure 8-6 Frequency overview of the total crankshaft torque, the gear box torque and the engine case torque simulated in x-direction and refernced to coordinate plane "CSYS centre of gravity".

SYSTEM EXTENTION

Next diagram (Figure 8-7) shows the most important signals of the power train system. As it can be seen the simulated acceleration signal is in a normal range.

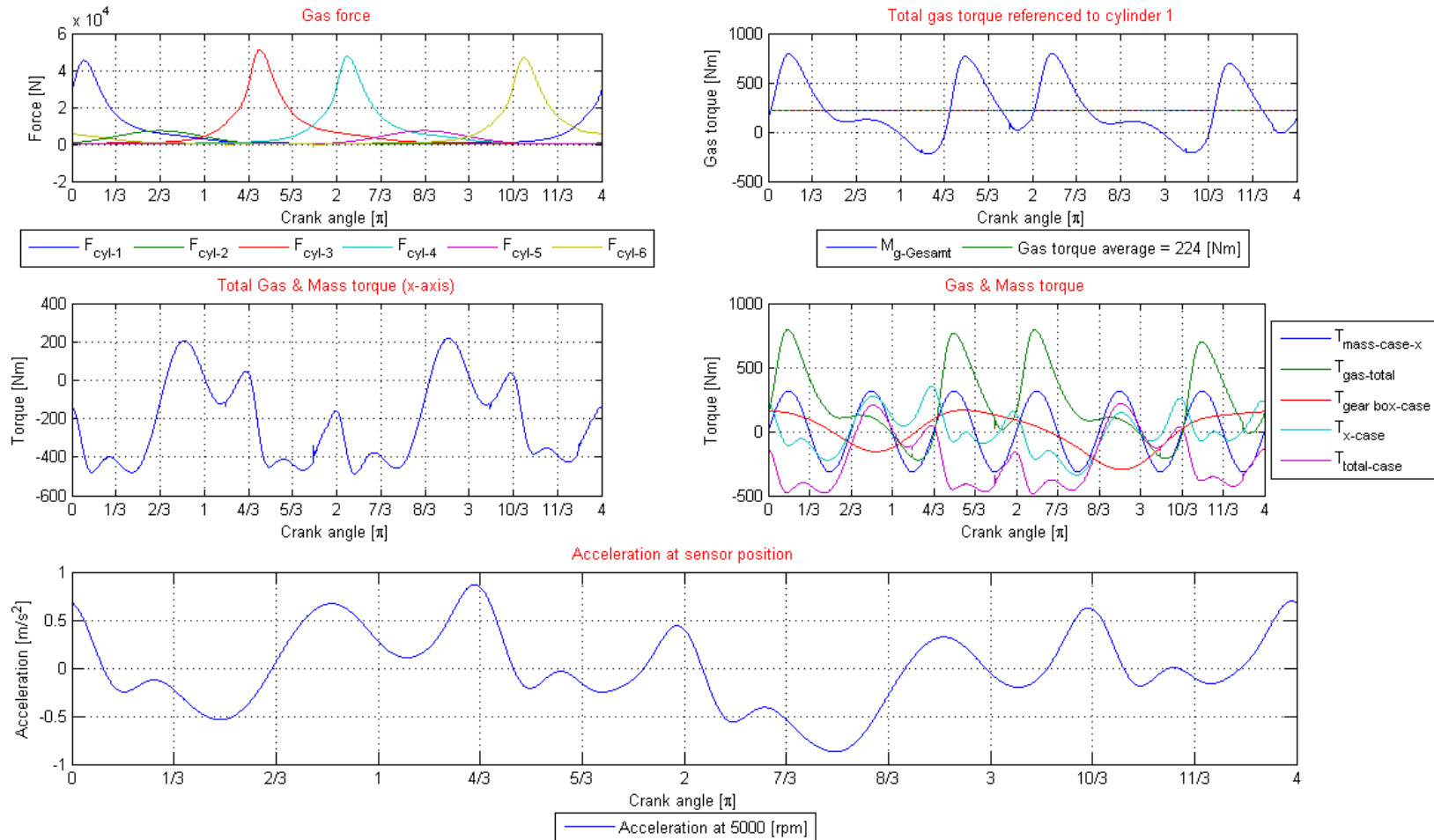


Figure 8-7 Overview of calculation steps from gas force to engine case acceleration if cylinder 2 is defect and cylinder 5 is switched off.

In Figure 8-8 the frequency spectrum of the engine case movement is drawn. It shows completely different spectral components compared to a faulty engine. It can be seen that the signal power is split on several spectral components. Especially the 0.5th engine oscillation mode is compensated.

SYSTEM EXTENTION

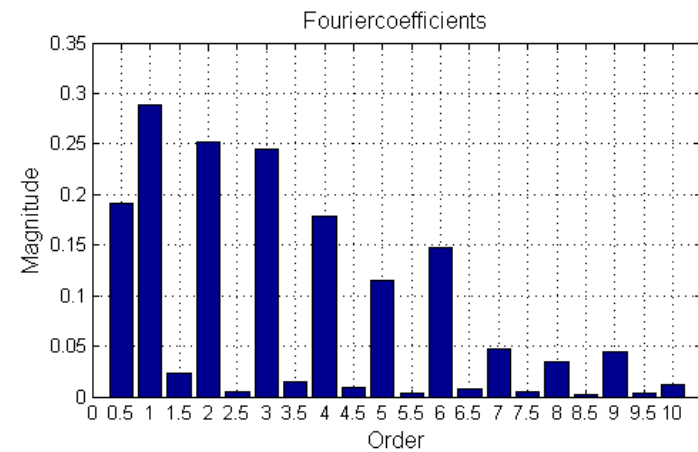
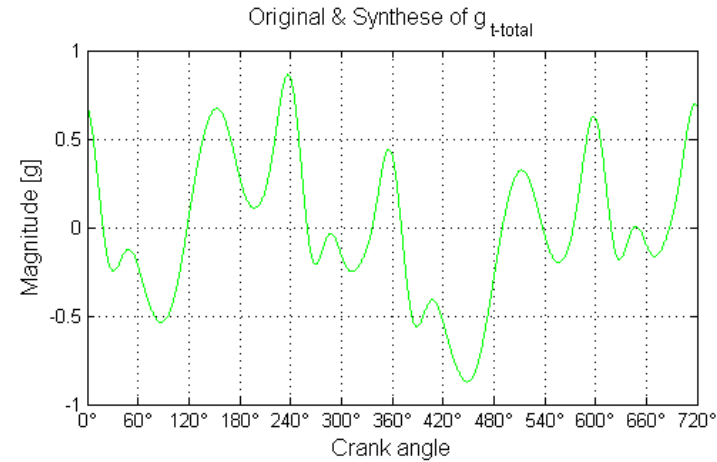
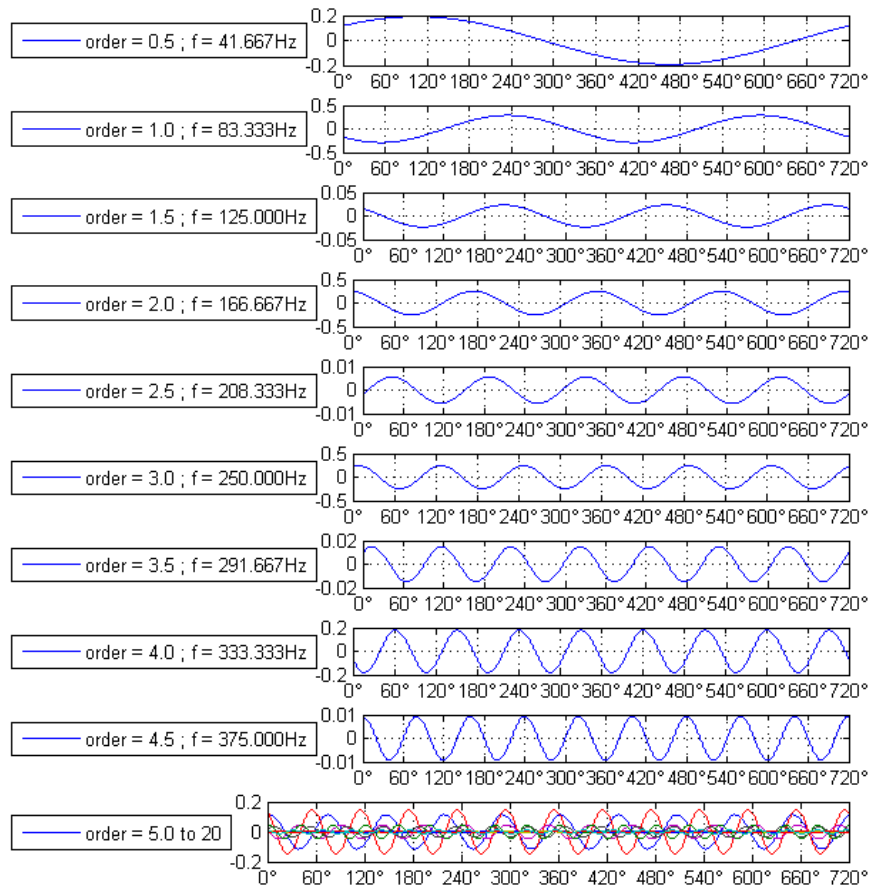


Figure 8-8 Simulated frequency spectrum of engine case acceleration with a faulty cylinder 2 and a deactivated cylinder 5 (misfiring compensated).

By using the signal processing method, which was proposed in chapter 6, the result shows a good engine with a slight tendency to higher vibration levels at high engine oscillation modes. This can be seen in Figure 8-9.

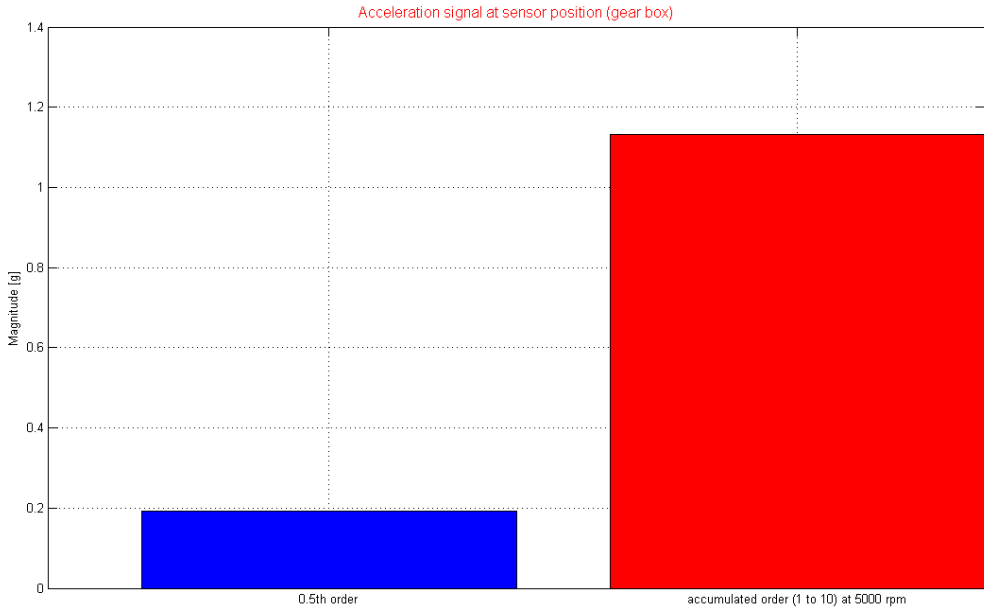


Figure 8-9 Computation of the signal power of the 0.5th engine oscillation mode and the sum from the 1st to the 10th engine oscillation mode with a faulty cylinder 2 and a deactivated cylinder 5.

If the disturbance due to a defect cylinder is compensated the mechanical stress of the internal parts is reduced to a normal value which is not further critical. This is shown in the next figure (Figure 8-10) last plot right hand side. This chart represents the torsion bar for example. A comparison with Figure 8-1 (good engine) and Figure 8-2 (poor engine) shows the stress reduction on this device.

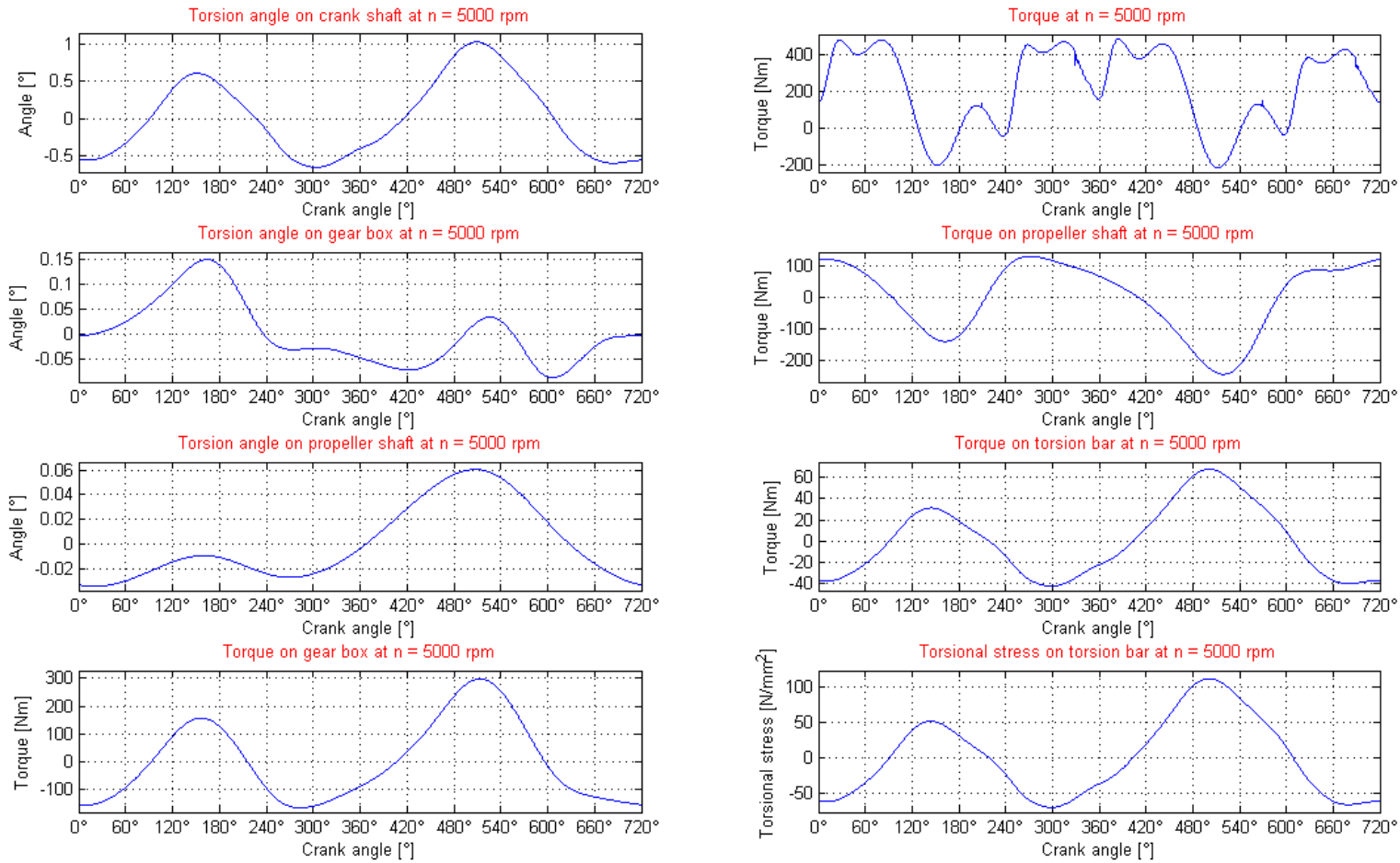


Figure 8-10 Overview of the stress analyses of the mechanical components of the power train system like crankshaft angle displacement, torsion angle on gear box, torsion angle on propeller shaft and torque on torsion bar. Cylinder 2 defect and cylinder 5 deactivated.

9 SUMMARY

In this thesis a new approach to detecting misfire of an aircraft combustion engine was described. Based on theoretical aspects, an analytic model was developed and the engine behaviour was simulated. A bottom up description of the system was established and proofed by comparing simulation results with real world measurements. The comparison of the analytic model with measurements completed on an aircraft show good agreements. The proposed condition monitoring system recognises misfire on a tested combustion engine with an amazing detection speed and a high detection probability rate.

An easy installation on the engine can be realized by using an acceleration sensor which has no restrictions to installation or location on the engine.

Due to the model description and the measured results, the signal processing leads to a simple signal algorithm with at least four samples per engine working cycle equal to 720° crank angle.

There is no system training required in order to acquire data from the engine under normal operating conditions.

In case of misfire, further actions based on the analytic model of the engine like cylinder shut down, variation of ignition angle and injected fuel quantity will mitigate mechanical stress from the engine.

Furthermore a preventive maintenance management can be established by monitoring the engine case acceleration. Existing condition monitoring system can be extended by adding this proposed method.

The described misfire detection method can be applied on engines with different cylinder counts as well.

Vibrations of engines that are designed with symmetric ignition angle offset can be reduced by applying controlled cylinder shut down.

Proposed misfire detection method could also be applied on remote controlled engines like compressor stages for pipe lines or power generations as well.

10 **OUTLOOK**

Some rig tests showed that an improvement of the model's sensitivity and the sensor signal processing will help to increase the dynamic range of the sensing system.

Misfire detection would benefit from improved acquisition quality of the acceleration signal, which reflects the engine block's displacement rate.

This opens new opportunities for the future, such as detecting deviations of the compression ratio between cylinders.

Durability tests involving different aircrafts with different propeller settings are essential to complete the definition of system limitations.

Information of the engine block vibration allows developing strategies for predictive maintenance as well.

Due to successful test series new ECU's have to be developed based on the functional prototype. Furthermore the implementation of the proposed misfire detection method in standard ECU's including test procedures and quality definitions are next steps which have to be done in the future.

Finally extensions of existing onboard diagnoses by adding the proposed method can be established.

BIBLIOGRAPHY

- [1] Anson Lee, Robert N.K. Loh and Zhijian James Wu. *Automotive Engine Misfire Detection Using Kalman Filtering*. Vehicular Technology Conference, IEEE, 2003.
- [2] Stefano Sgatti, Zanotti Massimo and Luigi De Luca. *Flywheel Learning for Multi-Cylinder Gasoline Engine Systems*. Industrial Technology, IEEE, 2003.
- [3] Matteo Montani and Nicol`o Speciale. *Multiple Misfire Identification by a Wavelet-Based Analysis of crankshaft Speed Fluctuation*. International Symposium on Signal Processing and Information Technology, IEEE, 2006.
- [4] C. Bohn, O. Magnor and M. Schultalbers. *State Observer based Analysis of Crankshaft Speed Measurements with Application to Misfire Detection*. International Conference on Control and Automation (ICCA2005), 2005.
- [5] Katsuhiko Kondo. *Electronic control apparatus of internal combustion engine*. Patent No.: US 6,530,360 B1.
- [6] Ruben Villarino and Johann F: Bohme. *Fast-in cylinder pressure reconstruction from structure born sound using the EM algorithm*. Acoustic Speech and Signal Processing, IEEE, 2003.
- [7] Michael Wagner, Jürgen Förster and Johann F. Böhme. *In-Cylinder Pressure Estimation from Structure-Borne Sound*. SAE 2000 World Congress, 2000.
- [8] James M. Slicker. *Knock and misfire detection system*. Patent No.: US 6,546,328 B1, 2003.
- [9] H. Heim and M. Mayer. *Engine misfire detection and engine exhaust systems*. Patent No.: WO 90/02871, 1990.
- [10] Environmental Conditions and Test Procedures for Airborne Equipment, RTCA incorporated 1828 L Street, NW, sweet 805 Washington DC, 20036, USA.
- [11] Schnell, Gross, Hauger: *Technische Mechanik 2(Elastostatik)*. Springer Verlag, ISBN 3-540-64147-5.
- [12] William A. Wisemann. *Vibratory Torque Control (VTC)*. Patent No.: US 3 421 343, 1969.
- [13] Hans Dresig, Franz Holzweißig, *Maschinendynamik*, ISBN 978-3-540-72032-4, 8. Auflage Springer Berlin Heidelberg New York.
- [14] P.Luger, K. Desoyer und A. Novak. *Technische Mechanik*, ISBN 3-211-81717-4.
- [15] Prof.Dr.-Ing. Erwin Haidbach. *Betriebsfestigkeit, Verfahren und Daten zur Bauteilberechnung*. VDI Verlag, ISBN 3-18-400828-2.
- [16] Barna Szabó and Ivo Babuska. *Finite Element Analysis*, ISBN 0-471-50273-1.
- [17] William H. Press, Saul A. Teukolsky, William T. Vetterling, Brian P. Flannery. *Numerical Recipes*, ISBN 0-521-43064-x.
- [18] MATLAB/SIMULINK™, <http://www.mathworks.de>.

- [19] Prof.Dr.Ing. Harald Maass. *Gestaltung und Hauptabmessungen der Verbrennungskraftmaschine*. Klöckner-Humboldt-Deutz AG Köln, ISBN 3-211-81562-7.
- [20] Jaroslav Kozesnik. *Maschinendynamik*, Hanser Verlag, 1966.
- [21] Heinz Ulbrich. *Maschinendynamik*. Teubner, 1996.
- [22] CAD Programme PTC-Wildfire V4.0, <http://www.ptc.com>.
- [23] Andreas Mair and Thomas Turner. *Condition Monitoring for Reciprocating Aircraft Engines using Fuzzy Logic*. Computational Intelligence for Measurement Systems and Application (CIMS), IEEE, 2010.
- [24] FlexPro, Version 8, <http://www.weisang.com>.
- [25] Ruben Villarino and Johann F. Böhme. *Misfire Detection in Automotive Engines Using Structure-Borne Sound*. SAE 2004 World Congress & Exhibition, 2004.
- [26] RTCA, Inc. Environmental Conditions and Test Procedures for Airborne Equipment. USA, 2004.
- [27] S.J. Loutridis. *Damage detection in gear systems using empirical mode decomposition*. Engineering Structures 26 (2004) 1833-18-41.
- [28] Daniel Ch. Von Grüningen. *Digitale Signalverarbeitung*. Fachbuchverlag Leipzig, ISBN 3-446-21445-3, 2001.
- [29] Stéphane Mallat. *A Wavelet tour of signal processing*. ISBN 0-12-466606-X, 1999.
- [30] STEVEN M. KAY. *STATISTICAL SIGNAL PROCESSING*. Prentice Hall PTR, ISBN 0-13-345711-7, 1993.
- [31] Steven Kay. *Intuitive Probability and Random Processing using MATLAB*. Springer. ISBN 0-387-24157-4. 2006.
- [32] HWEI P. HSU. *SIGNAL AND SYSTEMS*. SCHAUM'S OUTLINE SERIES, ISBN 0-07-030641-9, 1995.
- [33] Reinhard Lerch. *ELEKTRISCHE MESSTECHNIK*. Springer. ISBN 3-540-34055-6, 2006.
- [34] Bruno Assmann. *TECHNISCHE MECHANIK*. Oldenbuorg Verlag München Wien, ISBN 3-486-25597-5, 2001.
- [35] Ekbert Hering, Klaus Bressler, Jürgen Gutekunst. *Elektronik für Ingenieure*. Springer, ISBN 3-540-41738-9, 2001.
- [36] Alan V. Oppenheimer, Roland W. Schafer, John R. Buck. *Zeitdiskrete Signalverarbeitung*. PEARSON Studium, ISBN 3-8273-7077-9, 2004.
- [37] Jörg Hoffmann. *Taschenbuch der Messtechnik*. Carl Hanser Verlag, ISBN 3-446-22860-8, 2004.
- [38] Zhijian James Wu, Robert N.K. Loh and Anson Lee. *Automotive Engine Misfire Detection Using Kalman Fitering*. Vehicular Technology Conference, IEEE, 2003.
- [39] William G. Rado, Wayne J. Johnson. *Monitoring the Combustion Quality in Internal Combustion Engines Using the Spark Plug as a Plasma Probe*. Vehicular Technology, IEEE, 2002.

- [40] Guangyu DONG, Liguang LI, Shui YU and Xusheng ZHANG. *A Method of Torque Estimation Utilizing Ionization Sensing Technology in Internal Combustion SI Engine*. Vehicular Electronics and Safety, IEEE, 2006.
- [41] Yue-Yun Wang, Haskara, I. *Exhaust Pressure Estimation and Its Application to Variable Geometry Turbine and Wastegate Diagnostics*. American Control Conference (ACC), 2010.
- [42] Schroder A., Kupnik M., O'Leary P., Benes E., Groschl M. *A Capacitance Ultrasonic Transducer with Micro machined Back-plate for Fast Flow Measurements in Hot Pulsating Gases*. Sensors Journal, IEEE, 2006.
- [43] Takahashi, S.; Sekozawa, T. *Air-Fuel Ratio Control in Gasoline Engines Based on State Estimation and Prediction Using Dynamic Models*. Industrial Electronics, Control, and Instrumentation, 1995.
- [44] Samat S.A, Tahir S.M., Sha'ameri A.Z. *ENGINES CONDITION MONITORING BASED ON SPECTRUM ANALYSIS OF SOUND SIGNALS*. Signal Processing and its Application, IEEE, 2001.
- [45] S. V. P. Sankar Nidadavolu S.V.P.; Yadav S.K.; Kalra P.K. *Condition monitoring of Internal Combustion engines using empirical mode decomposition and Morlet wavelet*. Image and Signal Processing and Analysis (ISPA), IEEE, 2009.
- [46] Klaus Vogl. *Zustandsüberwachung eines 4-Zylinder 4-Takt-Otto-Motors für Fluganwendung mittels Abgastemperaturmessung*. FH-Wels, 2010.
- [47] Klee, Peter & Gebhardt, Wolfgang. *Die hochauflösende Messung von Abgasmassenstrom und – Temperatur mittels Ultraschall*. Bericht aus der Tätigkeit der Forschungsvereinigung Verbrennungskraftmaschine e.V.; MTZ 59. Jahrgang, Heft 3, 1998.
- [48] Wendeker M., Kamiński T. *Development of a Fibre-Optic Sensor for the Measurement of Dynamic Cylinder Pressure in Spark Ignition Engine*. Sensors, IEEE, 2005.
- [49] William B Ribbens, Jaehong Park and Deeeun Iom. *APPLICATION OF NEURAL NETWORKS TO DETECTING MISFIRE IN AUTOMOTIVE ENGINES*. Acoustics, Speech, and Signal Processing, IEEE, 1994.
- [50] A. Alkhateeb, M. Das. *A Model Based Data Normalization Technique for Improving Performance of Engine Misfire Detection Algorithms*. Electro/Information Technology Conference, IEEE, 2004.
- [51] Ashish Babbar, Estefan M. Ortiz, Vassilis L. Syrmos. *Fuzzy Clustering Based Fault Diagnosis for Aircraft Engine Health Management*. Mediterranean Conference on Control & Automation, 2009.
- [52] N.B. Jones, Yu-Hua Li. *A Review of Condition Monitoring and Fault Diagnoses for Diesel Engine*. Tribo test, 2000.

11 TABLE OF SYMBOLS

\mathfrak{I}_C	Moment of inertia of the car
\mathfrak{I}_c	Moment of inertia of the crank shaft
\mathfrak{I}_A	Moment of inertia of the aircraft
\mathfrak{I}_p	Moment of inertia of the propeller
$f_{excitation}$	Excitation frequency
$\omega = 2\pi f$	Angular frequency
t_a	Time of force transition
T_{real}	Period time of the real system
f_{real}	Frequency of the real system
\mathfrak{I}_a	Moment of inertia with a as reference axis
s	Distance from axis to the point of the body
\mathfrak{I}_{pq}	Product of inertia
p, q	Reference plane
m	Mass
\mathfrak{I}_{xy}	Product of inertia
\mathfrak{I}_{xz}	Product of inertia
\mathfrak{I}_{xy}	Product of inertia
\mathfrak{I}_{yz}	Product of inertia
\mathfrak{I}_{xz}	Product of inertia
\mathfrak{I}_{yz}	Product of inertia
\mathfrak{I}_c	Mass centre of the complete engine
x, y, z	Direction of orientation
\mathfrak{I}_{xx}	Moment of inertia in x-direction
\mathfrak{I}_{yy}	Moment of inertia in y-direction
\mathfrak{I}_{zz}	Moment of inertia in z-direction
\mathfrak{I}	Moment of inertia generally
$\underline{\underline{\mathfrak{I}}}$	Moment of inertia (matrix) generally
\mathfrak{I}_1	Moment of inertia of the crankshaft
\mathfrak{I}_{16}	Moment of inertia of crankshaft and hydro damper
\mathfrak{I}_2	Moment of inertia of the tooth wheel (gear box input)
\mathfrak{I}_2^*	Auxiliary variable for the Moment of inertia
\mathfrak{I}_4	Moment of inertia of the tooth wheel (gear box output)
\mathfrak{I}_5	Moment of inertia of the propeller
\mathfrak{I}_6	Moment of inertia of the hydro damper

TABLE OF SYMBOLS

$\ddot{\phi}_{16}$	Angular acceleration of crankshaft and hydro damper
$\ddot{\phi}_1$	Angular acceleration of crankshaft
$\ddot{\phi}_2$	Angular acceleration of the tooth wheel radius (gear box input)
$\ddot{\phi}_4$	Angular acceleration of the tooth wheel radius (gear box output)
$\ddot{\phi}_5$	Angular acceleration of the propeller
$\ddot{\phi}_6$	Angular acceleration of the hydro damper
$\ddot{\phi}$	Angular acceleration generally
$\underline{\ddot{\phi}}$	Angular acceleration (complex) generally
$\dot{\phi}_{16}$	Angular velocity of the crankshaft and hydro damper
$\dot{\phi}_1$	Angular velocity of the crankshaft
$\dot{\phi}_2$	Angular velocity of the tooth wheel (gear box input)
$\dot{\phi}_4$	Angular velocity of the tooth wheel (gear box output)
$\dot{\phi}_5$	Angular velocity of the propeller
$\dot{\phi}_6$	Angular velocity of the hydro damper
$\dot{\phi}$	Angular velocity generally
$\underline{\dot{\phi}}$	Angular velocity (complex) generally
ϕ_{16}	Angular of the hydro damper
ϕ_1	Angular of the crankshaft
ϕ_2	Angular of the tooth wheel (gear box input)
ϕ_4	Angular of the tooth wheel (gear box output)
ϕ_5	Angular of the propeller
ϕ_6	Angular of the hydro damper
ϕ	Angular generally
$\underline{\phi}$	Angular (complex) generally
ϕ_{real}	Real part of the angular (complex)
ct_4	Spring rate of the torsion bar
ct_6	Spring rate of the propeller shaft
c_1	Spring rate of the torsion bar
c_4	Spring rate of the propeller shaft
c	Spring rate generally
\underline{c}	Spring rate (matrix) generally
r_5	Tooth wheel radius (gear box input)
r_2	Tooth wheel radius (gear box input)
r_4	Tooth wheel radius (gear box output)
r_6	Tooth wheel radius (gear box output)
$\omega_{1,2}$	Angular frequency of the power train system without excitation
ω_0	Angular frequency of the power train system without excitation
ω_*^2	Auxiliary variable for the angular frequency
d_1	Damping factor of the torsion bar

TABLE OF SYMBOLS

d_4	Damping factor of the propeller shaft
d_6	Damping factor of the hydro damper
d	Damping factor generally
\underline{d}	Damping factor (matrix) generally
T_1	Crankshaft torque
T_2	Torque at the tooth wheel (gear box input)
T_2^*	Auxiliary variable for the torque
T_4	Torque at the tooth wheel (gear box output)
T_5	Propeller torque
T_6	Torque at the hydro damper
T	Torque generally
\underline{T}	Torque (complex) generally
T_a	Torque amount
\underline{T}_a	Torque amount (complex)
j	Imaginary unit
t	Time [sec]
x	Auxiliary variable
\underline{x}	Auxiliary variable (complex)
\underline{x}_{real}	Real part
$x_{n,real}$	Real part at oscillation mode n
\underline{x}_{imag}	Imaginary part
$x_{n,imag}$	Imaginary part at oscillation mode n
F	Force
A_s	Area of the silent block
E	Modulus of elasticity
\underline{A}	Auxiliary variable (matrix)
\underline{B}	Auxiliaire variable (matrix)
\underline{C}_a	Amplitude (complex)
$\underline{\phi}$	Phase angle (complex)
ϕ_n	Phase angle at oscillation mode n
$C_{a,n}$	Amplitude of oscillation mode n
M_{engine}	Engine torque
\mathfrak{S}_{engine}	Moment of inertia of the engine
F_{st}	Force (static)
\hat{x}	Deflection (dynamic)
b	Damping parameter
\hat{F}	Force dynamic
\hat{x}'	Velocity
\hat{x}''	Acceleration
A_*	Amplitude
A	Amplitude

TABLE OF SYMBOLS

B	Amplitude
$f_{(x)}$	Periodical signal
T	Period time
k	Factor
π	Number pi
a_0	Average value
a_k	Amplitude of the oscillation mode k
b_k	Amplitude of the oscillation mode k
a_q	Amplitude of the oscillation mode q
b_q	Amplitude of the oscillation mode q
$f_{(t)}$	Finite time signal
$\dot{\psi}$	Angular velocity (of the crank motion system)
n	Engine revolution [rpm]
$\ddot{\psi}$	Angular acceleration (of the crank motion system)
s	Distance from TDC to piston pin
R	Crankshaft radius
ψ	Angular (of the crank motion system)
l	Connecting rod length
β	Angle between connecting rod and cylinder axis
λ	Crankshaft radius to connecting rod length ratio
x	Piston position
\dot{s}	Piston velocity
\ddot{s}	Piston acceleration
F_G	Gas force or piston force
V_c	Combustion space volume
ε	Compression ratio
$f()$	Function generally
V_c	Combustion space volume of the cylinder
R	Gas constant
T_c	In-cylinder gas temperature
ε	Compression ratio
p_c	In-cylinder pressure
F_N	Transversal force of the gas force
$F_{N(\psi)}$	Transversal force of the gas force depending on the piston position
$F_{G(\psi)}$	Gas force depending on the crank angle
A_p	Piston area
M_{case}	Case torque
F_T	Tangential force
F_{Rs}	Radial force
F_{Tm}	Tangential force of a single mass point
m_{po}	Oscillating mass
m_{pr}	Rotating mass

TABLE OF SYMBOLS

$y_{(\psi)}$	Piston distance to the centre of rotation of the crankshaft
F_R	Radial force
U_{sensor}	Acceleration sensor output voltage
$f(a)$	Function depends on the acceleration
M_{g_tot}	Total gas torque amount
i, h	Index
N	Equivalent to the cylinder counts
Z	Equivalent to harmonic numbers
a	Acceleration
v	Velocity
F_o	Oscillating force
m_o	Oscillating mass
M_{mass}	Total mass torque
M	Torque generally
M_m	Mass torque
$f(n_{engine})$	Function of engine speed
$\mathfrak{S}_{(\psi)}$	Moment of inertia as function of the crank angle
$\mathfrak{S}'_{(\psi)}$	Derivation of the Moment of inertia as function of the crank angle
m_2	Connecting rod mass
m_3	Connecting rod mass
m_p	Piston mass
u', u''	geometrical parameters for the connecting rod
w', w''	geometrical parameters for the connecting rod
$M_{m_x_total}$	Engine case torque around the x-axis due to mass effects
$M_{b_y_total}$	Engine case torque around the y-axis due to mass effects
$M_{b_z_total}$	Engine case torque around the z-axis due to mass effects
n_{engine}	Engine speed [rpm]
M_{case_total}	Total engine torque
$M_{g_tot_i}$	Individual cylinder torque due to the gas phenomenon
$M_{m_total_i}$	Individual cylinder torque due to the mass phenomenon
$f(engine_load)$	Function of engine load condition
g	Gravitational acceleration
$m_{(failure)}$	Failure indicator
$T_{(0.5^{th})}$	Torque amount of the 0.5 th engine oscillation mode
$T_{(cyl1\&cyl4)}$	Sum of the torques from cylinder 1 and 4
$T_{(cyl1)}$	Torque of cylinder 1
$T_{(cyl2)}$	Torque of cylinder 2
$T_{(cyl3)}$	Torque of cylinder 3

TABLE OF SYMBOLS

$T_{(cyl4+180^\circ)}$	Torque of cylinder 4
$T_{(cyl5+180^\circ)}$	Torque of cylinder 5
$T_{(cyl6+180^\circ)}$	Torque of cylinder 6
$T_{(cyl2\&cyl5)}$	Sum of the torques from cylinder 2 and 5
$T_{(cyl3\&cyl6)}$	Sum of the torques from cylinder 3 and 6

12 TABLE OF FIGURES

Figure 2-1	Overview of methods for misfire detection.	10
Figure 3-1	Torsional amplitude versus engine speed –Dual frequency system.	17
Figure 3-2	Engine model overview.	18
Figure 3-3	Sectional representation of the power train system. (1) hydro damper, (8) silent block, (2) crankshaft, (3) piston, (4) torsion bar, (5) pinion shaft, (6) gear box and propeller shaft (7).	21
Figure 3-4	Overview of engine parts of the power train system. Top: Crankshaft left hand side and torsion bar right. Middle: Pinion shaft left hand side and silent block with fixation to the right. Bottom: Hydro damper with tooth wheel left hand side, to the right the connecting rod and the piston.	22
Figure 3-5	Sectional representation of the gear box.	23
Figure 3-6	Rigid body type model of the power train system.	24
Figure 3-7	Normalized eigen-mode magnitude of the power train system.	26
Figure 3-8	Torques on parts of the transmission system versus engine speed. Top torsion bar, middle propeller shaft and bottom gear box.	26
Figure 3-9	Dynamic model overview of the power train system.	31
Figure 3-10	Cylinder location, bracketed the firing order and coordinate plane "CSYS engine centre".	39
Figure 3-11	Cylinder coordinate system "CSYS cylinder coordinate" for cylinder 1 and rotation direction of crankshaft.	39
Figure 3-12	Coordinate planes "CSYS engine centre" top view.	40
Figure 3-13	Coordinate planes "CSYS engine centre".	40
Figure 3-14	Coordinate planes "CSYS centre of gravity" calculated of the whole engine and "CSYS engine centre".	41
Figure 3-15	Coordinate planes "CSYS centre of gravity" calculated of the whole engine (top view).	42
Figure 3-16	Coordinate planes "CSYS centre of gravity" of the whole engine.	42
Figure 4-1	Overview of the crank drive system.	45
Figure 4-2	Overview of forces on the crank drive system.	48
Figure 4-3	Typical characteristics of gas force F_G of a turbo charged combustion engine.	49
Figure 4-4	Pressure curve without ignition (no combustion process). In case of a total cylinder shut down this pressure characteristic will be applied in the analytic mode.	50

TABLE OF FIGURES

Figure 4-5	Characteristic of the transversal force calculated from the gas force.	50
Figure 4-6	Computed crank motion system (top). Calculated cylinder force (middle) and cylinder torque (bottom) based on measured in-cylinder pressure characteristics.	52
Figure 4-7	Calculated gas torques of the individual cylinders (top graph) and the calculated total gas torque on the crankshaft based on measured in-cylinder pressure characteristics (bottom graph).	52
Figure 4-8	Typical calculated gas torque curve of one cylinder based on measured in-cylinder pressure characteristics of a turbo charged combustion engine.	53
Figure 4-9	Model of forces of a rotating single mass point. The force is split to the tangential force F_{Tm} and centrifugal force F_{Rs} .	55
Figure 4-10	Three mass model of the connecting rod. Oscillating mass m_2 , rotating mass m_1 and the centre of gravity m_3 of the connecting rod.	58
Figure 4-11	Mass model of the connecting rod. Separation of the connecting rod to oscillating mass point m_{po} and rotating mass point m_{pr} .	60
Figure 4-12	Characteristic of the mass torque effect on engine case versus engine speed	62
Figure 4-13	Overviews of coordinate planes with the position of the acceleration sensor and direction of sensitivity.	63
Figure 4-14	Arrangement of a balancer shaft referenced to coordinate plane "CSYS cylinder coordinate".	64
Figure 4-15	Measured in-cylinder pressure curve of cylinder 5.	65
Figure 4-16	Simulated gas and mass torques based on measured in-cylinder pressure curves at 5000 rpm	66
Figure 5-1	Model overview of the mechanical system and the torque mechanism	69
Figure 5-2	Overview of the cylinder selective spectral components drawn versus crank angle	71
Figure 5-3	Spectral analyses of the transversal force of the gas force	72
Figure 5-4	Spectral analyses of the crankshaft torque of cylinder 1. Watch the different scales used for higher engine orders.	73
Figure 5-5	Simulated spectral components of transversal forces of the corresponding cylinder pairs and the total calculated sum of the transversal force on the crankshaft	74
Figure 5-6	Simulated gas and mass torques. Upper plot gas (blue) and mass torque (green). Middle plot: Total torque on crankshaft and bottom plot engine block torque.	75
Figure 5-7	Spectral analyses of the gear box torque appearing on the engine block.	77
Figure 5-8	Spectral analyses of the engine case torque around x-axis.	78

TABLE OF FIGURES

Figure 5-9	Frequency overview of total crankshaft torque, gear box torque and engine case torque simulated around x-axis.	80
Figure 5-10	Simulated torque signals on engine case around x-direction. Gear box torque (green), total crankshaft torque on case (red), mass torque (turquoise) and total engine block torque (blue).	82
Figure 5-11	Spectral analyses of the engine case excitation.	83
Figure 5-12	Overview of calculation steps from gas force to engine case acceleration if all cylinder work fine. Simulation was done at 5000 rpm.	85
Figure 5-13	Spectral analyses of the crankshaft torque (green line) based on an analytic in-cylinder pressure characteristic.	87
Figure 5-14	Overview of the cylinder selective spectral components with a simulated failure at cylinder 3.	88
Figure 5-15	Spectral components of transversal forces of the corresponding cylinder pairs and the total sum at the crankshaft.	89
Figure 5-16	Gas and mass torques with simulated engine failure at cylinder 3.	90
Figure 5-17	Spectral analyses of the total crankshaft torque with poor combustion process at cylinder 3.	91
Figure 5-18	Spectral analyses of the influence to engine case due to gear box torque.	93
Figure 5-19	Spectral analyses of the engine case torque around the x-axis referenced to coordinate plane "CSYS centre of gravity".	94
Figure 5-20	Frequency overview of the total crankshaft torque, the gear box torque and the engine case torque simulated around x-axis with the reference to "CSYS centre of gravity".	95
Figure 5-21	Torque signals on the engine case in x-direction referenced to coordinate plane "CSYS centre of gravity". Gear box torque, total crankshaft torque simulated on the engine case and mass torques on engine block.	97
Figure 5-22	Spectral analyses of the engine block excitation in case of misfire.	98
Figure 5-23	Overview of calculation steps from gas force to engine case acceleration if cylinder 3 is switched off.	100
Figure 6-1	Hierarchical data processing chain of a fuzzy based condition monitoring system.	102
Figure 6-2	Fuzzy map for health level estimation.	102
Figure 6-3	Condition monitoring results from a real world field test. Upper plot: Acceleration signal power from real world experiment: time evolution of overall signal power and signal power in order 0.5 for cylinder 1 being disabled and enabled. Lower plot: Engine condition health level from Fuzzy-based engine condition estimation.	103
Figure 6-4	EMD results. Calculated intrinsic mode function (IMF) and measured vibration signal coming from engine tests with cylinder 1 deactivated. Engine was operated at 2500 rpm. Bottom right hand side	

TABLE OF FIGURES

	the vibration signal is shown. Imf 1 to imf 11 represents the intrinsic mode functions derived from the vibration signal (vibr sign) with a signal length of 10000 sampling points.	105
Figure 6-5	EMD results. Calculated intrinsic mode function (IMF) and measured vibration signal coming from engine tests with cylinder 1 deactivated. Engine was operated at 2500 rpm. Bottom right hand side the vibration signal is shown. Imf 1 to imf 11 represents the intrinsic mode functions derived from the vibration signal (vibr sign) with a signal length of 15000 sampling points.	106
Figure 6-6	Computation of the signal power with no engine faults. The blue bar represents the 0.5 th engine oscillation mode and the red the sum from 1 st to 10 th .	108
Figure 6-7	Computation of the signal power with engine faults (misfire). The blue bar represents the 0.5 th engine oscillation mode and the red the sum from 1 st to 10 th .	109
Figure 6-8	Magnitude characteristics of the 0.5 th to 5 th engine oscillation mode of each cylinders.	111
Figure 6-9	Overview of the computed 0.5 th engine oscillation mode for each cylinder by simulating misfire events.	112
Figure 6-10	Magnitude curve of the 0.5 th engine oscillation mode versus engine speed. The picture represents results of simulated misfire events of each cylinder.	113
Figure 6-11	Angle offsets of certain engine oscillation modes (referenced to cylinder one) simulated at torsion bar and drawn versus engine speed.	116
Figure 6-12	Angle offset of the 0.5 th oscillation mode (referenced to cylinder one) simulated at the torsion bar versus engine speed.	118
Figure 7-1	Simulated phase angle curve of the 0.5 th engine oscillation mode versus engine speed referenced to cylinder one with good engine behaviour.	120
Figure 7-2	Engine test without failures. Acceleration of the engine from idle speed to maximum engine speed. Each plot shows the behaviour over engine cycles First plot 0.5 th engine oscillation mode, second plot phase angle referenced to cam shaft signal of the monitored vibration signal and last plot engine speed.	121
Figure 7-3	Cylinder failure on cylinder 3 at 4000 rpm. The misfiring event occurs aprox. after 175 engine cycles. First plot 0.5 th engine oscillation mode, second plot phase angle referenced to cam shaft signal and last plot engine speed versus engine cycles.	122
Figure 7-4	Amplitude curve of the 0.5 th engine oscillation mode at 4000 rpm after deactivating (172 nd engine cycle) an injector.	123
Figure 7-5	Cylinder 1 was switched off after reaching idle speed and engine was accelerated to maximum engine speed. First plot 0.5 th engine oscillation mode, second plot phase angle referenced to cam shaft signal and last plot engine speed versus engine cycles.	124

TABLE OF FIGURES

Figure 7-6	Cylinder 2 was switched off after reaching idle speed and engine was accelerated to maximum engine speed. First plot 0.5 th engine oscillation mode, second plot phase angle referenced to cam shaft signal and last plot engine speed versus engine cycles.	125
Figure 7-7	Cylinder 3 was switched off after reaching idle speed and engine was accelerated to maximum engine speed. First plot 0.5 th engine oscillation mode, second plot phase angle referenced to cam shaft signal and last plot engine speed versus engine cycles.	126
Figure 7-8	Cylinder 4 was switched off after reaching idle speed and engine was accelerated to maximum engine speed. First plot 0.5 th engine oscillation mode, second plot phase angle referenced to cam shaft signal and last plot engine speed versus engine cycles.	127
Figure 7-9	Cylinder 5 was switched off after reaching idle speed and engine was accelerated to maximum engine speed. First plot 0.5 th engine oscillation mode, second plot phase angle referenced to cam shaft signal and last plot engine speed versus engine cycles.	128
Figure 7-10	Cylinder 6 was switched off after reaching idle speed and engine was accelerated to maximum engine speed. First plot 0.5 th engine oscillation mode, second plot phase angle referenced to cam shaft signal and last plot engine speed versus engine cycles.	129
Figure 7-11	Measured magnitude of the 0.5 th engine oscillation mode during misfire events of the individual cylinders (cylinder 1 to 6) drawn versus engine speed.	130
Figure 7-12	Measured cylinder selective phase angle curve of the 0.5 th engine oscillation mode versus engine speed referenced to cam shaft signal.	131
Figure 7-13	Engine operated with 4 cylinder. Cylinder 1 and 2 were de-powered. Upper Plot: Magnitude of the 0.5 th engine oscillation mode versus engine cycle. Middle plot: phase angle of the 0.5 th engine oscillation mode referenced to cam shaft signal versus engine cycle. Last plot: engine speed versus engine cycle.	132
Figure 8-1	Overview of simulated stress analyses of the mechanical components of the power train system. Drawn are crankshaft angle displacement, torsion angel at gear box, torsion angle at propeller shaft and torque at torsion bar. Simulation was done with good engine condition.	134
Figure 8-2	Overview of simulated the stress analyses of the mechanical components of the powertrain system. Drawn are crankshaft angle displacement, torsion angle at the gear box, torsion angle at propeller shaft and torque at torsion bar. Simulation was carried out with bad engine condition.	135
Figure 8-3	Overview of the cylinder selective spectral components with a simulated failure at cylinder 2 and controlled cylinder shut off of cylinder 5.	137
Figure 8-4	Spectral components of transversal gas force of the corresponding cylinder pairs and the total sum at the crankshaft.	138
Figure 8-5	Torque signals on the engine case in x-direction referenced to coordinate plane "CSYS centre of gravity". Gear box torque, total	

TABLE OF FIGURES

	crankshaft torque simulated on the engine case and mass torques on engine block by a faulty cylinder 2 and deactivated cylinder 5.	139
Figure 8-6	Frequency overview of the total crankshaft torque, the gear box torque and the engine case torque simulated in x-direction and refernced to coordinate plane "CSYS centre of gravity".	140
Figure 8-7	Overview of calculation steps from gas force to engine case acceleration if cylinder 2 is defect and cylinder 5 is switched off.	141
Figure 8-8	Simulated frequency spectrum of engine case acceleration with a faulty cylinder 2 and a deactivated cylinder 5 (misfiring compensated).	143
Figure 8-9	Computation of the signal power of the 0.5 th engine oscillation mode and the sum from the 1 st to the 10 th engine oscillation mode with a faulty cylinder 2 and a deactivated cylinder 5.	144
Figure 8-10	Overview of the stress analyses of the mechanical components of the power train system like crankshaft angle displacement, torsion angle on gear box, torsion angle on propeller shaft and torque on torsion bar. Cylinder 2 defect and cylinder 5 deactivated.	145

13

**TABLE OF IDENTIFICATION
CODES**

MSE	Motorsteuereinheiten
ECU	Engine Control Unit
EMS	Engine Management Systems
LOPC	Loss Of Power Control
TBO	Time to Be Overhaul
EMC	Electromagnetic Compatibility
DO-160	Environmental conditions and test procedures for airborne equipment
OBD	On-Board Diagnostic
LTI	Linear Time Invariant
CSF	Crankshaft Speed Fluctuation
MDOF	Multiple Degree Of Freedom
FEM	Finite Element Method
CSYS	Coordinate System
TDC	Top Dead Centre
BDC	Bottom Dead Centre
EMD	Empirical Mode Decomposition
IMF	Intrinsic Mode Function

Eidesstattliche Erklärung

Ich erkläre an Eides statt, dass ich die vorliegende Dissertation selbstständig und ohne fremde Hilfe verfasst, andere als die angegebenen Quellen und Hilfsmittel nicht benutzt bzw. die wörtlich oder sinngemäß entnommenen Stellen als solche kenntlich gemacht habe.

Oberschlierbach, März 2011

Andreas Mair

ANDREAS MAIR

Familienstand: Ledig
Staatsangehörigkeit: Österreich
Geburtsort: Wels am 16.01.1973

Berufserfahrung:

1996-1997 Elektro- Eder 4600 Wels
 Radio und Fernsehmechaniker
 Reparaturen im Video Bereich
 Angebotserstellung im Bereich der Antennentechnik

1995-1996 Josef Silber 4600 Wels
 Radio und Fernsehmechaniker
 Leiter für Reparaturen diverser Geräte im Bereich der
 Unterhaltungselektronik.
 Planung und Errichtung von Satellitenanlagen.

1994 Fa. EHG Handel und Haustechnik GmbH 4560 Kirchdorf
 Radio und Fernsehmechaniker
 Leiter für Reparaturen diverser Geräte im Bereich der
 Unterhaltungselektronik.
 Betreuung mehrerer Antennengemeinschaftsanlagen.
 Planung und Errichtung von Satellitenanlagen.

2001 seit 2001 als Entwicklungsingenieur (Motormanagement)

Ausbildung:

Seit 2006 Dissertation am Institut f. elektrische Messtechnik u.
 Signalverarbeitung an der TU-Graz

1997-2001 Fachhochschule (mit gutem Erfolg bestanden) 4600 Wels
 Automatisierte Anlagen und Prozesstechnik, Ausbildung in den
 Bereichen Maschinenbau, Elektrotechnik / Elektronik, Informatik
 und Wirtschaft.
 Diplomarbeit: Automatisierte Schrumpfmessung von PVC-Profilen
 Ausbildung zum Wertanalytiker (Zertifikat)
 Ausbildung zum Junior Projektmanager (Zertifikat)
 Qualitätsmanagement Fachkraft (Zertifikat)
 Qualitätsmanagement-Beauftragter QMB-TÜV (Zertifikat)

1996-1997 Studienberechtigungsprüfung 4600 Wels
 Teilprüfungen in den Bereichen Mathematik, Deutsch, Englisch,
 Darstellende Geometrie und Physik.

1996 Unternehmerprüfung WIFI Kirchdorf
 Diverse Kurse im Bereich der Unterhaltungselektronik

1990-1993 Radio und Fernsehmechanikerlehre EBG Kirchdorf

1988-1990 Lehre als Elektromechaniker für Starkstrom EBG Linz

1987-1988 Polytechnischer Lehrgang 4560 Kirchdorf

1983-1987 Hauptschule 4560 Kirchdorf

1979-1983 Volksschule 4560 Kirchdorf

Kenntnisse: Elektronik; Verbrennungskraftmaschinen, erneuerbare Energien wie z.B.
 Windkraftanlagen und Photovoltaik

1994 8 Monate Präsenzdienst in Kirchdorf abgeleistet.